Proceedings of the "Pierre Beghin" international workshop on rapid gravitational mass movements = Compte-rendu du séminaire international " Pierre Beghin " sur les mouvements gravitaires rapides

L. Buisson, G. Brugnot

Proceedings of the "Pierre Beghin" international workshop on rapid gravitational mass movements

Actes de l'atelier international "Pierre Beghin" sur les mouvements gravitaires rapides

Coordination : L. BUISSON - G. BRUGNOT

Cemagref

10th December 1993 / 6-10 décembre 1993 - Grenoble

Proceedings of the "Pierre Beghin" international workshop on rapid gravitational mass movements

Actes de l'atelier international "Pierre Beghin" sur les mouvements gravitaires rapides

Grenoble
6-10th December 1993 /6-10 décembre 1993

Dans la même collection aux éditions du Cemagref

(prix TTC)

- Recherche et société, 10 ans d'expérience du Cemagref, oct. 1991, Paris, ISBN 2-85362-256-8, 1991, 204 p. - **200 F**

Équipements agricoles et alimentaires

- Equipements en production végétale et réduction des pollutions, 1994, ISBN 2-85362-405-6, 1995, 96 p. - **150 F**
- Plastiques et environnement, 1994, ISBN 2-85362- 396-4, 52 p. - **100 F**
- Maîtrise et prévention des pollutions dues aux élevages, *SIMA 94*, Paris, ISBN 2-85362-349-1, 148 p. - **200 F**
- La conduite autonome des engins agricoles, *SIMA 92*, Paris, ISBN 2-85362-266-5, 1993, 152 p. - **200 F**
- L'application de l'analyse d'images dans l'agro-industrie. De la production à la transformation des produits agricoles, 28 sept. 1994, Montpellier, ISBN 2-85362-372-6, 144 p. - **180 F**
- Use of on-machine vision systems for the agricultural and bio-industries. Systèmes de vision embarqués pour l'agriculture et l'industrie agro-alimentaire, sept. 1991, Montpellier, ISBN 2-85362-279-7, 1992, 176 p. - **200 F**
- Du concept de BVRE à celui de zone atelier dans les recherches menées en eaux continentales, 1994, Paris, ISBN 2-85362-400-5, 228 p. - **200 F**

Équipement pour l'eau et l'environnement

- Workshop on subsurface drainage simulation models. Atelier sur les modèles de simulation du drainage, 4-5 sept. 1993, La Haye, ISBN 2-85362-338-6, 1993, 338 p. - **150 F**
- Drainage agricole, fév. 1990, Le Caire, ISBN 2-85362-220-7, 1991, 340 p. - **220 F**

Gestion des milieux aquatiques

- ACIPENSER, colloque international sur l'esturgeon, oct. 1989, Bordeaux, ISBN 2-85362-208-8, 1991, 520 p. - **350 F**
- Measures for success. Metrology and instrumentation in aquaculture management. Mesures pour le succès. Métrologie et instrumentation appliquées à la gestion en aquaculture, *Aquaculture Bordeaux 94*, ISBN 2-85362-373-4, 328 p. - **275 F**
- Atelier international sur les bases biologiques de l'aquaculture des siluriformes. International workshop on the biological bases for aquaculture of siluriformes, 1994, Montpellier, ISBN 2-85362-365-3, 194 p. - **150 F**
- Dysfonctionnements biologiques dans les stations d'épuration en boues activées, 21 oct. 1994, Lyon, ISBN 2-85362-381-5, 82 p. - **200 F**
- Congrès international sur le traitement des effluents vinicoles. International specialized conference on winery wastewaters, 20 - 24 juin 1994, Narbonne / Epernay, ISBN 2-85362-366-1, 296 p. - **200 F**

Gestion des territoires

- Agriculteurs, agricultures et forêts, 1994, Paris, ISBN 2-85362-414-5, 1995, 208 p. - **190 F**
- Quelle mécanisation pour la forêt de demain ?, *SIMA 93*, Paris, ISBN 2-85362-324-6, 1993, 192 p. - **200 F**
- Ressources naturelles et développement montagnard, *SAM 92*, Grenoble, ISBN 2-85362-310-6, 1993, 154 p. - **200 F**
- Montagne = Qualité ?, *SAM 92*, Grenoble, ISBN 2-85362-332-7, 1993, 68 p. - **150 F**
- Territoires ruraux et développement. Quel rôle pour la recherche, 28 avril 1994, Paris, ISBN 2-85362-367-X, 246 p. - **170 F**
- Thermal remote sensing of the energy and water balance over vegetation in conjunction with other sensors. Télédétection infrarouge thermique des échanges énergétiques et hydriques de la végétation en combinaison avec d'autres capteurs, sept. 1993, La Londe Les Maures, ISBN 2-85362-371-8, 330 p. - **275 F**

Actes du colloque **Proceedings of the "Pierre Beghin" international workshop on rapid gravitational mass movements (Actes de l'atelier international "Pierre Beghin" sur les mouvements gravitaires rapides)**. 6-10 décembre 1993. Coordination de l'édition : L. Buisson et G. Brugnot - Suivi de fabrication : V. Goulette - Maquette de couverture : F. Cédra.
Impression et façonnage : imprimerie Louis Jean, 05003 Gap - Diffusion : Cemagref-Dicova, BP 22, 92162 Antony Cedex - Diffusion aux libraires : TEC et DOC Lavoisier, 19 rue de Provigny, 94236 Cachan Cedex
 ISBN 2-85362-411-0, dépôt légal : 2e trimestre 1995 - **Prix : 280 F**

Proceedings of the "Pierre Beghin" international workshop on rapid gravitational mass movements

Actes de l'atelier international "Pierre Beghin" sur les mouvements gravitaires rapides

December 6 to 10, 1993 / 6-10 décembre 1993
Grenoble, France

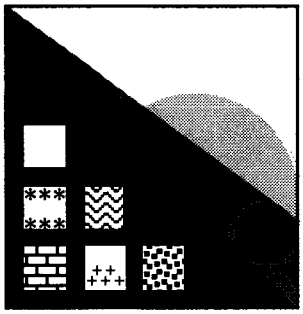

Co-ordination / Coordination

L. Buisson - G. Brugnot
Cemagref, France

Programme Committee / Comité de programme

G. Brugnot, *Cemagref, France*
J. Locat, *Université Laval, Canada*
H. Norem, *NGI, Norway*
K. Sassa, *Kyoto University, Japan*

Sponsors / Soutiens

Cemagref
Ministère de l'Environnement, Délégation aux risques majeurs (DRM)
Pôle grenoblois d'étude et de recherche sur les risques naturels (PGRN)
Délégation nationale aux actions de restauration des terrains en montagne (RTM)
Grenoble, pôle européen universitaire et scientifique (GPEUS)
Région Rhône-Alpes

L'atelier dont les actes sont présentés dans cet ouvrage a été dédié à Pierre Beghin, disparu dans la face Sud de l'Annapurna le 11 octobre 1992.

The workshop whose proceedings are presented in this book has been dedicated to Pierre Beghin who disappeared in the South Face of Annapurna on October 11, 1992.

Pierre Beghin, le 12 mars 1990, sur la zone de dépôt du site d'avalanche de Taconnaz, Haute-Savoie, France (photo de F. Rapin).

Pierre Beghin, on March 12, 1990, on the deposit zone of the avalanche path of Taconnaz, Haute-Savoie, France (photo by F. Rapin).

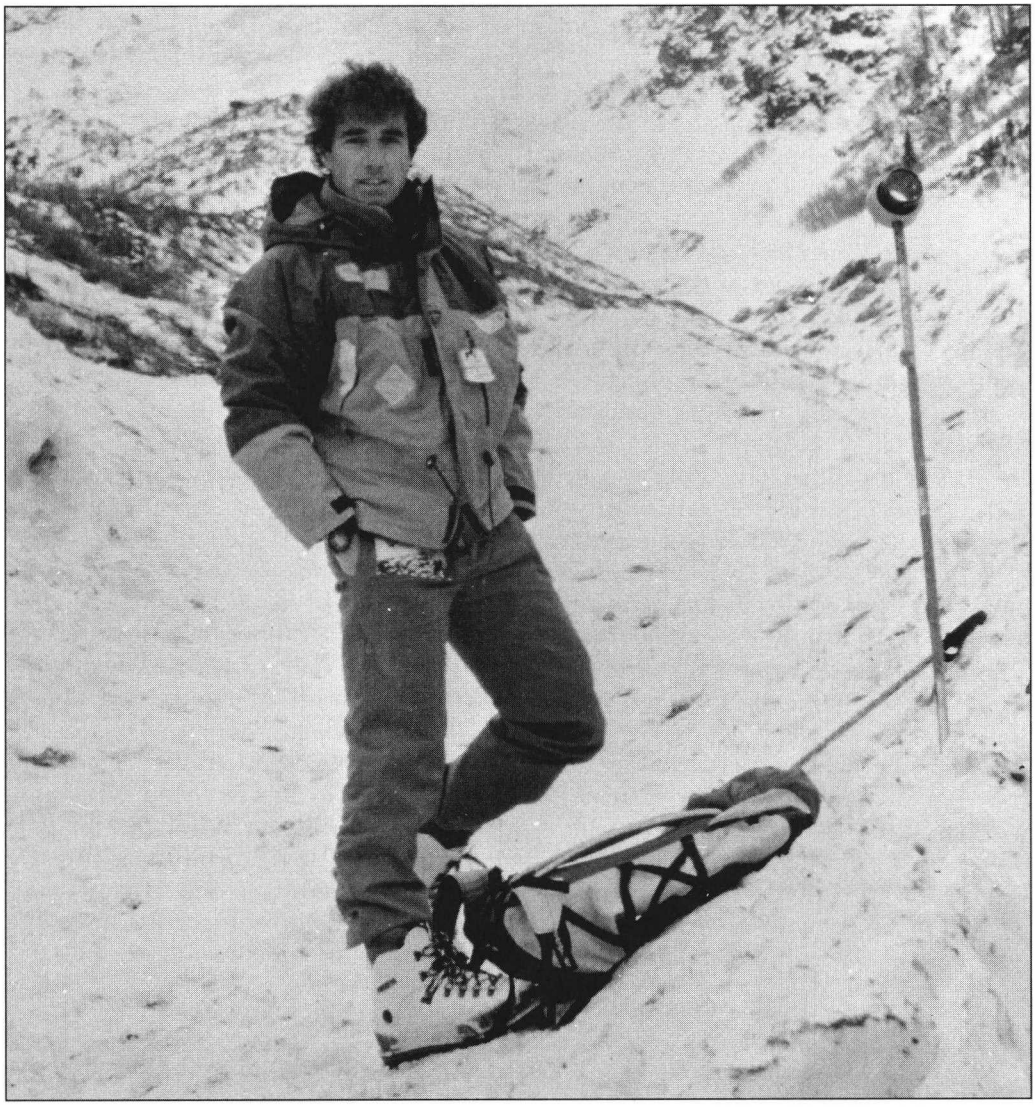

To Pierre Beghin

Several stirring ceremonies were devoted to the alpinist Pierre Beghin and to the numerous feats he accomplished in high mountain, especially in Himalayas where he performed impressive first ascents.
Along these ceremonies, those who didn't know his talents of photograph and author, took the opportunity to discover them. If naturally his eyes turned towards the roof of the World, they also came to rest on the earth of men.

In the same time, Pierre's scientific colleagues wanted to pay homage to Pierre Beghin as an engineer and a researcher. The following biographical note evokes shortly his work.
It is necessary to remind here, once more, that he was a forerunner in the field of multi-phenomena studies. Therefore, it was quite natural and logical to organize a scientific workshop on Rapid Gravitational Movements and to dedicate it to Pierre Beghin.
He would probably have attended it, listening to the presentations with curiosity and discretion, giving his talk with self-effacement and rigour, discussing with the others to share his knowledge and his experience.

Finally, for his collegues at Cemagref and especially at Division Nivologie, Pierre Beghin was not only an engineer, a researcher, a photographer, a writer and an alpinist. When he came back after each expedition, we had a confused feeling of relief to meet him again together with the wrong impression of having been always sure of his return home.
We wished also, as a matter of fact, to remember the fellow worker, the friend who shared with one or another, a meal, an office, a day in the Division Nivologie workshop, in its laboratory, on the field, a bike training, a mountain hike, a present... Along these ordinary days, when meanwhile a part of him was already leaving, or once a year, for a slide projection, Pierre allowed us to take advantage of his personnality and his character, showing, almost against his will, his huge qualities. For a while, we were also, with him, admiring and musing, in the land where oxygen is rare.

Laurent Buisson

Pour Pierre Beghin

Des cérémonies particulièrement émouvantes ont été consacrées à Pierre Beghin, alpiniste de haut niveau, et aux nombreux exploits qu'il avait accomplis en haute montagne, plus particulièrement en Himalaya où il avait réalisé d'impressionantes premières.
Ces cérémonies ont aussi donné à ceux qui ne les connaissaient pas l'occasion de découvrir ses talents de photographe et d'écrivain. Si son regard d'alpiniste portait, bien sûr, jusqu'au toit du monde, il savait aussi, avec une incroyable précision, se poser sur la terre des hommes.

Parallèlement à ces cérémonies, ses collègues scientifiques tenaient à rendre hommage à Pierre Beghin, ingénieur et chercheur. La notice biographique qui suit rappelle brièvement ce que fut son travail.
Il est nécessaire de préciser ici, une fois de plus, qu'il fut un précurseur en matière d'études multi-phénomènes. Organiser un colloque scientifique sur les Mouvements Gravitaires Rapides et le dédier à Pierre Beghin était donc tout naturel. Il aurait sûrement participé à cet atelier, écoutant les communications avec curiosité et discrétion, présentant ses travaux avec modestie et rigueur, discutant avec les uns et les autres de sorte que tous profitent de ses connaissances et de son expérience.

Enfin, pour ses collègues du Cemagref et de la Division Nivologie en particulier, Pierre Beghin n'était pas seulement l'ingénieur, le chercheur, le photographe, l'écrivain et l'alpiniste que nous voyions revenir après chaque expédition avec, au fond de nous, le sentiment mélangé que créaient le soulagement de le retrouver et l'impression, ô combien trompeuse, d'avoir toujours été sûrs de ce retour.
Nous souhaitions aussi, en effet, rappeler le souvenir du compagnon, de l'ami qui partageait, avec les uns ou les autres, un repas, un bureau, des journées à l'atelier, au laboratoire, sur un chantier ou sur le terrain, un entraînement à bicyclette, une course en montagne, un cadeau échangé... Que ce soit au cours de ces journées ordinaires où, toutefois, une part de lui-même était déjà en partance ou bien encore, à l'occasion, une fois l'an, d'une projection de diapositives devenue au fil du temps rituelle, Pierre nous faisait profiter de sa personnalité et de son caractère laissant apparaître, presque malgré lui, ses immenses qualités. L'espace d'un instant, nous étions nous aussi, avec lui, admiratifs et songeurs, au pays de l'oxygène rare.

Laurent Buisson

Pierre Beghin

(Rotterdam 1951 - Annapurna 1992)

Pierre Beghin began his undergraduate studies in l'Ecole des Mines de Saint-Etienne. After getting his engineering degree and his Master of Science, in 1974, he decided to prepare a PhD. He then worked at Institut de Mécanique de Grenoble with Emil Hopfinger as a PhD director. His work was funded and supported by the Division Nivologie which depended on former CTGREF (Centre Technique du Génie Rural, des Eaux et des Forêts). Louis de Crécy who was the head of the Division Nivologie especially helped him. His PhD thesis was mainly dedicated to the gravity currents with an application to "powder" snow avalanches.

After his PhD, he kept on working on powder snow avalanches and logically joined the Division Nivologie of Cemagref in 1981. Since, he has been able to go further on this issue thanks to some experimental devices he designed.

In his research, he put a constant emphasis on the physics of natural phenomena and has always been cautious in front of numerical modelling which were being developped in the eighties.

He has been able to study the fundamental laws of gravity flows in the frame of an international joint research programme on submarine gravity currents. Several Canadian and Norwegian laboratories were associated with Cemagref in this programme. In this context, he got the consideration of some of our colleagues from Université Laval, Norwegian Technical Institute, Atlantic Geoscience Center and of many others. He developed interesting theories concerning the effect of the sedimentation on the flow dynamics.

He always kept contact with snow and, because he was very interested in the physics of the phenomena, he worked on methodological and field studies with some of the consultants of Cemagref. His work made possible the development of computer tools available for practioners.

Along his research work, Pierre Beghin directed numerous students preparing an Engineering Degree or a Master of Science at ENSMHG (Ecole Nationale Supérieure de Mécanique et d'Hydraulique de Grenoble) of INPG (Institut National Polytechnique de Grenoble) or at Université Joseph Fourier.

Gérard Brugnot

Pierre Beghin

(Rotterdam 1951 - Annapurna 1992)

Pierre Beghin a commencé sa carrière dans l'enseignement supérieur en "intégrant" l'Ecole des Mines de Saint-Etienne. En 1974, après avoir obtenu son diplôme d'ingénieur, il a souhaité faire une thèse. Ce travail a été réalisé à l'Institut de Mécanique de Grenoble, sous la direction d'Emil Hopfinger et avec le soutien de ce qui était à l'époque le CTGREF (Centre Technique du Génie Rural, des Eaux et des Forêts), notamment de Louis de Crécy. Le thème fondamental était les courants de gravité, avec, comme application, les avalanches de neige "poudreuse".

Ayant obtenu son diplôme d'ingénieur-docteur, il a continué à travailler sur le thème des avalanches poudreuses, ce qui lui a permis d'être recruté à la Division Nivologie du Cemagref en 1981. A partir de cette époque, il a pu approfondir son sujet de prédilection, grâce notamment à la mise en place de dispositifs de simulation physiques qu'il a conçus lui-même. Son action peut, en effet, être caractérisée par un intérêt constant pour la physique des phénomènes naturels et il a toujours considéré avec une saine méfiance les méthodes numériques qui se sont développées de façon spectaculaire dans les années 80.

Il a pu revenir aux lois fondamentales des écoulements de gravité grâce à un programme portant sur les courants de gravité sous-marins associant le Cemagref à de nombreux laboratoires canadiens et norvégiens. Dans ce cadre, il a non seulement acquis l'estime de nos partenaires de l'Université Laval, du Norwegian Geotechnical Institute, de l'Atlantic Geoscience Center et de bien d'autres encore mais il a produit des développements très intéressants dans le domaine de la prise en compte de l'influence du facteur sédimentation sur la dynamique des écoulements.

Il n'a jamais quitté le domaine de la neige car, toujours sensibilisé par la réalité physique des phénomènes, il a toujours été très heureux de réaliser des études méthodologiques et des études de sites en liaison avec les experts de la Division Nivologie. Ces travaux ont conduit à des programmes informatiques utilisables par les praticiens.

Dans le cadre de ces travaux de recherche, Pierre Beghin a encadré de nombreux étudiants, principalement de l'ENSMHG (Ecole Nationale Supérieure de Mécanique et d'Hydraulique de Grenoble) de l'INPG (Institut National Polytechnique de Grenoble) et des DEA (Diplômes d'Etudes Approfondies) de l'INPG et de l'Université Joseph Fourier.

Gérard Brugnot

Préface

Objectifs de l'atelier

L'Atelier International Pierre Beghin a été organisé à partir de l'idée qu'il était intéressant de rassembler des chercheurs travaillant sur des phénomènes aussi différents que les coulées boueuses, les avalanches de neige, les écroulements rocheux, les coulées de cendres volcaniques et les avalanches sous-marines. Ces phénomènes ont en commun d'être des mouvements gravitaires rapides et d'avoir des comportements non newtoniens.

L'organisation de cet atelier s'inscrit dans le cadre plus général du Programme Mouvements Gravitaires Rapides soutenu à travers le Contrat de Plan Etat-Région Rhône-Alpes. Différents organismes grenoblois sont impliqués dans ce programme. Il s'agit, par exemple, du Cemagref, de l'ADRGT (Association pour le Développement de la Recherche sur les Glissements de Terrain), de l'IRIGM (Institut de Recherche Interdisciplinaire en Géologie et en Mécanique), de la délégation nationale aux actions RTM (Restauration des Terrains en Montagne)... De nombreuses coopérations existent avec d'autres équipes installées ailleurs en France ou dans d'autres pays.

De façon plus précise, les objectifs de cet atelier étaient au nombre de trois :

- Faire le point des travaux existants en matière de mouvements gravitaires rapides.
- Confronter les uns aux autres des spécialistes de différents phénomènes utilisant des techniques différentes.
- Susciter l'organisation d'une communauté internationale de travail sur les mouvements gravitaires rapides.

Organisation et déroulement

La méthodologie de travail retenue a consisté à faire connaître les avancées réalisées par des équipes avec des outils particuliers ou pour certains phénomènes afin que d'autres équipes travaillant sur d'autres phénomènes puissent en tirer profit. L'atelier était donc organisé en sessions centrées chacune autour d'un outil ou d'une approche.

Environ 60 scientifiques (dont cinquante extérieurs au programme Mouvements Gravitaires Rapides) ont été contactés pour intervenir. Les réponses positives ont permis d'atteindre le chiffre de 33 communications dont 8 provenant de membres du programme (Cemagref, ADRGT, IRIGM, RTM). Les scientifiques invités à présenter une communication voyaient leur mission prise en charge par l'atelier.

Environ 50 personnes (sans compter les intervenants) ont assisté en totalité ou en partie à l'atelier, ouvert par une intervention de Philippe Huet, Chef du Département Montagne du Cemagref. L'exposition de logiciels a permis de présenter une demi-douzaine de systèmes.

Une visite sur le terrain dans la vallée de la Romanche a permis aux participants d'observer écroulements rocheux, torrents et sites d'avalanches ainsi que les dispositifs de surveillance et de protection. La curiosité, l'enthousiasme des participants et un solide repas à Bourg d'Oisans ont fait de cette visite un moment fort de l'atelier malgré un véritable "temps de saison" avec vent, pluie et neige.

Une fin d'après-midi a également été consacrée, par le Groupement de Grenoble du Cemagref, à la mémoire de Pierre Beghin. Après une intervention de Raymond Pinoit, Directeur du Groupement, un montage que Pierre Beghin avait préparé avant sa dernière expédition a été projeté en "multi-vision". Un ensemble de panneaux présentait le travail scientifique qu'il avait réalisé ainsi que les activités de ses collègues au Groupement du Cemagref à Grenoble.

Les actes

Les articles sont pour l'essentiel rédigés en anglais. Chaque article dispose d'un titre en anglais et en français. Le titre original du ou des auteurs est présenté en premier. Le titre traduit est imprimé en italique. Les articles sont précédés d'un résumé en anglais et d'un résumé en français. Lorsque ces résumés n'ont pas été écrits par le ou les auteurs de l'article, ils sont imprimés en italique. La traduction des titres et la rédaction éventuelle de résumés complémentaires sont de la responsabilité des coordinateurs, auteurs de la présente préface.
Les articles sont présentés dans l'ordre alphabétique du nom de leur premier auteur. Le sommaire ("contents") présente les articles par leurs titres en français et en anglais.

Perspectives

A l'issue de l'atelier, les collègues canadiens, très présents, ont fait savoir qu'ils étaient prêts à organiser dans deux ans un atelier comparable, probablement en Colombie Britannique. Cet ouvrage n'est donc, probablement que le premier d'une longue série !

Remerciements

Un certain nombres d'organismes, outre le Cemagref, ont apporté leur soutien pour l'organisation de cet atelier. Il s'agit en particulier du Ministère de l'Environnement, plus particulièrement, la Délégation aux Risques Majeurs (DRM), du Pôle Grenoblois d'Etude et de Recherche sur les Risques Naturels (PGRN), de Grenoble-Pôle Européen Universitaire et Scientifique (GPEUS), de la Délégation nationale aux actions de Restauration des Terrains en Montagne ainsi que de son service départemental de l'Isère et de la Région Rhône-Alpes qui, conjointement avec l'Etat, soutient le programme "Mouvements Gravitaires Rapides".
D'autres organismes ont participé à l'organisation de la visite de terrain. Il s'agit de la Direction Départementale de l'Equipement de l'Isère et de la Société d'Aménagement Touristique de l'Alpe d'Huez.

Nos remerciements vont donc d'abord aux responsables des organismes associés au Cemagref qui viennent d'être cités et qui, convaincus de l'intérêt que présentait l'atelier Pierre Beghin ont accepté de soutenir ce projet.
Nous pensons à Jean-Marie Martin, Président de GPEUS, François Gillet, Directeur du PGRN, responsable du programme "Risque Naturel" dans le cadre du contrat de plan Etat-Région et Directeur de GPEUS, Patrick Deblonde de la DRM, Bernard Saillet, délégué national aux actions RTM, Jacques Tailhan de la Direction Départementale

de l'Equipement de l'Isère, Christian Blot et Hervé Lenoire des Subdivisions de l'Equipement de Vizille et de Bourg d'Oisans, Christian Reverbel de la SATA.

Nos remerciements vont également à tous les intervenants qui ont accepté de venir présenter leurs travaux à Grenoble après un voyage parfois très long.

Une assistance nombreuse est venue au Cemagref écouter les différentes interventions. Nous la remercions pour l'intérêt qu'elle a montré et la curiosité dont elle a fait preuve.

La visite de terrain n'aurait pas été possible sans Pierre Antoine de l'IRIGM, Robert Marie de la Délégation nationale aux actions RTM, de Michel Rouvrais du Service départemental RTM de l'Isère, Jean-Marc Daultier de la SATA et M. Rignon de la Subdivision de l'Equipement de Bourg d'Oisans. Nous tenons à les remercier pour leur aide précieuse.

Enfin, de nombreux membres de la Division Nivologie sont intervenus dans l'organisation de l'atelier.
Anne-Marie Uvietta a participé à la préparation du programme, de l'atelier, des actes provisoires. Au cours de l'atelier, elle a assuré en partie la permanence de l'accueil. De plus, elle a été la cheville ouvrière de la constitution définitive des actes qui sont entre vos mains. Qu'elle soit ici remerciée.
Dominique Strazzeri a, elle aussi, participé à la préparation des actes provisoires et à l'accueil des participants ainsi que Françoise Gay qui avait, par ailleurs, la lourde et durable responsabilité de la prise en charge des intervenants. Nous leur savons gré à toutes deux de leur disponibilité.
Vincent Cligniez a su habilement jouer les pompiers volants, intervenant dans la décoration de la salle de conférence, accueillant les participants, reproduisant des actes supplémentaires... Nous l'en remercions.
Pour terminer, nous remercions Gilles Borrel, Fabrice Moutte, Philippe Coussot et Maurice Meunier qui ont accepté de relire ce document afin d'en expurger les fautes d'orthographes et d'en rendre l'anglais plus correct.

Laurent Buisson et Gérard Brugnot

Preface

Aims of the workshop

The Pierre Beghin International Workshop aimed to gather researchers working on quite different phenomena such as mud flows, snow avalanches, rock avalanches, pyroclastic flows and submarine avalanches. As a matter of fact, these phenomena are rapid gravitational movements.
The organisation of this Workshop takes place in the framework of the Rapid Gravitational Movements Programme funded by the State-Region Planning Contract in Rhône-Alpes.
Different teams in Grenoble are involved in this Programme : there are, for instance, Cemagref, ADRGT (Association pour le Développement de la Recherche sur les Glissements de terrain), IRIGM (Institut de Recherche Interdisciplinaire en Géologie et Mécanique), Délégation nationale aux actions RTM (Restauration des Terrains en Montagne). Numerous cooperation actions exist with other teams in France and abroad.
This workshop had three identified targets :

- Provide a survey of existing works in the area of Rapid Gravitational Movements ;
- Gather specialists of different phenomena working with different techniques ;
- Promote the structuration of an international working community in the area of Rapid Gravitational Movements.

Organization and programme

The working methodology consisted in the presentation of advanced progress produced in one particular team with specific tools for peculiar phenomena in order to allow other teams to take advantage of this experience while working on different phenomena. For this reason, the workshop was organised with several sessions centered on one tool or one approach.
About 60 scientists, whose 50 were not already in the Rapid Gravitational Movements Programme, were invited to present a paper. 33 communications, including 8 from teams participating in the RGM Programme (Cemagref, ADRGT, IRIGM, RTM) were presented. Their travel expanses were to be paid by the Workshop organisation.
90 persons attended the workshop totally or partly. It was opened by a talk given by Philippe Huet, Head of Mountain Department. A software exibition gave the opportunity to present 6 systems.
During a field trip in the Romanche Valley, the attenders observed landslides, torrents and avalanche paths as well as monitoring and protection systems. Their curiosity and enthousiasm as well as a good meal in Bourg d'Oisans made this visit a good time during the workshop in spite of a windy, rainy and snowy winter weather.
Half an afternoon was dedicated by Cemagref Grenoble to the memory of Pierre Beghin. After a talk given by Raymond Pinoit, Head of Cemagref Grenoble, a multi-screen slides-projection prepared by Pierre Beghin before his last expedition was

shown. Posters presented the scientific work he had accomplished on the activities of his colleagues in Cemagref Grenoble.

The proceedings

The papers are mostly written in English. Each paper has a title and an abstract in English and in French. If these titles or these abstracts have not been written by the author(s) of the paper, they are printed in italic. The translation of titles and writing of abstracts, when required, were made by the coordinators, authors of this preface.
The papers are ordered by the first author name. The contents ("sommaire") lists the papers with their English and French titles.

Future

At the end of the workshop, Canadian colleagues, well represented, let us know that they were ready to organise an equivalent workshop in British Columbia. These proceedings should probably be the first of a long serie.

Acknowledgements

A few organisations, besides Cemagref, helped in the arranging of this workshop : Ministère de l'Environnement, and especially Délégation aux Risques Majeurs (DRM) Pôle Grenoblois d'Etude et de Recherche sur les Risques Naturels (PGRN), Grenoble Pôle Européen Universitaire et Scientifique (GPEUS), Délégation nationale aux actions de Restauration des Terrains en Montagne as well as its service départemental de l'Isère and Région Rhône-Alpes which, with the French Government, supports the "Rapid Gravitational Mass Movements" Programme.
Others organisations helped in the field trip preparation : Direction Départementale de l'Equipement de l'Isère and Société d'Aménagement Touristique de l'Alpe d'Huez.

We would like to thank the managers of these organisations, associated with Cemagref, which have just been listed. Convinced by the interest presented by the Pierre Beghin Workshop, they accepted to support it : Jean-Marie Martin, Président of GPEUS, François Gillet, Head of PGRN, responsible for the "Natural Hazard" Programme in Rhône-Alpes Région and Head of GPEUS; Patrick Deblonde, of DRM, Bernard Saillet, Délégué National aux Actions RTM, Jacques Tailhan, of DDE in Isère, Christian Blot et Hervé Lenoire, of the Subdivisions de l'Equipement in Vizille and Bourg d'Oisans, Christian Reverbel, of SATA.

We also thank all the people who gave a talk in Grenoble after, sometimes, a very long travel.

A large audience came in Cemagref to attend the Workshop. We thank it for its interest and curiosity.

The field trip would not have been possible without Pierre Antoine of IRIGM, Robert Marie of Délégation nationale aux actions RTM, Michel Rouvrais of Service départemental RTM de l'Isère, Jean-Marc Daultier, of SATA and Mr. Rignon, of Subdivision de l'Equipement in Bourg d'Oisans. We want to thank them for their useful help.

Finally, many membres of Division Nivologie helped in the organization of the Workshop.
Anne-Marie Uvietta, took part in the preparation of the programme, the workshop and the provisional version of the proceedings. During the workshop, she welcomed the participants. Moreover she was the king pin of the present proceedings preparation. Thank you, Anne-Marie.
Dominique Strazzeri also took part in the preparation of the provisional proceedings and in welcoming the audience as well as Françoise Gay, who was responsible for the travel expenses payment. This was a heavy task and... durable too.
Vincent Cligniez could play the "flying fireman", setting panels in the conference room, welcoming those taking part in workshop, copying new provisional proceedings... Thank you, Vincent.
To conclude we thank Gilles Borrel, Fabrice Moutte, Philippe Coussot and Maurice Meunier who accepted to read these lines in order to correct them and to improve the english.

Laurent Buisson and Gérard Brugnot

Sommaire / Contents

Programme de l'atelier / Programme of the workshop

Dimanche 5 décembre / Sunday, December 5

17:00	20:00	**Accueil à l'Hôtel ATRIA / Welcome at ATRIA Hôtel**

Lundi 6 décembre / Monday, December 6

8:00	9:30	**Accueil, enregistrement, ouverture de l'atelier** **Welcome, registration and opening of the workshop**
9:30	10:30	**Session "Présentation et classification des phenomènes I"** **Session "Presentation and classification of the phenomena I"** M. Meunier (Cemagref, Grenoble, France) *Classification of torrential flows.* J. Hutchinson (Imperial College, London, UK) *Types of rapid gravitational subaerial mass movements and some possible mechanisms.*
10:30	11:00	**Pause / Break**
11:00	12:00	**Session "Présentation et classification des phenomènes II"** **Session "Presentation and classification of the phenomena II"** O. Marco (Cemagref, Grenoble, France) *Snow Avalanches : classification and modelisation.* J. Locat (Université Laval, Québec, Canada) *Fra fell til fjord : Considerations on viscous flows.*
12:00	14:00	**Repas / Lunch**
14:00	15:30	**Session "Observations de terrain I" / "Field obsevations I"** S. Evans (Geol. Survey. Can., Ottawa, Canada) *The field documentation of highly mobile rock and debris avalanches in the Canadian Cordillera.*

J.-C. Thouret (Université Blaise Pascal, Clermont-Ferrand, France), J. Vandemeulebrouck (Université de Savoie, Chambéry, France), J.C. Komorowski (UNAM, Mexico)
Volcano-glacier interactions : field survey, remote sensing and modelling. Case study : Nevado del Ruiz, Colombia.

A. von Poschinger (Bayerisches Geologisches Landesamt, München, Germany)
Rapid Mass Movements in the Bavarian Alps and some Special Aspects of their "Impact" on the Valley Floor.

15:30 16:00 Pause / Break

16:00 17:30 Session "Observations de terrain II" / "Field observations II"

C. Ravenne and C. Ponsot (IFP, Rueil-Malmaison, France)
Gravitational Mass Movements and Resedimentation in Applied and Fundamental Geology.

H. Lee (USGS, Menlo Park, USA)
Evidence of Rapid Gravitational Mass Movement on the Submerged Flanks of the Hawaiian Islands.

19:30 22:00 Banquet de l'Atelier à l'Hôtel ATRIA
Workshop Dinner at ATRIA Hotel

Mardi 7 décembre / Tuesday, December 7

8:30 9:30 Session "Initiation du mouvement" / "Movement initiation"

P. Evesque (Ecole Centrale de Paris, Chatenay-Malabry, France)
Can we define a unique friction coefficient for a non cohesive granular material ? A temptative answer from the point of view of sand avalanche experiments.

J.A. Gili (UPC, Barcelona, Spain)
Contribution to the study of mass movements : mudflow slides and block fall simulations.

9:30 10:00 Pause / Break

10:00 12:00 Session "Modélisation I" / "Modelling I"

P. Coussot (Cemagref, Grenoble, France)

Wall shear stress of channelized debris flows deduced from rheological measurements.

N. Maeno (Institut for Low Temperature Science, Sapporo, Japan)
Rheological Characteristics of Snow Flows.

H. Norem (NGI, Oslo, Norway)
Ideas on a phase diagram for granular materials.

K. Sassa (Kyoto University, Japan)
Prediction of Landslide Motion ; Measurements of the apparent friction angle under undrained loading condition and the computer simulation based on it.

12:00 14:00 Repas / Lunch

14:00 15:00 Session "Outils informatiques pour les ingénieurs"
Session "Software tools for the engineers"

L. Buisson and C. Charlier (Cemagref, Grenoble, France)
Avalanche modelling and integration of expert knowledge in the ELSA system.

R.M. Faure (ENTPE, Vaulx-en-Velin, France)
Computer tools for risk management of slopes ; the XPENT system for slope stability analysis.

15:00 15:30 Pause / Break

15:30 17:00 Session "Modélisation II" / Session "Modelling II"

F. Hermann (ETH, Zürich, Switzerland), D. Issler (IFENA, Davos, Switzerland) and S. Keller (ETH, Zürich, Switzerland)
Numerical Simulations of Powder-Snow Avalanches and Laboratory Experiments on Turbidity Currents.

P. Sampl (AVL, Graz, Austria)
Current Status of the AVL Avalanche Simulation Model - Numerical Simulation of Dry Snow Avalanches.

P. Sampl (AVL, Graz, Austria) and H. Schaffhauser (Institut für Lawinenkunde, Innsbruck, Austria)
Simulation of powder avalanches by FIRE ; Verification of results on example of Wolfsgruben avalanche (march 1988), in St Anton, Tyrol, Austria.

17:00 19:30 **Exposition d'outils informatiques, projection d'un film de l'IFP sur les courants de gravité et cocktail**
Exhibition of software tools, projection of an IFP movie on gravity deposits and cocktail

Mercredi 8 décembre / Wednesday, December 8

8:00 19:00 **Visite de terrain "Risques naturels dans la vallée de la Romanche"**
Field trip "Natural Hazards in Romanche Valley"

Jeudi 9 décembre / Thursday, December 9

9:00 10:00 **Session "Modélisation III" / Session "Modelling III"**

P.Y. Julien and J. O'Brien (Colorado State University, Fort Collins, USA)
Rheology and modeling of mass movements deposits.

D. Takahashi (Kyoto University, Japan)
Fluid Mechanical Modelling of the Viscous Debris Flow.

10:00 10:30 **Pause / Break**

10:30 11:30 **Session "Modélisation IV" / Session "Modelling IV"**

D. Laigle and P. Coussot (Cemagref, Grenoble, France)
Numerical modelling of debris flow dynamics.

D. Rickenmann (IFRF, Birmensdorf, Switzerland)
Estimating debris flow parameters.

A. Kalinin (Lomonossov University, Moscou, Russia)
Seismic mapping of gravitational mass movements on the shelfs and continental margins.

12:00 14:00 Repas / Lunch

14:00 15:30 Session "Modélisation V" / Session "Modelling V"

O. Hungr (Thurber Engineering Ltd, Vancouver, Canada)
Mass-referenced flow model for dynamic analysis of flow slides and avalanches.

J. Syvitski and J.M. Alcott (Bedford Institute of Oceanography, Dartmouth, Canada)
Numerical simulation of basin sedimentation affected by slope failure and debris flow runout.

T. Davies (Lincoln College, Canterbury, New-Zealand)
Models for disastrous mass movements.

15:30 16:00 Pause / Break

16:00 19:00 Multi-vision sur Pierre Beghin, alpiniste, présentation des actions du Cemagref de Grenoble and cocktail
Multi-screen projection on Pierre Beghin, alpinist, presentation of the actions of Cemagref-Grenoble and cocktail

Vendredi 10 décembre / Friday, december 10

8:30 9:30 Session "Instrumentation"

H. Gubler (IFENA, Davos, Switzerland)
Dense Flow Avalanches, a Discussion of Experimental Results and Basic Processes.

M. Gay (Cemagref, Grenoble, France)
Sound wave propagation measurements in snow flows.

9:30 10:30 Pause / Break

10:30 12:00 Session des praticiens "Retour au terrain"
Practitionners session "Back to the field"

P. Antoine (IRIGM, Grenoble France)
Réflexions sur les conditions de déclenchement de mouvements gravitaires rapides sur les versants montagneux.

C. Azimi and P. Desvarreux (ADRGT, Gières, France)
Certains aspects dynamiques des mouvements de terrain.

R. Marie (RTM, Grenoble, France)
Le praticien RTM est-il un médecin généraliste ?

12:00	**14:00**	**Repas / Lunch**
14:00	**16:00**	**Session plénière / Plenary session**
16:00		**Fin de l'atelier / End of the workshop**

Réflexions sur les conditions de déclenchement de mouvements gravitaires rapides sur les versants montagneux

Discussion on initiation conditions of rapid gravitational movements on mountain slopes

P. ANTOINE

IRIGM
BP 53 X, 38041 Grenoble Cedex - France
Tel. (33) 76 51 49 82 - Fax (33) 76 51 49 00

Résumé

Après une description des conditions d'apparition de mouvements gravitaires rapides géologiques, cet article détaille les contextes favorables à cette apparition en présentant un certain nombre d'exemples. La présence de masses de roche cohérente, homogène, peu déformable et sur de fortes épaisseurs est très souvent vérifiée. L'existence d'une forte pente trouve fréquemment son origine dans l'action des glaciers. La position de cette masse dans le versant joue un rôle déterminant dans la propagation du phénomène.
Les causes possibles de déclenchement sont ensuite passées en revue, avec notamment les séismes et l'eau. Les situations de rupture progressive et de rupture différée sont également présentées.
L'article se termine par l'évolution de l'origine du glissement de Val Pola et par la description des problèmes qu'il faut résoudre avant de poursuivre les tentatives de modélisation,

Abstract

After a description of the possible conditions of initiation of geological rapid gravitational movements, this paper gives a few examples of such movements and presents the context in which they can occur.
A mass of cohesive homogeneous rock on a large depth is often encountered. Steep slopes are frequently created by glacier erosion. The relative position of this mass in the slope can determine the nature of the phenomenon propagation.
The main potential causes are then listed : earthquakes, water... Progressive and delayed rupture situations are also described.
At last, the paper considers the origin of the Val Pola rock avalanche and reviews problems which to be solved before going on modelling.

Introduction

Le qualificatif de mouvement gravitaire rapide recouvre en fait globalement un ensemble de phénomènes de causalités différentes dont les effets s'enchaînent plus ou moins rapidement dans le temps. Dans une première phase il s'agit essentiellement d'une évolution plus ou moins rapide vers la rupture, de la déformation gravitaire du versant. Une seconde phase correspond alors à la déformation et au déplacement post-rupture ce dernier représentant en fait la véritable menace lorsque l'on se place d'un point de vue de sécurité civile.

Pour préciser cette dernière il est séduisant d'envisager une modélisation du phénomène. Celle-ci doit-elle nécessairement prendre en compte les deux phases du phénomène, puisque, pratiquement, il paraît *a priori* suffisant de limiter la modélisation à la phase terminale de propagation? Il est,pour l'instant, difficile de répondre à cette question, le lien susceptible d'exister entre les modalités de la première phase du phénomène et le développement de la seconde n'étant pas évident (s'il existe). La présente communication vise simplement à établir quelques unes des conditions naturelles qui peuvent orienter un mouvement de versant vers une évolution rapide et à souligner les difficultés susceptibles de contrarier l'intention de modélisation. Nous nous limiterons, dans cet examen, au cas des versants de grande ampleur (au sens du colloque de Nainville-les-Roches c'est-à-dire supérieurs, en volume, au million de m^3). Ceux-ci sont essentiellement constitués de roches variées, organisés selon une structure géologique héritée de l'histoire tectonique locale. Dans cette hypothèse, nous écartons de l'analyse les chutes de blocs isolées ainsi que les coulées et laves torrentielles.

Conditions d'apparition des mouvements gravitaires rapides

L. Rochet a clairement résumé les conditions principales qui conduisent à l'apparition d'un mouvement gravitaire rapide. Il faut, tout d'abord, disposer d'une pente forte (disons, pour fixer les idées, supérieure à 40°) laquelle ne peut se rencontrer que dans un massif de roches de forte cohésion et de faible déformabilité intrinsèque. Pour que le mouvement ait lieu, il faut généralement qu'une action préliminaire (altération physico-chimique par exemple) vienne diminuer fortement, voire annuler cette cohésion. La résistance aux actions de cisaillement sous l'effet principal des forces de gravité est alors assurée par le seul frottement. Selon les conditions morphologiques et géologiques locales, il peut alors se faire que l'énergie potentielle disponible soit hors de proportion avec la résistance ultime du massif. La rupture sera alors brutale et, la déformation de la masse rocheuse n'en absorbant qu'une très faible part, le gros de cette énergie potentielle se transformera alors en énergie cinétique. Dans certains cas des énergies autres que celles dues à la gravité pourront ajouter leurs effets, en cas de secousse sismique par exemple.

Quelques contextes favorables à l'apparition de mouvements gravitaires rapides

L'analyse précédente permet de cerner (exemples réels à l'appui) les principales conditions géologiques et morphologiques qui vont favoriser ce type de mouvement.

Remarquons toutefois que les exemples utilisables ne peuvent être fournis que par des mouvements dont l'homme a été le témoin et bien souvent la victime. Les chaînes de montagnes comme les Alpes abondent en mouvement de versants très importants mais trop anciens pour avoir été observés et rapportés; c'est le cas de tous les mouvements post-glaciaires.
Pour nous limiter aux Alpes françaises nous citerons les écroulements du *Mont-Granier (1248)*, du *Claps de Luc (1442)*,de *Clavans (1418)*, du *Dérochoir (1751)*, et, plus près de Grenoble, des mouvements récents mais de moindre ampleur comme ceux de *Charmonétier* près de Bourg-d'Oisans (1987) et du *Ruisseau Blanc* dans la vallée de l'Eau d'Olle (1989)- Giraud et al.(1990)
Tous ces mouvements ont affecté soit des calcaires massifs soit des roches granitiques ou des schistes cristallins. Ceci confirme bien que les mouvements gravitaires rapides apparaissent préférentiellement dans des massifs de roches très cohérentes, homogènes sur de fortes épaisseurs et peu déformables; la rupture peut alors être matricielle (au sein du massif rocheux) ou bien se produire au long d'une discontinuité préexistante.
Les exemples cités correspondent tous (sauf le *Claps de Luc*) à des vallées alpines ayant subi l'action des puissants glaciers rissiens et würmiens. Cette action est bien connue, Antoine (1992) : l'érosion glaciaire raidit considérablement les versants dans les roches très cohérentes et la disparition du glacier met à nu une morphologie caractérisée par des pentes abruptes pouvant atteindre des valeurs comprises en 45° et la verticale. On admet couramment que l'évolution vers la rupture de la plupart des versants, dans les régions alpines englacées au quaternaire, a débuté avec la fonte des glaciers il y a de douze à quinze mille ans.
L'exemple du *Claps de Luc* montre qu'en matière d'instabilité, la raideur des pentes topographiques peut céder le pas à celle du pendage des couches sédimentaires. Au *Claps*, celui-ci varie de 42° à la partie haute du versant à 28° au niveau de la rivière *(La Drôme)* - Ramirez et al. (1988)
Un facteur extrêmement important de rapidité de l'évolution post-rupture est la position dans le versant de la base de la masse mobilisable (ou mobilisée); lorsque celle-ci est "perchée", c'est à dire située à une hauteur relativement importante au-dessus du fond de la vallée, la propagation sera évidemment extrêmement rapide comme cela fut au *Val Pola* en Italie (1987) où la dénivellation atteignait 700 m environ. Un effet de souffle peut alors être attendu en fin de propagation. C'est ce qui fait toute la différence entre les mouvements (potentiels pour l'instant) de *Séchilienne* (la base de la masse mobilisable domine d'environ 250 m le fond de la vallée) et de *La Clapière* où la surface de glissement du mouvement principal est au niveau de la rivière *(La Tinée)*.

Les causes possibles de déclenchement

La connaissance exacte des causes de déclenchement des mouvements de versants reste la plupart du temps très hypothétique. Seuls les séismes peuvent être invoqués avec certitude quand il y a coïncidence entre les deux phénomènes - Durville (1992). Cette cause ne peut être invoquée dans aucun des exemple français rappelés ci-dessus.
L'action de l'eau est le plus souvent retenue par les auteurs. Les forces hydrauliques mises en jeu sont en effet d'un ordre de grandeur comparable à celui des forces

gravitaires qui affectent l'équilibre naturel des massifs superficiels. Ceci explique que les pressions interstitielles et les pressions d'écoulement jouent un rôle déterminant dans la stabilité des massifs - Rochet (1983). Nous disposons actuellement de suffisamment de mesures sur des sites différents pour vérifier que, sur la quasi-totalité des mouvements instrumentés, l'évolution des vitesses de déplacement est sous la dépendance des facteurs climatiques. L'examen détaillé des courbes de pluviométrie et de vitesses en fonction du temps apporte généralement beaucoup à la compréhension de la réponse du massif rocheux aux fluctuations des niveaux d'eau qu'il contient. Ainsi, à *La Clapière*, des pics de vitesses très prononcés apparaissent parfois après un pic de précipitation, la vitesse chutant toutefois très vite après son maximum. Cela signifie qu'à une augmentation très rapide de pression, le massif a répondu par un déplacement, mais que ce dernier a eu pour effet de faire chuter très vite cette pression, provoquant une diminution rapide des vitesses. Un tel style de variation ne se comprend bien que si l'on a affaire à un milieu très perméable, bien délimité (et de volume relativement restreint), une zone de fracture par exemple. On conçoit bien que, si les conditions s'y prêtaient, cela pourrait dégénérer en une rupture généralisée.

D'autres causes de déclenchement sont moins bien définies et touchent au mécanisme même de la rupture. L'approximation couramment faite dans les calculs de stabilité de l'apparition instantanée d'une surface de rupture surlaquelle la distribution des contraintes est homogène, ne correspond généralement pas à la réalité. Dans les phénomènes naturels *la rupture progressive* ou *la rupture différée* sont des manifestations sans aucun doute beaucoup plus fréquentes.

La *rupture progressive* est probablement la règle dans les massifs de roche homogènes, parcourus par un réseau plus ou moins dense de discontinuités. L'extension individuelle de celles-ci est généralement trop faible à l'échelle du versant pour fournir une surface de rupture adéquate. Par contre, la présence de familles de fractures discontinues, d'orientation défavorable (plus ou moins parallèles à la pente topographique et recoupées par des fractures verticales, comme à Séchilienne par exemple), facilite la déformation du massif laquelle s'accompagne d'un phénomène de dilatance. La résistance au cisaillement est alors assurée, pour l'essentiel, par les ponts de matière subsistant entre les diverses discontinuités ou par l'intrication des blocs constituant le massif (ou de certains d'entre eux). Leur réarrangement et les ruptures successives des ponts de matière peuvent conduire à l'individualisation progressive d'une surface de rupture. Elle est bien difficile à mettre en évidence et sa géométrie ne peut être prévue *a priori*.

L'auscultation sismo-acoustique peut semble-t-il trahir l'approche d'une telle rupture, comme cela a été le cas lors de la seconde partie de l'écroulement de Randa en Suisse - C. Bonnard communication orale. Une tentative de ce genre est actuellement en cours à *Séchilienne*.

Une conséquence importante de la rupture progressive, à laquelle on ne pense peut-être pas suffisamment, est qu'un développement, somme toute limité, de la surface de rupture peut conduire à un accroissement très important de la masse mobilisable. L'énergie potentielle disponible peut alors dépasser très rapidement le seuil nécessaire pour la rupture par cisaillement et le déclenchement de la chute peut

apparaître très brutal. Cette apparence est trompeuse car la phase préparatoire (rupture progressive) a pu être très longue et passer inaperçue.
La *rupture différée* correspond à un autre type de phénomène dont l'occurence est très probable dans les massifs rocheux superficiels soumis à des actions gravitaires. Il a été mis en évidence expérimentalement, qu'un fluage maintenu pendant un certain temps sous une contrainte constante et à une valeur inférieure (de 80% par exemple) à la limite de rupture peut entraîner soudainement cette dernière - Goguel (1983). Ce type de rupture est tout à fait envisageable dans les massifs rocheux. Il reste pour l'instant très difficile à interpréter et marque probablement l'aboutissement d'un processus d'évolution lente (parfaitement envisageable à l'échelle de temps géologique) dont le mécanisme nous échappe.
On admet de plus en plus,sans en avoir de preuve (bien difficile, il est vrai, à obtenir) que des phénomènes que l'on peut qualifier de "vieillissement" se produisent certainement au sein des versants soumis depuis 10 à 15 000 ans à des déformations gravitaires. Les aspérités qui fournissent l'essentiel de la résistance au cisaillement s'altérent, s'épauffrent, et peuvent finir par céder après des déplacements, somme toute minimes, et très lents, d'où la soudaineté apparente de la rupture.
Le cas des roches sédimentaires est un peu différent puisqu'il existe en leur sein les surfaces de discontinuité très privilégiées que représentent les limites de couches. Leur extension peut être très facilement à l'échelle du versant et provoquer le mouvement de masses tout à fait considérables. Le meilleur exemple récent est fourni par la rupture en 1963 du versant Nord du *Mont-Toc (Longarone)* qui a mobilisé près de 300 millions de m^3 de roches calcaires litées.
Outre les raisons invoquées plus haut (séismes, fluctuations des pressions interstitielles), la question se pose de savoir s'il n'existe pas des facteurs minorants de la résistance au glissement couche sur couche. Dans le cas des terrains sédimentaires plissés il est connu que l'inévitable glissement des strates les unes par rapport aux autres durant le plissement, en raison des différences de courbure à l'extrados et à l'intrados du pli, peut fortement diminuer les caractéristiques au long de certains interstrates voire les amener au stade résiduel. La circulation de l'eau sur les limites de couches de perméabilités très différentes peut conduire à une altération qui changera peu à peu les caractéristiques mécaniques et pourra effacer la cohésion (décarbonatation par exemple) au long de surfaces très étendues. De telles actions peuvent expliquer des ruptures au long de pentes très faibles comme l'on en observe dans les argiles litées du Trièves par exemple.

Conclusion

Nous venons d'évoquer quelques unes des causes d'incertitude qui affectent la connaissance des mécanismes de déclenchement de la rupture au sein de massifs rocheux fracturés, homogènes ou stratifiés. Toutefois, à trop vouloir présenter objectivement des faits, l'on perd parfois de vue leur enchaînement et leurs interactions (dont nous ignorons sans doute bon nombre d'entre elles).
Pour ce qui est de la rupture par exemple, Durville (1992) a insisté sur le fait que les mouvements de grande ampleur passaient fréquemment durant leur évolution

temporelle d'un comportement mécanique à un autre. Deux types d'évolution peuvent se rencontrer:

• une masse stable évolue vers la rupture laquelle survient lorsque certains seuils sont franchis,

• un certain régime de mouvement s'installe et une divergence catastrophique se manifeste pour des raisons qui restent la plupart du temps hypothétiques.

Dans ce dernier cas, on est généralement dans l'incapacité de déterminer si la transition d'un régime à l'autre aura lieu et encore moins d'en prévoir la date.

L'écroulement catastrophique du *Val Pola* illustre parfaitement cela. Il s'agissait d'une rupture ancienne (très vraisemblablement "post-glaciaire"), stabilisée, ainsi qu'en attestent tous les caractères morphologiques observables sur les photographies aériennes antérieures à la catastrophe. Bien que cette partie du versant n'ait pas été auscultée auparavant, il est très probable que sa déformation fut minime pendant des siècles, voire des millénaires. Qu'est-ce qui a provoqué la divergence soudaine de 1987 conduisant à une évolution gravitaire extrêmement rapide ? Est-ce l'approfondissement post-glaciaire de la vallée, ou bien l'entaille érosive provoquée par les fortes pluies des semaines précédentes, ou tout simplement l'élévation anormale des pressions interstitielles qui en est résultée? Dans ce cas, le glissement réactivé étant très ancien, avait vraisemblablement dû subir quelques fois au cours des derniers millénaires des précipitations aussi importantes sans dommage.

Tout ceci montre bien que beaucoup de progrès restent encore à faire sur le plan théorique et dans de mutiples domaines touchant à la mécanique, à la géologie, à l'hydrologie, à l'hydraulique souterraine avant de pouvoir envisager une modélisation de tels phénomènes qui soit autre chose qu'un jeu de l'esprit.

Bibliographie

Antoine P. (1992) - Les problèmes posés par l'instabilité des versants de grande ampleur, Bull. AIGI, n° 45, pp.7-22.

Durville J.L. (1992) - Mécanismes et modèles de comportement des grands mouvements de versants, Bull. AIGI, n° 45, pp.23-40.

Giraud A., Rochet L., Antoine P. (1990) - Processes of slope failure in cristallophyllian formations, Engineering geology, 29, pp.241-253.

Goguel J. (1983) - Etude mécanique des déformations géologiques, BRGM, Manuels et méthodes n° 6, 193 p.

Ramirez A., Fabre D., Antoine P. (1988) - Enseignements tirés de deux écroulements couche sur couche en terrain calcaire, C.R. 5e Symp. Internat. Glissements de terrains, Lausanne, Balkema, pp.1359-1362.

Rochet L. (1983) - De la géologie aux propriétés mécaniques des terrains, E.N.P.C., Paris, Journées d'études "Grands travaux et Géologie", 13p.

Certains aspects dynamiques des mouvements de terrains

On few dynamical aspects of mass movements

C. AZIMI, P. DESVARREUX

A.D.R.G.T.
2, rue de la Condamine - Z.I. de Mayencin - BP 17
38610 Gières - France
Tel. (33) 76.44.17.55 - Fax (33) 76.44.20.18

Résumé

Après une description des différents états par lesquels passe un mouvement de terrain et l'exposé des deux questions principales concernant le moment et l'extension spatiale du mouvement, cet article détaille quatre exemples de mouvements gravitaires rapides. Pour chacun d'entre eux, il présente les différents outils utilisés pour surveiller le mouvement et pour protéger des équipements : relevés topographiques, piezomètres, pluviomètres et programmes de simulation de chutes de blocs. En conclusion, l'article recense les situations pour lesquelles existent des solutions pour la prévision et les difficultés principales.

Abstract

After a description of the different stages of a land movement and the presentation of the two basic questions concerning the time and the spatial extension of the movement, this paper deals with four examples of rapid mass movements. For each of them, it presents the different tools used to monitor the movement or to protect facilities : periodical topographical survey, piezometers, pluviometers and rock fall simulation programs. In conclusion, the paper reviews the situations for which solutions exist for the prevision along with the main difficulties.

Introduction

Particularités dynamiques des mouvements de sol

Un mouvement de terrain est un phénomène géologique qui évolue dans le temps. Quel que soit le matériau concerné *(sol ou roche)*, on peut distinguer 3 états, sur le plan cinématique *(voir fig. 1)*, qu'on peut rapprocher, par analogie, des divers stades de fluage mis en évidence sur échantillons [1].

L'état 1 correspond à la stabilité : toute nouvelle application de contrainte provoque alors une déformation instantanée. Il peut y avoir également une déformation différée mais celle-ci ralentit très vite *("fluage" primaire)*.

1 Pour cette raison, nous parlons ici de "fluage".

L'état 2 correspond à des mouvements à vitesse pratiquement constante, en général faible (quelques mm à quelques cm/an) qui peuvent durer très longtemps *(10 à 50 ans)* ou moins *(2 à 3 ans)* dans le cas de certains éboulements. Si la contrainte varie *(par exemple variation de pression interstitielle)*, la vitesse de déplacement varie aussi, mais on reste dans le même type de comportement, qui est celui du "fluage" secondaire. En particulier si les contraintes diminuent en deçà de la "limite de fluage", les mouvements s'arrêtent. En ce sens, tant qu'on est dans ce type de comportement, on peut considérer les mouvements de terrains comme un phénomène reversible, du point de vue de leur vitesse.
L'état 3 correspond à une accélération continue sous contrainte constante menant à la rupture 4. On atteint de très grandes vitesses et on peut avoir de grands déplacements. Cette accélération est très différente de celles qui peuvent se produire en phase 2. Elle correspond au "fluage tertiaire", lequel représente l'évolution ultime du fluage secondaire, la contrainte restant constante. Dans ce type de comportement, on considère les mouvements comme irréversibles.
Au cours des phases 3 et 4 les matériaux subissent une redistribution des masses qui conduit à un nouvel état de stabilité 5.
Devant un phénomène de mouvement de terrain, si on est confronté à des impératifs de gestion de la sécurité, les deux questions capitales auxquelles on doit s'efforcer de répondre sont :

- comment le phénomène peut-il évoluer dans le temps ?
- comment le phénomène peut-il s'étendre spatialement ?

La réponse à la première question est parfois tellement délicate qu'on se contente de chercher à répondre à la deuxième. C'est le cas des menaces de chutes de blocs et d'éboulements.
Compte tenu de ce qui précède, on doit distinguer 2 types très différents de phénomènes de mouvements de terrains :

- ceux dont la vitesse dépend des conditions hydrauliques[1],
- ceux dont la vitesse ne dépend pas des conditions hydrauliques.

Dans la suite nous allons illustrer par quelques exemples pris dans chacun des deux types de phénomènes comment on a pu chercher à répondre aux questions capitales ci-dessus.

Exemple du glissement de LEAZ (Ain)

Localisation - Circonstances

Ce glissement de terrain naturel domine la retenue de GENISSIAT sur le Rhône. Il était connu dès 1934 avant établissement de la retenue, mais n'avait pas fait l'objet d'études particulières. A partir de 1964, suite à une réactivation des mouvements, une surveillance a été progressivement mise en place, parallèlement avec des reconnaissances géologiques classiques. Le but de ces études était de préciser le volume

[1] On exclut du sujet de cet article les mouvements liés à des sollicitations dynamiques rapides (séismes).

en mouvement, le rôle éventuel de la retenue dans ces mouvements, de prévoir dans quelles conditions des masses importantes de matériaux pourraient arriver dans la retenue et à quelles vitesses *(ceci dans le but d'apprécier les conséquences du phénomène et en particulier les caractéristiques de l'onde hydraulique engendrée).*

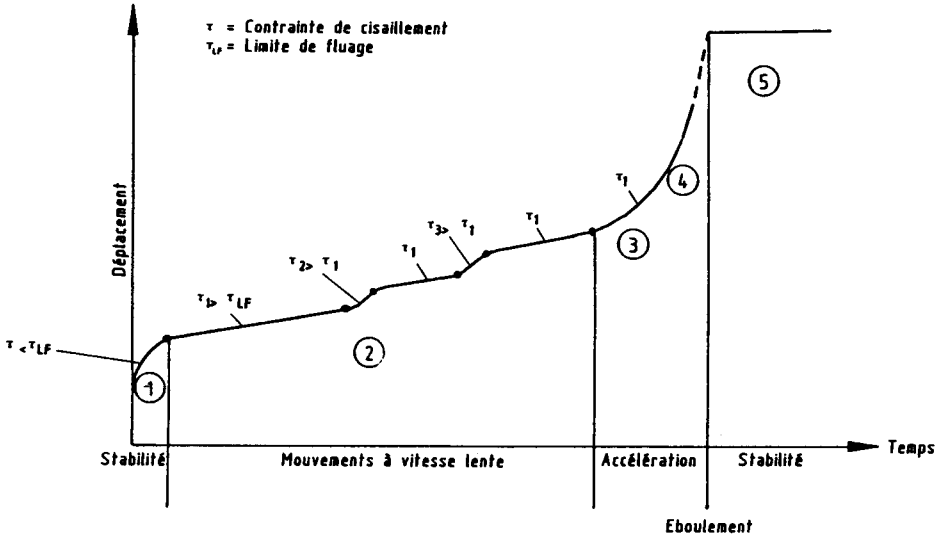

Fig. 1 - Différents états d'un mouvement de terrain

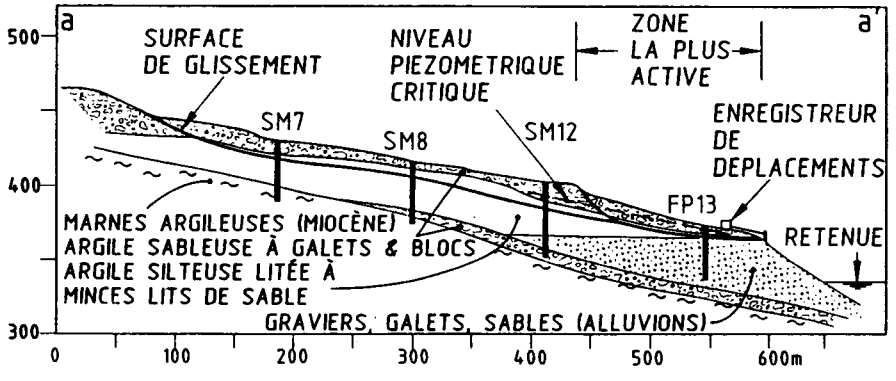

Fig. 2 - Glissement de Leaz. Coupe géologique schématique

Description du site

La synthèse des reconnaissances géologiques est présentée en figure 2 et on peut retenir les points suivants :

- le substratum de marnes situé à 30-40 m de profondeur est stable, de même qu'une terrasse d'alluvions anciennes *(aucun mouvement entre 1964 et 1993)*. La retenue n'a donc aucune influence sur le glissement.
- le glissement s'effectue au sein d'une formation d'argiles litées d'origine glacio-lacustre, très répandue dans la région et caractérisée par :

  WL = 35 - 50%
  Ip = 20 - 30%
  U = 19,5° c' = 0 *(cisaillement à 1 µ/mn)*

Le volume total des matériaux en mouvement est de $1{,}4.10^6$ m^3, caractérisés en 1969 par des vitesses de 5-10 cm/an et de 10-30 cm/an dans la zone la plus active représentant 100.000 m^3 *(vitesses maximales de l'ordre de 1 m/an pour certains points)*.

Surveillance et résultats

Les mesures de déplacements ont commencé en 1964, mais depuis 1977 le système de surveillance comporte :

- des mesures annuelles en triangulation sur 25 témoins,
- des mesures mensuelles au distancémètre sur 11 témoins répartis dans le glissement,
- un enregistrement en continu des déplacements d'un point de la zone la plus active,
- un enregistrement des niveaux d'eau dans 4 piézomètres et des mesures mensuelles dans 8 autres,
- un enregistrement de la pluviométrie.

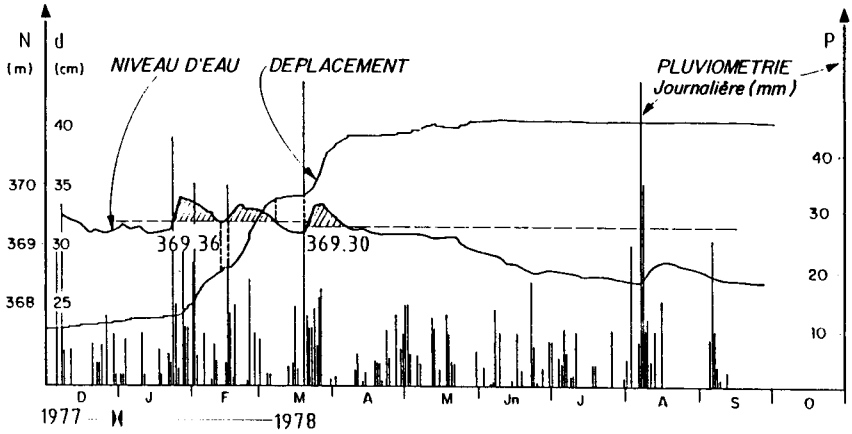

Fig. 3 - Glissement de LEAZ. Enregistrements simultanés de piézométrie et de déplacements

Sur la figure 3, on a représenté un exemple de 10 mois d'enregistrements corrélés avec des variations du niveau piézométrique à proximité de l'enregistreur.
On a ainsi pu mettre en évidence 3 points fondamentaux :

- les périodes d'activité sont réduites dans le temps alors qu'on a plusieurs mois - "d'arrêt" par an des mouvements *(à 1 ou 2 mm près)*, correspondant au stade 1 de stabilité.
- l'activité du glissement se produit lorsque le niveau d'eau dépasse une valeur critique N_0.
- en phase d'activité, on peut lier la vitesse instantanée des déplacements au niveau d'eau par une formule approchée du type $V = k\ (N-N_0)$. On est alors au stade 2 des mouvements réversibles.

On a donc pu proposer un certain schéma de comportement du glissement qui permettait de rendre compte des vitesses observées en fonction des niveaux d'eau dans le terrain.Ce schéma comporte un "modèle hydraulique" permettant à partir de la pluviométrie journalière de déterminer le niveau piézométrique au sondage FP13, et un "modèle mécanique" permettant de relier ce niveau piézométrique à la vitesse instantanée. On indique à la fig. 4, le résultat de l'application de ces modèles et on peut en conclure que, tant que ce mécanisme reste identique, pour les séquences pluviométriques connues, les vitesses pourront atteindre environ 10 mm/j puis diminueront.
Par conséquent dans ce type de mouvement, ni les mouvements, ni l'accélération seuls sont des critères suffisants pour déterminer le moment où le mouvement devient rapide et irréversible. Il faut considérer l'ensemble sollicitations + déplacements pour déterminer ce moment. Les critères de danger correspondent soit à une accélération sous contrainte constante, soit à des vitesses nettement supérieures *(pour une même contrainte)* à celles déterminées auparavant.

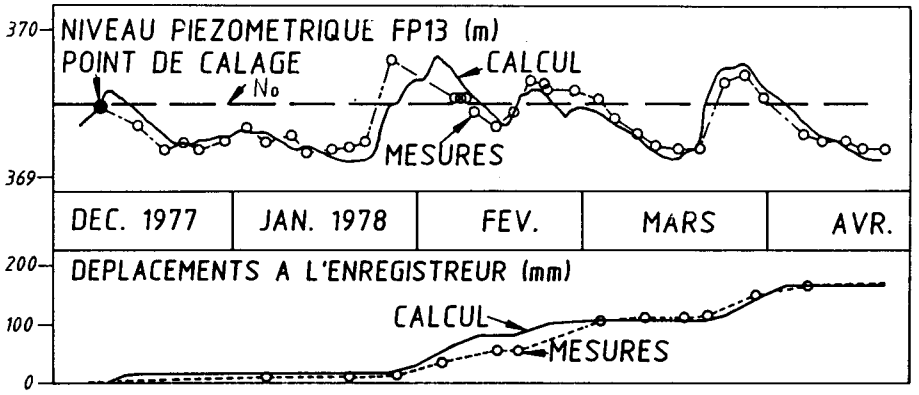

Fig. 4 - Comparaison des niveaux piézométriques et des déplacements calculés à partir de la pluviométrie avec les mêmes valeurs mesurées

Exemple de l'éboulement du CD 926

Localisation - Circonstances

Il s'agit d'un éboulement rocheux situé dans la vallée de l'ARVAN, à 5 km au Sud-Ouest de ST-JEAN-DE-MAURIENNE.

Fin 1975, suite à un éboulement de l'ordre 1.000 m^3 dans les gypses en contre-bas de la route départementale *(C.D. 926)*, deux fissures distantes de 50 m sont apparues dans la chaussée de cette route. Les questions qui se sont alors posées ont été les suivantes :

- l'affaissement observé sur la route est-il local ?
- y a-t-il un danger pour la route et lequel ?

Description du site

Pour la zone étudiée, le C.D. 926 se situe à 100 m au-dessus de l'ARVAN, dont il est séparé par des falaises de gypses à 45-50°.

Les terrains de couverture sont constitués d'éboulis de gypses et de dépôts morainiques *(silt sableux à blocs arrondis)*.

Dans le gypse, on a noté les trois familles de plans de discontinuité suivantes :

- les plans de stratification à pendage 50 à 60° vers l'aval donc défavorable,
- une grande fissure à pendage 73° vers le S.E. Cette dernière est ouverte et comporte des traces de mouvements anciens. Sa position a été représentée sur la coupe de la figure 5.
- des plans de diaclases à pendage 60° vers le S.E., donc également défavorable.

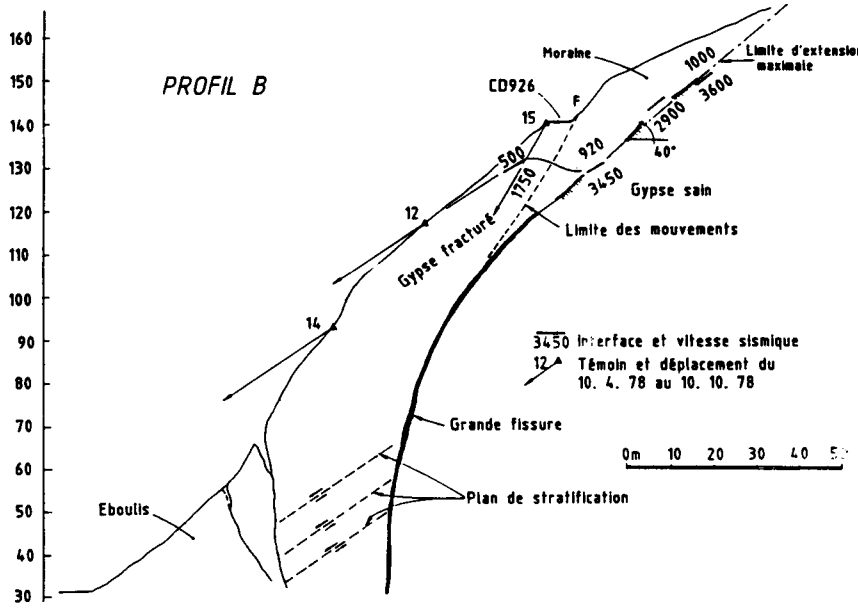

Fig. 5 -CD 926 - Profil en travers de l'éboulement

Dans tous les terrains *(substratum et couverture)*, on remarque l'absence de circulation d'eau importantes et de nappe.

Surveillance

En février 1976, on a mis en place 10 repères de nivellement sur la route, puis en avril 1978, 7 repères dont 5 en contrebas de la route.

Dès le mois d'octobre 1978, on a pu faire les 3 constatations suivantes :

- les vitesses de déplacements verticaux de témoins tels que 12 ou 14 étaient les mêmes que celles des repères de nivellement du C.D. 926, ce qui montrait bien qu'il y avait un mouvement d'ensemble *(figure 5)*.
- les directions des vecteurs de déplacements des témoins 11 à 14 étaient parallèles entre elles, non conformes à la pente topographique, et cohérentes avec les directions et plongements des stries observées sur les plans de stratification ou de diaclases.
- les vitesses des mouvements étaient sensiblement constantes et non influencées par la pluviométrie *(fig. 6)*.

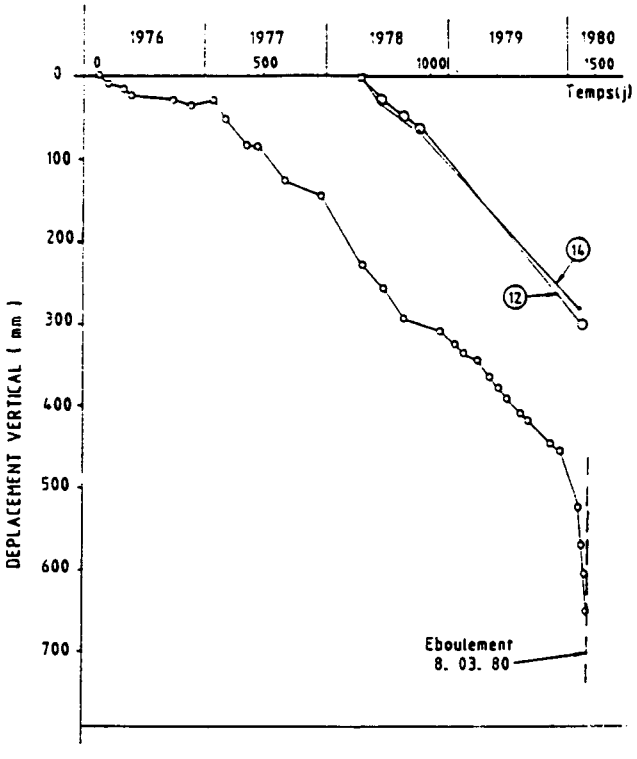

Fig. 6 - C.D. 926 - Courbe des affaissements verticaux

Mais, lors de la mesure du 11 février 1980, on a décelé une accélération, ce qui a conduit à resserrer les mesures *(tous les 10 jours, puis tous les 2 jours, puis tous les jours)*.

Au 5 Mars 1980, l'analyse de l'évolution des déplacements a montré que la date la

plus probable d'éboulement se situait le 8 ou 9 Mars. On a recommandé alors la fermeture du CD 926 avec continuation de la surveillance. Au moment de la fermeture de la route (6 Mars), les vitesses journalières d'affaissement ne dépassaient pas 5 à 7 mm/jour et l'accélération n'était pas décelable à l'oeil nu.
Le 8 Mars à 21 h.30, un éboulement estimé à 80.000 m3 emportait le C.D. 926 sur 50 m de long. Les limites de cet éboulement ont été sensiblement celles qui avaient été prévues.
Grâce à la fermeture préventive des routes, aucune victime n'a été à déplorer.

Méthodes de prévision

Etant donné la mesure de l'évolution d'un paramètre significatif X *(déplacement, ou vitesse)* en fonction du temps t, le problème se résume à la recherche d'une valeur finie tr pour laquelle X tend vers l'infini.
Le principe, dérivé de la méthode proposée par ASAOKA en 1978 pour le tassement oedométrique, consiste à découper les déplacements en intervalles égaux DD pour lesquels les temps successifs t_n, t_{n+1} tendent vers une valeur t_r. Mais, ici, la relation $t_{n+1} = f(t_n)$ n'est pas obligatoirement linéaire.

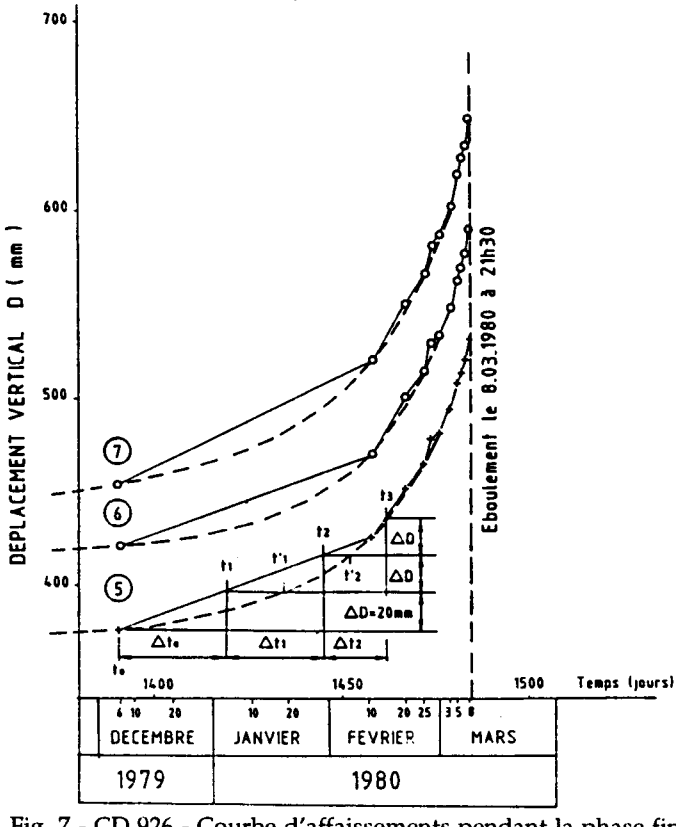

Fig. 7 - CD 926 - Courbe d'affaissements pendant la phase finale et principe du découpage des déplacements

On a représenté sur la figure 7, pour 3 témoins :

- les courbes brutes des déplacements verticaux mesurés au CD 926 dans les trois derniers mois*(phase finale)* ;

- les mêmes courbes, lissées ;
- le principe du découpage des déplacements en intervalles successifs égaux permettant de définir la suite t_0, t_1, t_2... t_n sur les courbes brutes, ou t_0, t'_1, t'_2,... t'_n sur les courbes lissées.

L'intervalle de déplacement DD est arbitraire. On a adopté, ici, DD = 20 mm.
Sur la figure 8, on a représenté, pour les 3 témoins 5, 6 et 7, l'ensemble des points représentatifs $t_n = f(t_{n-1})$ à partir des courbes lissées, en prenant t_0 = 1 391 j *(6 décembre 1979)* correspondant au dernier point connu de la phase à vitesse sensiblement constante. Si, à une date donnée où l'on dispose d'un certain nombre de points, on essaie d'ajuster une droite par la méthode des moindres carrés et que l'on calcule l'intersection de celle-ci avec la bissectrice, on constate qu'on arrive à une date comprise entre le 8 et le 9.03.1980.

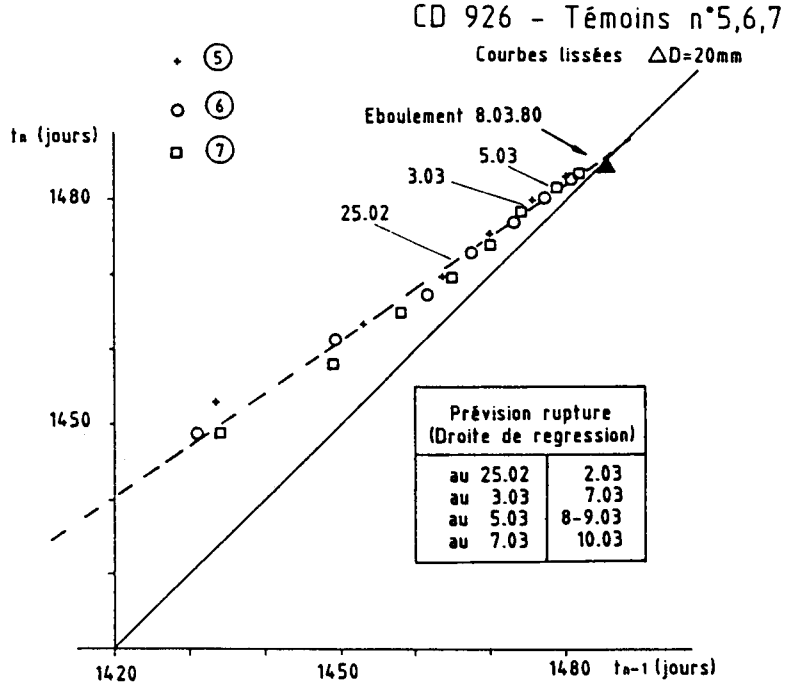

Fig. 8 - Courbes $t_n = f(t_{n-1})$ sur courbes lissées avec droite de régression au 5.03.1980

Si dans ce cas la prévision de la date l'éboulement a pu être effectuée précisément c'est à cause de 2 caractéristiques :

- le mouvement n'était aucunement influencé par les conditions climatiques et il s'agissait d'une rupture progressive dans le rocher,
- géométriquement, le mouvement ne pouvait se stabiliser en évoluant.

On va montrer dans les 2 cas suivants, les difficultés posées si ces 2 conditions ne sont pas remplies.

Exemple de l'éboulement de MONTVAUTHIER

Localisation - Contexte géologique

Ce cas concerne une falaise d'environ 40 m de haut sur la Commune des HOUCHES. Cette falaise est constituée de schistes gréseux et micacés du houiller comportant plusieurs directions de discontinuités dont au moins 2 familles ont un pendage vers l'aval.

En contrebas, il existe une route et plusieurs habitations.

Les mesures sur 4 témoins ont commencé en juin 1992 sur des fissures qui sont apparues au sommet de la falaise à 5 m en arrière du bord de celle-ci.

Une prospection sismique par transparence a permis de préciser que le rocher était décomprimé sur 7 à 10 m de hauteur et 5 à 6 m d'épaisseur. Le volume en mouvement a été estimé à 800 ou 1000 m^3.

Surveillance - Travaux de protection

La surveillance des mouvements a été réalisée par des mesures manuelles d'écartement des fissures avec une fréquence journalière.

L'appréciation des zones pouvant être atteintes par l'éboulement a été faite sur plusieurs profils selon la méthode de trajectographie de chutes de blocs mise au point par A.D.R.G.T. Il a été ainsi possible de vérifier que les maisons pouvaient être atteintes et de préconiser et dimensionner des merlons de protection qui ont été réalisés.

Problème de la prévision de l'éboulement

Sur la fig. 9, on a reporté les courbes d'écartement des fissures et la pluviométrie journalière en fonction du temps. On peut constater que les mouvements s'accéléraient après des précipitations dépassant 20 mm. Aucun niveau d'eau n'étant mesuré, il n'a pas été possible d'établir une corrélation entre les précipitations et les mouvements.

Ceci a été à l'origine d'une fausse alerte puisque l'analyse des mouvements au 6.09.1992 montrait une date de rupture probable *(selon la méthode exposée au paragraphe 3)* entre le 7 et le 9.09. Ceci était dû à l'accélération provoquée par les précipitations des 29 et 31.08.

Ce n'est qu'après le 9.09 que la courbe des déplacements a pris une allure régulière, sans ralentissement alors qu'il ne pleuvait pas. La rupture était amorcée, et la deuxième prévision effectuée le 17.09 indiquait une date de rupture la plus probable entre le 18 au soir et le 20 au matin. L'éboulement a eu lieu le 19 à 18 h. Il avait été précédé par quelques chutes de blocs plusieurs heures auparavant.

Sur la fig. 10, on a représenté schématiquement le corps de l'éboulement et les trajectoires des quelques blocs ayant été le plus loin. Ces dernières trajectoires correspondent bien à la prévision qui en avait été faite par les calculs trajectographiques.

Au contraire le corps de l'éboulement a parcouru une faible distance, ayant été arrêté par la plate-forme constitué par la route.

Il est frappant de constater que le calcul trajectographique indiquait que 63% des blocs *(donc une majorité)* partis du sommet de falaise s'arrêtaient sur la route. Cet aspect qualitatif n'a pas été vérifié quantitativement puisqu'une infime partie de l'éboulement a atteint la zone occupée par les maisons. Ceci montre que la méthode de

trajectographie pour le phénomène chutes de blocs ne peut être transposée d'une manière quantitative au phénomène éboulement.

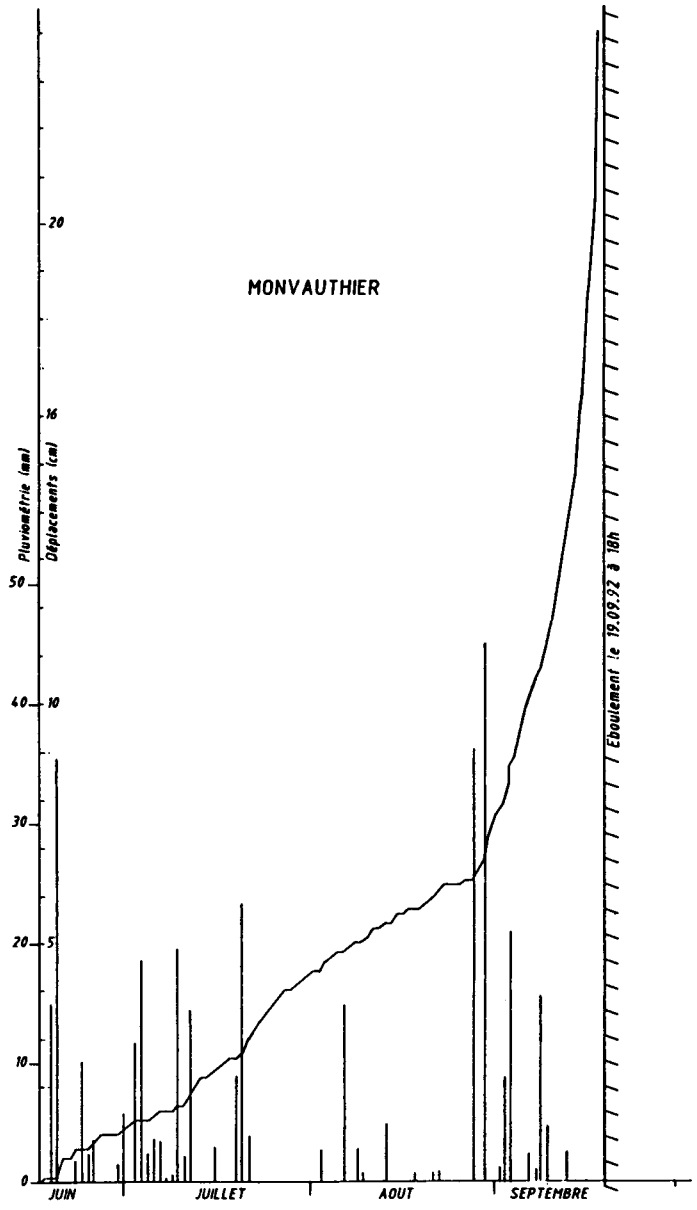

Fig. 9 - Eboulement de MONTVAUTHIER. Courbe des déplacements et précipitations

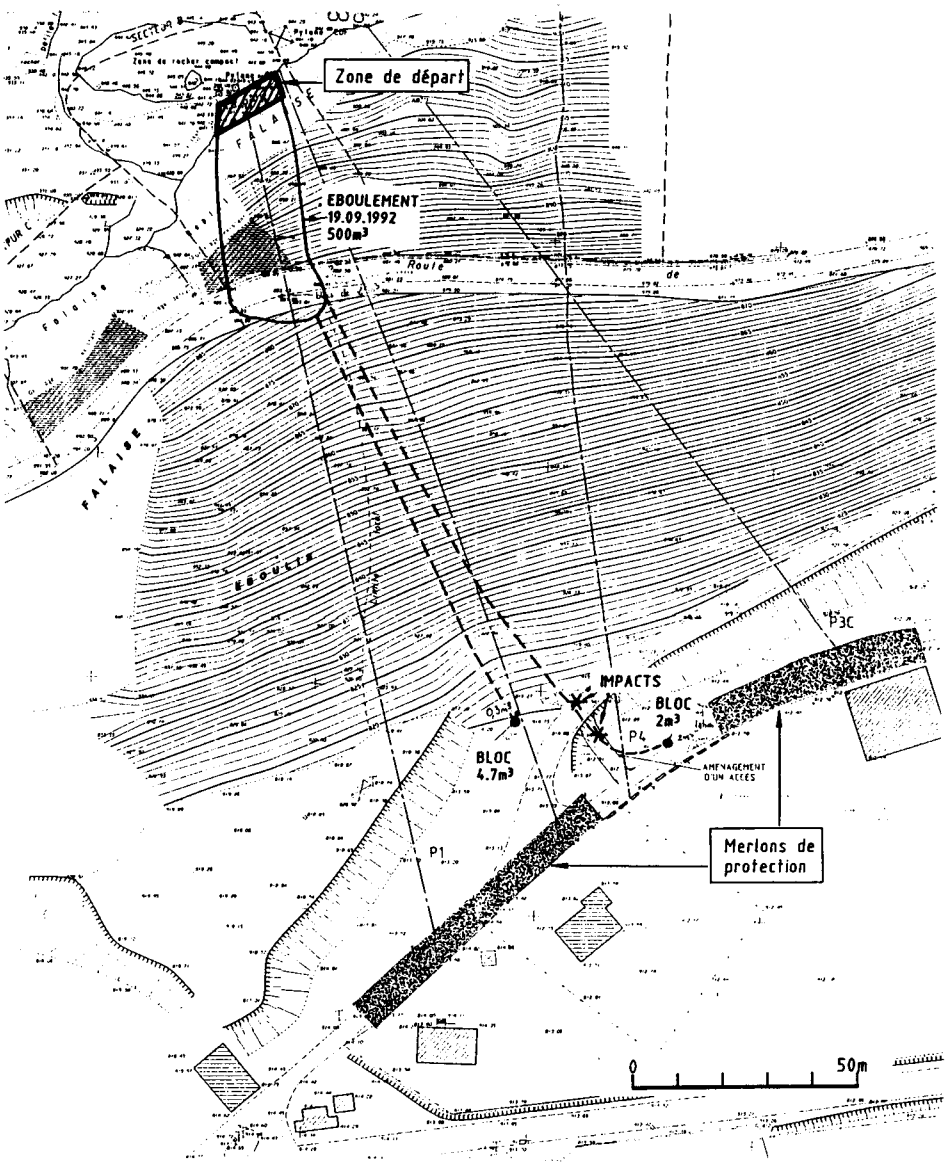

Fig. 10 - Eboulement de MONTVAUTHIER - Zones atteintes le 19.09.1992

Exemple du Glissement d'AUBERIVES

Localisation - Contexte géologique

Le glissement de terrain d'AUBERIVES est situé en rive droite de la rivière la Bourne, affluent de l'Isère, à 40 km au Sud-Ouest de GRENOBLE. Il est très ancien et

s'est réactivé 2 fois récemment, en 1983 et en Octobre 1988. Il affecte la route départementale C.D. 531 et, dans une moindre mesure, un canal d'irrigation *(canal de la Bourne)* qui a été implanté en tunnel à cet endroit dès 1875 à cause de ces mouvements.

La reprise des mouvements d'octobre 1988 s'est traduite par :

- une déformation du C.D. 531,
- une déformation du tunnel, beaucoup moins importante.

Le versant dominant la Bourne est haut de 120 m, penté à 30-35° en partie basse. La route se situe 15 m au-dessus de la Bourne. Les terrains sont composés de molasse : alternance de grès et marnes. Le pendage normal est dirigé vers l'E-SE, de 5 à 15°. Sur la fig. 11, on a représenté le profil en travers des glissements. Les mouvements détectés par les inclinomètres concernent :

- une partie superficielle de molasse sablo-gréseuse très décomprimée, épaisse de 5 à 10 m, dans laquelle ont eu lieu les mouvements les plus actifs (A sur la fig. 11)
- une zone profonde (B), descendant jusqu'à 15-35 m et affectée de mouvements lents, détectés dans le tunnel.

Dans la suite, on ne s'intéressera qu'aux mouvements les plus actifs.

Problème de la prévision

Lors de la reprise des mouvements en février 1989, un certain nombre de repères de nivellement ont été implantés sur le CD 531 et relevés avec une fréquence de 2 fois/semaine. En février et mai, la courbe des affaissements a montré une nette accélération (fig. 12), si bien qu'on a tenté de réaliser des prévisions sur les dates possibles d'éboulement. Cependant, dans ce cas, plus on avançait et plus les dates prévues reculaient.

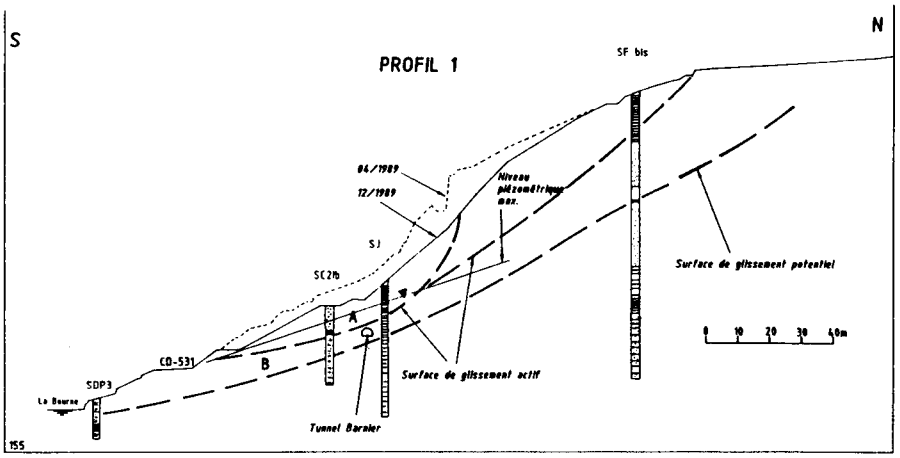

Fig. 11. - Glissement d'AUBERIVES - Profil en travers

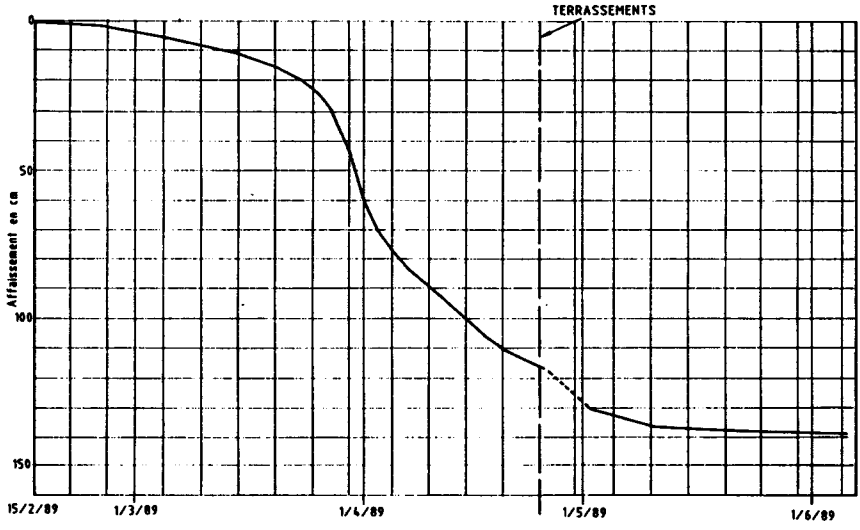

Fig. 12 - Glissement d'AUBERIVES - Affaissement du repère 125

Dates de la prévision	Date de rupture prévue
18-03	25-03
21-03	26-03
22-03	27-03
23-03	30-03

Finalement, la vitesse est passée le 1er avril par un maximum de l'ordre de 7 cm/j puis a ralenti. Ceci est dû à 2 phénomènes :

- modification de forme du glissement au cours des mouvements avec engraissement de la partie basse stabilisatrice et allégement de la partie amont motrice,
- la dissipation des pressions interstitielles au fur et à mesure des mouvements.

Conclusions

Les exemples ci-dessus montrent que certains problèmes ont actuellement une solution possible même si elle est parfois lourde :

- pour les mouvements de terrains dont la vitesse est variable dans le temps, il est possible par mise en place d'une surveillance judicieuse *(précipitations, déplacements et niveau piézométrique)* d'établir des corrélations entre sollicitations et déplacements et de déterminer les particularités dynamiques des mouvements.

Il est alors possible de discerner le passage des mouvements reversibles aux mouvements irréversibles accélérés avec grande vitesse.

- pour les petits éboulements et les chutes de blocs, quelques méthodes de calculs trajectographiques permettent de prévoir, avec une bonne

approximations, les probabilités d'atteintes de diverses zones et également de dimensionner des protections efficaces *(calcul de l'énergie et de la hauteur de passage).*

- pour des menaces d'éboulements rocheux répondant à certaines conditions, on peut apprécier avec une assez bonne précision le moment du passage aux mouvements accélérés rapides.

Au contraire, pour un grand nombre de mouvements affectant des matériaux rocheux, cette dernière prévision est plutôt aléatoire *(toutefois une augmentation de la fréquence des chutes de blocs constitue parfois un signe précurseur de grand éboulement).*

Les difficultés proviennent de plusieurs facteurs :

- les grandes masses rocheuses en mouvement souvent ne peuvent être considérées comme un système unique avec sa propre dynamique et doivent être subdivisées en plusieurs sous-ensembles, chacun d'eux pouvant avoir ses propres particularités dynamiques, d'où une complexité accrue du système de surveillance.
- les mesures sont difficiles à organiser s'il s'agit de falaises étendues.
- les corrélations entre pluviométrie et déplacements ne sont pas faciles à établir.
- on ne connaît pas, pour des matériaux rocheux, la durée du stade 2 mais on peut supposer qu'elle est réduite. Ce manque d'expérience ne facilite pas l'organisation de la surveillance systématique *(implantation des repères, espacement des mesures, interprétation).*

C'est pourquoi, sans négliger la recherche sur ce point, il est préférable de l'orienter sur la détermination de l'extension des éboulements, ou plus exactement sur la détermination des facteurs suivants :

- la distribution des masses à l'arrivée en fonction de la géométrie du terrain,
- la répartition des vitesses de passage et des énergies en différents points au cours de l'éboulement.

Bibliographie

ASAOKA, A. (1978). Observational procedure of settlement prediction. Soils and Foundations 18 (4) pp. 87-101

AZIMI, C. DESVARREUX P. et al (1982). Méthode de calcul de la dynamique des chutes de blocs - Bull. Liaison Labo P. et Ch. 122, pp 93-102.

AZIMI, C. BIAREZ, J. et al (1988). Prévision d'éboulement en terrain gypseux - Proc. 5 th Internat. Symp. on Landslides, Lausanne pp. 531-536.

AZIMI, C. BIAREZ, J et al (1992). Mecanisme des glissements de terrains argileux - Bilan de surveillance sur plusieurs années. Proc. 6 th Internat. Symp. on Landslides, Christchurch (vol. post-congrés).

Avalanche modelling and integration of expert knowledge in the Elsa System

Modélisation des avalanches et intégration de connaissances expertes dans le système ELSA

L. BUISSON, C. CHARLIER

Cemagref / Division Nivologie
BP 76, 38402 Saint-Martin d'Hères - France
Tel. (33) 76 76 27 95 - Fax (33) 76 51 38 03

Abstract

The choice of the best protection system against avalanches on a particular path requires an accurate description, or *image*, of these avalanches. In order to get this image, avalanche consultants can use several numerical models which are often difficult to handle. Moreover, these models deal only with a part of the phenomena involved in avalanches and ignore the others. As a result, the consultants must use their experience and knowledge to imagine avalanches on any particular path.
This paper presents ELSA (Etude et Limites de Sites Avalancheux), a computer system dedicated to the modelling of the avalanche expert knowledge and to the *integration* of the new symbolic computer models with the classical numerical models. The basic aim of integration is to build a unique computer system incorporating all these models.
After a description of the terrain representation, we present different scenarios that ELSA takes into account. Then, the methods which deal with some phenomena occurring in avalanches are described. The problems involved in the integration of these methods close this paper.

Résumé

Le choix de la meilleure protection contre les avalanches sur un site particulier exige une description précise, ou image, de ces avalanches. Afin d'obtenir cette image, les ingénieurs peuvent utiliser plusieurs modèles numériques qui sont souvent difficiles à manipuler. De plus, ces modèles ne traitent qu'une partie des phénomènes impliqués dans l'avalanche et ignorent les autres. Par conséquent, les ingénieurs doivent faire appel à leur expérience et à leur connaissance pour imaginer les avalanches sur un site particulier.
Cet article présente ELSA (Etude et Limites des Sites Avalancheux), un système informatique destiné à la modélisation de la connaissance des experts en avalanche et à l'intégration de nouveaux modèles symboliques et des modèles numériques

classiques. L'objectif de l'intégration est de construire un système informatique unique incorporant tous ces modèles.
Après une description de la représentation de terrain, nous proposons les différents scénarios qu'ELSA prend en compte. Ensuite, les méthodes qui traitent des différents phénomènes qui se produisent dans les avalanches sont décrits. L'exposé des problèmes qui apparaissent lors de l'intégration clôt cet article.

Introduction

The consultants responsible for avalanche path analysis must answer the following questions. Is there any avalanche hazard on the path ? Which kind of avalanche can occur ? In which conditions ? What are the properties of these avalanches (magnitude, velocity, extension, pressure fields...) ? These analyses will give the basic information to recommend the best protection strategy (Buisson and Charlier 1989).
The consultants have several tools to analyse an avalanche path. First of all, they can use their experience. They can make comparisons between a particular avalanche path and some other well-known paths. They can make assumptions based on terrain and vegetation features. But more and more, in avalanche hazard zoning, the velocity and the run-out distance of the flows are required for building design. Snow specialists can use simulation methods based on mechanical equations. Numerous models have been developed from Voellmy's model mainly to describe a flowing avalanche (Bakkehoi *et al* 1981, Beghin *et al* 1983, Brugnot *et al* 1985, Norem *et al* 1989, Salm, Burkard and Gubler 1990, Brandstatter, Wieser and Schaffhauser 1992, Martinet 1992 unpublished)
ELSA is a computer tool dedicated to avalanche path analysis (Buisson and Charlier 1989). It tries to provide, not only some of these numerical simulation methods, but also some empirical methods developed by using the experience of avalanche experts. These methods provide input data for the numerical models. Recent developments in Computer Science enable the knowledge of avalanche experts to be captured. *Symbolic models* based on this knowledge can then be implemented (Buisson 1990a).
There is no conflict between these two kinds of methods. They are complementary and can be combined to produce an improved output.

Description of terrain

ELSA must be provided with an accurate description of terrain. Terrain plays an important part in avalanche path analysis. Topography, vegetation and the nature of the soil surface are the parameters which, in combination with meteorological conditions, control the release and flow behaviour of avalanches. In numerical models, the terrain profiles are used to describe the geometry of the avalanche track. The vegetation and the soil surface are important in the choice of roughness coefficients. In symbolic models, slope, topography around the ridges and exposure to prevailing wind direction are used as determinants for the computation of snowdrift, snow cover stability and fracture propagation.

Three zones

The different models available in ELSA cannot be used on the whole avalanche path. As a result, we assume that the user is able to clearly define the *starting zone*, the *avalanche track* and the *run-out zone* (Figure 1).

This decomposition is common. The starting zone is that part of the terrain where the mass of snow which will be involved in the avalanche is released. The fracture propagation and the acceleration of the avalanches are of principal features of this zone. The avalanche track is where the avalanche simply flows and the run-out zone is where the avalanche decelerates and finally stops.

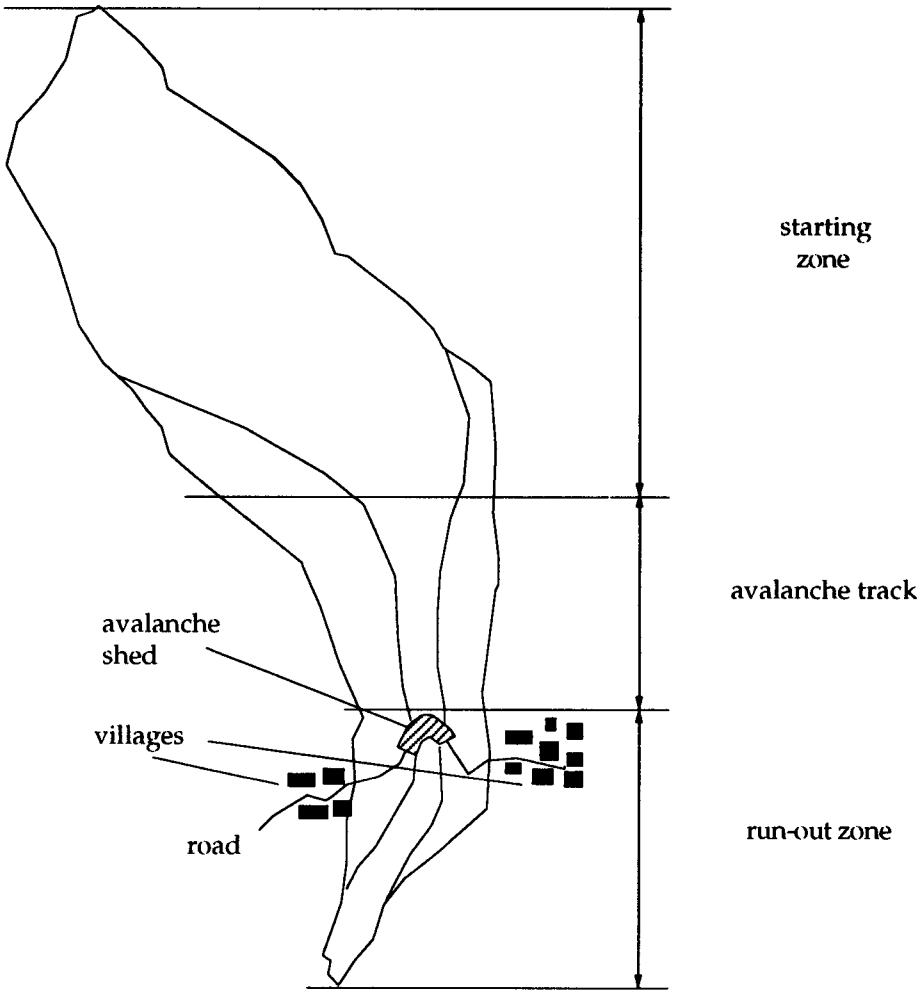

Fig.1. : The Drayre avalanche path in Vaujany, Isère, Région Rhône-Alpes, France.

Triangles and topography

In order to describe the topography mathematically, a digital terrain model (DTM) is required. A triangulation method is used which describes the natural terrain as planar triangles. Each triangle is defined by the coordinates of its vertices.
Toppe (pers. comm.), suggested using this method to keep the number of triangles rather low and to get an accurate DTM adapted to the terrain features.

Panels

The symbolic models are based on experts knowledge. As a result, ELSA must use the same terrain analysis methodology as these experts do. The experts do not reason in small triangles. Instead, they use a unit of terrain called a *panel*. A panel is considered homogeneous according to the criteria of the avalanche path analysis : slope, exposure, vegetation, soil and distance to the main ridges. Panels are represented in ELSA as *polygons* defined by the union of several connected triangles. The panel represents the minimum topological decomposition of the terrain. ELSA does not consider units of terrain which are less than the size of a panel.

A construction system

The triangle and panel specifications suggest the process of their construction. The basic idea is to use the data which are easily obtained, i.e. contour line maps (1), ridges and breaks of slope maps (2), singularity line maps (changes in aspect, gullies, furrows...) (3) and vegetation and soil surface maps (4). All these polygonal lines are going to become constraints in the building of triangles. In other words, these lines can not cut through a triangle.
According to the specifications of the panels, these polygonal lines may have several meanings. Some must be panel boundaries (e.g. vegetation or ridge line); others may be included in the interior of a panel (a contour line for instance). In this latter case, the lines are used only for the construction of the triangles.

The terrain construction system is based on polygonal lines. Each vertex of these lines must be known through its three coordinates. If x and y are defined through the digitisation of the map, the z-coordinates can be provided *only by the contour line map*. As a consequence, we decided not to work with the initial data map (2), (3) and (4) (Fig. 2a.) but with the lines defined by the intersection of these data with the contour lines (1) (Fig. 2b.).

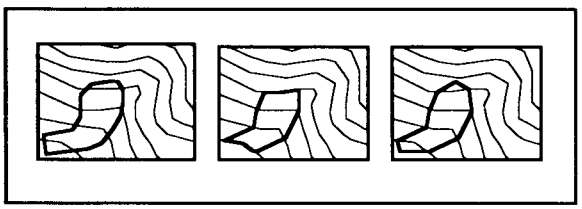

Fig. 2a., 2b. : Lines used in the construction

The contour lines maps are purchased at l'Institut Géographique National which is in charge of mapping in France. The available digitised contour lines are adapted to

a scale of 1/10 000. The other maps (2), (3) and (4) are digitised by the user on the graphic interface of ELSA. This operation requires a good analysis of the natural terrain.

Meteorological conditions

An avalanche occurs when a particular scenario takes place on an avalanche path.
A *scenario* is described through an *initial condition* and a sequence of *events*. An initial condition defines the distribution of the snow in the starting zone. The last event is called the *critical event* and it ends with an avalanche release.
ELSA is able to deal with one family of scenarios where a heavy snowfall triggers an avalanche.
In these scenarios, the snow fall event can occur with or *without snowdrift*. The user can choose the wind direction and the empirical level of snowdrift. The user can also choose the character of the snow available for avalanche i.e. the new snow from a snowfall. The character is defined by physical parameters : density, cohesion, friction angle.

Modelling several phenomena

During an avalanche occurrence, several phenomena take place in the avalanche path as shown in Figure 3.
Four phenomena are analysed : snowdrift, snow cover stability, release propagation and avalanche flow and stopping. The first three are located mainly on the starting zone, the last on the avalanche track and on the run-out zone

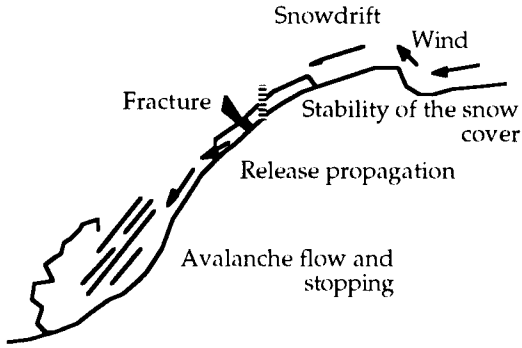

Fig. 3 : Avalanche phenomena taken into account by ELSA

Snowdrift

Snowdrift and its influence on avalanches have been studied for several years from both the theoretical and experimental points of view (Föhn *et al* 1983, Meister 1989). In ELSA, a symbolic simulation of snowdrift is based on empirical knowledge. The first assumption is that the spatial analysis of panels is *relevant* and yields homogeneous units with reference to this phenomenon.

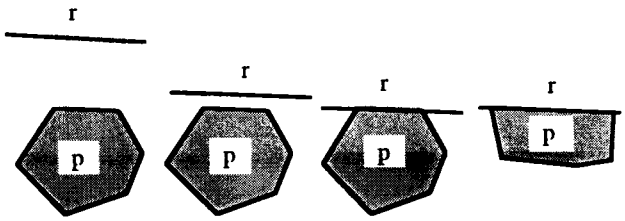

Fig. 4 : Four relative positions between a ridge r and a panel p considered by ELSA : *near, very near, juxtaposed* and *on*.

Several parameters are used to estimate snowdrift on each panel. They are the relative position of the panel to the ridge (Fig. 4.), shape of the ridge (assumed to be symmetric), distance to the ridge, incidence angle between the wind and the ridge and position of the panel and the ridge relative to wind (*lee-* or *windward*). The result of the snowdrift analysis is an empirical distribution of a coefficient between 0 and 5. A coefficient of 1 means that snowdrift has no effect. A coefficient lower than 1 means that there is wind erosion, a coefficient greater than 1 means that there is wind deposit. The limit of 5 is the maximum value.

Snow cover stability

This stability is used in the analysis of release propagation. A very simple model is used in the starting zone to calculate the stability. It is based on the soil mechanics interpretation which gives, for a homogeneous material and a infinite domain, the critical depth hcrit (measured vertically) of material above which a slide can appear,

$$h_{crit} = \frac{c \cos \varphi}{d\, g \cos i \sin (i - \varphi)}$$

where g is acceleration due to gravity, i is slope angle, d is density of the material (in this case, the snow layer), c is cohesion of the material, and φ is internal friction angle of the material.

In this case, the condition for stability is : $h_{crit} \leq h$

If $h > h_{crit}$, the snow layer is considered as unstable. If there is a release, the whole unstable snow layer is considered to be involved.
In order to take into account the vegetation and the soil surface, we use an empirical association between types of vegetation and soil surface and the values of a factor used to modify the crtitcal height.
Also, in ELSA the user is always allowed to control the stability in a particular panel.

Release propagation

In the release propagation, two phenomena occur with two different characteristic times. The fastest is considered as a wave propagation. It takes place in a cohesive snow layer where the slab stability condition is exceeded. It is the *fracture propagation*. The slowest is considered as the gradual entrainment of snow masses

moving down slope. It is called *movement propagation*. These two phenomena act together to determine the part of the starting zone released.
In the ELSA, these two phenomena are mixed in an empirical model to determine which panels are going to be realeased. This model takes into account the stability inferred for each panel, the neighbourhood relations between panels, the organization of the panels according to the slope line and the mass of snow on each panel.

Avalanche flow

As explained above, the avalanche motion can be simulated by several methods, but only one of them is available in ELSA through one method presented by Bakkehøi *et al* (1981, modified from the Voellmy's method).
This method requires an estimation of the mass of snow involved in the avalanche and the values of two parameters m and D (friction and drag coefficients).

Integration

Integration is used here to mean the introduction and the articulation of several methods in the same computer system.
This paper presents several methods used in ELSA. Some of them have been already used (especially the last ones, dedicated to avalanche flow). Some of them are new and need more work to be validated. These methods are integrated in ELSA. The knowledge based system architecture allows for the development of *problem solving environments* (Buisson, 1990b).
ELSA is built on an object-oriented knowledge representation system : SHIRKA (Rechenmann *et al* 1992, unpublished) which is written in Le-Lisp, a Lisp dialect (Ilog 1991). ELSA runs on a SUN IPC workstation with UNIX.

Sharing data

One of ELSA's main strength is the sharing of data between several methods. The best example is topography. All the different methods use triangulation to represent terrain. However, the first three methods make intensive use of the decomposition in panels. The main advantage of data sharing lies in consistency and in time-saving.

Cooperation

The output of the symbolic simulation can drive the numerical simulation and vice versa. As a result, all the phenomena described above are linked to one another in the analysis.

An interactive interface

The interactive interface allows non-computer specialists to use ELSA. The user-friendly colour interface based on a mouse and a high definition screen highlights the important parameters. The keyboard of the workstation is hardly used and the user doesn't need to know or use the computer operating system or programming languages.
The language Le-Lisp is provided with Aïda, an object-oriented environment for the development of graphic applications (Ilog 1992). The figures in this paper come from the interface. It is used for the construction process (definition of the lines presented

in figure 4a) and for the presentation of results : snow heights map, stability distribution, initial fracture location and release propagation. The scenarios are also displayed in a graphic representation.

Future developments

ELSA is still being developed. Besides the capabilities presented in this paper and which have already been implemented, further developments are being considered : terrain validation of some methods, further analysis of stability in a forested or tree-covered area, integration of the AVAER (AValanche AERosol) program for aerosol avalanches (Rapin 1991, unpublished), integration of the Voellmy-Salm model (Salm *et al* 1990) and integration of a statistical method for the estimation of the run-out distance such as described by Bakkehoi *et al* (1981).

Acknowledgements

A very near version of this paper has already been presented in the International Symposium de l'IGS "Snow and snow related problems" held in Nagaoka, Japan, from the 14th to the 18th September 1992.
These research actions have been supported by grants of La Région Rhône-Alpes in 1989 and 1990 and grants of La Délégation aux Risques Majeurs (Ministère de l'Environnement) in 1990 and 1991.
We would like to thank Harald Norem from NGI in Oslo (Norway), Ronald Toppe formerly from NGI, David Mc Clung from UBC in Vancouver (Canada) and Hansueli Gubler from IFENA in Davos (Switzerland) for their relevant advice.

References

Bakkehøi, S., T. Cheng, U. Domaas, K. Lied, R. Perla and B. Schieldrop. 1981. On the computation of parameters that model snow avalanche motion. *Canadian Geotechnical Journal*, Vol. 18, 121-130.

Beghin, P. and G. Brugnot. 1983. Contribution of theoretical and experimental results to powder-snow avalanche dynamics. *Cold Regions Science and Technology*, Vol. 8, 66-73.

Brandstätter, W., K. Wieser and H. Schaffhauser. 1992. Three-dimensional simulation of powder avalanches. *to be published.*

Brugnot, G. and J.P. Vila. 1985. Investigation théorique et expérimentale des caractéristiques dynamiques des avalanches de neige dense. *La Houille Blanche*, n°2, 133-142.

Buisson, L. and C. Charlier. 1989 Avalanche starting zone analysis with a knowledge-based system. *Ann. Glaciol.*, 13, 27-30.

Buisson, L. Unpublished. Le raisonnement spatial dans les systèmes à base de connaissances ; application à l'analyse de sites avalancheux. (Thèse d'Informatique, Université Joseph Fourier, Grenoble, 1990a).

Buisson, L. 1990b. ELSA : a problem solving environment for avalanche path analysis. *In* Pavé, A. and G.C. Vansteenkiste, *ed. Artificial intelligence in numerical and symbolic simulation*. Lyon, ALEAS, 25-50.

Föhn, P. and R. Meister. 1983. Distribution of snow drifts on ridge slopes : measurements and theoretical approximations. *Ann. Glaciol.*, 4, 52-57.

Ilog S.A. 1991. Le-Lisp de l'INRIA, Version 15.24. Le manuel de référence. Gentilly.

Ilog S.A. 1992. Aïda, Version 1.54. Reference Manual. Gentilly.

Martinet, G. Unpublished. Contribution à la modélisation numérique des avalanches de neige dense et des laves torrentielles. (Thèse de Mécanique, Université Joseph Fourier, Grenoble, 1992).

Meister, R. 1989. Influence of strong winds on snow distribution and avalanche activity. *Ann. Glaciol.*, 13, 195-201.

Norem, H., F. Irgens and E. Schieldrop. 1989. Simulation of snow-avalanche flow in run-out zones. *Ann. Glaciol.*, 13, 218-225.

Rapin, F. Unpublished. Utilisation du programme de calcul d'avalanche à aérosol. (Document Interne, Division Nivologie, Cemagref, 1991).

Rechenmann, F., P. Fontanille, P. Uvietta. Unpublished. Shirka : manuel d'utilisation. (Document interne, IRIMAG, 1992).

Salm, B., A. Burkard and H. Gubler. 1990. Berechnung von Fliesslawinen ; eine Anleitung für Praktiker mit Beispielen. *Mitteilungen des Eidgenössischen Instituts für Schnee- und Lawinenforschung*, 47.

Vila, J.P. 1984. Modélisation mathématique et simulation numérique d'écoulements à surface libre. *La Houille Blanche*, n°6/7.

Wall shear stress of channelized debris flows deduced from rheological measurements

Détermination de la contraintesà la paroi dans une lave torrentielle à partir des mesures rhéologiques

P. COUSSOT

Cemagref / Division Protection contre les Erosions
BP 76, 38402 St-Martin-d'Hères - France
Tel. (33) 76 76 27 66 - Fax (33) 76 51 38 03

Abstract

Debris flow behaviour depends essentially on clay fraction and total solid concentration. For clay fraction less than a few percents, the obtained suspension has an unstable behaviour (which may be represented, in certain conditions, by a flow curve with a minimum). When the ratio of clay to total solid fraction is more than about 10 % the corresponding natural suspension behaviour in simple shear follows a Herschel-Bulkley model. Using rheological parameters one can deduce theoretically the exact wall shear stress for flow on an inclined plane. This result is here compared with experimental data concerning fine mud flows in open channel. Additionally, semi-empirical wall shear stress expressions corresponding to flow in rectangular and trapezoidal channels are established.

Résumé

Les lois de comportement des laves torrentielles dépendent essentiellement de leur fraction argileuse et de leur concentration solide totale. Lorsque le rapport du volume d'argile et du volume solide total est inférieur à quelques pourcents, la suspension a un comportement "instable" (qui, dans certaines conditions, peut être représenté par une courbe d'écoulement avec un minimum). Quand ce rapport est supérieur à environ 10%, la suspension correspondante possède un comportement du type Herschel-Bulkley rhéofluidifiant. En utilisant les paramètres rhéologiques du fluide et les conditions aux limites d'un écoulement sur un plan incliné infiniment large, on peut déduire l'expression exacte de la contrainte à la paroi. Dans cet article, cette formule est comparée aux résultats expérimentaux obtenus pour des écoulements à surface libre de mélanges boueux fins. De plus, des expressions semi-empiriques de contrainte à la paroi sont proposées pour des écoulements dans des canaux de section trapézoïdale et rectangulaire.

Introduction

Debris flows are large masses of water, clay, silt, sand, pebbles, boulders and organic matter, with a high total solid concentration, which sometimes flow in mountain streams after long or intense rains. Since they can cause much damages to inhabited areas, it is important to improve protection or prevention techniques (dams, channels, runout extent). In this aim the knowledge and understanding of debris flow characteristics appear to be a basic means. Furthermore, either for estimating steady flow characteristics or studying numerically transient flows a local wall shear stress expression would be a fundamental tool. Since most debris-water mixtures flow in laminar regime the corresponding wall shear stress should be determined directly from rheological and flow characteristics. In this paper we first review debris flow characteristics. Then we propose wall shear stress expression for uniform flow in open channel.

Rhéological debris flows characteristics

Hypotheses

Debris flows are pulsing flows [1] of a bulk including water, clay, silt, sand, pebbles and boulders, either rolling, slipping or flowing. If one tries to take into account all these local phenomena, flow description will be rather complex. However, to start with, at a global scale, we can distinguish different parts in motion: a bouldery front (representing a small fraction of the whole mass) followed by a large body and finally a low viscous tail (that we shall neglect because of its weak impact). We shall make the important assumption that, despite fluctuations in concentration from one point to another, and despite some local discontinuity in strain field due to local fractures, slip at the wall, segregation or sedimentation, body and front can be considered as homogeneous fluids flowing in a steep channel.

Rheological behaviour of water-debris mixtures

Neglecting organic matters, a debris flow can be regarded as a certain volume of water in which one adds successively coarser solid particles (from clay to boulders). This idea enables us to review and understand from a microstructural viewpoint the various possible water-debris behaviour types. In the following we only consider mixtures having a solid concentration in such a range that neither fracture nor settling occurs during most flows.

Fine mud suspensions

Though purified clay-water mixtures often exhibit complex thixotropic properties, the simple shear behaviour of natural cation-saturated clay-water mixtures generally follows [2-4] a Herschel-Bulkley model, which may be expressed as follows:

$$\tau = \tau_c + K\,\gamma^n \text{ when } \gamma \neq 0\text{, and } \tau \leq \tau_c \text{ when } \gamma = 0 \qquad (1)$$

where τ is the shear stress, γ the shear rate, and τ_c, K, and n are fluid parameters. These three latter parameters do not vary too much with pH or temperature (at least

within limited ranges corresponding to natural conditions) [4-5]. τ_c is the fluid "yield stress" and constitutes the minimum shear stress value to impose for flow to start. This appears to be a key parameter of any water-debris mixture. For most muds and water-debris mixtures, n is around 1/3 [4, 6-7]. K and τ_c vary widely with solid volumic concentration (Cv) and we can write:

$$\tau_c = a \exp(k\, Cv)\ ;\ K = a' \exp(k'\, Cv) \qquad (2)$$

where a, a' and k, k' are fluid parameters. k and k' are generally comprised between 10 and 30 (with Cv expressed in percent) [3-4, 8]. These parameters are different from one material to another and depend on clay types and pH.

Muddy debris flows

Debris flow grain size distribution varies from clay to boulders. The clay-water fraction forms an interstitial matrix in which coarse particles (grains) are embedded. When the initial clay concentration is low enough, the effect, on the suspension yield stress, of such an addition is negligible [6]. When the initial clay concentration is high enough or when the total solid fraction becomes large enough (Cv_0), the suspension yield stress increases rapidly with concentration of added grains (thus also with total solid fraction) [6]:

$$\tau_c = A \exp(\chi\, Cv) \text{ when } Cv > Cv_0 \qquad (3)$$

where A and χ are fluid parameters. These two parameters are all the smaller than the added coarse particle grain size distribution is more expanded. In nature it is likely that debris flow grain size distribution is so expanded that large grain volumes can be added in the initial clay-water mixture before a significant yield stress change occurs. So, as long as a strong grain packing network does not form (see I.2.3), the order of magnitude of the fine matrix yield stress is not too far from the one of the whole mixture. In this case, we shall call the whole material a muddy water-debris mixture because its interstitial clay-water matrix lubricates every relative grain motion. Finally the rheological model to be used for this debris flow type is also given by equation (1).

Granular debris flows

Another completely different debris flow type consists in granular debris flows for which grain concentration is so high that grain contacts affect predominantly the behaviour at least for slow flow. It seems that this debris flow type was modelled by Takahashi [9] on the basis of Bagnold's work [10] concerning rapid shear of force-free particles suspensions. Bagnold distinguished a macroviscous regime (low shear rates) for which viscous energy dissipation due to interstitial fluid shear is predominant from an inertia regime (high shear rates) for which grain collisions are predominant. Unfortunately it is not clear whether these results are or not appliable to flows of complex natural highly concentrated suspensions with an expanded grain size distribution. At least a great defect of this approach is that it does not predict any fluid yield stress which necessarily exists since the material does not flow at rest on a smooth slope.

Our personal view that we shall now present is supported by recent works concerning dry granular flows in open-channel [11] or rheological tests with concentrated force-free particle suspensions [6-7, 12]. Granular water-debris mixtures have such a low clay content (about 1% of the solid fraction) that, at rest, a continuous packing network of direct grain frictional contacts exists althrough the material and explains the material yield stress. The global behaviour is "unstable". This means that, when progressively increasing shear stress from zero, one will suddenly observe a rapid shear rate increase to a high steady state value just when shear stress becomes higher than yield stress value. This effect is probably due to dilatancy or change in grain configuration: it globally results that, during shear, strong direct frictional contacts at low shear rates are partly replaced by lubricated contacts which dissipate less energy. This behaviour type can be represented by a flow curve with a minimum like the one proposed by Phillips & Davies [13]. Unfortunately such a flow curve can hardly be found experimentally because rheometrical flows are often unstable [7, 12]. At least one can say that, in nature, this fluid type can suddenly stop or start to flow at a high velocity for a small change in boundary conditions (slope, channel section).

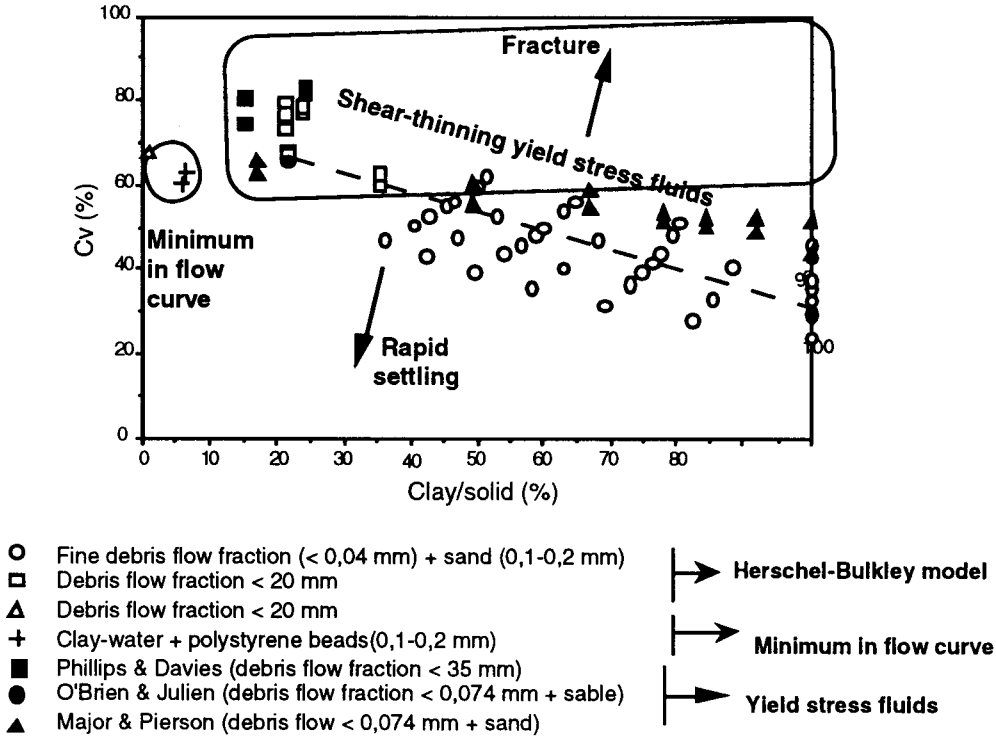

Figure 1: Results of rheometrical tests on natural saturated mixtures.

Debris-water mixture classification

From experimental field tests it appears that there does not exist any natural flows of intermediate material between muddy and granular "unstable" debris flows because it would immediately fracture or settle [6]. We can see the clear separation between these two material types depending on clay fraction in Figure 1 diagram. In this diagram we included both our results obtained with laboratory and field rheometers and those obtained by other researchers with large rheometers.

Further progress is needed concerning granular debris flow behaviour and thus our following development will only concern muddy debris flows.

Flow characteristics of muddy debris flows

Generalities

Because of their high yield stress most natural debris-water mixtures flow in laminar regime (this can be proved easily by using a generalized Reynolds number). Here we consider only muddy debris flows whose behaviour can be well described by a Herschel-Bulkley model with n equal to 1/3. In these conditions the three non-dimensional numbers governing flow are :

$$F = \sqrt{\frac{U^2}{gh}} ; G = \frac{\rho g h}{\tau_c} ; Hb = \frac{\tau_c}{K} \left(\frac{h}{U}\right)^{1/3} \qquad (4)$$

where U is the mean velocity through a cross-section. For studies in similarity one has to respect the equality of these three parameters between prototype and reality. This requires to use a model fluid with lower τ_c and K values. In this aim it is possible to use for example the debris flow fine fraction (at a particular concentration) [14].

Open channel flow

In the case of uniform flow without slip at the wall on an inclined plane and under gravity, flow equations can be solved completely. The exact solution of flow equations is given in terms of the fluid velocity component (in the direction of plane slope):

$$u(y) = \frac{\alpha}{4} [y_0^4 - (y_0 - y)^4] \text{ when } y \leq y_0$$

$$u(y) = u(y_0) = \frac{\alpha}{4} y_0^4 \text{ when } h \leq y \leq y_0 \qquad (5)$$

$$y_0 = h - \frac{\tau_c}{\rho g (\sin i)} ; \alpha = \left(\frac{\rho g \sin i}{K}\right)^3$$

where y_0 is the sheared zone height (the plug depth is $h-y_0$). The discharge by unit of length (q) through a vertical cross-section is equal to :

$$q = \frac{\alpha}{4} y_0^4 \left[h - \frac{y_0}{5}\right] \tag{6}$$

Then the shear stress at the wall (y=0) is :

$$\tau_{xy} = \rho g(\sin i)h \tag{7}$$

We made open channel flow tests [15] with mud mixtures whose behaviour was approximated by a Herschel-Bulkley model (in a wide shear rate range). In the case of uniform flows in rectangular channel the theoretical normal depth (h_n) using equation (6) is compared with experimental normal depth (h_{ne}) in Figure 2. It is clear from these results that the theory based on the infinitely wide inclined plane hypothesis is valid as long as the aspect ratio is less than 0.1. We also deduced [14] from (6) a more practiceful wall shear stress approximated expression:

$$\tau p = \tau_c \, (1+1.93(Hb)^{-0,9}) \tag{8}$$

This expression can be written as a relation between two non-dimensional numbers:

$$G = (1+1.93(Hb)^{-0,9}) \tag{9}$$

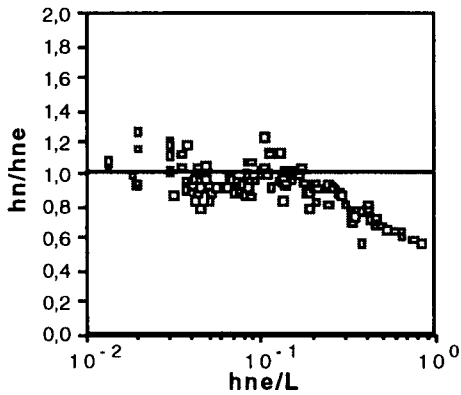

Figure 2 : Ratio of theoretical (using eq.6) to experimetal normal depth as a function of the aspect ratio.

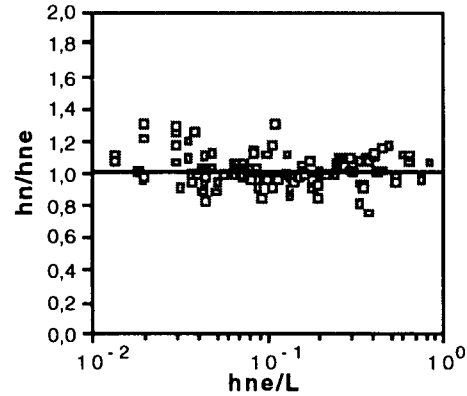

Figure 3 : Ratio of theoretical (using eq.11) to experimetal normal depthas a function of the aspect ratio.

For uniform flows in an open channel of any cross-section we assume that such an equation relating G, H_b and now aspect parameters may be found [14]. Here G is taken as the ratio of mean wall shear stress to fluid yield stress and H_b is computed using the maximum fluid depth. We showed from experimental results [15] (cf Figure 3) that we could take:

$$\tau_p = \tau_c \, (1 + a \, (Hb)^{-0,9}) \tag{10}$$

with:

• Rectangular channel

$$a = 1{,}93 - 0{,}43 \arctan[(\frac{10h}{L})^{20}] \; ; \frac{h}{L} < 1 \qquad (11)$$

• Trapezoidal channel (bottom width B, edge slope : 45°):

$$a = 1{,}93 - 0{,}6 \arctan[(\frac{0{,}4h}{B})^{20}] \; ; \frac{h}{B} < 4 \qquad (12)$$

With these formulae the normal depth (corresponding to uniform flow) may be found using:

$$\tau_p = \rho g R \sin i \qquad (13)$$

Gradually varying flow

Gradually varying flows of muddy debris flow are quite analogous to usual water flows on smooth slopes in the sense that all the main properties are similar: super-critical and sub-critical regimes, hydraulic jump, roll waves on steep slopes and at high discharges. A complete mathematical description of gradually varying flows can be done as soon as the wall shear stress and the velocity distribution are approximately known [14, 16].

Flow stability

In some cases roll waves similar to those occurring in water flows can form. Waves (visible at the surface of the flow) grow and develop in large rolls which have larger height and velocity than mean values of the corresponding theoretical uniform flow. A criterion deduced from Trowbridge's one-dimensional analysis formula [17] for flow instability in an infinitely wide channel can be obtained using wall shear stress expression [14-16].

Conclusion

For steady flows of water-debris mixtures one can obtain simple analytical formulae relating flow depth, discharge and slope. However transient flows are transient and in this case flows can only be studied numerically [18]. Calculations with the help of steady regime formulae are hoped to rapidly provide rough flow characteristics estimations.

However that may be these results still correspond to idealized flows of homogeneous materials and were established in laboratory. Further studies will determined the exact influence of the various peculiar phenomena occurring during flows: bouldery front, archeing process, mean boulder velocity higher than mean flow velocity, particle segregation, erosion, roll waves.

References

Davies, T.R.H., (1986), "Large Debris Flows : A Macro-Viscous Phenomenon", Acta Mechanica, 63, pp.161-178.

Locat, J., and Demers, D., (1988), "Viscosity, yield stress, remolded strength, and liquidity index relationships for sensitive clays", Canadian Geotechnical Journal, 25, N°4, pp. 799-806.

Major, J.J., and Pierson, T.C., (1992), "Debris flow rheology : Experimental analysis of fine-grained slurries", Water Resources Research, 28, N°3, pp. 841-857.

Coussot, P., and Piau, J.-M., (1993), "On the behaviour of fine mud suspensions", to be printed in Rheologica Acta.

Chang, S.H., Ryan, M.E., and Gupta, R.K., (1993), "The effect of pH, ionic strength, and temperature on the rheology and stability of aqueous clay suspensions", Rheologica Acta, 32, pp. 263-269.

Coussot, P., (1992), "Rhéologie des laves torrentielles", thèse de Doctorat de l'Institut National Polytechnique, Grenoble, France, 420p.

Coussot, P., and Piau, J.-M., (1993), "A large-scale field coaxial cylinders rheometer to study the rheology of natural coarse suspensions", submitted to Journal of Rheology.

O'Brien, J.S., Julien, P.Y., (1988), "Laboratory analysis of mudflows properties", Journal of Hydraulic Engineering, 114 (8), pp.877-887.

Takahashi, T., (1981), "Debris flow", Annual Review of Fluid Mechanics, 13, pp. 57-77.

Bagnold, R.A., (1954), "Experiments on a gravity free dispersion of large solid spheres in a Newtonian fluid under shear", Proceedings of the Royal Society of London, A.225, pp. 49-63.

Jaeger, H.M., Chu-dependent shearing of concentrated suspensions", Powders & Grains, Thornton Heng Liu, Nagel, S.R., and Witten, T.A., (1990), "Friction in granular flows", Europhysics Letters, 11 (7), pp. 619-624.

Kytomaa, H.K., and Prasad, D., (1993), "Transition from quasi-static to rate (ed.), Balkema, Rotterdam.

Phillips, C.J., and Davies, T.R.H., (1991), "Determining rheological parameters of debris flow material", Geomorphology, 4, pp. 101-110.

Coussot, P., (1993), "Steady, laminar yield stress fluid flow on an inclined plane - I General theory - ", to be printed in Journal of Hydraulic Research.

Coussot, P., and Bossan, E., (1993), "Steady, laminar yield stress fluid flow on an inclined plane - I experiments and comparison with theory - ", submitted to Journal of Hydraulic Research.

Bossan, E., (1993), "Lois d'écoulement des laves torrentielles", DEA de Mécanique, INPG.

Trowbridge, J.H., (1987), "Instability of concentrated free surface flows", Journal of Geophysical Research, 92 (C9), pp.9523-9530.

Laigle, D., and Coussot, P., (1993), "Numerical modelling of muddy debris flows", Pierre Beghin Workshop on Rapid Gravitational Mass Movements, Cemagref.

Models for disastrous mass movements

Modèles pour des mouvements en masse catastrophiques

T. R. DAVIES

Department of Natural Resources Engineering
Lincoln University, Lincoln - New Zealand
Tel. (64) 33 25 38 13 - Fax (64) 33 25 38 45

Abstract

This essay first examines the potential of theoretical and simulation models to predict the behaviour of mass movements, and shows why field data for calibrating semi-empirical and 'black-box' models will always be inadequate. The potential of small-scale physical models to fill this knowledge gap is then examined, and some difficulties and limitations of such models discussed. Finally, some experiences in physical modelling of powder-snow avalanches and debris flows are described, and the potential for modelling rock avalanches is investigated briefly.

Résumé

Cet article examine dans un premier temps, l'intérêt de modèles théoriques de simulation pour prévoir le comportement de mouvements en masse et montre pourquoi les données de terrain pour caler des modèles semi-empiriques ou "boîtes noires" seront toujours inadaptées. Les avantages présentés par des modèles réduits physiques pour combler les lacunes dans la compréhension des phénomènes sont ensuite détaillés. Les difficultés rencontrées lors de l'utilisation de ces modèles et leurs limites sont discutées. Enfin, quelques expériences de modélisation physique d'avalanche de neige poudreuse et d'écoulement de débris sont décrites et la possibilité de simuler des avalanches de roches est envisagée de façon succincte.

Introduction

Large-scale rapid mass movements have a serious impact on people living in hill and mountain regions. Each year many deaths and much damage result from landslides, debris flows, mudflows, rock avalanches, snow avalanches and lahars. There is an urgent need for better prediction of the hazard zone and potential magnitude of such events.

There is substantial research literature related to this subject, but there has been little direct application of this knowledge to the problem of saving lives. Recent developments in the understanding of non-linear processes, and of the nature of disasters, suggest that some redirection of effort is needed to develop the capability to predict and mitigate the effects of large rapid mass movements.

General Characteristics of Natural Processes

In recent years a radical development has occurred in the understanding of natural systems behaviour. It has become clear that many, if not most, natural processes that occur in the landscape can behave in a strongly nonlinear fashion, and that the behaviour of many landscape phenomena is thus likely to be chaotic;excellent examples are turbulence in flowing fluids, and weather systems. It is a characteristic of chaotic systems that, even if the equations governing the system behaviour are known, under some conditions the system is so sensitive to the precise value of initial conditions that its behaviour beyond a short time into the future simply cannot be predicted. Although more detailed knowledge of individual processes, and increased computing power, will undoubtedly allow better incorporation of more variables into more sophisticated simulations of system behaviour, repeating the simulation exercise with very slightly different initial conditions still leads to wildly different behaviour after a number of time steps, when the system is in the chaotic range. It is simply not practicable to define the initial conditions with the degree of precision needed to avoid this effect.

This idea, which is now widely accepted (Davies, 1989), implies a fundamental change in scientific investigations of landscape processes. There is little point in adding to the precision of the governing equations if the ability to predict the system behaviour is not thereby improved.

Predictive Possibilities

Since theoretical prediction is of very limited use in reality, emphasis could shift to empirical or semi-empirical models, perhaps guided by theory, but with a number of variables that can be adjusted empirically, or by trial and error, until the model fits well with the known field behaviour of the system. A major difficulty with the use of such models for predicting the behaviour of events that cause disasters, is that, by definition, field data describing such events are sparse and unreliable.

A natural event causes a disaster only if it significantly impinges on the lives and investments of people. People are not completely stupid; they do not live in such a way that ordinary natural events will threaten them. People locate themselves and their investments to be beyond reach of the usual behaviour of mass movements, floods, etc. Thus it is only the less usual events that cause disasters; events that tend to recur, on average, so infrequently that people `forget' that a particular location has been affected in the past. It is very difficult to collect field data on rock avalanche or debris flow processes, for example, because these events occur at times and places that are quite unpredictable and often difficult and dangerous of access - for example, at night, in severe storms, or earthquakes, in remote inaccessible valleys. Even when one is there, gathering useful data on velocity, depth, density, basal shear, etc., can be extremely dangerous. Clearly, we cannot expect good field data to be available to calibrate models of disastrous events.

There is an additional difficulty in that the behaviour of mass movement events will be location-specific, and empirical data relating to one location might not be transferable to others.

Dynamically Similar Small-scale Physical Models

River engineers have difficulties similar to those described above, in predicting the behaviour of rivers and their response to management, and have developed the art of physical modelling to a useful degree. In outline, a small-scale laboratory representation of the field (prototype) situation is constructed, using the laws of dynamic similarity deduced from dimensional analysis. This ensures that, although the detailed processes in the prototype are unknown, the model processes are dynamically similar and hence the model will behave in the same way as the prototype. This technique has been used routinely and successfully for many years, and is transferable to the behaviour of mass movement phenomena.

Dynamic similarity between model and prototype requires that certain dimensionless parameters must be the same in model and prototype; identification of these parameters requires a comprehensive list of the variables that characterise the situation. Omission of important variables leads to an incomplete set of dimensionless parameters, and therefore incomplete dynamic similarity; inclusion of unnecessary variables leads to unnecessary dimensionless parameters, which does not lead to incorrect results, but complicates the situation. Often, some knowledge of the processes involved in the physical situation allows relaxation of these criteria - for example, Reynolds' number similarity can be relaxed if the Reynolds' number of both model and prototype is greater than a few thousand.

Value and Uses of Physical Models

The great advantage of physical models is that the details of processes of the phenomenon need not be known; if we are confident of dynamic similarity, we can confidently predict prototype behaviour from that of the model. Thus, if the prototype behaves chaotically, so will the model. The problem of obtaining field data to calibrate semi-empirical models is much reduced, because data from physical models can be used instead; the latter are much more easily, reliably and precisely obtainable (under controlled laboratory conditions) than are the corresponding field data. In addition, it is often possible to build a location-specific physical model of a field situation with realistic topography (boundary conditions), in order to predict the hazard extent and to compare the effectiveness of a range of hazard modification strategies; alternatively, a "characteristic" or "general" model can be built, with rather simple boundary conditions, for calibrating an empirical model to which location-specific topography can subsequently be introduced.

In using physical models, a crucial requirement is to "prove" the model by demonstrating that it adequately represents prototype behaviour. For this, prototype data are again needed; however, because we can be reasonably confident of dynamic similarity, the amount of information needed for this is much less than is needed to calibrate semi-empirical or empirical models over a wide range of behaviour.

In essence, the great advantage of physical modelling is that process details are not necessary; we can be much more confident of achieving dynamic similarity than we can be of adequately describing processes, particularly in large rapid mass movements.

In practice, however, achieving dynamic similarity can be difficult; a variety of scale effects' can arise, circumventing which requires some ingenuity. Sometimes complete similarity is impracticable, and the model data must then be used with caution; even then, however, certain ranges of model behaviour can represent prototype behaviour very well.

It is interesting that making simplifications to the prototype situation, for example using single-sized spheres in a model to represent rocks in a rock avalanche, is not a constructive thing to do, since dynamic similarity between model and prototype is thereby endangered.

In summary, small-scale physical models offer access to improved data describing infrequent mass movement phenomena, which can be used to calibrate and test semi-empirical or black box models for predicting the behaviour of the phenomena. They can also be used directly to model specific mass movement hazards and devise mitigation strategies. The process of designing and proving such models is well known in hydraulic engineering (e.g., Yalin, 1971) and can be transferred to mass movement phenomena.

Examples of Mass Movement Models

Powder-snow Avalanches

This phenomenon is at the borderline between solid mass movement and fluid motion, but illustrates some useful points. Davies (1979) and Scheiwiller (1986) used respectively sand in water and polystyrene particles in water to model the density-current phenomenon of snow grains in air. The major criterion for dynamic similarity was a density-adjusted Froude number (ratio of inertial to gravity forces), and consideration was also given to the ratio of particle translation velocity to fall velocity. The linear scale of the model was 1 : 500, and the ratio of corresponding velocities 1 : 1000; Reynolds number of the model was 10^4, and of the prototype 10^8, which was satisfactory. This model was specifically designed to study the internal dynamics of powder-snow avalanches and to develop theoretical explanations, rather than to predict runout distances and pressure intensities. The main difference between model and prototype was in the nature of the solid grains; snow grains exhibit a wide range of shapes, sizes, densities and strengths, while the polystyrene grains were uniformly shaped, dense and strong while varying from 200 - 400 in size. The only attempt to demonstrate or "prove" the model was by observing that avalanches' in the model looked very much like real powder-snow avalanches, but, given the objectives of the study, this is understandable. Had prediction been the objective, more rigorous quantitative comparison between model and prototype would have been undertaken; gross data for this purpose on large avalanches are available from films.

Debris Flows

Again, these are somewhat intermediate between mass movements and channelised fluid flows, having some of the characteristics of both. During the last decade a lot of theoretical research on debris flows has made very little predictive progress, and little progress also in agreed understanding of processes, largely due to lack of field

or laboratory data on debris flow behaviour. Most laboratory work has involved severe simplification of the field phenomena, e.g., using bentonite clay, or PVC granules in water, or sand in water, to represent the behaviour of a huge range of grain sizes (metres to microns) in water; using steady flows to represent the highly unsteady surging behaviour of debris flows; and using Newtonian fluids to represent the strongly non-Newtonian behaviour of debris flow material. There is reliable velocity, depth and density information from one or two field sites in Japan and China. A very wide range of models for predicting debris flow hazard zones has appeared, all of which claim success.

To date there has been no published attempt to create a small-scale debris flow in the laboratory that is dynamically similar to field flows. The dimensional analysis is, however, relatively straightforward and suggests that a 1 30 model, using coal slack (density 1.5T m^{-3}) to represent large grains and a solution of wallpaper paste in water (viscosity ten times that of water) to represent the intergranular slurry of fine solids in water, should be able to satisfy Froude number and Reynolds' number similarity to a sufficient extent; I hope to report results of this exercise soon. Criteria by which the success of the attempt will be judged include its ability to display the significant differences in behaviour observed in the field between large (Jiangjia Ravine, China) and small (Mt Thomas, New Zealand) debris flows (Davies, 1993), and to represent accurately the quantitative behaviour of large flows reported by Kang *et al.* (1987). The major value of the technique, if successful, would be in predicting the height, velocity and runout path of debris flows resulting from known volumes of erosion in channels and on fans of known geometry, thus allowing reliable design of bridges and land use zoning.

Large Rock Avalanches ('Sturzstoms')

Rock avalanches with volumes greater than about 10^7 m^3 show mobility that increases with size; while the equivalent friction coefficient for events of less than 10^7 m^3 is about 0.5, that for events of 10^9 m^3 is about 0.1-0.2, and for a lunar event of 10^{12} m^3 is 0.06 (Hsü, 1975). A number of hypotheses to explain this phenomenon have been proposed, but no generally-accepted explanation has been adopted. It is clear that the local topography, as well as the volume of material, seriously affect the deposit location (or destruction zone). In this case, dimensional analysis must include the factor(s) that give rise to the varying friction coefficient. The most successful attempt at a physical model has been Hsü's (1975) representation of the Elm event at a scale of 1 : 4000 using a bentonite slurry to represent the mass of rocks that fell. This is clearly more of an analogue than a physical model, in that relevant factors such as the coefficient of restitution of the rocks have been subsumed into the rheology of the bentonite slurry, and to that extent dynamic similarity was not achieved. Thus, while the exercise gave valuable suggestions and possible insights (and, indeed, testable hypotheses - Davies, 1982), one cannot confidently use its results for the calibration of semi-empirical models or for direct prediction of specific situations.

It is nonetheless intriguing that the behaviour of the Elm event can be so well simulated by a very different material; in much the same way, fluid meanders in a very wide range of physical situations have startlingly similar geometries. Modelling by analogy is sometimes very successful in an *ex post facto* sense, but, until

we understand why, it cannot confidently be used for prediction, in case it doesn't work.

Conclusions

- Prediction of the behaviour of disastrous mass movements is hampered by the nonlinear and sometimes chaotic nature of the events.
- Since disastrous events are, by definition, rare, reliable field data are difficult to obtain.
- Small-scale laboratory physical models can provide reliable data on large mass movements.
- These data can be used to calibrate empirical or semi-empirical predictive models of disastrous mass movements.

References

Davies, P.C.W. (1989). The Cosmic Blueprint. Simon and Schuster, New York, 224 p.

Davies, T.R.H. (1979). The investigation of avalanche processes by laboratory experiments;exploratory tests. Internal Report, VAW, ETH-Zürich, 31p.

Davies, T.R.H. (1982). The spreading of rock avalanche debris by mechanical fluidisation. Rock Mechanics 15, 9-24.

Davies, T.R.H. (1993). Large and small debris flows occurrence and behaviour. Proceedings, Int. Workshop on Debris Flow, Kagoshima, Japan, 11-22.

Hsü, K.J. (1975). Catastrophic debris streams (Sturzstoms) generated by rockfalls.

Bulletin, Geological Society of America, 86, 129-140.

Kang Zicheng et al. (1987). A Comprehensive Investigation and Control Planning for Debris

Flow in the Xiaojiang River of Yunnan Province. Scientific and Technical Publishing Co., Changching, Sichuan, China, 285 p. (in Chinese).

Scheiwiller, T. (1986). Dynamics of powder-snow avalanches. Mitteilung No.81, VAW, ETH-Zürich.

Yalin, M.S. (1971). Theory of Hydraulic Models. MacMillan, London.

The field documentation of highly mobile rock and debris avalanches in the Canadian Cordillera

Les observations de terrain relatives à des avalanches très mobiles de rochers et de débris dans la Cordillère Canadienne

S. G. EVANS

Geological Survey of Canada
601 Booth Street Ottawa, Ontario - Canada K1A 0E8
Tel. (1) 613 996 76 48 - (1) 613 992 24 68

Abstract

Three highly mobile landslides, all of which have occured in this millennium, have been documented in the Canadian Cordillera. They are the Pandemonium Creek rock avalanche, which occurred in 1959 in the southern Coast Mountains of British Columbia (Evans et al. 1989) ; the 1984 debris avalanche from the western flank of Mount Cayley volcano in the Garibaldi Volcanic Belt of southwestern British Columbia (Evans et al. in prep.), and the Avalanche Lake rock avalanche, which occurred in the Mackenzie Mountains of the Northwest Territories sometime after the middle of the 15th century (Evans et al. in press).

Résumé

Trois mouvements de terrain très mobiles qui se sont tous les trois produits durant le présent millénaire ont été observés dans la Cordillère Canadienne. Il s'agit de l'avalanche de roches de Pandemonium Creek qui est survenue en 1959 dans le sud de la Chaîne Côtière de Colombie Britannique (Evans et al. 1989) ; l'avalanche de débris de 1984 descendue du flanc ouest du volcan du Mont Cayley dans la ceinture volcanique Garibaldi au sud-ouest de la Colombie Britannique (Evans et al., à paraître) et l'avalanche de roches d'Avalanche Lake survenue dans les montagnes Mackenzie, Territoires du Nord-Ouest, dans la deuxième moitié du 15e siècle (Evans et al. à paraître).

Pandemonium Creek rock avalanche

In 1959, a rock spur became detached from the headwall of a cirque near Pandemonium Creek in the southern Coast Mountains of British Columbia. Approximately 5 Mm^3 of blocky, quartz diorite debris travelled 9.0 km along a highly irregular path, descending a vertical distance of 2 km to the valley of South Atnarko River. The high mobility of the rock avalanche debris is manifested by

superelevation in valley bends in Pandemonium Creeck, two run-ups (the vertical) height of the first run-up in Pandemonium Creek was 335 m), and two right-angle changes in flow direction. Although most of the debris came to rest on the upper part of a fan at the mouth of Pandemonium Creek, one lobe traversed the fan and entered Knot Lakes where it generated displacement waves that destroyed trees along the shore.

Evans et al. (1989) present run-up and superelevation data which indicates that the debris was moving between 81 and 100 m/s as it entered the run-up at Pandemonium Creek and 21-38 m/s as it moved through the bends in Pandemonium valley. These velocities were analysed by applying the dynamic model of Körner (1976) to the path of the landslide. The analysis suggests that the rock avalanche had two phases : a very rapid initial phase from detachment to the beginning of the run-up (mean velocity 74 m/s), and following, sudden energy losses at the run-up, a second phase involving much lower velocities (mean velocity 22 m/s).

Mount Cayley debris avalanche

In 1984, a mass of Quarternary pyroclastic rock (est. vol. 0.52×10^6 m^3) detached from the western flank of Mount Cayley volcano, in the Garibaldi volcanic belt of southwestern British Columbia. The rock mass formed a debris avalanche that travelled up to a horizontal distance of 3.46 km from its source over a vertical distance of 1.18 km yielding a fahrboschung of 19° before being transformed into a debris flow. From the superelevation of the debris trimlime it is estimated that velocities in the debris avalanche reached at least 31 m/s.

The debris avalanche deposits consist of large fragments up to 3 m in diameter set in a finer matrix of pulverised tuff. Above the trimlines pulverised tuff is found on the upslope side of trees and branches are stripped off up to 20-30 m above the trimline indicating that the passage of the debris was accompanied by an airbourne cloud. Such evidence of an airbourne cloud was not observed along the margins of the Pandemonium Creek event where similar velocities were calculated from superelevation of trimlines in bends.

The damage to vegetation along the debris avalanche path is very similar to that observed along the margins of a snow avalanche path and suggests that the avalanche moved partly as a turbulent powder avalanche of pulverised tuff, a movement mechanism that is consistent with the evidence of remarkable wind damage to trees along the margins of the path documented by Lu (1988) and Cruden and Lu (1992).

The debris avalanche exhibited mobility characteristics of debris/rock avalanches with debris volumes approximately two orders of magnitude greater and is termed hyper-mobile. The event shows similar mobility characteristics to hyper-mobile slides of comparable volume in porous Chalk and loosely compacted coal mine waste. An impact collapse mechanism is hypothesised to account for the hyper mobility of the 1984 Mount Cayley event in which pore pressures are generated by the impact collapse of the highly porous tuff structure. The debris avalanche is one of seven high velocity debris avalanches to have occurred in the Garibaldi Volcanic Belt of southwestern British Columbia since 1855.

This interpretation of the Mount Cayley event differs substantially from that of Cruden and Lu (1992).

Avalanche Lake rock avalanche

The landslide is located in the Backbone Ranges of the Mackenzie Mountains, in Canada's Northwest Territories and was first described by Gabrielse et al. (1973) and Eisbacher (1979). The landslide involved the detachment of about 200 x 10^6 m^3 of rock from a dip slope in massive Denovian carbonates. It is noteworthy because of a remarkably planar detachment suface consisting of bedding planes in the carbonate sequence dipping at 30°, and a spectacular run-up on the opposite valley side onto a topographic feature called the Shelf.

The interpretation of events at Avalanche Lake has recently been subject to controversy. Kaiser and Simmons (1990) presented a reassessment of transport mechanisms of several rock avalanches in the Mackenzie Mountains of northwest Canada in which their central hypothesis is that the mobility of some rock avalanches was "assisted" or influenced by the presence of glacial ice, supposed by the authors to have existed at the time of rock avalanche occurence, i.e. the late Pleistocene. With respect to the Avalanche Lake rock avalanche, Kaiser and Simmons (1990) assert that the mobility noted above could only have been achieved with ice in the valley and that without it the runup would be "physically impossible" (p.137). This finding is in contrast to Evans (1989) who presented evidence which suggested that the Avalanche Lake event occurred in the Holocene sometime after 1450 A.D., that the mobility of the rock avalanche is real and not apparent, and that is was not assisted by the presence of glacier ice in the valley.

In a further work, Evans et al (in press) present additional evidence which indicates that the rock avalanche occurred in an ice-free environment. It consists of observations on the nature of the detachment surface, the morphology and location of the rock avalanche debris, the presence of levees in the debris and isolated patches of debris on valley side slopes, and the entrainment of alluvial deposits and conifer fragments from the valley floor in the Shelf Lobe debris. Additional raidocarbon dating of the entrained wood in the debris indicates that the landslide took place in this millennium, no earlier than about 1460 A.D.

Based on this evidence the behavior of the rock avalanche is reconstructed. It is characterised by dramatic mobility in which the rock avalanche split into two parts. The west part smashed into the opposite valley side and about 5 x 10^6 m^3 rode up onto the Shelf. The remainder (155 x 10^6 m^3), fell back into the valley, partially running back up the detachment surface to an elevation 360 m above the valley, and then, reversing direction again, ran back into the valley bottom where it was deposited. The east part, the South Lobe (40 x 10^6 m^3) ranout down a valley re-entrant opposite the detachment surface. The maximum vertical drop in the path is 1220 m, the maximum run-up is 640 m. The fährboschung for the Shelf Lobe is 8° and for the South Lobe is 10°.

In a paper at this symposium, Hungr (1993) simulates the run-up onto the Shelf indicating that the presence of glacier ice is not necessary to account for the run-up magnitude. It is estimated that maximum velocities during the movement reached 80

m/s. The run-up (640 m) is the highest recorded in the world and on an empirical run-up plot is highly anomalous in relation to the height of the descent slope. The case history demonstrates that massive detachments have taken place in the Mackenzie Mountains in the comparatively recent past.

All three rapid mass movements exhibit several aspects of mobility, the simulation of which are useful tests of a dynamic model. It is hoped that other specialists in the field may wish to use these data to test or calibrate their dynamic models. In addition, the case histories illustrate the importance of detailled field observations in the reconstruction of rapid mass movement events and that major differences in the interpretation of the timing and sequence of events may result.

References

Cruden, D.M. and Lu, Z.Y., 1992. The rockslide and debris flow from Mount Cayley, B.C. in June 1984. *Canadian Geotechnical Journal*, 29: 614-626.

Eisbacher, G.H. 1979. Cliff collapse and rock avalanches (sturzstroms) in the Mackenzie Mountains northwestern Canada. *Canadian Geotechnical Journal*, 16: 309-334

Evans, S.G. 1989. Rock avalanche run-up record. *Nature*, 340: 271.

Evans, S.G., Clague, J.J., Woodsworth, G.J., and Hungr, O. 1989. The Pandemonium Creek rock avalanche, British Columbia. *Canadian Geotechnical Journal*, 26, 427-446.

Evans, S.G., Hungr, O., and Enegren, E. (in press). The Avalanche Lake rock avalanche, Mackenzie Mountains, Northwest territories, Canada : description, dating, and dynamics. *Canadian Geotechnical Journal*, 31.

Evans, S.G., Hungr, O., and Clague, J.J. (in prep.). A hyper-mobile debris avalanche in the Garibaldi Volcanic Belt, *British Columbia*.

Gabrielse, H., Blusson, S.L., and Roddick, J.A., 1973. Geology of Flat River, Glacier Lake, and Wrigley Lake Map-areas, District of Mackenzie and Yukon Territory. *Geotechnical Survey of Canada*, memoir 366.

Hungr, O. 1993. Mass-referenced flow model dynamic analysis of flow slides and avalanches. Paper presented to the Pierre Beghin International Workshop on Rapid Gravitational Mass Movements, Grenoble, France.

Kaiser, P.K., and Simmons, J.V., 1990. A reassessment of transport mechanisms of some rock avalanches in the Mackenzie Mountains, Yukon and Northwest Territories, Canada. *Canadian Geotechnical Journal*, 27: 129-144

Körner, H.J., 1976. Reichweite und Geschwindigkeit von Bergstürzen und Fließschneelawinen. *Rock Mechanics*, 8: 225-256.

Can we define a unique friction coefficient for a non cohesive granular material ? A temptative answer from the point of view of sand avalanche experiments

Peut-on définir un coefficient de frottement unique pour un matériau granulaire sans cohésion ? Une tentative de réponse fondée sur des expériences avec des avalanches de sable

P. EVESQUE

Laboratoire de Mécanique : sol-structures-matériaux
Ecole Centrale de Paris, 92295 Chatenay-Malabry - France
Tel. (33) 41 13 12 18 - Fax (33) 41 13 14 37

Abstract

We demonstrate using centrifuge experiments (10-1000m/s^2) on sand avalanches with different piles built at different densities that
i) grain cohesion is negligeable,
ii) the avalanche size and the average maximum angle of repose depend on the initial pile-density and on the mean stress. Our data are quite consistent with those obtained from other tests of soil mechanics in particular on what concerns the friction angle.
iii) but that the internal friction angle fluctuates within 2° from experiment to experiment so that this parameter is not a well defined macroscopic quantity.

Résumé

A l'aide d'expériences en centrifugeuse (10-1000 m/s^2) réalisées sur des avalanches de sable avec des densités initiales variables, nous démontrons les points suivants :
i) la cohésion entre les grains est négligeable ;
ii) la taille de l'avalanche et l'angle maximum moyen de repos dépendent de la densité initiale et de la contrainte moyenne.
Nos données sont cohérentes avec celles obtenues lors d'autres tests en mécanique des sols, en particulier pour ce qui concerne l'angle de frottement ;
iii) cependant, l'angle de frottement interne varie dans une fourchette de 2° d'une expérience à une autre ; il ne constitue donc pas une grandeur bien définie d'un point de vue macroscopique.

Introduction

Since Coulomb, we know that the mechanics of soil is mainly governed by a friction angle ϕ; since Reynolds we know that granular materials which deform generate dilatancy effect. More recently, experiments using triaxial test [1-4] have measured these effects quantitatively and demonstrated that this dilatancy effect depends on the mean stress supported by the material and on the initial pile density. In particular, it has been proved that this dilatancy effect modify the effective stiffness and the stress-strain behavior of the material. But a question arises then: are these quantities perfectly well defined at a macroscopic level or not; are they fluctuating; are they equal when measured by two different methods?

As a matter of fact, much work has been done recently to understand the mechanism of sand avalanches [2-13]; this is mainly due to the pionnering discrete model of Bak, Tang and Wiesenfeld (BTW) which generates a self-organized critical state [5,6]; it considers the problem as a true 2-D surface flow; it predicts large fluctuations of 2-D avalanche sizes and 1/f noise. On the other hand, most experimental investigations on real pile do not get such large 2-D fluctuations [3, 8-10, 12, 13], except when very small piles are concerned [3, 11-13]; for instance, it has been observed experimentally that the typical avalanche volume scales as the pile volume and not as the pile surface [3, 8-10, 12-13]; this means in particular that its size is characterized by a variation $\delta\theta$ of the free surface inclination and that two different values of the free surface inclination, before θ_b and after θ_e the avalanche, have to be defined. ($\delta\theta = \theta_b - \theta_e$; θ_b is also called the maximum angle of repose (MAR)).

Owing to this, I have proposed [3] to make a parallel between sand-avalanche behaviour and typical results of triaxial test in soil mechanics. Using such an analogy, I have been able to predict that the maximum angle of repose (MAR) θ_b should reflect mainly a unique friction coefficient ϕ, but differs from it by a quantity $\delta\theta = \theta_b - \phi$ which depends on the difference $d - d_c$ between the real pile density d and a reference one d_c (which is also called the "critical" density by soil mechanics); from this point of view, $\delta\theta$ is a measure of the dilatancy effect and is expected to tend to zero when $d \to d_c$. Grain elasticity, grain cohesion, water pressure and water flow are also quite relevant parameters and determine the avalanche size too. One way of separating dilatancy- and cohesion-&/or-elastic-effects is to vary gravity and density.

So, this work is devoted to study the physics of sand avalanches under gravity using a centrifuge and at controled density, to determine if the maximum angle of repose (MAR) θ_b and the avalanche size $\delta\theta$ are governed by the sand density, by grain cohesion or by grain elasticity and to demonstrate that sand avalanches may be understood within the same concepts as triaxial test results. More details may be found in [13]. I will focus here *on discussing whether the friction angle ϕ is unique or not.*

Experimental set-up and procedures

We have prepared by pluviation different homogeneous parallelepipedic samples (0.4*0.4*O.15 m3) of the same "normalized" Hostun sand [14] at different densities and have performed on each of them a series of avalanches at different gravity fields using the 5.5 m-radius centrifuge of the Laboratoire Central des Ponts et Chaussées in Nantes. Due to sample- and centrifuge-sizes, the acceleration homogeneity is not better than 3%. Vibrations inside the centrifuge may be neglected, but a special careenage has been designed to prevent any wind perturbation.

Hostun sand [14] is a sieved ground silicate sand from Grenoble neighbourhood. The density range which may be achieved by varying the pluviation parameters (which are the flow and the fall height) is 1.45-1.68; but keeping the same pluviation parameters leads to the same pile density within less than 1%.

The experimental avalanche device is sketched on Fig. 1: it is located in the centrifuge nacelle. It consists in a parallelepipedic container filled with Hostun sand, which can rotate slowly around an horizontal axis; this generates a set of successive avalanches; the flowing sand is collected by a box, where it is weighted. A video camera records the surface flow and allows to measure the height of the remaining sand. So, we have determined the angles of the free surface just before (qb) (qb=MAR) and just after (qe) any avalanche, their difference dq and the avalanche weight as functions of the gravity and of the initial density d.

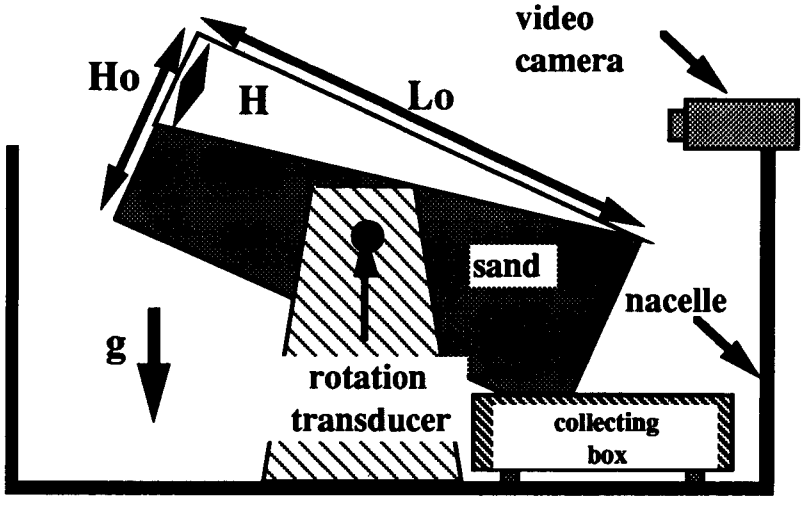

Figure 1: Experimental set-up.

The experimental procedures

The process to fill the box with sand at a controled density uses the pluviation method; it lasts about 5 hours, which is quite large compared to the running time of the centrifuge.

As a result, we have decided to record a whole series of avalanches for each sample preparation for most experimental procedures, even if the real pile density

was well defined for the first avalanche of each sample only. But sandpiles exhibit story effect, so that we expect that the results depend on the protocol, which has to be defined rigourously.

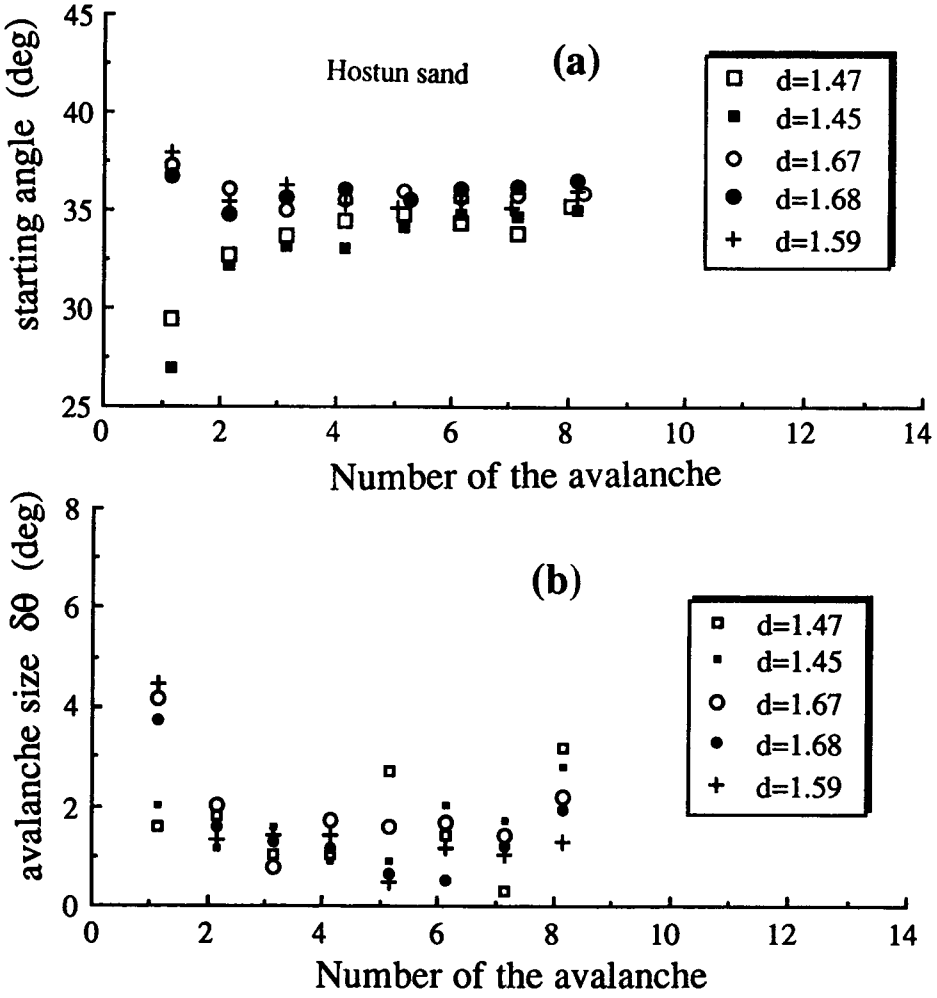

Figure 2: Evolution of the avalanche characteristics after a series of avalanches at 100G, for different initial densities.

One way to proceed is to increase gravity to a given value G_1=100G and to perform a series A_1 of few (A_1=8) avalanches and to record the evolution of their characteristics (θ_b(i), $\delta\theta$(i), θe (i), mass(i)) as a function of their number i in the

series ($1 \leq i \leq A_1$). These results are reported in Fig. 2a for θ_b, and in Fig.2b for $\delta\theta$. This set of experiments was devoted also to check the reproducibility of the results and we have repeated this experiment, on the two extreme packing densities. Indeed, Fig.2a demonstrates that the data are reproducible (within a given uncertainty).

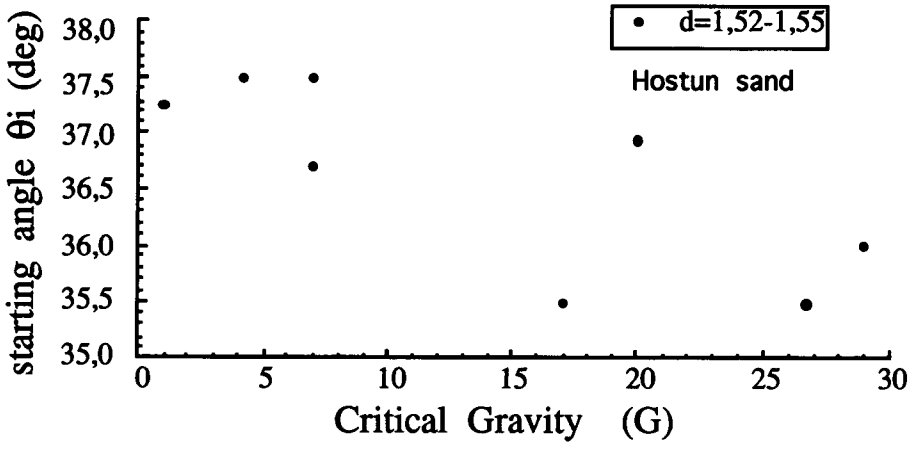

Figure 3: Dilatancy as function of G.

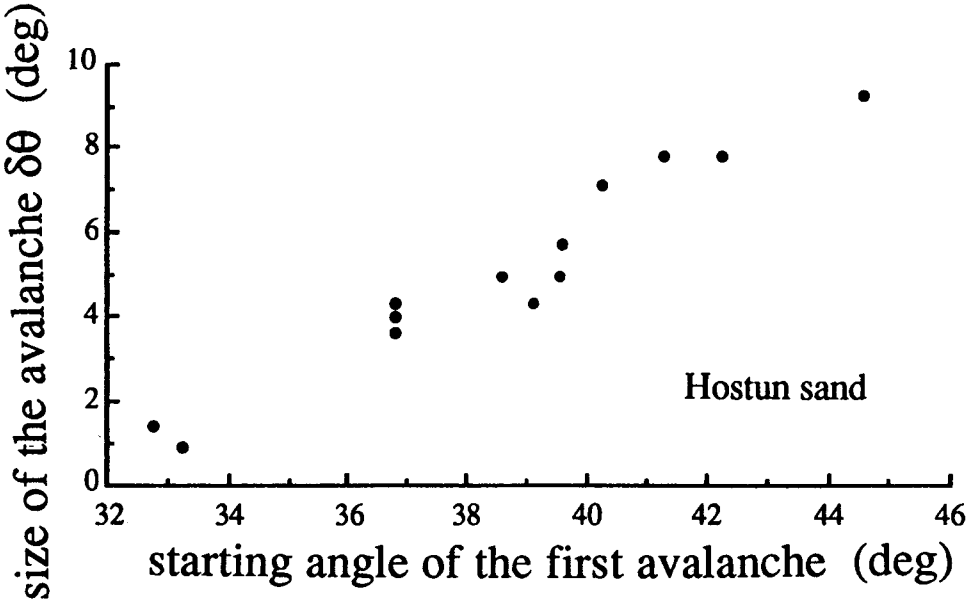

Figure 4: $\delta\theta$ vs. θ_b for Hostun sand.

However, an other way to proceed is to begin increasing the angle θ from 0 to a given value θ_b at G=1 and then to increase G till an avalanche occurs; this last procedure allows to demonstrate that the maximum angle of repose θ_b depends on the gravity field (cf Fig. 3). Furthermore, looking for a protocol dependence, we have tried other procedures, which have lead to other results published elsewhere [13]. But we can sum up part of these data by plotting $\delta\theta$ as a function of θ_b,; this is reported in Fig. 4.

Data analysis

Fig.2a confirms that our experiments are reproducible. We observe also from Fig. 2 that θ_b evolves spontaneously as a function of the number of the avalanche in the series; obviously, this evolution depends on the initial pile density since θ_b is continuously increasing for the loose packings (d=1.45) and continuously decreasing for the dense packings; but they both converge eventually to a common limit value which is about 34°-35°, rather independent of the initial density.

Coherence with triaxial test results

These behaviors may be understood within the framework of the "critical" state model of avalanches [3]: let us assume that the pile density d near the free surface evolves spontaneously due to successive avalanche processes till it reaches the so-called "critical" state density dc eventually. In this case the limit value of θ_b (i.e. 34°) will be equal to the internal friction angle ϕ measured at large deformations by triaxial cell apparatus, so that it will be independent of d. From the literature, we find that ϕ=33-35° for Hostun sand [14], [Biarez private communication]; this is the value found here. Furthermore, this theoretical approach agrees also with the facts that θ_b should increase continuously when the initial pile is loose and should decrease when the initial pile is dense, which confirms then the "critical" state analysis.

However the "critical" state analysis [3] does not explain the existence of macroscopic events when the pile is loose since this model predicts a small and continuous evolution of the pile slope instead of the observed macroscopic variations of the slope inclination $\delta\theta$=1° as exhibited in Figs. 2b for d=1.42, 1.45, 1.47. Looking for more information on these events, we have measured the weight of the flowing sand using the box device of Fig. 1 and have found that these events do not correspond to a real flow, (no sand has been collected in the box after these events); this demonstrates that these two first events correspond to macroscopic volume-change, each of them being of about 5%, so that the mean pile density after these two events is increased to about 1.6. To the best of our knowledge, this is the first evidence of such a macroscopic densification process. These two features -existence of "avalanches" for slopes smaller than ϕ and existence of a macroscopic densification- might perhaps be understood within the frame work of Evesque and Sornette [15] on the dynamical system approach of the deformations in non-cohesive soil which demonstrates that deformation localizations in soil are sub-critical bifurcations.

Effect of gravity on the maximum angle of repose θ_b

Fig. 3 results have been obtained using the second protocol (i.e. the container has been first inclined at 1G at a given initial angle θ_b, the gravity has then been increased till the first avalanche occurs, this value of Gas then been plotted as a function of θ_b. The aim of this experiment is to focus on the behaviour of a sample built at a density just above the critical density d_c (i.e. 1.52-1.54 for Hostun sand) and to determine the variations of its dilatancy -or-cohesion effect as a function of gravity.

Fig. 3 demonstrates that the larger the gravity, the smaller the maximum angle of repose. Our data prove either the existence of a cohesion effect, the strength of which diminishes when increasing gravity, or that the "critical" density d_c increases when increasing G, which reduces also the dilatancy effect. (This is predicted by the Schofield & Wroth approach of avalanches [2, 3] since d_c increases with the mean stress). Anyway, we remark that the width of the curve corresponds to about 2° and is independent of gravity so that these fluctuations are not linked to cohesion.

Relationship between density, avalanche size and maximum angle of repose θ_b

Turning now to the variations of the avalanche size, (cf Fig. 2b), we note first that a correlation exists during the first avalanches of each series between the initial density and the avalanche size $\delta\theta$, (the larger the density the larger the avalanche); for instance we find first avalanche sizes of about $\delta\theta$=4° for the densiest packing instead of 1 or 2° for the looser packings. (This is confirmed by fig. 4 data).

In soil mechanics, the notion of the "critical" state is linked to the existence of a unique macroscopic friction coefficient ϕ and of a dilatancy effect. This last one depends on the difference d-d_c between the real pile density and the so-called "critical" one d_c. Furthermore, one finds that d_c depends on the mean stress. When one applies this theory to avalanches [3], one can define an effective friction coefficient ϕ_{eff} which depends on d and which is equal to the maximum angle of repose θ_b; as ϕ is the ending angle, the avalanche size $\delta\theta$ is ϕ_{eff}-ϕ. So this theory predicts a linear dependence between $\delta\theta$ and θ_b-ϕ, the slope of which should be equal to 1; this is what we observe experimentally on Fig. 4 where we have collected most of the data obtained on Hostun sand. However, we observe also large fluctuations on this figure.

Analysis of the fluctuations

We note that the widths of the curves in Figs. 3 & 4 correspond to uncertainties of about 2°. In the same spirit, we note in Fig. 2 that the limit value of θ_b fluctuates within 2°, that a mean avalanche size $<\delta\theta>$ of about 2° is reached after the transient regime a limit regime. We note also that this $<\delta\theta>$=2° value compares well with the other data from the literature [3,8-13] obtained with other devices on different silicate granular materials (glass spheres of different diameters, sand of different size).

It seems to us that the simplest way to integrate these fluctuations into the physics of the avalanche size is to assume the "critical" state to be governed by an erratic

process as if the internal friction angle ϕ is not be defined within an accuracy better than 2°. We can try and test this hypothesis and look at triaxial test curve to demonstrate the existence of such fluctuations in the internal friction angle ϕ. It is accepted that the scatter of the experimental data from a triaxial test to an other one allows to measure the friction angle within an accuracy of 2°, since large deformations without yieldings and localizations in a homogeneous sample are extremely difficult to obtain; however, if we examine carefully each triaxial test curve, we find that the stress-strain experimental curves are smooth in general; its fluctuations correspond to $\delta\phi$=0.5°, so that we cannot be completely certain that these $<\delta\theta>$ and θ_b fluctuations in avalanche experiments are completely linked to fluctuations of ϕ and not induced directly by some non-linear relaxation process involved in the avalanche mechanism.
One can ask whether the fluctuation amplitude ($\delta\phi$=2°) depends on the material or not. This is why we have studied recently avalanches on Fontainebleau sand and on rice, for which we have measured different mean experimental avalanche fluctuations $<\delta\theta>=\delta\phi$: 1° and 4° respectively.

Conclusion

As a conclusion, we think that these experiments demonstrate the existence of a density effect which is more or less in agreement with triaxial data [2, 3] and with the "critical" state analysis [2, 3]: in particular, we have shown that the denser the packing the larger the maximum angle of repose and that the first avalanche size $\delta\theta$ depends on the packing density and on the maximum angle of repose θ_b.
We have found that a limit regime is reached after few avalanches. It is characterized by a typical avalanche size $<\delta\theta>$=2°. These results seem to us very stimulating since they demonstrate that the typical limit of the avalanche size ($<\delta\theta>$=2°) is gravity independent. The simplest way to interprete these facts is to assume that the friction angle is a random value, within an uncertainty of 2°. An other important result is that a macroscopic discontinuous densification occurs in the case of very loose packings. These two effects were not known and not forecast by soil mechanics.
As a final remark, part of this work was motivated by the search of a parameter controling the avalanche size; it succeeded clearly to demonstrate that density is one of them (as we thought), but it appears that we are not able to make the avalanche size to vanish and to get a state of critical bifurcation, obeying the BTW model, as we were hoping. It is still possible that an other parameter controls the avalanche size, so that we hope that this work will stimulate further developments on avalanche experiments in centrifuge.

Acknowledgement

I want also to thank E.S.A., M.R.T., L.C.P.C., Région Nord-Pas-de-Calais, GRECO-géomatériaux, GDR milieux hétérogènes complexes and C.N.R.S. for partial financial support.

References

A.N. Schofield & C.P. Wroth, 1968, Critical State of Soil Mechanics (Londres, Mc Graw-Hill).

P. Evesque, 1990, J. Phys. France, 51, 2515-2520.

P. Evesque,1991, Phys. Rev. A43, 2720.

Habib, 1986, Revue Franç. Géotechnique, 31, 5

P. Bak, C. Tang & K. Wiesenfeld, 1987, Phys. Rev. Lett., 59, 381.

C. Tang & P. Bak, 1989, Phys. Rev. Lett., 60, 2347.

L.P. Kadanoff, S.R. Nagel, L. Wu & S.-M. Zhou, 1989, Phys. Rev. A39, 6524.

P. Evesque & J. Rajchenbach, 1988, C. R. Hebdo. Acad. Sci. Paris Série II, 307, 223.

H.M. Jaèger, C.H. Liu & S. Nagel, 1989, Phys. Rev. Lett., 62, 40.

P. Evesque& J. Rajchenbach, 1989, Poudres et Grains, Eds. J. Biarez et R. Gourvès (Balkema, Rotterdam), p. 217-224.

G.A. Held, D.H. Solina, D.T. Keane, W.J. Haag, P.M. Horn & G. Grinstein, 1990, Phys. Rev. Lett., 65, 1120.

P. Evesque, D. Fargeix, P. Habib, M.P. Luong & P. Porion, 1993, Phys. Rev. E47, 2326

P. Porion &P; Evesque, 1993, pp. 327-332, in Powders & Grains, ed. C. Thornton, Balkéma, Rotterdam

E. Flavigny, J. Desrues& B. Palayer, 1990, Rev. Franç. Géotech. 53, 67.

P. Evesque &D. Sornette,1993, Phys. Lett. A173, 305-10

Computer tools for risk management of slopes ; the XPENT system for slope stability analysis

Outils informatiques pour la gestion des risques liés à la pente ; le système XPENT pour l'analyse de la stabilité des pentes

R-M. FAURE

ENTPE
Rue Maurice Audin, 69518 Vaulx en Velin Cedex - France
Tel (33) 72 04 70 25 - Fax (33) 72 04 62 54

Abstract

Computer tools for risk management in case of slope instability are presented in this paper. With them, the geotechnician will be able to face any emergency and provide the best analysis of the slope.

Résumé

Cet article présente des outils informatiques destinés à la gestion du risque dans le cas des pentes instables. Avec l'aide de tels outils, le géotechnicien sera capable de faire face à toute situation de crise et de réaliser la meilleure analyse de stabilité pour une pente donnée.

Introduction

The expert system, XPENT, for slope stability, was presented in 1988, (Faure et al. 1988) at the Lausanne International Conference. The aim of the research presented was to provide the geotechnician with help in analysis of a failure and in definition of the best reinforcement design. In figure 1 one can see that other aspects were also taken into account, such as computer aided teaching and diagnosis during crisis. The latter point was made in a recent thesis (Mascarelli D, 1994) and consequently it is possible to decide upon some tools for risk management (Mascarelli D, Faure R.M, 1993). In the case of a crisis, the slide has just occured and the expert is not in a good position to perform a detailed analysis. Everybody is in a hurry, the data, most of which incorporate visual facts, are uncertain and incomplete and the expert has to produce the design which will best avoid the risk. One of the best aids that he can have is a computer aided design system which can take into account all kinds of data and can simulate all kinds of reinforcement design. That is to say, that we have to build a complete model of the slope with very little numerical informations, that are enhanced, step by step, using powerful tools of simulation. The present paper

tries to describe this challenge and defines the necessary computer tools that are useful for the expert.

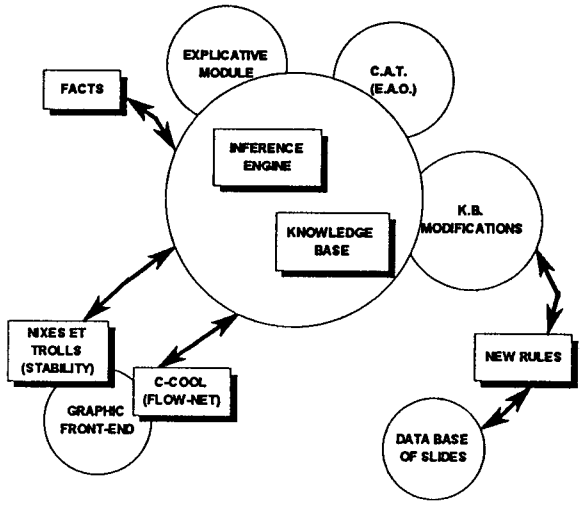

figure 1 GENERAL CHART OF **XPENT** (1988)

An accurate definition of a landslide

In order to help the expert in his analysis or reinforcement design, the computer model is built with a very accurate description of the world of landslides. This large description and the need for reasoning imply some important consequences such as :

Powerful computer software

To facilitate the use of empirical knowledge and declarative facts an object oriented language is necessary. In order to provide reasoning capacities the "Le Lisp" language was choosen. In fact we have used in the development of the expert system higher level languages such as Aida, Masai, Smeci, all from the Ilog company, which are layers of software that are easy to use (Neveu et al, 1990).

A new and more accurate classification of slides

For more than a century geotechnicians have tryed to classify earth slides. Numerous classifications have been developed and the last one was given by the World Landslides Inventory working group (Cruden, 1991). We find in this classification an attempt to go beyond the descriptive geology, but the mechanical aspects are not sufficiently taken into account. To overcome this weakness, a new description including the velocity and the stage of movement has been proposed (Vaunat et al, 1994).

A detailed description of the actions

When actions are combined to secure a slide they are not employed without order. By means of a SADT (structured analysis design technique) approach the sequences of all possible actions are established and put in the computer as guideline for reasoning. So the program can only propose realistic scheme of repair. This very important job is done through two thesis (Ke, 1990), (Mascarelli, 1994).

Quick input

One of the most important features of the system is the speed of the input. But with this speed, integrity of the data have to be ensured. Happily graphic input can provide both safety and speed.

Input of visual facts

Iconography is now available on small computers and with it, it is possible to propose to the user a description by means of images or sketches for the necessary concepts we use in the study. However, the textual input is still used by means of checking lists which are displayed to the user. We have simple choice lists where the computer checks the unicity of the answer, and several choices lists. All these inputs are gathered in screens that we can access in any order, and consequently the input time is considerably reduced. This approach gives new ideas for the agreement of a data base for landslides. Following the works done by the World Landslides Inventory, a version has been developed with the parameters used by the Working Group. It will be soon available on international networks to facilitate data exchanges on landslides, with full details as to permit comparative studies.

Simplified ground model

Ground Elevation Models (GEM) are powerful tools but are scarcely useful for the management of a crisis. This is for two main reasons: first, the geometrical data are too accurate and are stored in a very big file not easy to use on a PC, and, second, the indices useful for the geotechnician are not available in it. A specialised GEM. has thus to be built by the user. The starting point is the usual map of the site that is first digitalised through a scanner and then displayed on the screen. An extensive icon menu allows the setting on the map three kinds of feature that are localized on the map by the use of the computer mouse. Thus, they are:

- points, such as springs, blocks, boreholes, etc ;
- linear details such as electric wires, fences, roads, etc ;
- surface details such as buildings, woods, wet areas, etc.

The reference of the map allows the coordinates of those elements to be obtained directly and thus, knowledge of the relative position of each element with respect to others is easily available. For the elevations, the user can define specific lines such as crests, wedges and particular points. Subsequently, the elevation at any particular point can be determined through linear interpolation. Very quickly, all the remarkable features are placed on the map and the data of the ground note-book, filled during the site visit, are easily stored in the computer. The GEM with such

data can be recognised as a Geographic Information System (GIS) for the management of landslides (Faure and Mascarelli, 1993).

Vulnerability

A special item can be associated to each object entered in the GIS showing, either the value of a specific parameter, or a particular attention for works, and in that way, to give some orientation for the reasoning. The remedial works can be thus, clearly defined in terms of values. For the evaluation of hazard, discussed later on, the vulnerability is settled and to compute the risk the well known equation, Risk=Hazard*vulnerability, is used (Vaunat et al,1992).

Underground representation

To define the sub-soil the behaviour of an expert is followed step by step, the geotechnician makes hypotheses that have to be confirmed by other data or reasonings. The user starts with a borehole and sets some hypothesis about the layers. The neighbouring borehole can confirm or contradict this hypothesis. In the case of contradiction the user has to propose a new hypothesis. The process goes on for all vertical profiles and finally a complete 3D model is developped. At each step the computer can display the consequeces of the hypothesis on the screen under the form of diagrams, profiles or maps. Some geostatistical checks can be done layer by layer and the data of a borehole can be verified by an expert system (Zelfani, 1993 ; Zelfani et al, 1992). Figure 2 shows the general sketch for establishing the 3D description of the subsoil.

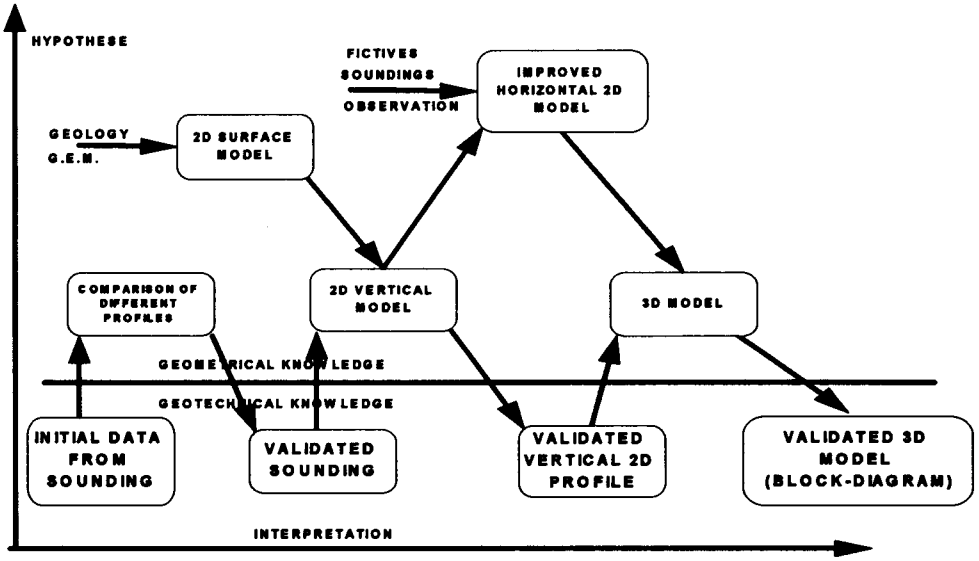

SKETCH FOR COMPLETE ELABORATION OF SUB-SOIL MODEL

Figure 2.

Geotechnical and spatial reasoning

Expert rules

To give an efficient help to the geotechnician, reasoning is introduced as expert rules with regard to geotechnics and spatial relations. It is very useful to be able to manage the relative position of two layers following the correspondance of two boreholes. Other more simple rules are used for setting the range of the soil parameters for the soils known only by their name. It is the completeness of this set of rules which gives the reasoning power to the system.
The establishment of the rules has been made using the Knowledge Oriented Design (KOD) method for the analysis of the speach of the experts (Vogel, 1988), (Faure et al, 1991).

Checking consistency

Through his answers to the system the geotechnician may introduce non consistent facts that ought to be discovered by the computer as to follow a realistic and logical reasoning. At each step, tools from geostatistics can be used to evaluate the consistency of the soil model, and the dialog between the expert and the computer allows back trials.

The slope simulator

Real data and computed data

At this stage of the study geotechnical profiles may be given by the computer with all the necessary informations. An editor profile allows this operation and it is a profile validated by the user, that is used for the following calculations.

Links with calculus codes

Analysis methods give a quantification of the stability. It is a particular useful tool for comparing two designs of reinforcement. In slope stability the most important input is quite often the hydraulic flownet and it is necessary to check that the hypotheses which define it gives results corresponding to pore pressure observations or field measurements, otherwise an adjustment of the parameters is necessary. It is done by C-COOL, a finite element program for saturated and unsaturated soils (Vaunat,1990). For the calculation of the stability, a profile editor sets up a data file used by NIXES ET TROLLS, a versatile slope stability program developed in France (Faure et al., 1985).
The interface between these programs is very complete providing the user with a powerful slope simulator. He is thus able to check, in real time, the importance of each parameter involved in the stability of the slope. It is easy to recognize the most important parameters for which a more accurate and detailed investigation is necessary. The user can appreciate the c-ϕ curve corresponding to conditions at failure, or the diagram giving the safety factor F as a fonction of the water level. To some extend that gives an estimation of the hazard for evaluating the risk (Vaunat et al., 1992).

Sketches of reports

All the information, that supplied by the user, and the rest deduced or calculated by the computer, is well ordered and stored in the computer. Consequently, it is easy to use the computer in order to elaborate and present different kinds of report with graphics, pictures and charts needed in a slope study. For this, links are established with an usual word-processing software that allows an individualization the report.

Conclusion

All these functions are being integrated in the expert system XPENT, and some aspects have been down sized for use on a 486 PC. The development on workstation is going ahead with the help of several universities. This year the use of "fuzzy logic" will be introduced for the definition of the reinforcement. In another way, the use of international network ought to enhance this cooperation, for the first time with the WASSS project following the work of the Word Landslide Inventory.
Ultimately, XPENT will be a complete and powerful tool for crisis management in the situation where a slide occurs, and also for the design of any kind of reinforcement.

References

Cruden D. (1991) A simple definition of a landslide. Bul. of the Int. Association of Engineering Geology pp27-29.

Faure R.M., Leroueil S., Rajot J.P., Larochelle P., Sève G., Tavenas F. (1988) XPENT, système expert en stabilité des pentes. Int. conf. on Slope stability, Lausanne, Suisse.

Faure R.M., Magnan J.P., Moreau M., Pilot G., (1975) Calcul sur ordinateur des ouvrages en terre. Revue gen. routes et aérodromes. n°338, pp23-38.

Faure R.M., Mascarelli D., Chaveriat L., Zelfani M., Gandar J., Mosuro O. (1991) XPENT, expert system of slope stability. 2nd Conf. on the applications of artificial intelligence techniques to civil and structural engineering. Oxford, England

Faure R.M., Mascarelli D., Vaunat J.,Leroueil S., Tavenas F.(1992) Present state and development of XPENT, expert system for slopes stability problems. Proc 6th Int symp. on Landslides, Christchurch.

Ke C.(1990) Un système de représentation des connaissances et d' aide à la décision pour la prévention des mouvements de terrain. PhD Thesis U.Claude Bernard Lyon1, France, n°213-90

Mascarelli D. (1994). PhD Thesis in preparation INSA-ENTPE, Lyon, France

Mascarelli D., Faure R.M. (1993) XPENT, slope stability expert system for managing the risk. Int. emergency management and engineering conf. Arlington, Virginia USA.

Mascarelli D., Faure R.M., Kastner R. (1992) Anatomie d'un projet à base de connaissance : XPENT, Système de travail en ingénierie des pentes. Coll. Int Géotechnique et Informatique, ENPC, Paris, France

Neveu B., Trousse B., Corby O. (1990) SMECI, an expert system shell that fits enginering design. 3rd Int.symp. on artificial intelligence, Monterey, Mexico

Vaunat J. (1990) Programme C-COOL, simulation des écoulements dans une pente naturelle. Internal report, Laval university, Quebec

Vaunat J. (1994) Risk Analysis PhD Thesis U.Laval Quebec, Canada

Vaunat J., Leroueil S., Tavenas F. (1992) Hazard and risk analysis of slope instability. Conf. Canadienne de géotechnique. Vancouver Canada.

Vaunat J.,Leroueil S.,Faure R.M. (1994).Material behaviour otientd caracterization of slope movements. 7th I.A.E.G. Congress, Lisbon.

Vogel C. (1988) Génie cognitif. Ed. Masson Paris, France pp196

Zelfani M, Faure R.M. (1992) Représentation, modelisation et traitement des connaissances spatiales en géotechnique. Coll. Int Géotechnique et Informatique, ENPC, Paris, France.

Zelfani M. (1993) Ingéniérie de la connaissance et raisonnement dans un univers multi-agents : XPENT-CASSIS un système à base de connaissance en géotechnique. PhD Thesis U.J. Monnet, St Etienne, France.

Sound wave propagation measurements in snow flows

Mesures de la propagation d'ondes sonores dans des écoulements de neige

M. GAY

Cemagref / Division Nivologie
BP 76, 38402 Saint-Martin d'Hères - France
Tel. (33) 76 76 27 27- Fax (33) 76 51 38 03

Abstract

We are introducing a new acoustic wave propagation measurement system to obtain the variation of the time of attenuation and sound speed inside the flow. These measurements are carried out in two points in space and enable us to find the speed of the flow through an intercorrelation data processing. We show different experiments carried out at the Federal Institute for Snow and Avalanche Research (Switzerland). We describe the sensor and the results and thus validate its principle. By a treatment of the signal we obtain some parameters in simulated avalanches that are :

- the speed of the front,
- the sound attenuation variation in this environment,
- the speed of the snow flow.

Résumé

Nous développons un système de mesure de propagation des ondes acoustiques pour obtenir les variations de temps d'atténuation et de vitesse du son dans un écoulement. Ces mesures sont réalisées en deux points de l'espace et nous permettent de trouver la vitesse de l'écoulement par un traitement d'intercorrélation. Nous présentons différentes expériences effectuées à l'Institut Fédéral pour l'Etude de la Neige et des Avalanches (Suisse). Nous décrivons le capteur, les résultats et validons ainsi son principe. Par un traitement du signal, nous obtenons différents paramètres dans des avalanches simulées :

- *la vitesse du front ;*
- *la variation de l'atténuation du son dans cet environnement ;*
- *la vitesse de l'écoulement de neige.*

Introduction

The physical parameter measurements inside the snow flow is essential to identify and to characterise numerical models. When the stage of model realization is finished, it's necessary to look for measurement results for identification and validation.

The difficulties of snow flow measurements are the selection of a sensor, its installation and the interpretation of the results. The two methods to know the avalanche kinematics are the sound wave propagation and the electromagnetic wave propagation. We have chosen the first solution because we want to know the mechanical parameters of the snow flow. We describ the designing and realization of the sound sensor.

Previous data

The electrical properties of the snow are in relation with different parameters : density, temperature, structure, etc.
Debye's model :
The dielectric constant

$$\varepsilon(f) = \varepsilon'(\mathrm{f}) - j\varepsilon''(\mathrm{f}) \qquad (1)$$

ε' is the relative permittivity and ε'' is the loss factor (it shows the absorption). Water, ice and for a great part snow are described like this :

$$\varepsilon(f) = \varepsilon_\infty + \frac{\varepsilon_0 - \varepsilon_\infty}{1 + 2\pi j f \tau} \qquad (2)$$

ε_0 is the dielectric constant in static

ε_∞ is the optical limit of the dielectric constant

τ is the relaxation time.

We find in relation with EQ(1) and EQ(2) that the loss factor reaches a maximum for the frequency :

$$f = \frac{1}{2\pi\tau}$$

The optical limit of the dielectric constant is controlled by the porosity, the liquid water content and the relative permittivity of the components ice, air and water. In the microwave range, ε' and ε'' depends strongly on the frequency.

Look at the Doppler effect. Quadrivector of wave : an electromagnetic plane wave polarized rectilinear is propagated through the vacuum with a speed v=c. The propagation direction representation is the wave vector k :

$$\vec{K} = (\vec{k}, \frac{i\omega}{c}) \qquad \text{Quadrivector of wave}$$

Its scalar square is invariant in relation with the Lorentz transformation (L). We have :

$$\vec{K'} = (L)\,\vec{K} \quad \text{with} \quad \begin{aligned} k'_x &= \gamma_u (k_x - \beta \frac{\omega}{c}) \\ k'_y &= k_y \\ k'_z &= k_z \\ \frac{\omega'}{c} &= \gamma_u (\frac{\omega}{c} - \beta k_x) \end{aligned} \tag{3}$$

to observe :

$$k_x = -\left\| \vec{k} \right\| \cos\theta = -\frac{\omega}{c}\cos\theta,$$

the fourth relations give us :

$$\frac{\omega'}{c} = \gamma_u \frac{\omega}{c}(1 - \frac{u}{c}\cos\theta) \tag{4}$$

Thus:

$$\boxed{\frac{\Delta\omega'}{\omega} = -\frac{u}{c(\varepsilon)}\cos\theta} \tag{5}$$

About this relation, and the dependence of the snow permittivity, we suggest to work with sound waves, to make the data interpretation easier.

Hydrodynamic equation :

$$\rho\frac{\partial u}{\partial t} + \rho u \frac{\partial u}{\partial x} + \frac{\partial P}{\partial x} = 0 \tag{6}$$

Continuity equation :

$$\frac{\partial \rho}{\partial t} + u\frac{\partial \rho}{\partial x} + \rho\frac{\partial u}{\partial x} = 0 \tag{7}$$

State equation:

$$\frac{dP}{d\rho} = V^2 \tag{8}$$

To solve this system, we notice that presently u and P are too small as well as their derivative.We can remove the second term in the hydrodynamic and continuity equation :

$$\rho\frac{\partial u}{\partial t}+\frac{\partial P}{\partial x}=0$$

$$\frac{\partial \rho}{\partial t}+\rho\frac{\partial u}{\partial x}=0$$

With $\frac{dP}{d\rho}=V^2$

Let:

$$\boxed{\frac{\partial^2 u}{\partial t}=V^2\frac{\partial^2 u}{\partial x^2}} \tag{9}$$

It's the wave propagation equation. V is the velocity of the wave propagation. The time integration gives :

$$\boxed{\begin{aligned} u &= f(t-\frac{x}{V})+\varphi(t+\frac{x}{V}) \\ P &= \rho V\left[f(t-\frac{x}{V})-\varphi(t+\frac{x}{V})\right] \end{aligned}} \tag{10}$$

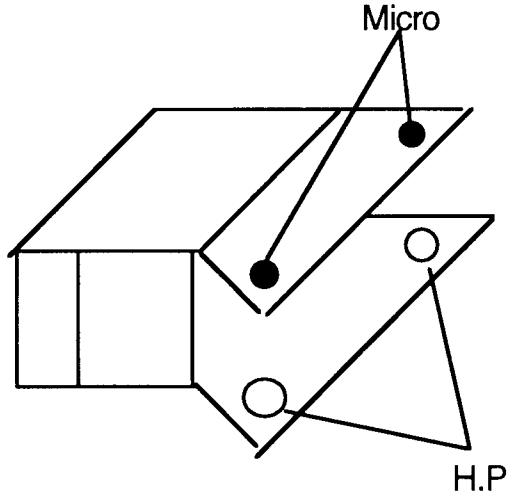

Fig. 1 Sensor, 8 March 1993.

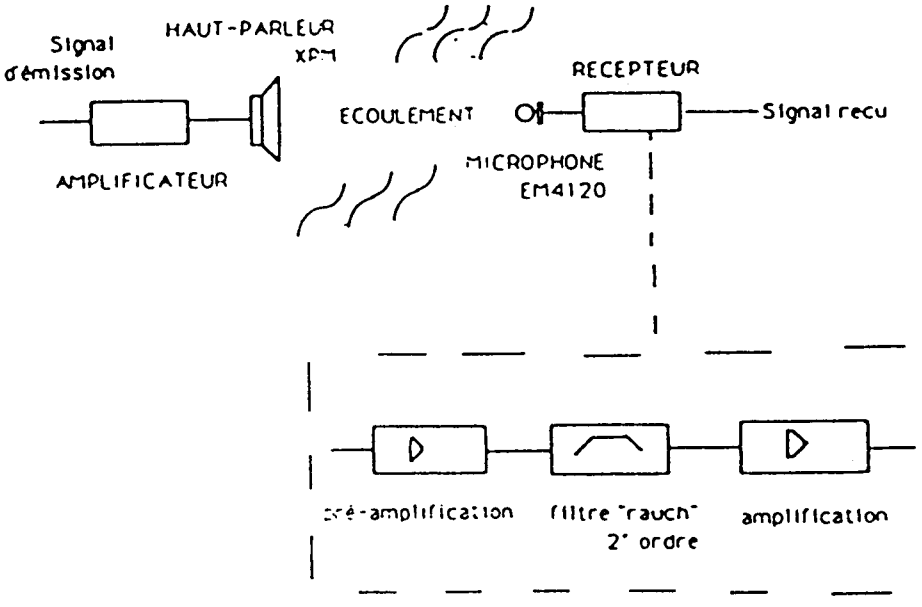

Fig.2 Schematic representation of transmitter and receiver. The frequency is respectively 2 kHz and 2.5 kHz, according to the static experiments.

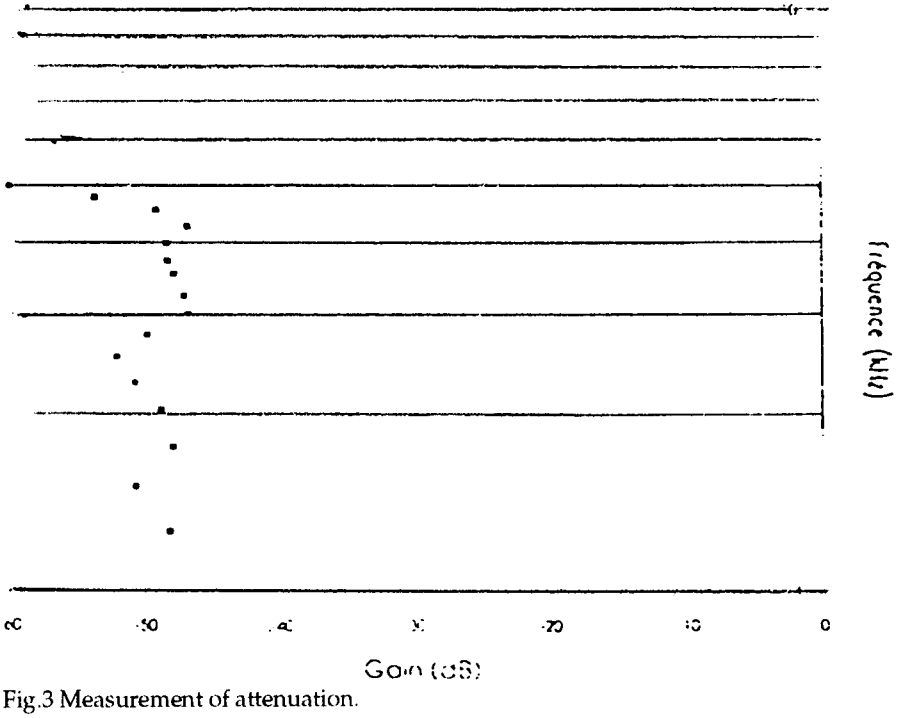

Fig.3 Measurement of attenuation.

Instrumentation and techniques

The speed measurement of snow flow consists in obtaining two signals in the space and in relation, in inter-correlationing analysis to obtain the speed.
Attenuation and propagation speed are function of the environment characteristics.
The loud speaker sends out a sound wave through the snow flow.

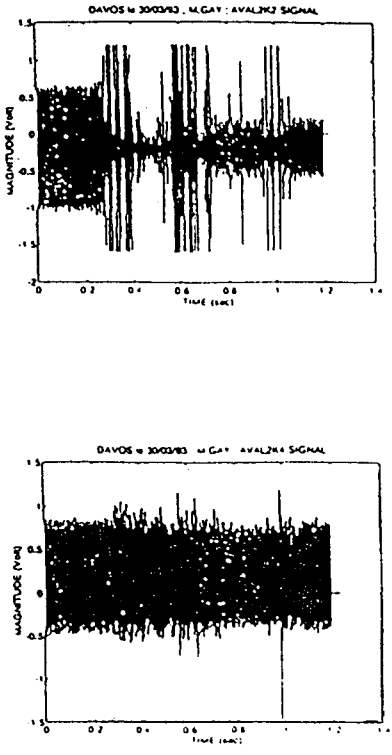

Fig. 4 Signal according to time

The important stage is the test of the sensor. There is a typical experimental installation to test the sensor at the Federal Institut for Snow and Avalanche Research in Davos.
We can see the recorded signal in the time domain and frequency domain.

Results

The design of this sensor was mainly directed towards two different goals : the first was to determine the speed in snow flow, the second one consisted in recording the variation of sound attenuation and phase in the hope of knowing the density during the flow.

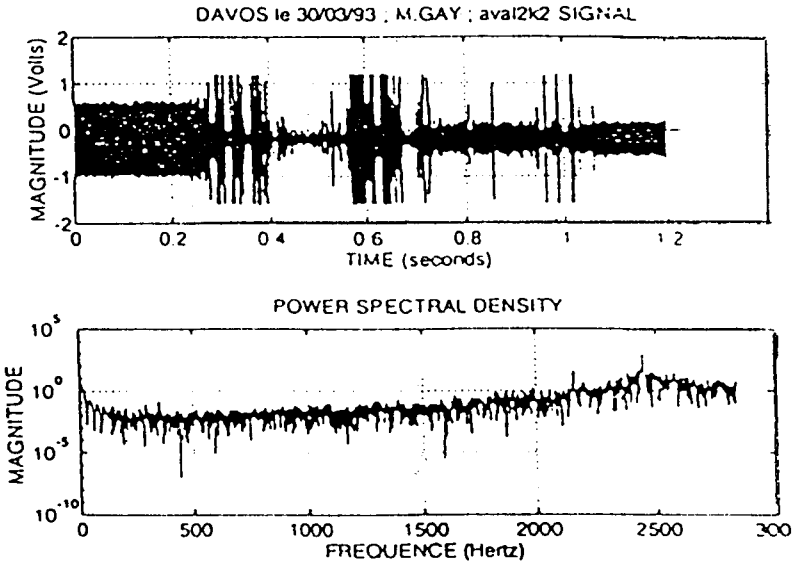

Fig.5 Spectrum of received signal.

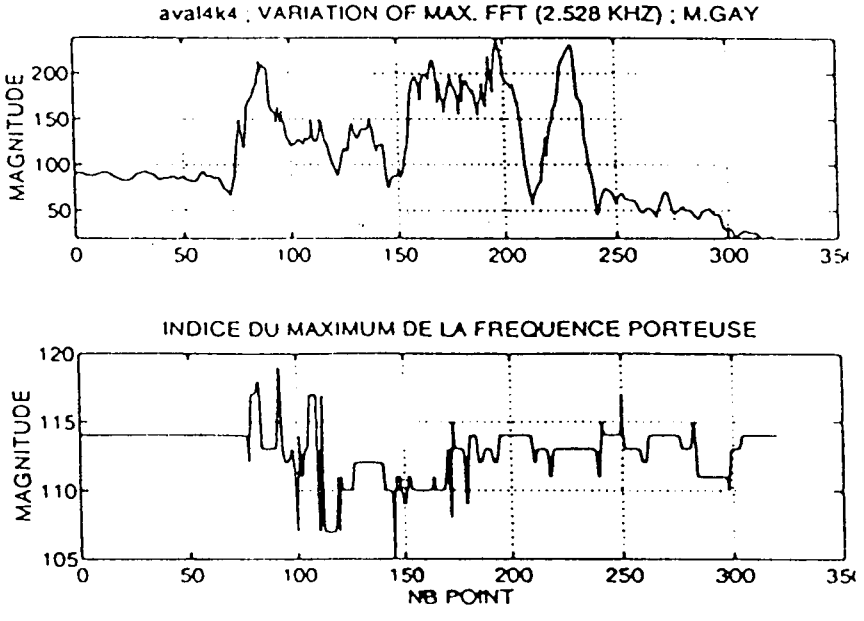

Fig.6 Maximum peak variation and frequency rating.

Speed inside snow flow : the spectral analysis is the signal processing method that characterises the frequency content of a measured signal. We look at carrier frequency modulation. The simple demodulation consists in taking the fast Fourier transform with slippery window of 64 points. The modulation is obtained with the maximum peak variation.
Some problems exist which are the variations of the frequency rating.
We can see the rating change from 105 to 120, let 2.33 kHz to 2.66 kHz, or we give out a 1.1 kHz frequency. It's a noise that disturbs the signal.

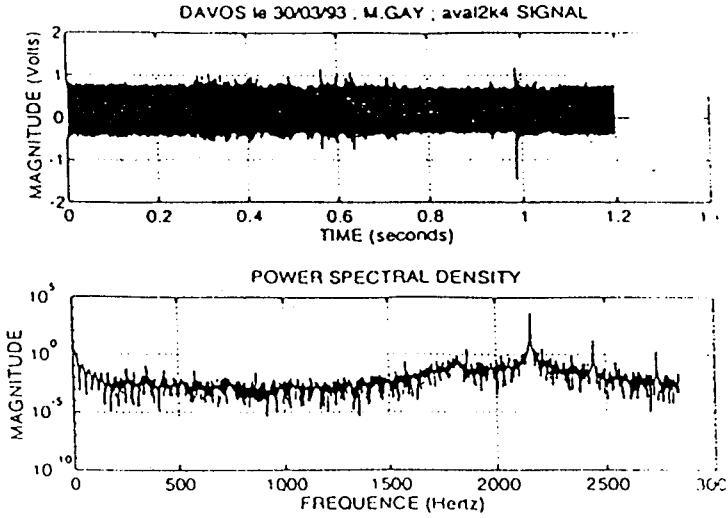

Fig.7 Spectrum of received signal

We have a peak of frequency 2.29 kHz, in that case we give out 1.1 kHz. We must use an another method of demodulation.

$$\gamma_{xy}(\nu) = TF\left[\Gamma_{xy}(\tau)\right] \tag{12}$$

or:

$$\Gamma_{xy}(\tau) = \int_{-\infty}^{+\infty} X(\nu) Y^{*}(\nu) e^{2\pi j \nu \tau} d\nu = TF^{-1}\left[S_{xy}(\nu)\right]$$

$S_{xy}(\nu) = X(\nu)\, Y^{*}(\nu)$ is the energy spectral density.

We obtain the inter-correlation of signal E1->R1 and E2->R2, and calculate the covariance of (E1,R1)->(E2,R2).

$$\boxed{C_{xy}(\tau) = \lim_{T \to \infty} \frac{1}{T} \int_0^T y(t)x(t-\tau)dt}$$

Finally, we obtain the speed of the avalanche front, and inside the snow flow. For example :

Avalanche N°2 : **V1(t) = 8.4 m/s.**
Avalanche N°4 : **V1(t) = 3.37 m/s.**
Avalanche N°6 : **V1(t) = 4.21 m/s.**

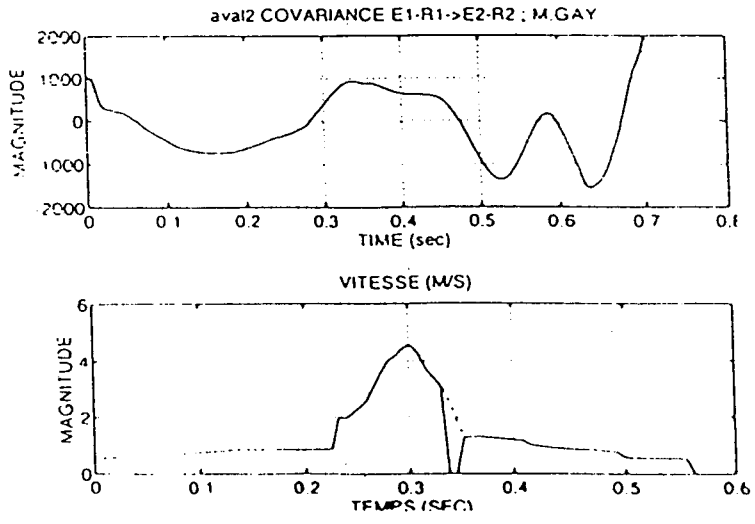

Fig.8 Speed of snow flow

Attenuation and phase : the amplitude variation is function of attenuation and phase but we can adjust the measurement of amplitude to obtain the attenuation in the snow flow.

Conclusion

The above-described experiments demonstrate the possibility to measure some physical parameters inside a snow flow. The digital signal processing allows to extract information in spite of noice. One of the important unsolved problems is the filtering of the received signal. Last the sensor resists to the snow flow.

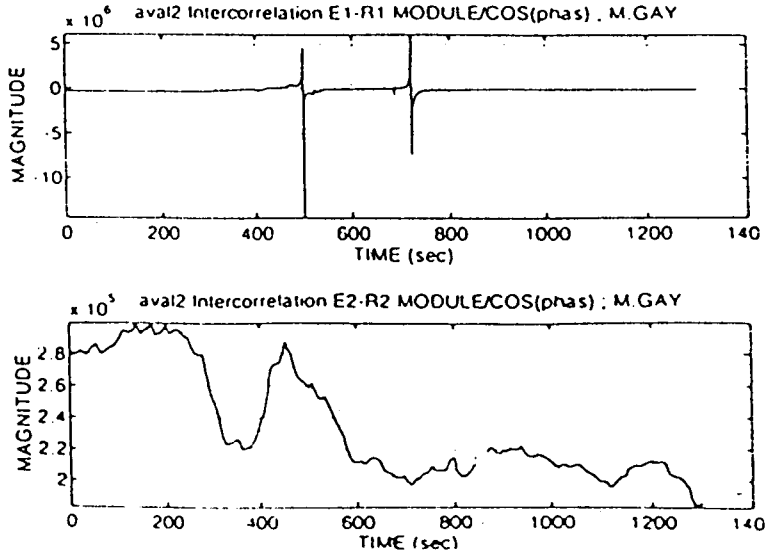

Fig. 9 Attenuation in the snow flow.

References

O.BUSER : On the application of rigid porous models to impédance data for snow,1987.

C.GROSSETETE : Relativité restreinte, 1985.

H.GESPAC : Manuel de spécification du bus G64-96.

H.GUBLER : Electrical, optical and acoustical properties of snow.

H.GUBLER : Measurement and modelling of snow avalanche speeds.

GUBLER & WEILEMAN : Seasonal snow cover monitoring using FMCW radar, 1986.

HEWLETT PACKARD : Standard commands for programmable instruments, 1991.

M.LACOUME : Cours de traitement du signal, 1993.

D.MARBOUTY : La neige : Propriétés Physiques.

J.MAX : Méthodes et techniques de traitement du signal et applications aux mesures physiques, 1971,1985.

M.SOUTIF : Vibrations, propagation diffusion, 1970.

TRAN TIEN LANG : Systèmes de mesures informatisés, 1991.

TRAN TIEN LANG : Électronique des systèmes de mesures, 1984.

ZWIKKER & KOSTEN : Sound aborbing materials, 1949.

Contribution to the study of mass movements : mudflow slides and block fall simulations

Contribution à l'étude de mouvements en masse : simulations de coulées de boues et de chutes de blocs

J.A. GILI, A. HUERTA, J. COROMINAS

Technical University of Catalonia (U.P.C.)
08034 Barcelona - Spain
Tel. (34) 34 01 68 63 - Fax (34) 34 01 65 04

Abstract

Several theoretical and practical developments in relation with mass movements (rock blocks, rockslides, mudflows) are presented as a contribution to the discussion. Some of them are field based, and others are numerical simulations. First of all we present briefly some *generalized Newtonian* fluid models. Then the Arbitrary Lagrangian-Eulerian (ALE) formulation for viscous flows with free surface is described and an example of its applicability is discussed. A rock avalanche simulation using some simplifications within a F.E. or a Finite differences scheme is developed next. Then the mudflow balance of energy study technique is outlined. Finally, we explain our experiments in rock block simulations, and we present a tentative graph runout distance vs. volume of material.

Résumé

Plusieurs développements théoriques et pratiques sur les mouvements en masse (chutes de blocs, écroulements rocheux, coulées de boues) sont présentés. Certains d'entre eux sont basés sur des observations de terrain, d'autres relèvent de la simulation numérique. Dans un premier temps, nous présentons brièvement quelques modèles de fluides de type Newtonien généralisé. Ensuite, une formulation Lagrangienne-Eulérienne pour les écoulements visqueux à surface libre est décrite et un exemple d'applicabilité est discuté. Une simulation d'avalanche rocheuse utilisant des simplifications au sein de schémas aux éléments finis ou aux différences finies est ensuite développée. Par la suite, la technique du bilan d'énergie pour une coulée de boue est détaillée.
Enfin, nous expliquons nos expériences de simulations avec des blocs rocheux et nous proposons un graphe de la distance d'arrêt par rapport au volume de matériau.

Introduction

To study natural flow phenomena (rock or mudslides, snow avalanches, breaking of a dam or mine tailings impoundments, lava flow...) one must consider behaviours other

than newtonian (μ=constant). Among all the possible models, a set of practical engineering ones are pointed up: the so called Generalized Newtonian fluids. These models are characterized by a viscosity which depends on the shear rate: $\mu=\mu(\dot{\gamma})$. In table 1 and fig.1 some of them are presented (Huerta & Liu, 1988).

Model 1	1D viscosity	3D generalization
Newtonian	μ_0 = constant	$\sigma' = 2\mu_0 D'$
Power law	$\mu = m\dot{\gamma}^{n-1}$	$\sigma' = 2m(\sqrt{2\,\mathrm{tr}(D'^2)})^{n-1}D'$
Truncated Power Law	$\mu = \mu_0 \quad \dot{\gamma} \leq \dot{\gamma}_0$ $\mu = \mu_0(\dot{\gamma}/\dot{\gamma}_0)^{n-1} \quad \dot{\gamma} \geq \dot{\gamma}_0$	$\sigma' = 2\mu_0 D' \quad \sqrt{2\,\mathrm{tr}(D'^2)} \leq \dot{\gamma}_0$ $\sigma' = 2\mu_0(\sqrt{2\,\mathrm{tr}(D'^2)}/\dot{\gamma}_0)^{n-1} \quad D' \leq \dot{\gamma}_0$
Carreau	$\frac{\mu - \mu_\infty}{\mu_0 - \mu_\infty} = [1 + (\lambda\dot{\gamma})^2]^{(n-1)/2}$	$\sigma' = 2(\mu_0 - \mu_\infty)[(1 + 2\lambda^2\,\mathrm{tr}(D'^2)]^{(n-1)/2}D' + 2\mu_\infty D'$
Carreau-A	$\mu_\infty = 0$	$\sigma' = 2\mu_0[1 + 2\lambda^2\,\mathrm{tr}(D'^2)]^{(n-1)/2}D'$
Bingham	$\mu = \infty \quad \tau \leq \tau_0$ $\mu = \mu_p + \tau_0/\dot{\gamma} \quad \tau \geq \tau_0$	$D' = 0 \quad \frac{1}{2}\,\mathrm{tr}(\sigma'^2) \leq \tau_0^2$ $\sigma' = 2\mu_p[1 + \tau_0/\sqrt{2\,\mathrm{tr}(D'^2)}] \quad D' \geq \tau_0^2$
Herschel and Bulkley	$\mu = \infty \quad \tau \leq \tau_0$ $\mu = m\dot{\gamma}^{n-1} + \tau_0/\dot{\gamma} \quad \tau \geq \tau_0$	$D' = 0 \quad \frac{1}{2}\mathrm{tr}(\sigma'^2) \leq \tau_0^2$ $\sigma' = 2m(\sqrt{2\,\mathrm{tr}(D'^2)})^{(n-1)}D'$ $+ 2\tau_0/\sqrt{2\,\mathrm{tr}(D'^2)}D' \quad \frac{1}{2}\,\mathrm{tr}(\sigma'^2) \geq \tau_0^2$

where σ' and D' are the deviatoric part of the stress and stretch [i.e. $\frac{1}{2}(\nabla v + v\nabla)$] tensors, respectively

$$\sigma_{ij} = -P\delta_{ij} + 2\mu D_{ij}$$

$$D_{ij} = \frac{1}{2}\left(\frac{\partial v_i}{\partial x_j} + \frac{\partial v_j}{\partial x_i}\right)$$

In addition to one of this constitutive relationships, the material has to verify the field equations (continuity and momentum conservation) and the proper initial and boundary conditions.

In order to simulate the flow with free surface, we can solve the *complete* problem (next section), or, under certain circumstances, use a simplified approach.

Application of arbitrary lagrangian-eulerian (ALE) techniques for viscous flow with large free surface motion

This is a recent development on the Finite Element Method (FEM), one of the most powerful and sofisticated numerical techniques available to solve partial differential equations.

The kinematic relationship between the moving fluid and the F.E. grid is extremely important in multidimensional fluid dynamics problems. Two classical descriptions are usually used:

- *Lagrangian*: the mesh, in motion, follows the particles. As there are no convective effects, the calculations are quite simple, but the mesh is not able to follow big material distortions.
- *Eulerian*: The mesh is fixed; although the previous drawback (mesh distortion) is overcome, now the convective effects arise, as well as problems to follow the free surface.

$$\sigma_{ij} = -P\delta_{ij} + 2\mu D_{ij}$$

$$D_{ij} = \frac{1}{2}\left(\frac{\partial v_i}{\partial x_j} + \frac{\partial v_j}{\partial x_i}\right)$$

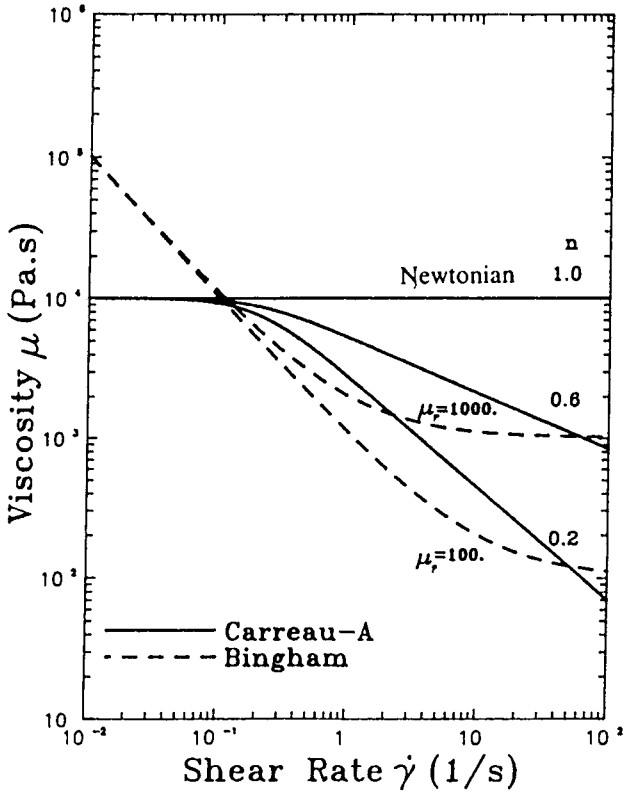

Fig.1 Viscosity as a function of shear rate as predicted by the Carreau and Bingham models.

Because of the shortcomings of purely Lagrangian and Eulerian descriptions, the arbitrary Lagrangian-Eulerian (ALE) technique has been developed (see e.g. Huerta & Liu, 1988). This new approach is based on the arbitrary movement of the reference frame, which is continuously rezoned in order to allow a precise description of the moving interfaces and to maintain the element shape. Convective terms are still present in the ALE equations, but the ability to prescribe the mesh movement may allow them to be reduced. There are various mesh rezonning algorithms to update the mesh following the moving domain, one of the major problems with the ALE description. Previously to solve the boundary value problem, all the field and constitutive equations have to be reformulated in this new mixed referencial form.

In order to apply the FEM, all the differential equations (field eq., constitutive relationship, and mesh updating eq.) must be transformed into equivalent integral equations. This transformation is based in the weighted residual theory, which can be formulated in different manners. In the quoted work, the streamline-upwind/Petrov-Galerkin formulation is used for the equilibrium and mesh updating eq., while the Galerkin method is applied to the continuity eq. This approach leads to a system of partial differential eq., solved using a predictor-multicorrector algorithm.

Dam-break example

The ALE technique, exposed here in brief, can be used to solve typical problems with large free surface motion (e.g.: propagation of long waves -"tsunamis"- onto a shelf off coast (Huerta et al., 1990), or seismic fluid-structure interaction problems -tanks, storage pools (Huerta & Liu, 1990)...-). Next, the ALE formulation is applied to model the so called "Dam-break problem" (see Huerta and Liu, 1988). Notice that we can deal with any kind of propagating fluid, not only water (e.g. tailing dams, muds, debris).

This problem, classic in mathematical hydraulics, has been solved through different approaches: Ritter, in 1892, using the method of characteristics, with frictionless bed. Later the effect of bed resistance was introduced, and also sloping beds and finite reservoirs were accounted for. In some cases a small but finite depth of still fluid was used as downstream boundary condition (Dressler, 1952; Chen, 1980; Jeyapalan, 1980).

All the previous work are based on shallow water theory (i.e. the Saint-Venant equations) and assume that the velocity distribution over a cross-section is essentially uniform, and that the streamline curvature is small (i.e. parallel flow, it means that the pressure distribution with depth is hydrostatic). The dissipation takes place through the boundary shear, that can be evaluated by means of 3 terms: the static (constant), the laminar (pp.to the velocity), and the turbulent (pp. to the square of the velocity), with constants that can be assigned depending on the assumptions, or adjusted in order to match the theoretical and the experimental results (Brugnot and Pochat, 1981).

In fact, using the MEF with the ALE approach all the above simplifications can be avoided or reduced. The problem is interesting and difficult:

- There are regions with flow mainly diffusive or convective
- High velocity gradients near the boundary
- Big accelerations in the first seconds, that enhances numerical oscillations.

In Fig.2 the two cases solved with this technique are presented. Both can be checked with the analytical solution provided by the Saint-Venant eq. for the inviscid case. The characteristic quantities used to scale the problem (get dimensionless values) are: length: H; velocities: $\sqrt{(gH)}$; pressure: ρgH; time: $H/\sqrt{(gH)}$. Another important dimensionless value is the Reynolds number ($Re= H\sqrt{(gH)}/\nu$, with kinematic viscosity $\nu=\mu/\rho$). But, as the fluid is non-newtonian (real fluid), the problem is influenced by the constitutive law and also by H, ΔH.... (Huerta,1987).

Through Fig. 2 to 11 (Huerta and Liu, 1988) the example results can be seen, as well as the potential of the ALE method.

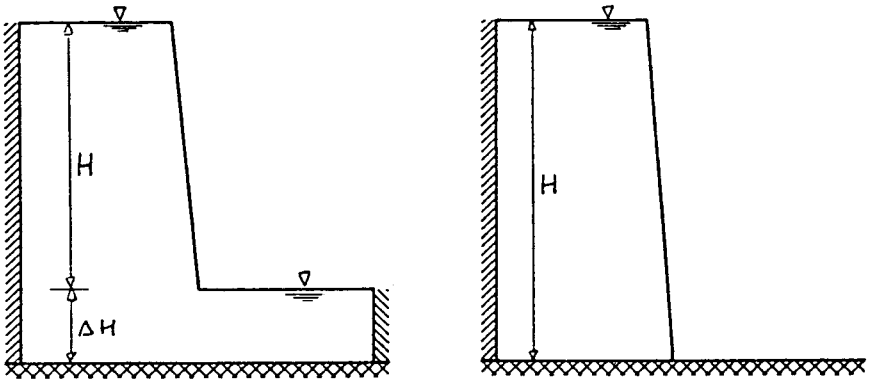

Fig. 2 Schematic representation of the dam-break problem (Huerta & Liu,1988):
a) Flow over a Still Fluid (FSF case) b) Flow over a dry bed (FDB case)

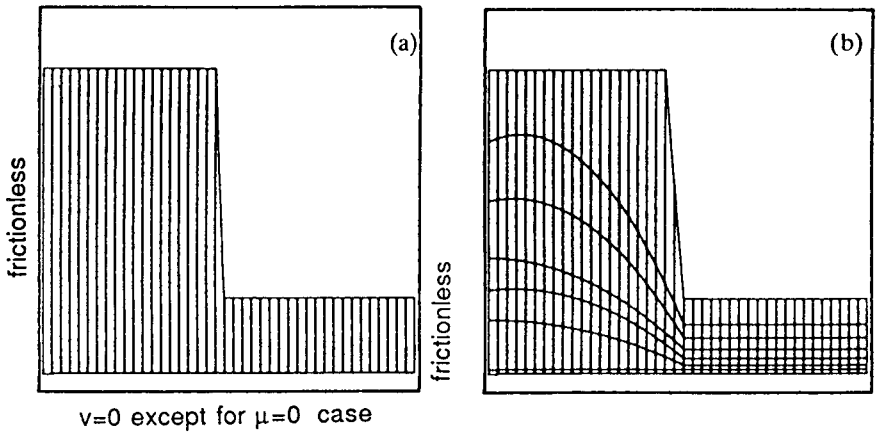

Fig. 3 Dam-break. The mesh discretizations employed in the FSF case are: 41x1(a), 41x3, 41x5, 41x7(b)

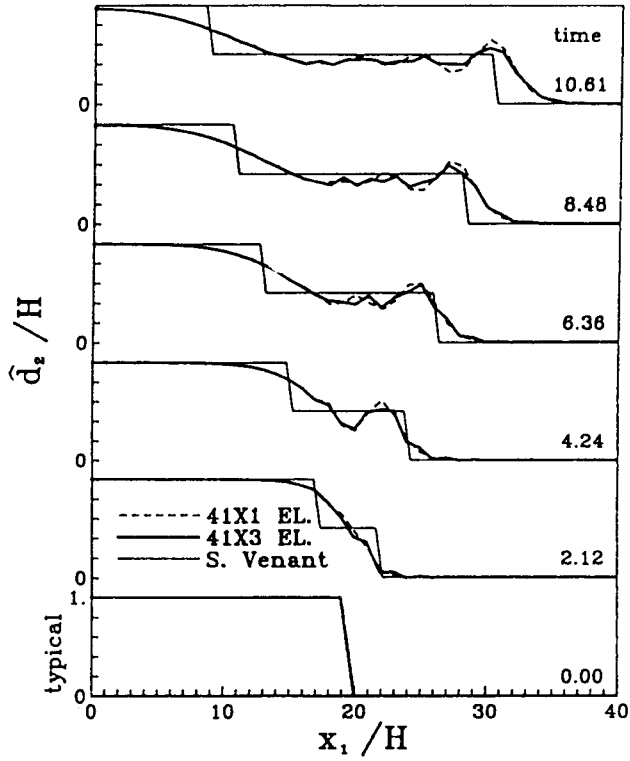

Fig.4 Dam-break. FSF case.Inviscid(μ=0). Comparison of the Saint Venant analytical solution (shallow water theory, straight lines) and ALE formulation (2 discretizations). All the axes are dimensionless. H/ΔH=1. The method smoothes the "wave". No big differences between 2 discretizations.

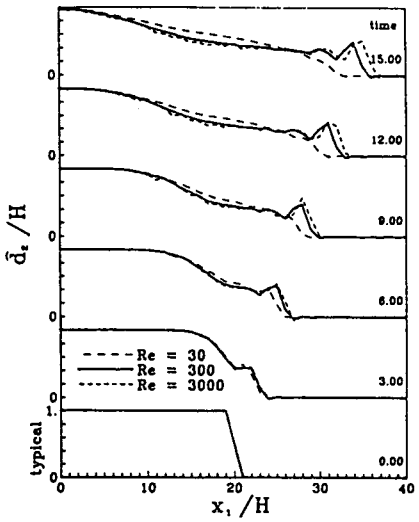

Fig.5 Dam-break. FSF case. Slope 2h:1v ,H=15m, ΔH=5m. Newtonian material, ρ=1600 Kg/m^3 ; μ=10^3 Pa.s (Re=300), and also lower (Re=3000) and higher (Re=30) viscosity. The last one smoothes the surface due to viscous dissipation of energy.

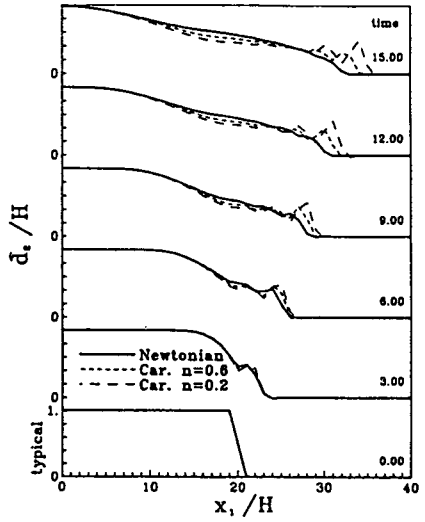

Fig.6 Dam-break. FSF case. Non-Newtonian material. Carreau model, with n=0.2 and 0.6 (see fig.1).

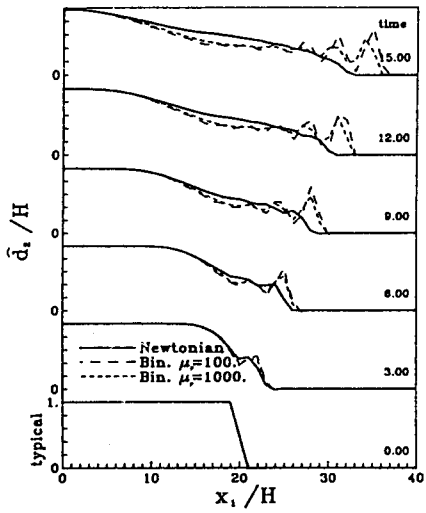

Fig.7 Dam-break. FSF case. Non-Newtonian material. Bingham model (see fig.1).

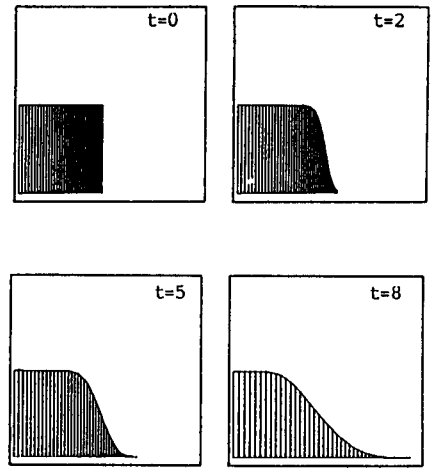

Fig.8 Dam-break. FDB case. Finite element mesh motion for the inviscid case (μ=0),mixed formulation.

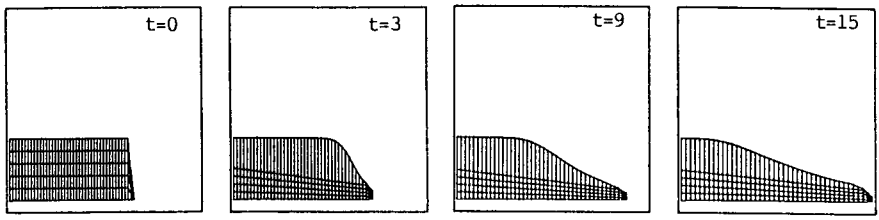

Fig.9 Dam-break. FDB case. Finite Element mesh motion, Carreau fluid.

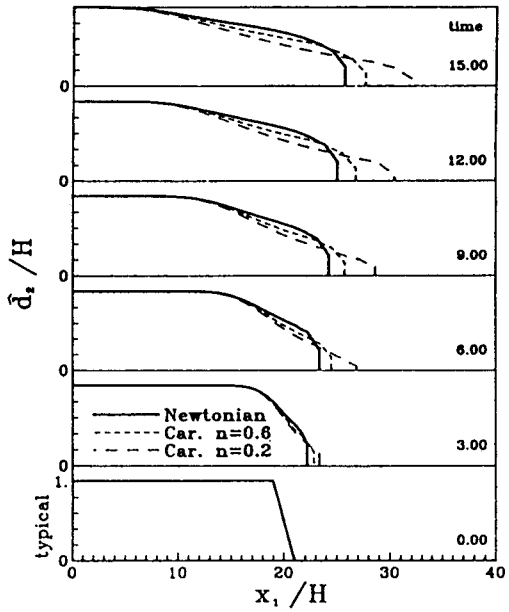

Fig.10. Dam-break. FDB case. Non-Newtonian material: Carreau model.

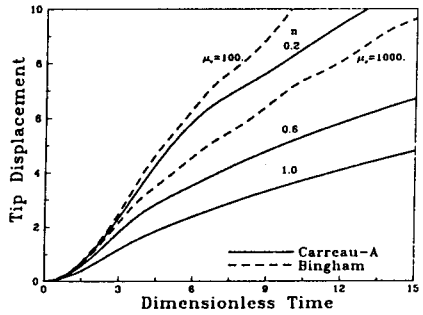

Fig.11 Dam-break. FDB case. Tip displacement vs time for the non-Newtonian materials studied.

Future works

It is obvious that the problem offers room for improvement, even though an important step forward has been achieved by the complete integration of the field equations through depth and the improved automatic rezonning technique. In the example, better descriptions of the initial instants of flow and the downstream boundary tip condition are needed. The future works should include sloping beds, 3D extensions (mudflow with lateral expansion), and non zero velocities at the base (yield function), as well as more sophisticated constitutive models. In fact, recent extensions to non linear continuum mechanics in transient analysis (Huerta et al., 1992, and Huerta & Casadei, 1993) have increased the field of applicability of this formulation in the context of constitutive relations for materials with memory.

Simplified numerical finite elements or finite differences technique to study flow of materials downhill a slope

In certain situations where the mass movement has a dimension (the thickness) smaller than the others (e.g. mudflows, avalanches, volcanic stuff flow, flow failures of mine tailing impoundments...), it is possible to simplify the problem; the formulation is reduced to 2 or even 1 spatial dimension (similarly to the shallow water theory).

Effectively, in those cases you can (see Vulliet & Hutter, 1988, Tolós & Huerta, 1992):

Effectively, in those cases you can (see Vulliet & Hutter, 1988, Tolós & Huerta, 1992):

1)change the coordinate system to have the axis aligned with the major mean directions.
2)formulate the eq. in a dimensionless manner, scaling the variables with certain characteristic quantities ([Lx], [Ly], [H], etc, see fig.12).
3)study the free surface, **Zs**, vs. time integrating the Navier-Stokes eq. through depth.
4)by a carefull perturbation analysis, disregard those equation terms extremely small.
5)and finally, reduce the problem to 2D or usually 1D by stating that the differential variables (velocities, **u,v**) depend only of **x**, and that there is no sliding in the base.

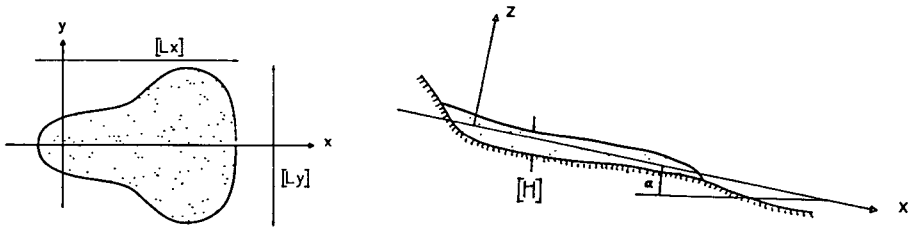

Fig.12 Reference system and some characteristic quantities.

At the end we obtain a set of non linear differential partial derivative quasi-hyperbolic equations in **Zs(x,t)**:

$$\frac{\partial Zs}{\partial t} + f(Zs,x)\frac{\partial Zs}{\partial x} = g\,(Zs,x)$$

These equations can be solved either by finite differences (F.D.)or by the finite element method (F.E.M.), but with special algorithms to handle the extremely high gradients near the tip of the flow, with enough numerical stability (Lax-Wendroff algorithm): in 2 steps in Finite Differences, resulting a explicit scheme; in 1 step in F.E. (implicit scheme).

The final implementation proceeds through time with variable time scaling. The Δt is choosed small enough to assume stability(checked by an extension of *Courant number* to nonlinear case)

Rockslide example

Only as a factibility test, the Madison Canyon rockslide (1959), reported by Trunk et al.1986, has been simulated. The material values are : $\rho=2100$ Kg/m^3, $\nu_{kinematic}=380$ m^2/s.

The scaling values are: [Lx]=1500m, [H]=100m, [Ux]=40m/s (probable speed, according to Trunk), and [Time]=[Lx]/[Ux]=37.5 s.

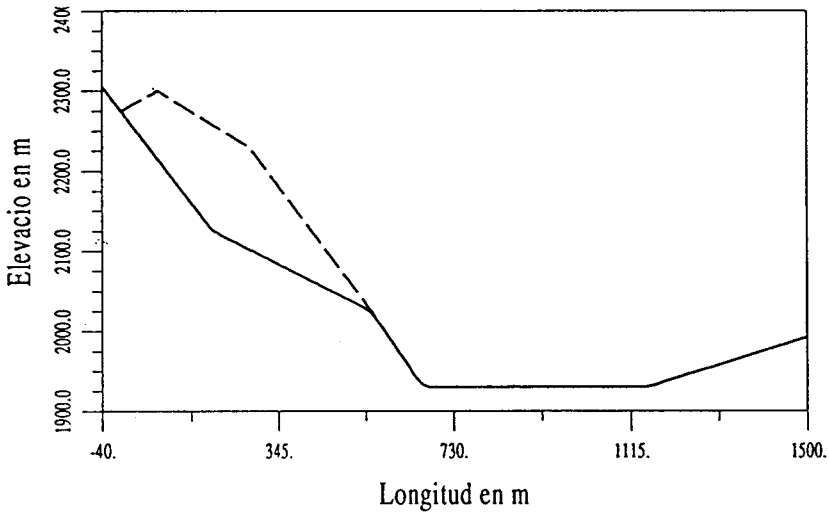

Fig.13 Madison Canyon Rockslide simulation: Initial situation (note uneven scales)

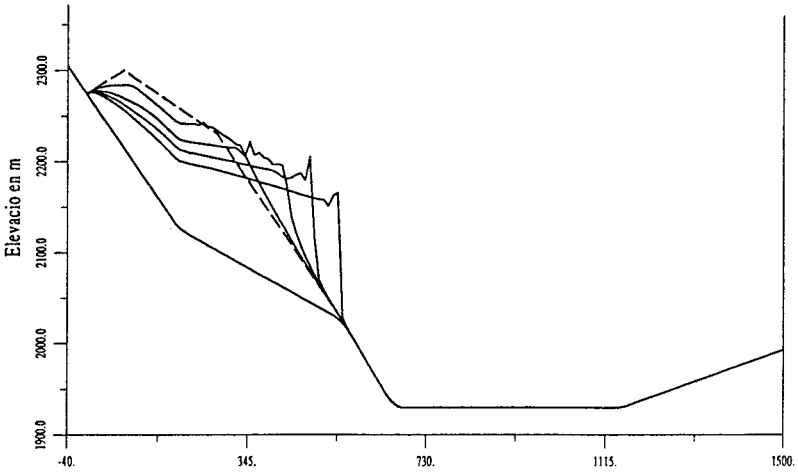

Fig.14 Madison Canyon Rockslide simulation: First seconds (accumulation at the toe).

The discretization consists of 205 elements, 10 m each. The main objective is to solve the quasi-hyperbolic eq. in the free surface position (**Zs**) as a function of **x** and **t**. A set

of runs with DF and with FE in 1st order or 2nd order precision formulation has been made.

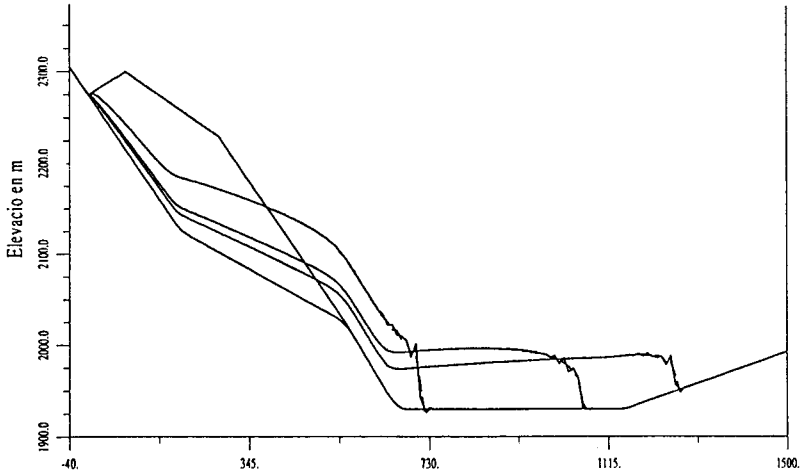

Fig.15 Madison Canyon Rockslide simulation: intermediate states.

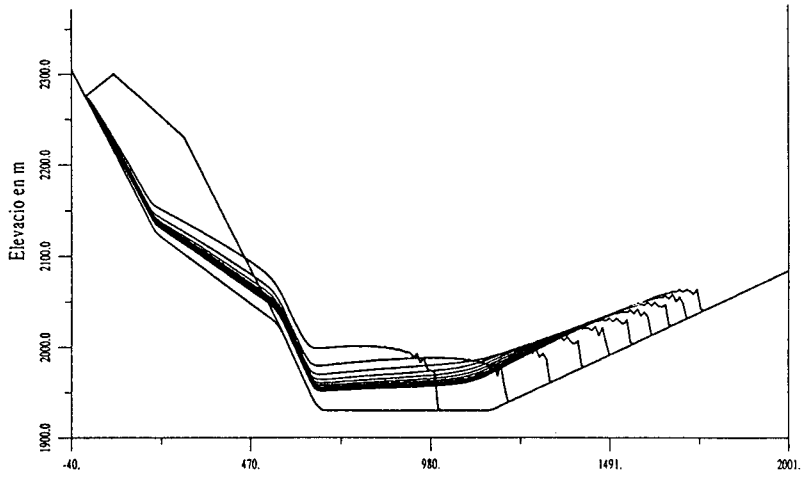

Fig.16 Madison Canyon Rockslide simulation: Last situation simulated.

Some typical results are presented in the figures 13 to 16. It can be concluded that:
-FE & DF give very similar results;
-2nd order analysis is better (accuracy and stability);

-The variable Δt scheme is better (optimize CPU[1]with best stability conditions, see fig 17);
-Results are consistent with those of Trunk, with peak velocities in the range 30-40 m/s.

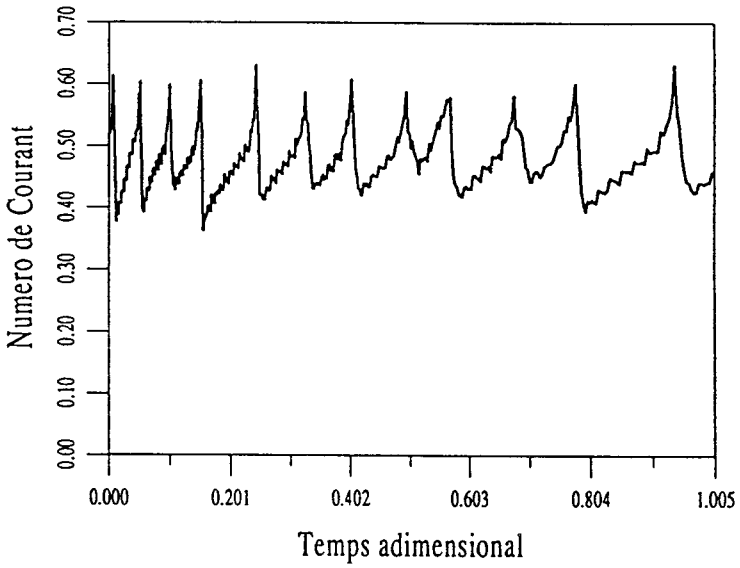

Fig. 17 Madison Canyon Rockslide simulation: Courant number vs time with variable Δt scheme.

Future works

As can be seen in fig.16 the tip velocity decreases when the material reach the other slope of the valley. However the final stop are not registered, due to the fact that the fluid in this situation has a too simple rheology (law without shear threshold) and the lateral spread has been disregarded (1D formulation). For these reasons the following improvements are considered:

- Viscous law with threshold
- 2D formulation Zs=Zs(x,y,t) to allow lateral expansion.
- Improved boundary condition at the base (v#0, sliding)
- Later, the hypothetical erosion to the still substratum can be incorporated to the model.

The last three ideas will permit, perhaps, to model the lateral levées formation.

Mudflow analysis through energy considerations

A quite simple approach is to model the behaviour of mudflows on the basis of energy balance.

[1] Up to the 92% of number of cycles can be saved.

In general, mudflows start at the foot of complex rotational slides, sometimes with solifluction processes, most of them in silty-clayey lithologies, reaching speeds in the range from 1m/h to 1m/min. In November 1982, after two days of heavy rain (200-400 mm/24h), several landslides were triggered in our region (Catalonia, Spain), the "La Coma" and "Gòsol" mudflows (Eastern Pyrenees) among them (Corominas, 1984). In April 1986, in Olivares,near Granada, another mudflow took place. The La Coma mudflow is very ilustrative (see fig.18), and has been studied in some extent (Corominas et al. 1988a).

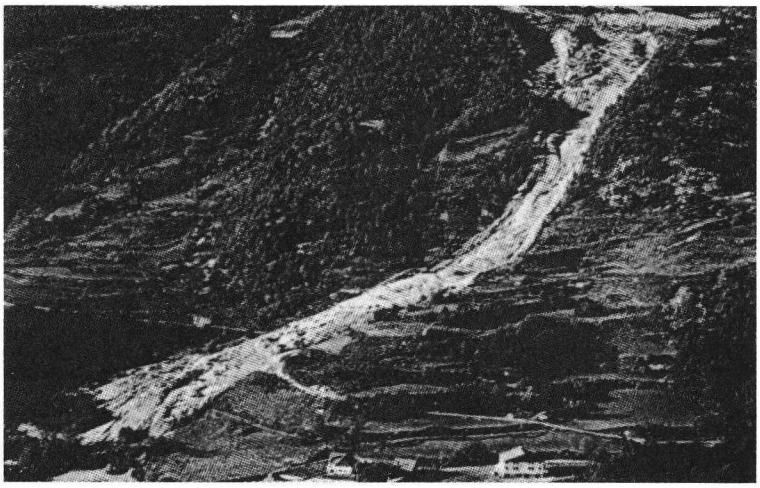

Fig.18 General view of La Coma mudflow, November 1982.

In the morning of November 8th, a large mud tongue was noticed, sliding down the slope at a speed of several meters per hour. After nine hours the mudflow stopped behind some buildings, having travelled 820 m (slope distance) and 298 m (vertical drop).
Three zones can be distinguished: the *head* (average slope ~ 21.5°); the main *channel*, that covers almost two thirds of the total (slope ~ 26°) and presents two lateral levées; and the *foot*, where the slope decreases to 17° (see fig.19).

Through detailed composition studies, pits, samples, test and field observations, it is possible to suggest some mechanisms. As stated in Corominas et al. 1988b, it seems that the development of lateral levées and the substratum erosion process under the main channel are heavily linked. It has been possible to establish that the levées are developed by "subsidence" of the mudflow surface (fig.20).

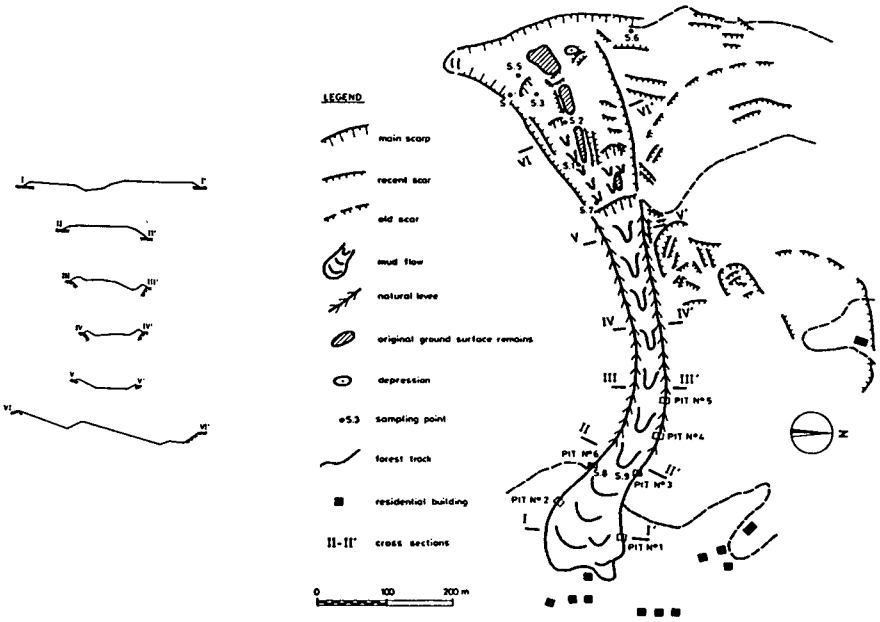

Fig.19 Scheme of La Coma mudflow with sections (x2 enlarged).

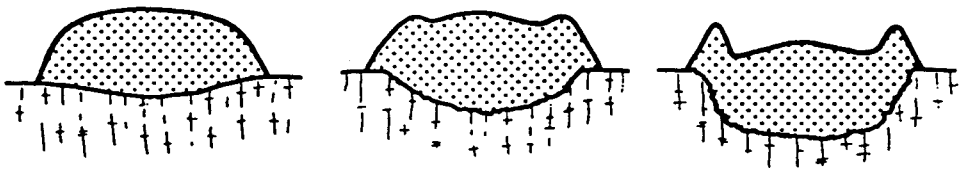

Fig.20 Development of natural levées by progressive erosion of the bottom channel.

In order to achieve a better understanding of the mudflow behaviour, a tentative energy balance can be established for the channel part of the flow (where the sliding conditions had been fairly constant. The potential energy (finally lost) can be calculated under certain assumptions ($\Delta Ep \sim 5.9 \times 10^{11}$ J), as well as the work done by the shear force at the contact tongue-substratum, (without erosion in a first attempt, $\sim 3.7 \times 10^{11}$ J). Thus losses by frictional sliding are not enough to justify the total energy dissipated.

A better match is obtained by assuming that when the mudflow slides down the channel, a shear zone at its lower part appears, with a parabolic velocity

distribution (fig.21). At the upper part of the channel, this shear zone begins over the substratum, but from there it can erode progressively a certain depth of the natural soil. This implies that a plug of "frozen" mud moves at uniform velocity above the shear zone and that the material is incorporated to the flow.

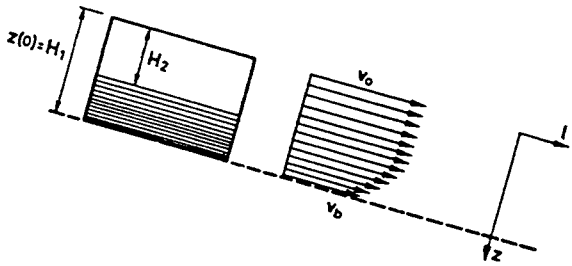

Fig. 21 "Plug" and shear zone at the bottom.

Now the dissipated energy is due to the friction between successive shear planes in this intermediate zone (H_1-H_2, variable), from the base of the plug to the bottom (including eroded substratum).

The integration of this work from the upper to the lower part of the channel must be equal to the total amount of dissipated energy. After several simplifications, assuming that the velocity at the bottom Vb>0 and that the thickness of the mudflow is continuously increasing, it is possible to balance ΔEp, obtaining a mudflow thickness increase between 5 and 6.7 m and total erosion thicknesses at the bottom channel between 9 and 11.5 m, that are compatible with the field observations.

Thus it seems clear that erosion not only explains the formation of the lateral levées, but it is necessary to balance the energy loss. Although the above calculations are very simplistic (and difficult to employ in a prediction model), they are a first step to take the erosion into account in the mudflow propagation mechanism.

Future works

In this field they may include field displacement measurements in a slow earthflow (triggered by rain periods) with EDM and GPS techniques (Gili & Corominas. 1992), and the physical modelling of the mudflows with scale models in the laboratory.

Block fall simulation models

Slightly out of the main scope of this contribution, this well-known type of models have been widely used to simulate the motion of a single block falling down a mountain side. The code developed (Gili & Gutierrez, 1992) is in the line of those developed by Azimi et al., 1982; Falcetta, 1985; Rochet, 1987, and others. P.Cundall's "Distinct Element Method" is used. The slope is partitioned into straight elements (2D). The block itself is prismatic. Sliding, rolling, impact and free flight are taken into account.

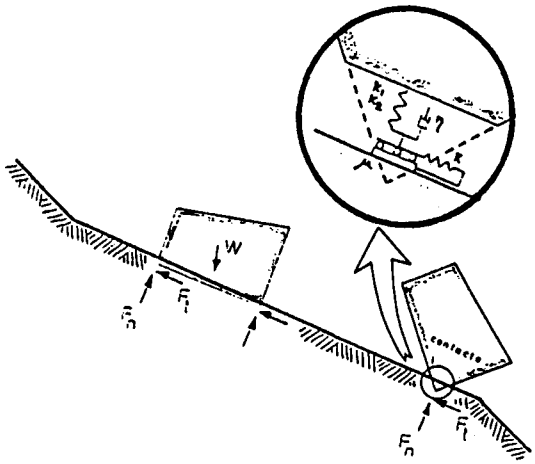

Fig.22 Block-slope contact forces, and rheological conceptual behaviour.

The model parameters (fig.22) are calibrated with observed field data; the best is to carry out many "in situ" block fall tests. For a given location, after the "tuning" of the model has been achieved, it can be used to design remedial measures.
As an example of application the model has been used in a old quarry reclamation case (St. Carles, Tarragona, fig.23). It is easy to realize the positive effect of the embankment comparing the frequency graph (before and after).
A careful use of such a tool may be helpful in risk assessment studies. But the model calibration is a major step.

Future (or in course) works

Block fall test with bigger blocks, study and implementation of the block breakage, model catch fence behaviour and block-wire net interaction, use of the same approach to study the drop of several blocks at a time (rock slide or avalanche).

Concluding remarks

In some hazard areas, the interest of mapping studies is to predict the runout distance that the landslide will reach, more than the flow or the exact speed. In those cases it is very common to use the "sled model", proposed by Heim in 1932, because, although neglecting secondary factors, it is the simplest one. This kind of simple approach has been widely used and improved (Sassa, 1988; see fig.24). The main hypothesis is that all energy loss during motion is caused by friction.

Thus, given an apparent friction angle, Φa, it corresponds to the gradient of energy line. Then, if $tan(\Phi a)=H/L$ is known, we can estimate the moving distance and the velocity (intersection of the line dipping Φa degrees from the source with the ground surface).

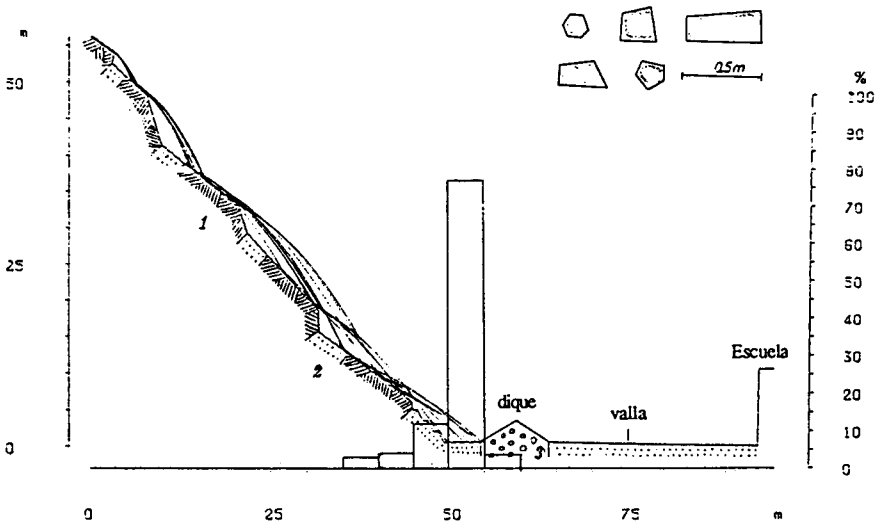

ST CARLES (OLIVERA)

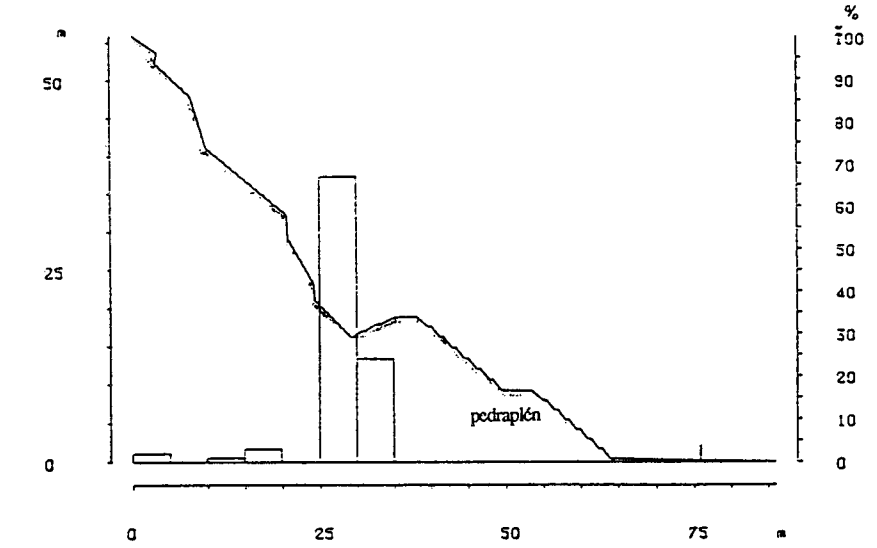

Fig.23 St. Carles quarry (1:fresh bedrock,limestone;2: grass or green;3: rock debris, scree deposit)
a) Results adjusted for the previous situation. The block shapes, the simulated paths and the frequency graph vs run-out distance are shown.
b) Results predicted for the new situations with a rock embankment.

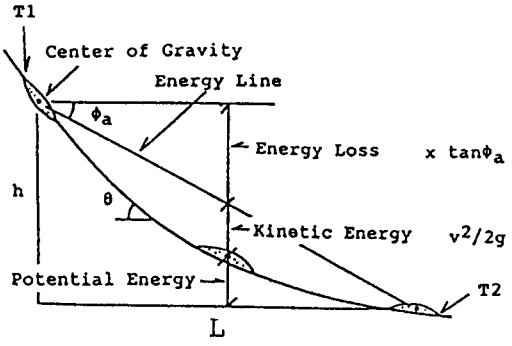

Fig.24 Sled model for the landslide runout distance.

The inventory graphs usually integrate information from various types of mass movements. Relationships has been found between the volume of a fallen mass and its reach. Hsü (1975) observed a decrease of the equivalent coefficient of friction (H/L) with the rockfall volume (fig.25a). This friction decrease is more evident in bigger rockfalls. Hutchinson (1988) found a new envelope for chalk failures and flow slides of coal mine wastes. He observed a different reach for talus formation derived from chalk rockfall from that attained by chalk flows (fig.25b). Specific lithology and type of movement seems to have more important influence with volume reduction. Corominas et al. (1988c) observed a different behaviour depending on the type of failure mechanisms for less voluminous movements (fig.25c). This fact may be explained by considering that big rockfalls dissipate a lot of energy by hitting the substratum and breaking into small rock fragments, whereas shallow slab slides should only dissipate energy as friction in the shear surface.

Debris flows presenting a thick basal shear zone or dispersivity of their clastic components (grain flow), will occupy an intermediate place. The use of this empirical relationship is still limited due to the lack of more representative data.

For very small movements the material of the substratum below the landslide source may have a significant influence on the progression of the displaced mass. This fact can be seen at the rockfalls inventored in the Pyrenees area (Corominas et al. 1990) where the presence downslope of grassland, bedrock, scree deposits or forest is a conditioning factor for material progression.

As can be seen the volume is a conditioning factor of landslide mobility. Unfortunately its prediction is very difficult unless the failure has started and visible scars limit the landslide. For these reasons, this kind of runout graphs give only a crude approximation.

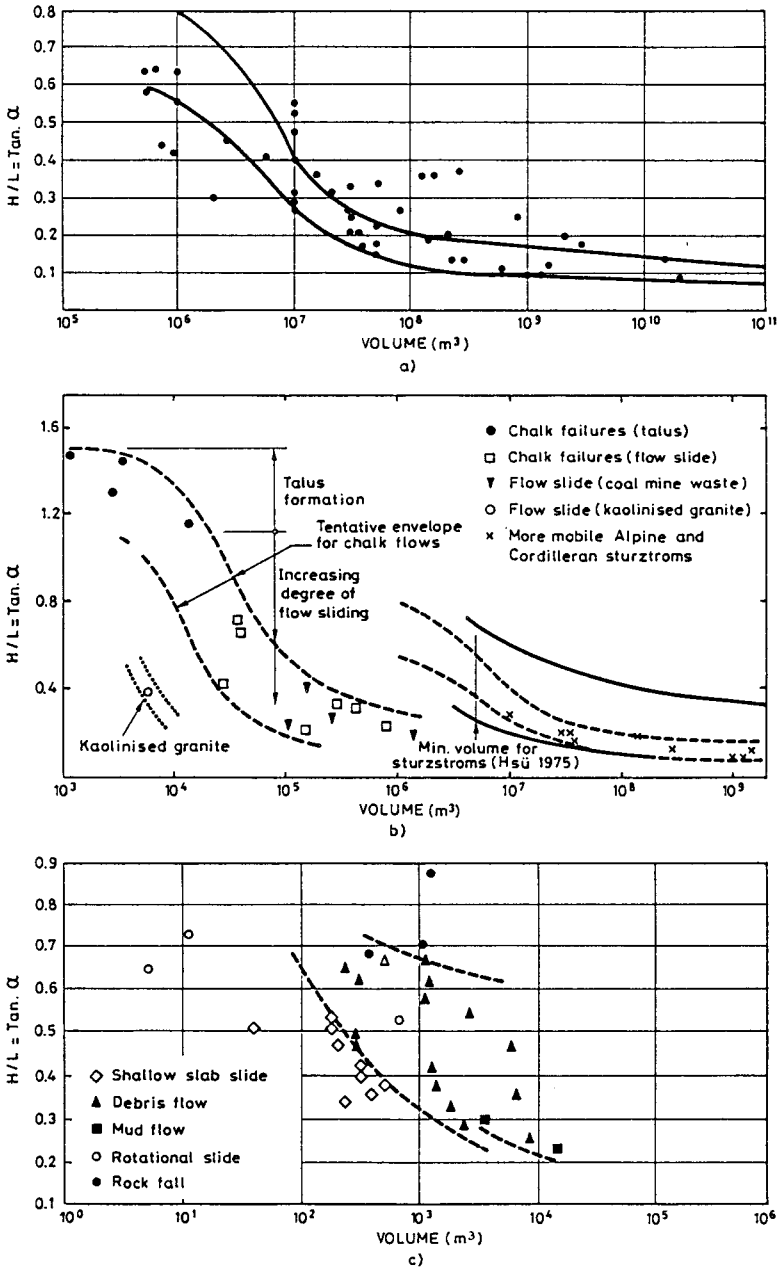

Fig. 25 Landslide mobility. Volume of fallen mass is plotted against height drop and the horizontal distance travelled ratio (H/L): a) data for huge rock avalanches (Hsü, 1975). b) data from Hutchinson, 1988. c) data for small volume movements (Corominas et al. 1988c).

All the models and works developed and presented until here have some good capabilities, but also serious drawbacks and disadvantages when trying to apply to a given case: Which set of parameters are the most representative?; How to measure them?; internal hidden values and details; scale effects; underground heterogeneities: natural variability (space and time); etc. However, when attempting to match the field behaviour, they may help to improve our basic knowledge of the phenomena, giving more mean "key parameters" values and experience, or forcing to adapt the conceptual model to new situations. Becoming, in this sense, an excellent tool for understanding and discussion.

Acknowledgements

We would like to acknowledge basic work and advice of the following students: V. Tolós, M. Moreno, C. Baeza, J. Gutierrez.

References

Azimi, C., Desvarreux, P., Giraud, A., Martin-Cocher, J. (1982) "Methodes de calcul de la dynamique des chutes de blocs. Application a l'etude du versant de La Pale". Bull. de Liaison des Lab. des Ponts et Chaussees, 122, pp.93-102.

Brugnot, G., Pochat, R. (1981) "Numerical simulation study of avalanches". J. Glaciology, 27 (95), pp.77-88.

Chen, C., Armbruster, J.T. (1980) "Dam-break wave model: formulation and verification, ASCE J. Hydraulics Div. 106 (HY5), pp.747-767.

Corominas, J. (1984) "Sobre la formación de coladas de barro en el Pirineo catalán". Procc. Jornadas sobre inestabilidad de laderas en el Pirineo, pp.I.9.1-I.9.10.

Corominas, J., Moreno, M., Pujals, J.M. (1988a) "El comportamiento de las coladas de barro. Análisis mediante balance de energía". Proc.II Symp. sobre taludes y laderas inestables. Andorra,pp.183-194

Corominas, J., Moreno, M. (1988b) "Mechanism of mudflows: A case study in the Spanish eastern Pyrenees". Proc.5th. Int. Congress on Landslides, Laussanne. pp.589-594.

Corominas, J., Peñaranda, R., Baeza, C. (1988c) "Identificación de factores que condicionan la formación de movimientos superficiales en los valles altos del Llobregat y del Cardener". Proc.II Symp. sobre taludes y laderas inestables. Andorra,pp.195-207.

Corominas, J., Esgleas, J., Baeza, C. (1990) "Risk mapping in the Pyrenees area: a case study". Hydrology in mountainous regions II, I.A.H.S., Publ. n.194, pp.425-428.

Dressler, R.F. (1952) "Hydraulic resistance effect upon the dam-break functions". J. Res. Nat. Bur. Standards 49 (3), pp.217-225.

Falcetta, J.L. (1985) "Un nuveau modele de calcul des trajectoires de blocs rocheux". Revue Francaise de Geotechnique, N. 30, pp.11-17.

Gili,J.A.,Corominas,J. (1992)"Aplicación de técnicas fotogramétricas y topográficas en la auscultación de algunos deslizamientos".III Simp. Nac. sobre Taludes Laderas Inestables, La Coruña, pp.941-952.

Gili, J.A., Gutierrez, J. (1992) "Aplicación de un modelo de simulación de caida de bloques rocosos a casos reales". Proc. III Simp. Nac. sobre Taludes y Laderas Inestables, La Coruña, pp.15-26.

Huerta, A. (1987) "Numerical modeling of slurry mechanics problems". PhD Dissertation, Northwestern University, Evanston, IL.

Huerta, A.,Liu, W.K.(1988) "Viscous flow with large free surface motion". Computer Meth. in Applied Mech and Eng., 69, pp.277-324.

Huerta, A.,Liu, W.K.(1990) "Large amplitude sloshing with submerged blocks". J. pressure vessel technology, ASME, vol.112, N.1, pp.104-108.

Huerta, A., Sierra, J.P., Arcilla, A., Navarrina, F. (1990) "Numerical modelling of Tsunamis: generation and propagation". Proc. 2nd World Congr. on Comp. Mech., Stuttgart, vol.1, pp.136-139.

Huerta, A., Casadei, F., Donea, J. (1992) "An arbitrary Lagrangian Eulerian stress update procedure for coining simulations". Proc. 4th. Int. Conf. on Num. Meth. in Industrial Forming Processes, Balkema, Sophia-Antipolis, pp.261-266.

Huerta, A., Casadei, F. (1993) "New ALE applications in non-linear fast-transient dynamics". Engineering Computations (to appear).

Hutchinson, J.N. (1988) "Morphological and geotechnical parameters of landslides in relation to geology and hidrogeology". Proc. 5th.Int.Congr. on Landslides, Laussanne, Vol.1, pp.3-35.

Hsü, K.J. (1975) "Catastrophic debris streams (sturzstroms) generated by rockfalls" Geol. Soc. Am. Bull., N.86, pp.129-140.

Jeyapalan, J.K. (1980) "Analysis of flow failures of mine tailing impoundments". PhD Dissertation, University of California, Berkeley, CA.

Rochet, L. (1987) "Application des modeles numeriques de propagation a l'etude des eboulements rocheux". Bull. de Liaison des Lab. des Ponts et Chaussees, 150/151, pp.84-95.

Sassa, K. (1988) "Geotechnical model for the motion of landslides". Proc. 5th.Int.Congr. on Landslides, Laussanne, Vol.1, pp.37-55.

Tolós, V., Huerta, A. (1992) "Comparació de dues tècniques numèriques per la resolució d'equacions diferencials quasi-hiperbóliques. Aplicació als moviments de superficie lliure". Internal technical report. ETSECCP Barcelona, 117 pag.

Trunk, F.J., Dent, J.D., Lang, T.E. (1986) "Computer modeling of large rock slides". Journal of Geotech. Eng., Vol.112, N.3, pp.348-360.

Vulliet, L., Hutter, K. (1988) "Continuum model for natural slopes in slow movement". Geotechnique, Vol.38, N.2, pp 199-217.

Dense-Flow Avalanches, a Discussion of Experimental Results and Basic Processes

Avalanches à écoulement dense, une discussion sur des résultats expérimentaux et sur les mécanismes élémentaires

H. GUBLER

SFISAR
CH-7260 Weissfluhjoch, Davos - Switzerland
Tel. (41) 81 417 01 11 - Fax. (41) 81 417 01 10

Abstract

This paper deals with dense flow avalanches measurements and the basic process involved. After a short classification of avalanches, the author describes field experiments performed on 20 artificially released avalanches. Two kinds of X-band radars have been used to measure the velocities in the avalanche body. Some conclusions draws from these experiments are then presented. They introduce two kinds of dense flow avalanches and discuss the velocity distribution in the avalanche body and along the path. The influence of the snow temperature is also shown. The author also gives some explanation on dissipative processes based on the ice crystals structure and describe the start of the flow and other processes at work in the steady flow and in the flow retardation.
In conclusion, the processes which are not taken into account in existing models are listed and the emphasis is put on the most important parameters.

Résumé

Cet article traite de mesures sur des avalanches à écoulement dense et sur les mécanismes physiques impliqués dans ces avalanches.
Après une classification succincte des avalanches, l'auteur décrit des expériences de terrain réalisées sur 20 avalanches déclenchées artificiellement.
Deux types de radars X ont été utilisés pour mesurer les vitesses dans l'avalanche. Des conclusions tirées de ces expériences sont ensuite présentées. Elles introduisent deux types d'écoulement dense d'avalanche et discutent de la distribution des vitesses dans l'avalanche et le long du site. L'influence de la température de la neige est également mentionnée.
L'auteur donne aussi des explications sur les processus de dissipation qui sont basées sur la structure du cristal de neige. Il décrit le départ de l'avalanche et d'autres mécanismes à l'oeuvre dans l'écoulement et dans l'arrêt de l'avalanche.
En conclusion, les phénomènes qui ne sont pas pris en compte dans les modèles existants sont rappelés. L'accent est mis sur les paramètres les plus importants.

Classification of avalanches

Snow avalanches are classified based on the starting mechanisms, the position of the sliding surface, liquid water content of the snow, form of the avalanche path and type of movement. Typically large snow avalanches release as large slabs. Primary fracture propagates along a weak shear layer parallel to the slope and ends in slope perpendicular fractures in the upper part and at the sides of the slab. Mean fracture heights vary usually between 0.2 and 2 m, but may be significantly higher occasionally. By this mechanism large volumes of snow (typically 10'000 -100'000 m^3) start to move almost simultaneously. The movement depends on snow temperature/liquid water content, the form and length of the avalanche path, inclination of the path and the size of the avalanche. If the shear stresses at the upper boundary of the dense flow are high enough to transfer small particles from the disintegrated slab into suspension a snow cloud will be formed. In the following discussion we will concentrate on dense-flow avalanches.

Field experiments

Particle speed distributions in artificially released dense flow avalanches from start to stop have been measured using oversnow-vehicle based X-band microwave Doppler radars (Fig.1). Frequency-modulated continuous-wave (FMCW) X-band radars buried in the avalanche tracks provide localized flow height and slope-perpendicular particle speed-profile recordings. So far, measurements on 20 avalanches have been performed. Avalanche sizes varied from a few hundred to several tens of thousand cubic meters of snow, total drop height from release to run-out from 150m to 1000m. Most avalanches were channelled at least in their middle part.

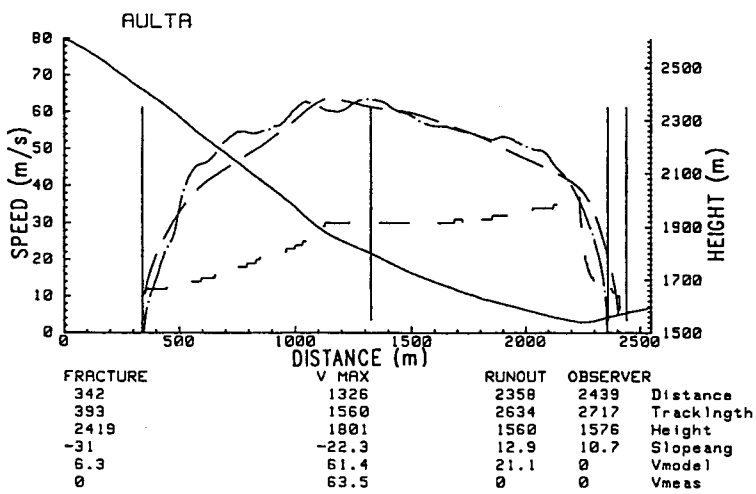

Fig.1 Front speed of a large avalanche as a function of distance. Solid line: track profile, dash-point: measured speed.

The basic results of Doppler measurements are speed spectra. Narrow-beam radars deliver time series of speed distributions of snow particles moving through a given location. The variation of the particle speeds in the flow from the front to the tail of the avalanche is recorded as the avalanche moves through the illuminated cross section. The shape of the spectra depends on the type of avalanche. Small avalanches consisting mainly of sliding snow blocks, low speed wet flows and slow movement of locked snow in the run-out produce fairly narrow, almost symmetric speed spectra (Fig.2). High speed avalanches are characterized by wider spectra (Fig.3) that often show a sharp cutoff at the high speed end, a wide asymmetric peak toward lower speeds and a long tail often reaching down to zero speed. These spectra correspond roughly to what is expected if a flow with an exponential flow-speed profile perpendicular to the gliding plane is probed at a low incidence angle with a radar.

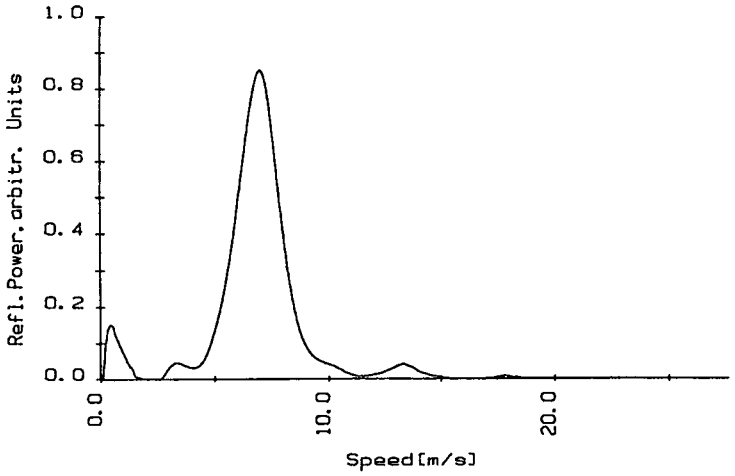

Fig. 2 Typical speed distribution in a cross section of the avalanche body of a slow moving avalanche.

Time series of particle speed spectra show a sharp increase of speed at the front of the avalanche. The rise time is determined by the instrument's spacial resolution.) The highest particle speeds of the avalanche are measured near or at the front (Fig. 4). In large flows particles in the segment of the avalanche immediately following the front move at about front-speed. The existence of this segment of constant flow-speed (avalanche body) is essential for the development of the avalanche. In the tail portion of the avalanche, speed decreases almost linearly with time.
A set of two FMCW radars buried at a distance of about 15 m from each other along the main flow direction were used to measure the slope perpendicular flow speed profile (Fig. 5). The radars measure slope perpendicular distances to the moving particles. If the internal structure of the avalanche does not change significantly within the short distance between the two radars, the speed profile can be determined from cross correlations of reflected power from different levels in the

flow. The distance-measurements may be significantly Doppler-widened if the particles have high slope-perpendicular fluctuation speeds. Especially at the location of the upper radar particles close to the flow surface have speed components perpendicular to the main flow direction. This fluctuation may be caused by a small cliff some ten meters above the upper radar.

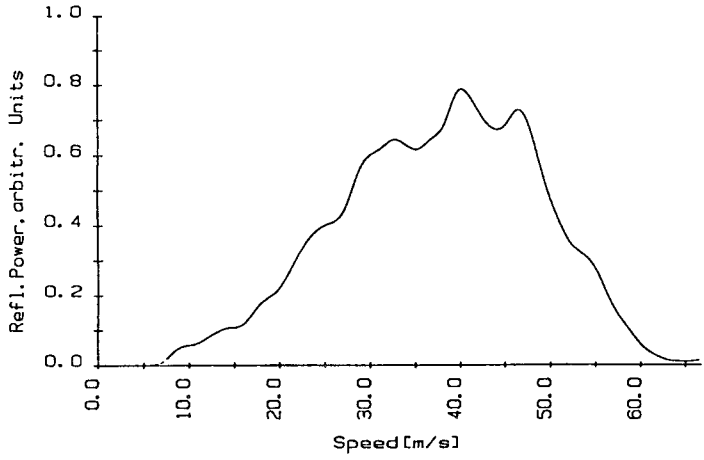

Fig. 3 Typical speed distribution in a cross section of the avalanche body of a fast moving partially fluidized avalanche.

Fig. 4 Particle speed in a fixed cross section in function of time, or particle speed along the avalanche.

Summary of conclusions from the measurements

There are two types of flows: a) Partly fluidized flow with significant fluctuation of particle speeds in flow direction and perpendicular to the flow. The shear zone in the flow close to the sliding plane extends over at least ten cm. In the upper part of the flow the speed profile may still be quite uniform. b) The avalanche moves more like a flexible body. Particle speeds are very uniform throughout the flow. There is very little particle fluctuation. The avalanche slides on the bed.

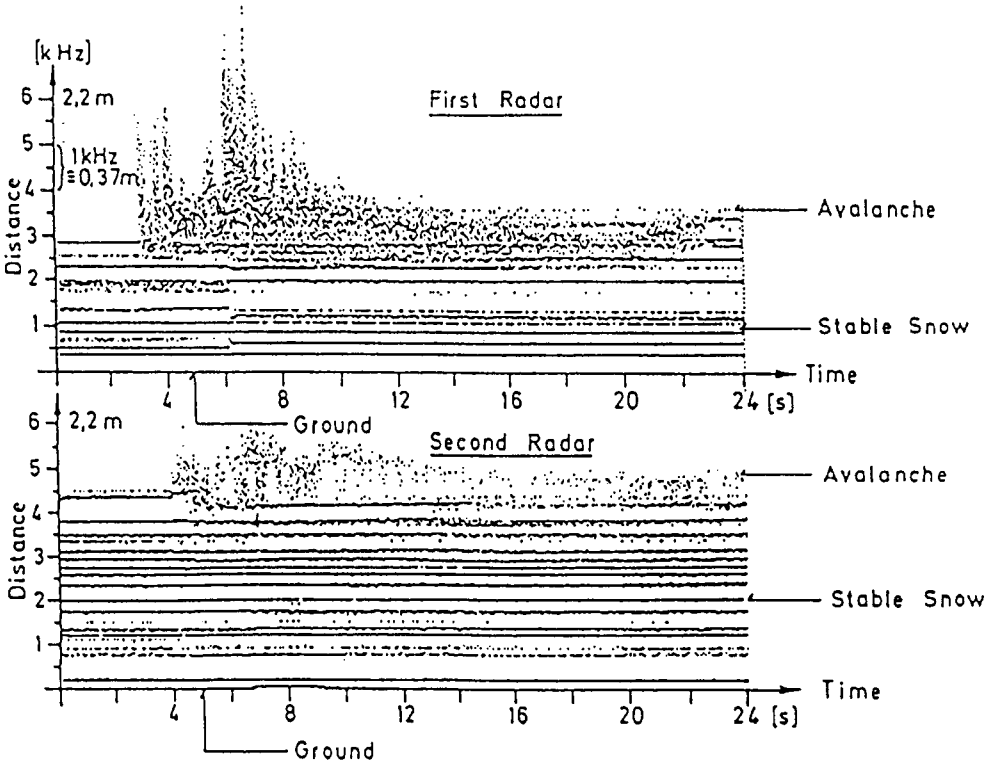

Fig. 5 Avalanche flow as seen from the two buried FMCW radars. Horizontal lines are layer interfaces in the static snow cover.

The front velocity of dense flow avalanches depends on the size of the avalanche body (section of avalanche with constant flow velocity and flow height immediately be hind the front). The highest particle velocities are found immediately behind the front in the avalanche head. The front flow velocity starts to decrease rapidly if the avalanche body disappears completely. This effect may stop an avalanche even in steep terrain (slope angles above 25°). The amount of transfer of avalanche snow from the avalanche head and body to the avalanche tail is important for the development of the flow. High track roughness increases the snow transfer from body to tail. The relative velocities of particles (width of

velocity spectral line) in the avalanche head and body increase with increasing characteristic speed and avalanche size. This is interpreted as an increase of fluctuation speed of larger snow clods. At least for small avalanches, snow temperatures near the melting point result in lower flow speeds, lower particle relative velocities and very long avalanches without typical head and body structures. At high snow temperatures larger avalanches tend to solidify in the run-out and to move as flexible bodies pushed by the snow behind.

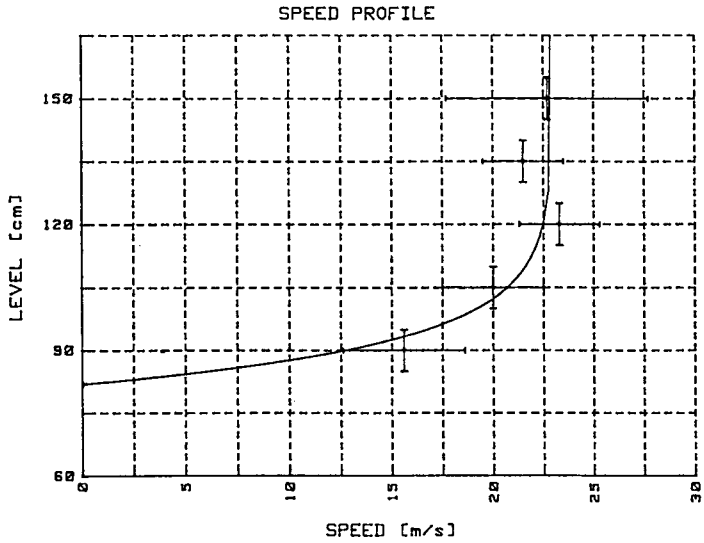

Fig. 6 Slope perpendicular speed profile

Discussion of dissipative processes

Snow changes its bulk properties significantly from start to stop of an avalanche. Snow consists of ice-crystals. The intergranular bonding depends on the shape and packing of the grains. The strength of the bonds between the crystals depends on bond size and ice-temperature. The formation of bonds and the rate of increase of their strength at new contact points between grains strongly depend on time of contact, contact pressure and ice temperature. Close to the melting point of ice bonding develops very fast. Although small ice grains have a high coefficient of restitution, collisions between snowballs are completely inelastic.

Start of flow

A short time after a slab is released it starts to disintegrate into smaller particles. Energy is dissipated by increasing the specific ice surface. The energy is supplied to the system in the form of fluctuation energy (relative motion of the snow clods). The fluctuation energy is generated by deflection and impact of the clods with the ground

roughness. A granulation model could be based on the assumption that the probability for breaking a snow clod into parts is proportional to the exponential

$$p = \exp\left(-\frac{\text{increase of surface energy per collision}}{\text{fluctuation energy of particle}}\right)$$

Steady flow

In a granular flow the fine material accumulates at the base of the flow, the larger clods swim on top. Different distributions of shearing within the snow and between snow and ground (sliding) are possible. The contact forces within the flow are the friction between the fluctuating particles, increasing cohesion if fluctuation and internal shear cease, and impact forces between particles with a coefficient of restitution $e \approx 0$ for snow clods and $e \leq 1$ for small ice particles.

a) Smooth sliding surface

If the sliding friction is smaller than the shear strength within the flow pure sliding will occur. This is the typical situation for wet snow avalanches in a smooth channel.

b) Microscopic roughness of the sliding plane large enough to induce shear in the fine grained bottom layer

Because of the high coefficient of restitution for the very small ice particles the decay length for the fluctuation velocity is large compared to the particle diameter. If the fluctuation pressure equals the static pressure from the overburden flow the fine grained material fluidizes, reducing friction between ground and flow.

c) Macroscopic roughness of track:

The coarse grained material will not fluctuate unless there is a significant macroscopic roughness of the sliding plane. Because of the very low coefficient of restitution for the snow balls true fluidisation is not possible. There is very little shearing in the upper part of the flow. Nevertheless these larger clods of snow will collide with each other, effectively dissipating energy and slowing down the avalanche. In a uniform, smooth channel or on a smooth slope the coarse material may start to lock, especially at high snow temperatures.

Other important mechanisms are:

- Entrainment of loose snow from the track at the avalanche front increasing the avalanche volume. Entrainment retards the flow but feeds snow to the avalanche body.
- Loss of snow from the avalanche body to the avalanche tail, reducing length and flow-height of the avalanche body. Small avalanches on rough terrain may lose enough material by this mechanism to be stopped in relatively steep terrain.

Flow retardation

During the retardation process high slope parallel normal stresses are generated in the flowing material. Depending on whether avalanche speed, roughness of the sliding plane and snow temperature cause partial fluidisation, sliding of cohesionless material or locking of the material, different scenarios may develop: lateral spreading in the run-out, flow of backward material on top of front material causing shear planes in the deposit, or fingering. The fingers consist of locked snow. Normal pressure along the fingers may significantly extend the flow distance. Because these fingers are very flexible laterally, the direction of their movement has a chaotic character.

Conclusion

Many models for simulating snow avalanches have been developed during the last 15 years. Today numerical simulations can quite easily be done as long as the constitutive equations for the material are not too complicated. Many approaches are based on the Bingham model. None of them take into account that the constitutive behaviour of flowing snow significantly varies from start to stop of the flow. Also the effects of roughness of the sliding plane, snow type, entrainment and loss of snow are not modeled. Maybe we will never be able to take all possible parameters into account and still keep the models manageable and useful. This raises the question of what is really needed: The ultimate goal of avalanche dynamics is the assessment of potential hazards. Safety theory defines the requirements on avalanche models: runout distances and pressures exerted on obstacles have to be known as a function of probability of occurrence. Therefore models must be applicable for different terrain and snow conditions. The most important parameters are the extent of the starting zone, total released snow mass as a function of recurrence period, and the constitutive behaviour of snow.

References

Bakkehoi, S., Domaas, U., Lied, K. (1983) Calculation of snow avalanche runout distance. Annals of Glaciology 4, 24 - 29.

Brugnot, G., Vila, J.P. (1985) Investigation théorique et expérimentale des caractéristiques dynamiques des avalanches de neiges dense. La Houille Blanche, no. 2, 133 - 142.

Dent, J.D., Lang, T.E. (1983) A biviscous modified Bingham model of snow avalanche motion. Annals of Glaciology, Vol 4, 42 - 46.

Eybert-Bérard, A., et al. (1978) Mesures dynamiques dans l'avalanche. Résultats expérimentaux du Col du Lautaret (1971 - 1978). ANENA, Comptes Rendus, 2e Rencontre Int. sur la Neige et les Avalanches, 12 - 14 Avril 1978, Grenoble, p.202 - 224.

Gubler, H. (1982) Strength of bonds between ice grains after short contact times, Journal of Glaciology, 28, no. 100, 457 - 473.

Gubler, H. et al. (1986) Messungen an Fliesslawinen, Mitteilung des Eidg. Institutes für Schnee- und Lawinenforschung Nr. 41.

Gubler, H. (1987) Measurements and modelling of snow avalanche speeds. In: Avalanche Formation, Movement and Effects, Proceedings of the Davos Symposium, Sept. 1986, IAHS Publ. no. 162, p. 405-420.

Hutter, K., Szidarovszky, F., Yakowitz, S. (1987) Granular shear flows as models for flow avalanches. In: Avalanche Formation, Movement and Effects, Proceedings of the Davos Symposium, September 1986, IAHS Publ. No. 162, p.381-394.

Maeno, N., Nishimura, K. (1989) Contribution of viscous forces to avalanche dynamics. Annals of Glaciology Vol. 13, p. 202 - 208.

Martinet, G. Contribution à la modélisation numérique des avalanches de neige dense et des laves torrentielles. Thèse, 1992, Université Joseph Fourier, Grenoble France.

McClung, D., Schaerer, P.A. (1983) Determination of avalanche dynamics friction coefficients from measured speeds. Annals of Glaciology Vol. 4, p.170 - 173.

Norem, H., Irgens F., Schieldrop B. (1987) A continuum model for calculating snow avalanche velocities. In: Avalanche Formation, Movements and Effects, Davos, September 1986, IAHS Publication No. 162, p. 363 - 379.

Norem, H., Irgens, F., Schieldrop, B. (1989) Simulation of snow avalanche flow in run-out zones. Annals of Glaciology, Vol. 13, p. 218-225.

Norem, H., Nishimura, K., Maeno, N. (1992) Comparing model and full-scale experiments on snow avalanche dynamics. IGS Symposium, Japan 1992. To be published in Annals of Glaciology.

Salm, B., Gubler, H. (1985) Measurement and analysis of the motion of dense flow avalanches. Annals of Glaciology Vol. 6, p.26 - 34.

Salm B. (1992) Flow, flow transition and runout distances of flowing avalanches. Presented to the IGS-Symposium, Japan 1992. To be published in Annals of Glaciology.

Tesche, T.W. (1986) A three dimensional dynamic model of turbulent avalanche flow. Snow Science Workshop, Lake Tahoe, California, October 22 - 25, p.111 - 137.

Numerical Simulations of Powder-Snow Avalanches and Laboratory Experiments on Turbidity Currents

Simulation numérique d'avalanches de neige poudreuse et expériences de laboratoires sur les courants de turbidité

F. HERMANN*‡, D. ISSLER†, S. KELLER*§

*Lab. of Hydraulics, Hydrology and Glaciology, ETH Zürich
CH-8092 Zürich - Switzerland

†SFISAR
CH-7260 Weissfluhjoch, Davos - Switzerland
Tel. (41) 81 417 01 11 - Fax. (41) 81 417 01 10

*Tel. (41) 16 32 41 48 - Fax. (41) 12 52 01 47

§Tel. 41-1-632-52 79 - Fax ++41-1-252-01 47

Abstract

This paper begins with a description of the physical processes at work in powder snow avalanches and in turbidity currents. A comparison between these two kinds of phenomena is presented. In a second part, a mathematical model is given with a special emphasis on turbulence and erosion/sedimentation processes. The paper deals then with an experimental study of powder snow avalanches by means of laboratory models. The experiments look realistic, no quantitative conclusions can be drawn.
Finally, different numerical simulations are described. Some of them are adapted to laboratory experiments, some others to actual powder snow avalanche events.

Résumé

Cet article commence par une description des mécanismes physiques à l'œuvre dans les avalanches de neige poudreuse et dans les courants de turbidité. Une comparaison entre ces deux types de phénomènes est présentée. Dans la seconde partie, un modèle mathématique est proposé avec une prise en compte spécifique de la turbulence et des mécanismes d'érosion et de sédimentation. L'article traite ensuite d'une étude expérimentale des avalanches de neige poudreuse à l'aide de modèles de laboratoire. Si les résultats obtenus semblent proches de la réalité, aucune conclusion quantitative ne peut être tirée.
Finalement, différentes simulations numériques sont décrites. Certaines correspondent aux expériences de laboratoire ; d'autres à de véritables avalanches de neige poudreuse.

Basic physical processes at work in powder snow avalanches

Under conditions of dry and cold fresh snow, dense-flow avalanches (DFAs) may become partially suspended in the air, forming so-called powder-snow avalanches (PSAs) which can cause enormous damage over large areas. We are developing computational methods for calculating runout distances, velocities and pressures so as to create a useful tool for avalanche danger mapping. Since PSAs are difficult to investigate in the field, we take recourse to experimental studies of turbidity currents (TCs, particle suspensions in a water tank) for validating our numerical models. This paper aims at giving an overview of our general approach, emphasizing open questions and problems.

Both powder snow avalanches in nature and turbidity currents in the laboratory exhibit the characteristic features of gravity currents [1], such as a distinct head with a raised nose in front of the body of the avalanche, and air entrainment along the upper and lateral surfaces. The flows are highly turbulent, with Reynolds numbers of the order of 10^8 and $2 \cdot 10^4$, respectively. The fine particles impart their momentum gained from gravity to the air around them whose turbulence, in turn, keeps them suspended. Turbulence thus plays a double role as the main decelerating mechanism on the macroscopic scale and the suspending mechanism on the mesoscopic scale. At least in PSAs, where the fluid density is much smaller than the mixture density, fluid turbulence will be significantly affected by the presence of particles.

Under certain conditions, snow from the avalanche track or sand from the bed of a submarine canyon may be entrained into the cloud, increasing further the speed and erosive power of the avalanche. Without snow entrainment, however, the settling velocity of the particles (about 1 m/s for snow grains) causes sedimentation and reduces the gravitational force on the flow. This being a positive feedback mechanism, the balance between erosion and sedimentation can strongly influence the dynamics of the avalanche.

The quartz or polyester particles in the laboratory flows have Stokes numbers (the ratio of particle and fluid time scales) well below 0.1 and thus follow the turbulent fluctuations of the fluid velocity very closely. In contrast, the snow grains have intermediate Stokes numbers in the range $0.1 < St < 10$ so that they are able to follow the larger eddies in the fluid flow but not the smaller ones. As a consequence, snow grains are expected to get trapped in regions of high shear and vorticity.

Of special importance are the processes taking place at the bottom of the flow. Studies of blown sand and snow revealed a thin but dense layer where particles hop in the direction of the wind, picking up a significant amount of momentum from the fluid while near the summit of their trajectories. A fraction of this energy - depending on the cohesion of the material - serves to eject other particles on impact while the rest is dissipated. The upper boundary of this saltation layer also marks the transition from the laminar sublayer to the turbulent regime. Near the apex of their trajectories particles may thus be lifted into suspension by a turbulent eddy. It follows that correct modelling of the suspension transport rate requires an adequate understanding of the structure of the saltation layer.

One expects to encounter similar conditions at the bottom of a PSA or of a TC because the high speed of the flow creates a shear layer, particles may fall into it from the

suspension cloud and impinge on the ground. Since the trajectory height and thus the height of the saltation layer increase with the shear stress, the thickness of the saltation layer in a PSA should be of the order of 1 m rather than 2-5 cm as in snow drift. Observations from the runout of real PSAs seem to be consistent with this conclusion.

Mathematical modelling of powder snow avalanches

In order to capture the effects of sedimentation and erosion that are important in TCs and PSAs, a model with two fully dynamical phases (fines and water or snow and air, i.e., the particles are treated like a fluid with volume concentration $c(t,\mathbf{x})$) would represent a useful framework. However, before this approach becomes fully viable several theoretical and numerical issues need to be resolved, among them the proper treatment of the particle-phase pressure and the interaction between particle and fluid turbulence.

For simplicity, let us therefore first neglect erosion and sedimentation and consider the limiting case where the coupling between the particles and the ambient fluid (air, water) is so strong that both components move at the same velocity U. One thus obtains the equations describing density currents (e.g., brine in fresh water, as studied by Beghin [2]):

$$\partial_t \rho + \nabla \cdot (\rho \mathbf{U}) = 0 \tag{1}$$

$$\partial_t (\rho \mathbf{U}) + \nabla \cdot (\rho \mathbf{U}\mathbf{U}) = -\nabla p + \nabla \cdot (\mu_{eff} \nabla \mathbf{U}) + \Delta\rho \mathbf{g} \tag{2}$$

$$\partial_t c + \nabla \cdot (c\mathbf{U}) = \nabla \cdot \left(\frac{\mu_{eff}}{\rho \sigma_c} \nabla \mathbf{U} \right) \tag{3}$$

where $\rho = \rho_f + \rho_p = \hat{\rho}_f + \Delta\rho$ is the mixture density, $\Delta\rho = c\Delta\hat{\rho} = c(\hat{\rho}_p - \hat{\rho}_f)$; $\hat{\rho}_f$ and $\hat{\rho}_p$ designate the intrinsic densities of pure particles and fluid, respectively. σ_c is the turbulent Prandtl number for the particle concentration. Use has been made in eqns. (2) and (3) of Reynolds averaging and the eddy-viscosity hypothesis; some way for determining the contribution from turbulent diffusion to the effective viscosity μ_{eff} needs to be prescribed, e.g., the two-equation k-ε model.

As a first step towards a more comprehensive model one may introduce the slip velocity $\mathbf{u} = \mathbf{u}_p - \mathbf{u}_f$ and approximate it by the settling velocity of the particles: $\mathbf{w} = w\mathbf{g}/g$. The mixture mass balance (2) remains unchanged. The particle mass balance (3) becomes

$$\partial_t c + \nabla \cdot (c\mathbf{U}) = \nabla \cdot \left(\frac{\mu_{eff}}{\rho \sigma_c} \nabla \mathbf{U} \right) - \mathbf{w} \cdot \nabla \left(c \frac{\rho_f}{\rho} \right) \tag{4}$$

In the momentum balance of the mixture, an extra term arises from the momentum flux of the sedimenting particles:

$$\partial_t(\rho \mathbf{U}) + \nabla \cdot (\rho \mathbf{U}\mathbf{U}) = -\nabla p + \nabla \cdot (\mu_{eff} \nabla \mathbf{U}) + \Delta\rho \mathbf{g} - \mathbf{w}\mathbf{w} \cdot \nabla \left(\frac{\rho_f \rho_p}{\rho} \right) \tag{5}$$

In most cases, however, this new contribution is negligible compared to the convective term on the left hand side since $|\mathbf{w}| << |\mathbf{U}|$.
The settling particles bring along the turbulence level at their previous location which - on the average - receives the same volume of fluid with the turbulence level from below. Assuming very low Stokes numbers, we modify the turbulence equations in the k- ε model in the following way:

$$\partial_t(\rho k) + \nabla \cdot (\rho k \mathbf{U}) - \nabla \cdot \left(\frac{\mu_{eff}}{\sigma_k} \nabla k \right) = \mathbf{P} + \mathbf{G} - \rho\varepsilon + \mathbf{w} \cdot \nabla (k \Delta\rho) \tag{6}$$

and analogously for the ε equation. P and G are the usual production terms due to shear and gravity, respectively, and ε is the dissipation term.

It should be kept in mind that the widely used k-ε turbulence model may not be adequate for our purposes. It is known to perform poorly in regions of high shear or of strongly curved streamlines. Both these situations occur in PSAs, but it is not known yet whether a more sophisticated turbulence model - such as a differential Reynolds stress/flux model or a renormalization group-improved k-ε model - will be required.
Inclusion of the settling velocity as sketched above will modify the concentration, momentum and turbulence profiles somewhat, but realistic results can be expected only when the saltation layer is adequately modelled. We are just beginning the development of such models and no definite mathematical scheme can be presented yet. First analyses suggest treating the saltation layer separately from the powder snow cloud, each system providing the boundary conditions for the other; we envisage an iterative solution procedure for the coupled system.
There is a rich literature, both experimental and theoretical, on the problem of Aeolian transport of sand or snow, with sometimes conflicting results. It appears, though, that the critical ingredients of any model are (i) an estimate of the ejection rate distribution as a function of wind shear, snow drift density and snow properties, (ii) the modification of the wind velocity profile in the saltation layer, and (iii) the correct determination of turbulent suspension of snow from the saltation layer.

Turbidity currents as a laboratory model of powder snow avalanches

High-quality field data on PSA events is very rare. So, in order to test our numerical models in a physically similar but experimentally accessible situation, we investigate turbidity currents of polyester or quartz powder (grain sizes 100-400 μm and 30-120 μm, respectively) in a large water tank. Various geometrical configurations can be used : plane chutes or open-channel chutes at various inclinations and with variable inclinations in the runout, or even 1/1000 scale models of real avalanche tracks. An ultrasonic Doppler device allows quasi-simultaneous measurement of particle concentration and speed at 16 different locations with good time resolution. So far, measurements of the velocity were restricted to the component in the main flow direction, but the full velocity vector and selected correlations of velocity and/or density fluctuations may be measured in the near future if desired.

In the first stage of our experimental work [3,4], quasi-twodimensional and quasi-stationary flows were investigated. One of the most interesting results was the consistent appearance of high-density regions at various locations in the TCs, generally coupled with increased velocities. If this phenomenon also occurs in real PSAs, simple one- or two-dimensional models may underestimate the relevant dynamic pressures by an order of magnitude.

Current experiments investigate the three-dimensional behaviour of transient TCs on inclined planes with or without slope change. Comparing runs with differently-sized quartz particles will allow us to study the influence of particle deposition. (Particle entrainment from the ground is strongly suppressed in our setup because the grains roll downhill on the relatively steep slopes used in these experiments.) We anticipate an extensive set of high-quality, high-resolution data that will comprehensively test our numerical models. At a later stage, we plan to measure the flow field around obstacles such as buildings, dams, power line pylons, etc.

Prompted by the absence of reliable calculational tools for PSAs and the very close agreement in the qualitative behaviour of TCs and real avalanches, our group was charged with the laboratory modelling of a large PSA event that occurred in 1984, and with an expertise on the residual danger after the construction of defence structures in the concerned area. While the experiments on a 1/1000 scale model of the affected area looked stupendously realistic even to an expert, careful analysis of the scaling behaviour revealed that no quantitative conclusions can be drawn from the measurements.

The difficulty stems from the fact that the ratio of gravitational to inertial forces is almost independent of snow concentration in PSAs but varies linearly with particle concentration in turbidity currents; this is due to the fact that PSAs are much denser than air while our TCs are only slightly denser than the surrounding water:

$$\frac{\Delta\rho}{\rho} = \frac{\kappa c}{1 + \kappa c} \approx \begin{cases} 1 - \frac{1}{\kappa} c \approx 0.9 \ldots 0.1 & \text{for PSAs;} \\ \kappa c \approx 0.02 \ldots 0.00002 & \text{for TCs.} \end{cases} \tag{7}$$

where $\kappa = \Delta\hat{\rho} / \hat{\rho}_{fluid}$ is about 900 for snow in air and 1.65 for quartz in water. The scaling factor for the velocities is determined by the requirement that the effective densimetric Froude numbers be the same in the laboratory *(M)* and in nature *(N)*:

$$U_N = \beta U_M \tag{8}$$

where

$$\beta^2 = \frac{1}{\lambda^2} \cdot \frac{\int dV \Delta\rho / \rho}{\int dV' \Delta\rho' / \rho'} \tag{9}$$

with λ the geometrical scale factor. The integrations in (9) are to be carried out over the entire flow domain. Accordingly, the velocity scale factor β depends on the solid concentration and increases along the avalanche track as the flow dilutes itself. In contrast, one finds that the scaling factor for the particles' settling velocities should decrease in the course of the experiment, rather than increase. There are additional violations of true scaling behaviour due to the variability of the scaling factor (additional pseudo-force like terms, increasing excess of turbulence energy in the laboratory flows, etc.). Even small errors in the evaluation of β will produce significant errors in the calculation of dynamic pressures.

Numerical simulations

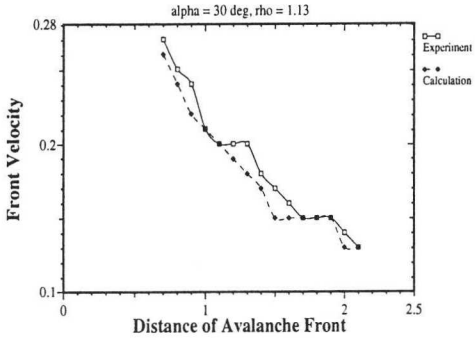

Figure 1: Comparison of three-dimensional numerical simulations of a brine current in fresh water with experimental data from [2]. Front velocity is plotted against front location. Slope angle: 30°, initial mixture density: 1130 kg/m^3.

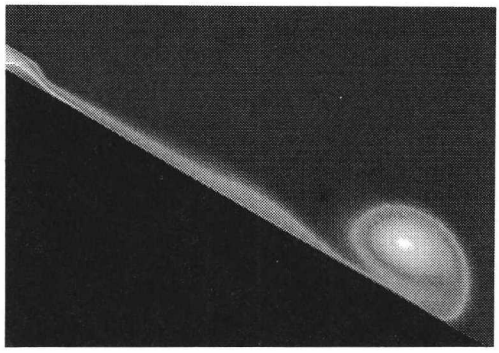

Figure 2: Numerical simulation of a density current. A two-dimensional grid with 150× 80 cells was used to resolve the raised nose and the high-density region in the rear part of the head.

We are developing a numerical PSA model on the basis of a commercial flow solver (CFDS-FLOW3D) that implements the finite volume method for stationary and transient flows. Besides the stability and relative ease of use of the code, its most important property for our purposes is the well-defined yet flexible interface to user-supplied routines describing extra source terms, special boundary conditions, etc. Other useful features are the option of including passive scalar equations, a variety of turbulence models, (structured) multi-block grid capabilities, and a choice of methods for doing the spatial discretisation and for solving the resulting system of equations. Furthermore, test runs with the two-phase code gave encouraging results despite the unresolved theoretical issues mentioned in a previous section.

The simplest approach to modelling a PSA treats it as a density current (cf. eqns. (1)-(3)), neglecting the relative velocity between the particle phase and the surrounding fluid and thus erosion and/or deposition of particles. The concentration of the particle phase may be described by a passive scalar field. No-slip boundary conditions are applied on the ground. Essentially the same model was developed independently by an Austrian group [5]. We tested our model against experimental data on pure density currents [2] as well as on suspension flows in our laboratory. A three-dimensional grid consisting of 10'000 cells per half field (assuming symmetrical avalanches) was used for the first case. The results agree satisfactorily with the laboratory density currents with respect to the development of the front velocity, but the shape of the avalanches is less well reproduced (see Figure 1). This led to some runs with a high resolution 150×80 two-dimensional grid along the centerline of the avalanche; now, very good agreement with the observations in the laboratory was found (Figure 2). A consequence of these runs is that even simple flows on simple geometries require fine grids, but once this condition is met the dominant physical processes are correctly captured by the model.

The density-current model was also used for a comparison with laboratory suspension flows over a model topography as described in the previous section. The calculations were done on reasonably big grids of 66×28×27 nodes or a total of approximately 55'000 cells (including boundary cells). A coarse comparison of the physical model with the calculations, limited to the front position and the internal velocities in the avalanche head, shows fair agreement even though this simple model incorporates neither snow erosion and deposition (which are clearly at work in the laboratory model) nor any relative velocity between the two phases. Simulating real PSAs on the scaled-up terrain model and with realistic density values is much ore delicate due to the huge density difference of the two materials. As far as our experience goes, smaller time steps or a better time step adaption algorithm must be applied.

The simulations just mentioned were useful in estimating the degree of scaling violation in the laboratory avalanches compared to real events. We found the TCs to grow in size much more rapidly and to reach their peak speed after a much shorter distance than the PSAs. Similarly, the typical structure of a gravity current head develops more slowly in our simplified simulations of real PSAs.

The next major step in the development of our numerical model will be the implementation of boundary conditions that model erosion and sedimentation effects in response to snow cover properties and avalanche velocities. Our measurement techniques do not permit resolution of the tiny saltation layer in laboratory

experiments, so the verification of the model will be possible only through data on snow drift. This opens yet another area of application for our model: Snow drift is a key factor in the assessment of avalanche danger because the winds at mountain crests may charge leeward slopes with enormous quantities of snow and because the runout distances of dense flow avalanches and PSAs grow strongly with avalanche snow volume. Even the best avalanche model one can imagine depends crucially on the estimate of the initial conditions.

References

J. E. Simpson. *Gravity Currents: In the Environment and the Laboratory*. Ellis Horwood Series in Environmental Science. Ellis Horwood Ltd., Market Cross House, Cooper Street, Chichester, West Sussex, PO19 1EB, England, 1987.

P. Beghin and X. Olagne. Experimental and theoretical study of the dynamics of powder snow avalanches. *Cold Regions Sci. Technol.* **19**:317-326, 1991.

T. Scheiwiller, K. Hutter, and F. Hermann. Dynamics of powder snow avalanches. *Annales Geophysicae* **5B**(6):569--588, 1987.

F. Hermann. *Experimente zur Dynamik von Staublawinen in der Auslaufzone*. Mitteilungen der VAW No. 107. Ph.D. thesis, ETH Zürich, 1990.

W. Brandstätter, F. Hagen, P. Sampl, and H. Schaffhauser. Dreidiensionale Simulation von Staublawinen unter Berücksichtigung realer Geländeformen. *Wildbach- und Lawinenverbau* **56**(120):107-129, 1992.

Mass-referenced flow model for dynamic analysis of flow slides and avalanches

Modèle d'écoulement pour l'analyse dynamique des glissements et des avalanches

O. HUNGR

Geotechnical Research Inc.
4195 Almondel Rd., West Vancouver, B.C. - Canada V7V 3L6
Tel. (1) 604 926 91 29 - Fax (1) 604 684 51 24

Abstract

This paper presents a generic flow model which can be used to model different kind of rapid flow-slides and avalanches. After a description of the interest of dynamic modelling, the author discusses the existing programs.
He then proposes a single dynamic model able to take advantage of different rheological laws. The model configuration is developed and two examples of application are given. They are both related to two experiments and they require different constitutive relationships adapted to the materials. Finally, two applications to an actual rock avalanche are described. For each of these attempts, a specific expression of the internal pressure term has been used.

Résumé

Cet article présente un modèle générique d'écoulement qui peut être utilisé pour modéliser différents types d'écoulements rapides et d'avalanches. Après une description de l'intérêt de la modélisation numérique, l'auteur traite des programmes existants. Il propose alors un modèle dynamique unique capable d'exploiter différentes lois rhéologiques. La configuration du modèle est développée et deux exemples d'application sont détaillés. Ils sont relatifs à deux expériences et nécessitent des lois constitutives différentes adaptées aux matériaux. Enfin, deux applications à une avalanche de roche sont décrites. Pour chacun de ces tests, une expression spécifique du terme correspondant à la pression interne a été utilisée.

Introduction

Rapid flow-slides, including debris flows, debris avalanches, rapid earth flows, rock avalanches and failures of mining waste, are the most dangerous and damaging of all landslide phenomena. In their extremely rapid motion and flow-like behaviour, they are similar to snow avalanches. Risks of rapid flow-slides often cannot practically be eliminated by stabilization of the source areas. The risks must

therefore be accepted, but this requires predictions of the likely runout area, motion velocity, discharge, behaviour in bends and in front of barriers and other similar atributes. One of the means of achieving such predictions is dynamic modelling.
Dynamic models of flow slides fall into two broad categories: lumped-mass models idealizing the motion of a flow -slide as a single point and models based on continuum mechanics, which are capable of tracing the internal distortions of the moving mass. A number of models of each type have been developed in the fields of snow avalanche science, materials handling, hydrology and engineering geology.
No single model has so far been accepted as a widely accepted practical tool. Even the selection of basic rheological constitutive equations is unsettled. Some authors prefer frictional models with pore-pressure but no velocity dependence. Another group favours the Bingham model which is linearly dependent on velocity and yet another the turbulent model dependent on velocity squared.
This paper presents a dynamic model designed to allow for a range of different rheologies and for certain important aspects of non-homogeneity which are often recognized in actual flow-slide events. Although simple in formulation, the model is capable of accounting for the special character of flow-slide behaviour, comprising elements which are both fluid-like and plastic. The model is thus capable of operating in the "grey area" between fluid dymamics and elasto-plasticity of solid or granular materials.

Model Configuration

The Author's initial idea was an extension of the lumped-mass approach. The slide mass was to be represented by a number of blocks contacting each other and retaining fixed volumes of material in their descent down the path. The integrated one-dimensional momentum equilibrium equation was used in an explicit manner. The forces acting on each block include gravity, basal resisting forces and side thrusts from adjacent blocks ,calculated as hydrostatic fluid thrusts or with the use of the theory of plastic states as discussed below. Each block was displaced with the requisite acceleration in a time step. Then, the block geometry was re-established using the continuum equation. The equations of motion were referenced to the constant mass of each moving block, instead of a fixed reference grid.

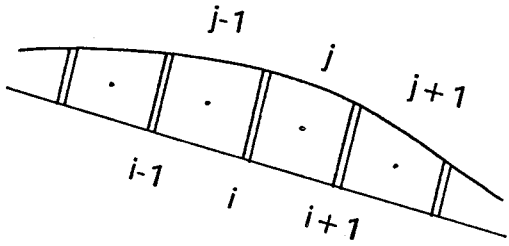

Figure 1 : The configuration of the model.

The original "Mass-Referenced Model" produced some interesting results, but was plagued by numerical instability. The Author therefore adopted an alternative formulation suggested by Savage and Hutter (1989), which is shown in Figure 1. In the new formulation, the integrated momentum equation is applied to infinitesimal columns of the flow, termed boundary columns and numbered i=1 to n in Figure 1. The continuity equation is then applied to the mass blocks of fixed volume numbered j=1 to n-1, separating the boundary blocks.
The solution is still explicit and occurs in time steps. At first, a block assembly is set up to approximate the initial configuration of the slide mass. The forces on each boundary block consist of the tangential component of gravity, G, the basal resisting force, T and the pressure term, P, which depends on the flow surface gradient. Integrating the resultant force twice, a new position of each boundary block is obtained. The average depth of the flow in the mass blocks is then determined to maintain their constant volume. New surface gradients are established by interpolation and the solution proceeds to the next time step.

The Flow Resistance Term

The flow resistance term, T, can be determined as a function of several different known parameters of the flow. The following constitutive relationships can be accommodated at present:

- Constant strength, such as the steady state undrained strength of liquefied material (plastic model).
- A function of the effective normal stress on the flow boundary (frictional model). The effective stress can depend on flow depth, density, pore-pressure, and gravity and centrifugal acceleration. The friction coefficient can be made a function of displacement to simulate the decay of strength from peak to residual. The pore-pressure can be a function of location, normal stress or elapsed time (drainage).

Linear function of velocity (Newtonian laminar flow model).

- A function of velocity squared (turbulent model).
- Combination of a frictional term and a turbulent term (Voellmy model, see Voellmy, 1955).
- A function of flow depth, velocity, constant yield strength and viscosity (Bingham model).

Two example applications of the above models are presented. Figure 3 shows a small scale experiment on the flow of sand down a steeply inclined sand-lined chute carried out by Huber (1980) and described by Savage and Hutter (1989). The sand is dry, with a dynamic internal friction angle of 29° and a bed friction angle of 23°. The present model closely simulates the travel of the sand throughout its path and its internal distortions, as did the model of Savage and Hutter (1989). The centrifugal forces have a strong influence in the curved segment of this flow path.

Figure 4 shows a flume experiment on the sudden break of a dam in a purely viscous material (oil), described by Jeyapalan (1981). The oil had a viscosity of 0.03 kPa.sec

and a density of 800 kg/m^3. Again, the model correctly simulates the propagation of the dam break wave. It is of interest to note that the simulated flow is laminar in this case, with a strong vertical velocity gradient. Thus, material must be continually crossing the boundaries of the reference blocks, without influencing the validity of the two governing equations or of the solution scheme.

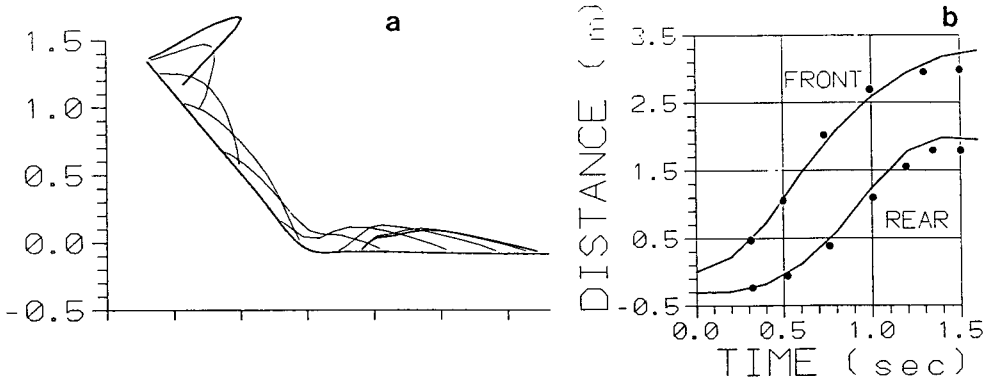

Figure 2 :Analysis of a sand flume experiment. (a) Flow profiles drawn at 0.2 sec. intervals. The flow depth is exaggerated five times. (b) Calculated motion of the flow front and rear. The dots show observations by Huber (1980).

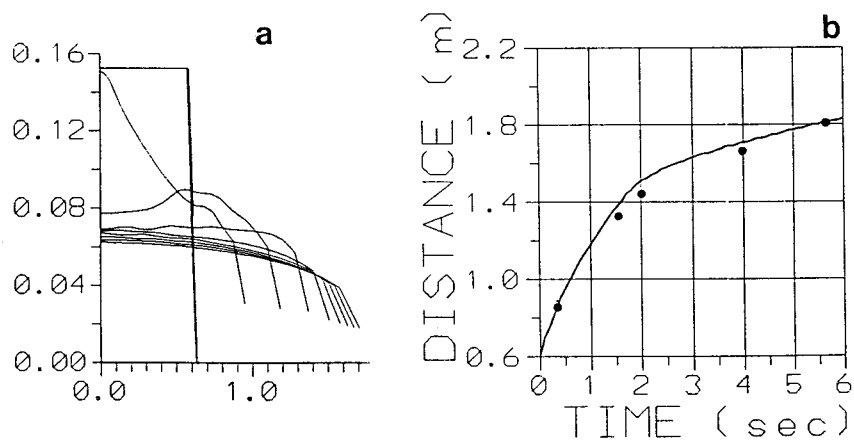

Figure 3 : Analysis of a dam break experiment in oil. (a) Flow profiles drawn at 0.2 sec. intervals. (b) Calculated motion history of the flow front. The dots show observations by Jeyapalan (1981).

Internal Pressure and Strain

It is usual in Fluid Dynamics to assume that the internal lateral stresses in the fluid are hydrostatic. This is, of course, not true in a frictional material, where the lateral stress is dependent on strain and varies between the Rankine limits of plastic equilibrium. Thus, while the ratio between the principal stresses is always 1.0 in a fluid, it may vary between 0.33 and 3.3 in a dry sand with an internal friction angle of 30°.

The transition from the active to passive state occurs in response to strain. Herein lies the main advantage of the mass-referenced approach, as compared to the conventional methods using a fixed reference grid. Strain is a quantity which travels with the mass and it can easily be monitored in the system of moving blocks, as they expand or contract during motion. The model connects incremental strain with internal stress through a pair of stiffness factors, s_l and s_u - a smaller one for loading and a larger for unloading (spreading). A possible sequence of internal stress changes in a block is shown in Figure 4. After each time step, an incremental strain is calculated in each block and the lateral stress coefficient, k, is modified to follow a path similar to that shown on the figure.

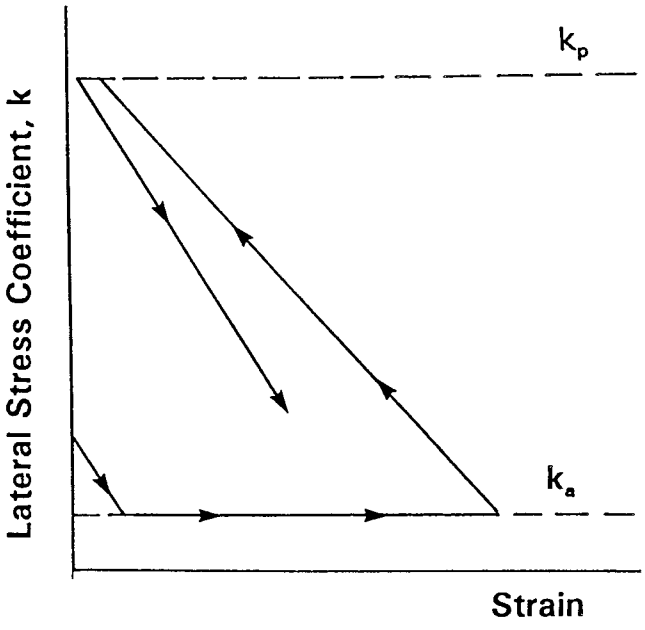

Figure 4 : Relationship between changing strain in an element and the coefficient of lateral pressure, as used in the Mass-Referenced Flow Model.

The importance of the pressure term is dramatically shown by the analysis of a major rock avalanche moving against a steep adverse slope (Figure 5). The example is an actual case: the Avalanche Lake rockslide in Canada's Northwest Territories,

described by Evans (1989) and Evans et al. (1993). One part of this gigantic rock avalanche ran up to a shelf at Elevation 1660 metres, 640 metres above the lowest point of the path. Only the extreme leading edge of the avalanche reached the shelf, depositing a few percent of the total volume there; the bulk of the debris fell back into the valley and even ran up the source slope.

Figure 5a shows an attempt to analyse the runup using the Mass-Referenced Model configured for a fluid, i.e. with the lateral pressure coefficient set to a constant 1.0. The fluid runs up a little over one half the height of the valley wall, but then stops and forms a giant standing wave or eddy, before falling back into the valley. The rheology used in this case was the Voellmy model, with a friction coefficient of 0.02 and a turbulence coefficient of 400 m/s^2. This, however, is not significant. The standing wave would occur even if the analysis were conducted using much lower resistance parameters.

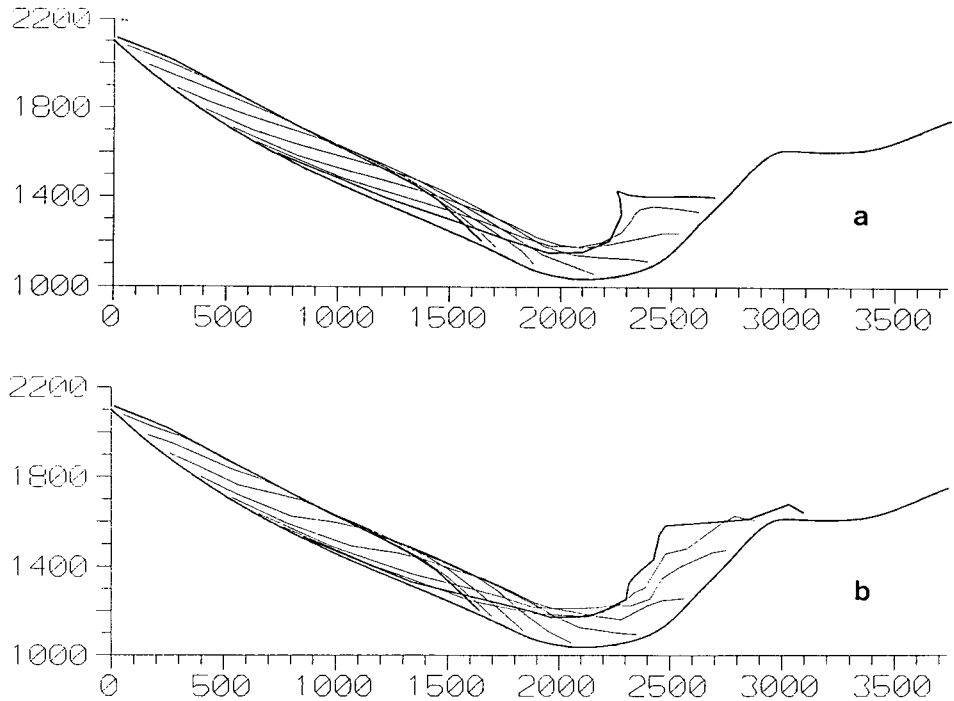

Figure 5 : Analyses of the Avalanche Lake rock avalanche runup. The flow profiles are plotted at 5 sec. intervals. (a) A fluid dynamics solution. (b) A solution using an internal friction coefficient of 38°.

The analysis of Figure 5b uses a k ranging between 0.24 and 4.2, corresponding to an internal friction angle of 38° typical for angular crushed rock. The Mass-Referenced Model realistically simulates the marginal runup onto the shelf, as well as a part of

the fallback. As would be expected, the internal lateral stresses in the debris during its precipitous climb towards the shelf correspond mainly to the passive condition.
In conclusion, flow slide models must recognize the special character of some of these phenomena, which involves the movement of a relatively rigid sheet of dry material over a thin liquefied layer. No existing fluid mechanics model, or even a physical model using real fluid, can simulate such behaviour. The Mass Referenced Model is capable of monitoring lateral strain and can thus account for the internal rigidity. At the same time, however, it can be used succesfully for simulating fluid behaviour as well.
This approach can also take into an account the three-dimensional effects of prescribed variable width of the path. It is also possible to have materials of different rheologies coupled in a single mass, as in boulder-fronted debris surges. At present, the model is being applied to the analysis of large debris avalanches resulting from failures of coal mining waste piles in British Columbia.

References

Evans, S.G., 1989. Rock avalanche runup record. Nature, Vol. 340, p. 271.

Evans, S.G., Hungr, O., and Enegren, R., 1993. The Avalanche Lake rock avalanche, Mackenzie Mountains, Northwest Territories, Canada; description, dating and dynamics. Can. Geotechnical Journal, in press.

Huber, A., 1980. Schwallwellen in Seen als Forge von Felssturzen. Mitt. No. 47 der Versuchsanstalt fur Wasserbau, Hydrologie und Glaciologie an der ETH Zurich, pp. 1-122.

Jeyapalan, K., 1981. Analysis of flow failures of mine tailings impoundments. Ph. D. Thesis, University of California, Berkeley.

Savage, S.B. and Hutter, K., 1989. The motion of a finite mass of granular material down a rough incline. Journ. Fluid Mechanics, Vol. 199, pp. 177-215.

Types of rapid gravitational subaerial mass movements and some possible mechanisms

Différents types de mouvements gravitaires rapides et quelques mécanismes possibles associés

J. N. HUTCHINSON

Dept. of Civil Engineering, Imperial College
London, SW7 2BU - U.K.
Tel. (44) 71 589 51 11 - Fax (44) 71 823 85 25

Abstract

After a classification of sub-aerial mass movements and the definition of a terminology, this paper deals with some mechanisms wich can be involved in rapid mass movements. First, sudden triggering mechanisms which provide an initial impetus to a slide mass are described.
Then, mechanisms which tend to accelerate and sustain movement are presented. As a conclusion, the paper gives some comparisons between the relative mobility of different types of rapid mass movements.

Résumé

Après une classification des mouvements en masse existant à la surface de la terre et la définition d'une terminologie, cet article traite des mécanismes impliqués dans les mouvements gravitaires rapides. Tout d'abord, sont décrits les mécanismes qui déclenchent le mouvement d'une masse de façon soudaine en lui communiquant une impulsion.
Ensuite, l'article présente les mécanismes qui entretiennent ou acccentuent le mouvement. Il se termine par une comparaison entre la mobilité apparente de différents types de mouvements gravitaires rapides.

Introduction

Rapid movement of a landslide was defined by Varnes (1978) as being between 1.5m/day and 0.3m/min, with 0.3m/min to 3m/sec termed very rapid and speeds greater than 3m/sec, extremely rapid. These ranges were thought to be too slow and are redefined by Cruden & Varnes (in press) as, respectively, between 1.8m/hour and 3m/min, 3m/min and 5m/sec and greater than 5m/sec. In the present connection, it is chiefly the last two categories which claim our attention.
Mass movements may be divided into those, like rock slides, which involve relatively intact masses and those, like rock avalanches, which consist of well broken debris. Their initial stages may also be divided into first-time slides and

slides on pre-existing shear surfaces (Skempton & Hutchinson, 1969). The former exhibit strain-softening stress-strain behaviour, following a peak, and thus have a degree of brittleness. This will itself tend to produce a degree of rapid slide movement. The stress-strain behaviour in renewals of movement on pre-existing shears, however, is elasto-plastic with little or no brittleness and these movements are, as a result, often quite slow. However, important exceptions to this are noted by Hutchinson (1987).

Classification and terminology of sub-aerial mass movements

A classification employing an eightfold primary division, A to H, is given by Hutchinson (1988). Here we can disregard (A) Rebound, (B) Creep and (C) Sagging of mountain slopes as being slow and (F) Topples and (G) Falls as being rapid in a free fall rather than in a sliding or flowing sense. Complex slides (H) are omitted. This leaves (D) Landslides and (E) Debris movements of flow-like form to be considered.
Landslides are subdivided into; (D1) Confined failures, (D2) Rotational slides, (D3) Compound slides and (D4) Translational slides. Confined failures are incipient and very slow. Rotational slides tend to be self-arresting by virtue of their form in section and thus are not normally particularly rapid. Very rapid movements are exhibited by some Compound and Translational slides, for example, Vaiont, c. 25m/sec (Hendron & Patton, 1985) and Goldau, 70m/sec (Heim, 1932), respectively.
Debris movements of flow-like form are subdivided into; (E1) Mudslides, (E2) Flow slides, (E3) Debris flows and (E4) Sturzstroms. Mudslides are characterised by having a high clay content (often > 40% <2μ) and are generally slow-moving, the clay perhaps acting as a viscous brake. However, through undrained loading by debris accumulation at their heads, mudslides can surge rapidly, as illustrated by that at Minnis North, Antrim, in which a surge exceeded 8m/sec (Hutchinson *et al.*,1974). Flow slides, sometimes termed liquefaction slides, occur through the sudden collapse of metastable structure in loose,saturated cohesionless materials and in cohesive deposits of low plasticity and high porosity (quick clays) and by the collapse under impact (impact collapse) of saturated pore spaces in cemented, highly porous soft rocks, e.g. loess and soft chalk (Hutchinson, 1980,1988). Flow slides move fast, for example at 8 to 11m/sec on average in the 1966 failure in a tip of coal mine waste at Aberfan (Hutchinson,1986) and probably at about 5m/sec in the chalk flows on the Kent coast.
Non-volcanic debris flows are normally associated with mountains and are caused by a sudden access of water, usually from rain, snow-melt or thawing permafrost, to slope mantles of weathered, non-argillaceous debris (clay fraction usually < 5 to10% <2μ). The soaked debris translates into the local stream network becoming ,as it does so, thoroughly mixed and increasingly mobile. Debris flow movements commonly exhibit surging and often reach speeds of between 3 and 12m/sec (Campbell,1975) and sometimes higher. More violent debris flows, termed lahars, result from volcanic activity, where the water derives from condensing steam, the melting of snow and ice and from crater lakes.
Sturzstroms, or catastrophic rock avalanches, are features of high mountains. They generally originate in a major and energetic rock slide or fall which breaks down into debris. This essentially dry debris is highly mobile, often travelling for kilometres

over fairly gentle and even reverse slopes. Average speeds are very high. They were estimated for Mayunmarca, 1974, for example, at between 33 and 39m/sec (Kojan & Hutchinson, 1978) and for Elm, 1881, at about 50m/sec (Heim,1932). It may be desirable to subdivide this group of phenomena into sturzstroms, with extreme run-outs, and rock avalanches, with more modest ones.

Possible mechanisms of rapid mass movements

These are listed in Table 1 and described below.

Sudden triggering mechanisms providing an initial impetus.

These mechanisms result in a sudden drop in factor of safety which provides an initial impetus to a slide mass. They are effective for both first-time failures and for renewals of movement on pre-existing shear surfaces. Most of these mechanisms have their maximum effect initially, with a diminishing influence thereafter.

External triggers

a) *Entry of surface water into a slide :* An abrupt cessation of surface water flow over a feeder mudslide at Minnis North, Antrim, was reported by Hutchinson *et al.* (1974) to have been followed immediately by a rapid surge movement. Fresh tension cracks are believed to have opened in the already only marginally stable mudslide. These "swallowed" the surface water, which generated the rapid failure through the consequent water pressure on the crack walls and possibly also, depending on the depth of the cracks in relation to the depth of the movement, through an increase in the ground-water pressures acting on the adjacent parts of the slip surface.

b) *Undrained loading of the head of a slide :*The power of undrained loading of the heads of, for example, accumulation mudslides by the rapid emplacement of debris from steeper feeder slides is described by Hutchinson & Bhandari (1971) and Hutchinson *et al.* (1974). The associated impetus for rapid movement arises partly from the direct weight of the emplaced debris, particularly where situated upslope of the drained neutral point, N_d (Hutchinson,1984), and partly from the undrained pore-water pressures set up by this on the sub-adjacent slip surface (Fig. 1a). More sudden effects are naturally produced by rock falls from a precipitous rear scarp (Fig. 1b).

c) *Undrained unloading of the toe of a slide :* The effects on stability of unloading the toe of a landslide, for instance by rock fall or excavation, are discussed in terms of the influence line approach by Hutchinson (1984,1987). This indicates that where a slide toe is rapidly unloaded, at a position between the drained and undrained neutral points (i.e. where the slip surface is inclined valleywards at an angle of between Φ_{mob} and zero, Fig.2a), the factor of safety of the overall slide, F, will be increased in the short term and reduced only in the long term, that is after some delay. However, if the unloading occurs valleyward of the undrained neutral point, N_u (i.e. where the slip surface is inclined into the valley slope, Fig.2b), the reduction in F will be immediate and will become larger in the long term. In the latter case, the potential for the triggering of rapid movements in the overall slide is evident. Rapid draw-down is a further type of unloading, essentially undrained in clays, which can lead to fast slides.

d) *Seismic effects, direct and indirect* : Seismically induced slides may be divided into direct failures, occurring synchronously with the earthquake shaking, and indirect failures, occurring some time (up to a few days) after the shock (Hutchinson, 1987). The former category are usually much more rapid. It is suggested by Hutchinson (1987, following Ambraseys, 1977) that such direct failures will have a limited length in a cross-valley direction, $< \lambda/2$, where is the seismic wavelength (Fig.3). $\lambda/2$ is typically about 15 to 30m. Rate effects on shear strength, discussed below, are also relevant.

e) *Magma intrusion and other volcanic phenomena.* These effects were well illustrated by the Mount St Helens volcanogenic landslide of 1980, when magma emplacement and associated earthquakes caused lateral displacements well in excess of 100m at rates of up to nearly 10m/day culminating in the violent failure of 18th May (Voight *et al., 1983).*

Coalescence of landslides

Salt (1985) points out that the coalescence of landslides in plan will result in a proportionate reduction in the restraining effect of the shear forces acting on the sides of the slipping mass, which will tend to reduce its three-dimensional factor of safety and thus cause an acceleration of movements. Related, but more violent effects would result from the coalescence of landslides in down-slope section (Hutchinson,1987).

Brittle failure within intact, quasi-stable slide mass.

a) *Internal shear failure towards the rear of compound slides.* Compound slides are unable to fail unless they are broken down into kinematically admissible mechanisms by internal shear failures. Thus, a compound slide may have a three-dimensional factor of safety, F_3', of significantly less than 1.0 on its non-brittle, bounding slip surface, but be prevented from behaving in accordance with this value (i.e. running away) by the restraints exerted by its brittle, but still unfailed internal shears, which hold its effective F_3 to about 1.0. Once failure on these internal shears takes place, the overall F_3 will drop suddenly from 1.0 to F_3', giving a corresponding acceleration to the freshly released slide mass (Hutchinson, 1987).

A striking example of this phenomenon is provided by the 1963 Vaiont slide, where the constraint on movement imposed by the internal shears was much increased by the great contrast in strength between the clay gouge forming much of the bounding slip surfaces and the hard limestones and cherts which constituted the bulk of the sliding mass. The resulting impetus, although important, does not account wholly for the rapidity of the succeeding events. Other factors are discussed below.

b) *Passive shear failure in the toe of translational slides.* Failures of this nature are most important in translational slides, as exemplified by that at Timpone, 1986 (Del Prete & Hutchinson,1988). The sliding surface there was pre-existing as a result of flexural slip. It followed a thin, planar clay layer, inclined at between 17 and 18°, within a thick sequence of littoral sands. The rapidity of the slide resulted chiefly from a passive failure through the brittle, slightly cemented sands at the toe. Similar results can also arise from the failure of inadequately designed restraining structures at slide toes.

c) *Buckling in the toe region of translational slides.* For Coal Measure sequences in opencast mines, Walton & Atkinson (1978) describe cases where a translational slide of an exposed, steeply dipping sandstone bed occurred through the sudden buckling of this, followed by wedging.

Mechanisms tending to accelerate and sustain movement

These phenomena come into play once movement has begun and generally tend to increase in effect with increasing movement, in a feed-back manner.

Slip surface phenomena

a) *Smoothing.* Rugosities on failure surfaces, particularly but not only in rock, tend to be smoothed off by continuing movements. The mobilised friction angle is thus reduced from Φ (basic) + i (roughness) towards Φ (Patton,1966; Barton,1973), with consequent acceleration of movement.

b) *Collapse of loose, saturated, metastable structure.* In material prone to flow sliding, the collapse of loose structure in saturated zones of a slope can occur as a result of various types of disturbance. The sudden transfer of load from the soil structure to the pore water gives rise to a sudden increase in pore water pressure through undrained self-loading, with a corresponding reduction in normal effective stresses and shear resistance. Such drained-undrained failures generally lead to very rapid and destructive landslide movements, as in the quick clay slide at Furre (Hutchinson, 1961). A sliding-consolidation model for flow slides, based on an effective stress approach and using geotechnical rather than rheological parameters, is proposed by Hutchinson (1986).

c) *Heating.* Frictional heating can be expected to occur on slip surfaces during sliding. Habib (1967) and Goguel (1969) suggested that where water is present it would be vapourised, thus creating a cushion and reducing the friction mobilised. Subsequently Voight & Faust (1982) argued that a significant frictional strength loss will result from the warming and expansion of the pore water, without proceeding to high temperatures and vapourisation. In this way they were able to offer a rational explanation of the very high speeds attained in the Vaiont failure.

The frictional melting of rocks, leading to the formation of pseudotachylytes, commonly occurs (at much higher temperatures than evisaged above) in fault zones at crustal depths of up to about 10km (Koch & Masch,1992). The occurrence of such rock-melt products on the slip surfaces of old landslides, originally up to perhaps 500 to 800 m deep, in Austria (Kofels) and Nepal (Langtang) is reported by Masch *et al.* (1985). Both landslides involved felsic gneiss: temperatures of the order of 1200° C or more may have been associated with the melting (Maddock, 1986), which could doubtless have led locally to an almost complete loss of frictional strength (Sibson,1977). In limestones, dissociation would occur at such temperatures.

d) *Negative rate effects in rapid shear.* Rapid ring shear tests on clayey samples show that after an initial peak the strength falls, usually to a value greater than the slow residual strength (positive rate effect) but, in a few cases, of particular interest here, to a value below this (negative rate effect) (Lemos *et al.*,1985).

Recent rapid ring shear tests on slip surface gouge from Vaiont (Tika-Vassilikos & Hutchinson, in prep.) exhibit a high negative rate effect. This is illustrated in Fig.4 for Sample 3 (w_P =30%, w_L = 49% & CF(<2μ) = 27%), which at a displacement rate

of 2600mm/min has a residual friction angle of about 4°, i.e. 60% below the slow residual value, after a displacement of less than a metre. This result, if reasonably representative, provides an explanation for the high speeds at Vaiont without invoking slip surface heating.

e) *Ball-or roller-bearing action.* It is conceivable that in certain rocks, clasts or broken fragments might act as ball- or roller-bearings in a basal zone during shear displacement. In describing a sturzstrom (Triple Slide) in lower Paleozoic carbonates in the Mackenzie Mountains, Eisbacher (1979) suggests, from observations of large angular blocks rotated up to 30° forward in the basal breakaway zone, in what appears to approximate to a multiple topple, that during an earthquake these could act as "roller bearings" with respect to the overlying rock mass. This proposal goes well beyond the field evidence. A related mechanism, as yet unreported, in which the resistant, rounded grains in weakly cemented sandstones or conglomerates could become detached from their matrix and act as ball-bearings on a basal failure surface, may well exist.

Mechanisms within rapidly moving debris

a) *Repeated undrained self-loading.* In debris flows, excess pore-water pressures may be generated by two forms of this mechanism; a) internal over-riding (Sassa,1984) and b) continuing upsetting of the debris fabric, throwing clasts into suspension (Pierson, 1981; Hutchinson, 1988).

b) *Bagnoldian grain flow.* A possible mechanism for sturzstroms, independent of the presence or nature of pore fluids, is momentum transfer leading, through dispersive stresses, to grain flow (Bagnold,1954; Hsü,1975; Campbell, 1989).

c) *Acoustic fluidisation.* A suggested alternative mechanism for sturzstroms, preferred by Melosh (1987), is acoustic fluidization. This appears to be related to grain flow, but the reduction of effective overburden pressures which permits the rapid flow is believed to occur on a more energy-efficient, lumped, rather than grain-to- grain basis.

Relative mobility of rapid mass movements

For the various types of rapid mass movement discussed above, it is of interest to compare their relative mobilities by means of a plot of H/L (= tanα, where α = fahrboschung) against log. debris volume. This is done in Fig.5 for rock avalanches and sturzstroms, distinguishing between those involving predominantly sedimentary rocks, predominantly crystalline rocks and those which are volcanogenic. The lowest bound to the data considered is the line AB or, if failures from volcanoes are excluded, the line AC.

The volcanogenic rock avalanches and sturzstroms have a fairly concentrated distribution, outlined by the line G. As noted by Voight *et al.* (1983), these lie in the more mobile region of the overall rock avalanche spectrum. With a couple of exceptions, rock avalanches involving crystalline rocks occupy the smaller volume, less mobile region of the overall spectrum, outlined by the line F. The data points for rock avalanches and sturzstroms involving predominantly sedimentary rocks are more dispersed: they tend to be concentrated between the other two types, but also

overlap with the crystalline data and with the intermediate to less mobile part of the data for volcanogenic rock avalanches.

The greater mobility of the volcanogenic rock avalanches is not surprising in view of the size and often unstable nature of volcanic cones and the destabilising effects of gas and magma intrusion and explosion and the accompanying seismicity. The generally greater mobility of the failures involving sedimentary rocks than those from crystalline rocks seems not to have been noted earlier. It may derive from the fact that, unlike the latter, sedimentary rocks are characterised by bedding, which tends to facilitate the formation of large landslides. The sedimentary rocks also have, on average, a lower frictional resistance and may break down more readily into fine debris. On the other hand, their coefficient of restitution (Richards, 1993) may generally be lower than for the crystalline rocks.

In the related plot of Fig.6, the mobility of rock avalanches and sturzstroms (the boundaries AB and DE are taken from Fig.5) is compared to that of chalk flows and flow slides from tips of coal mine waste. As noted by Hutchinson (1988), this shows that the latter group has a mobility equivalent to all but the most mobile rock avalanches and sturzstroms at debris volumes approximately two orders of magnitude smaller.

Data from a number of debris flows are also plotted (Fig.6). There is more doubt concerning the debris volume in these cases as the deposits are frequently emplaced in several increments. The volumes shown may thus be too high. Nevertheless, the plot shows that debris flows are usually significantly more mobile than the chalk flows and flow slides, though also overlapping with these, and are markedly more mobile than the rock avalanches and sturzstroms, with no overlap in the distribution of the present data points. The wide variation in the mobility of debris flows doubtless refects their very wide range of water content. Any correction of the debris flow points for volume, as discussed above, would emphasise their superior mobility. With debris flows, as with rock avalanches and sturzstroms, the volcanic variety are the biggest and most mobile.

The broad indications of Figs 5 & 6 would appear to be that while the high mobility of the essentially dry sturzstroms, especially at large debris volumes, is remarkable, rapid mass movements involving water are more effective, providing both higher debris mobility at similar volumes and similar mobility at much smaller debris volumes.

Although outside the classification used above, data for pyroclastic flows are also shown on Fig.6. These must be regarded as very tentative in view of the considerable likely inaccuracies, to which attention is drawn by Hayashi & Self (1992). The available data-points overlap with the fields occupied by those for rock avalanches/sturzstroms, chalk flows /flow slides from tips and the non-volcanic debris flows. The most mobile pyroclastic flows appear to be of similar, or slightly greater mobility to the most mobile rock avalanches/sturzstroms, but are surpassed in mobilty, like all other gravitational sub-aerial mass movements, by the lahars.

Acknowledgements

The author is grateful to T. R. Davies, I. E. Higginbottom, J. A. Hudson, R. H. Maddock and D. Shelley for help.

References

Abele, G. 1974. Bergsturze in den Alpen. *Wissenschaftliche Alpenvereinshefte,* Heft **25**, 1 - 230.

Ambraseys, N.N. 1977. On the response of structures to travelling waves. *Proc. CENTO Seminar on Earthquake Hazard Minimization,* Tehran, 410-414.

Bagnold, R.A. 1954. Experiments on a gravity-free dispersion of large solid spheres in a Newtonian fluid under shear. *Proc. Roy. Soc. Lond.,* Ser. A, **225**, 49 - 63.

Barton, N.R. 1973. Review of a new shear strength criterion for rock joints. *Engrg Geol.,* **7**, 287 - 332.

Campbell, C.S.1989. Self-lubrication for long runout landslides. *J.Geol.,***97**,653- 665.

Campbell, R.H. 1975. Soil slips, debris flows and rainstorms in the Santa Monica Mountains and vicinity, southern California. *U.S. Geol. Surv. Prof. Paper,* **851**,1-51.

Clague, J.J., Evans, S.G. & Blown, I.G. 1985. A debris flow triggered by the breaching of a moraine-dammed lake, Klattasine Creek, British Columb'a. *Can. J. Earth Sciences,* **22**, 1492 - 1502.

Cruden, D.M. 1976. Major rock slides in the Rockies. *Can. Geotech. J.,* **13**, 8 - 20.

Cruden, D.M. & Varnes, D.J. (in press). Chap. 3 in *Landslides : Investigation and Mitigation.* Transportation Res. Board, Nat. Acad. of Sciences, Washington, D.C.

Cummans, J. 1981. Chronology of mudflows in the South Fork and North Fork outle River following the May 18 eruption. In: The 1980 eruptions of Mount St Helens, Washington (P.W. Lipmann & D.R. Mullineaux, eds), *U.S. Geol. Surv. Prof. Paper,* **1250**, 479 - 486.

Curry, R.R. 1966. Observation of Alpine mudflows in the Tenmile Range, central Colorado. *Geol. Soc. Amer. Bull.,* **77**, 771 - 776.

Del Prete, M.& Hutchinson, J.N. 1988. La frana di Senise del 26-7-1986 nel quadro morfogico del versante meridionale della collina Timpone. *Rivista Italiana di Geotecnica,* Anno **22**, 7-33.

Eisbacher, G.H. 1979. Cliff collapse and rock avalanches (sturzstroms) in the Mackenzie Mountains, northwestern Canada. *Can. Geotech. J.,* **16**, 309 - 334.

Eisbacher, G.H. & Clague, J.J. 1981. Urban landslides in the vicinity of Vancouver, British Columbia, with special reference to the December 1979 rainstorm. *Can. Geotech. J.,* **18**, 205 - 216.

Goguel, J.1969. Le role de l'eau et de la chaleur dans les phenomenes tectoniques. *Rev. Geogr. Phys. Geol. Dyn.* ,**11**, 153-163.

Habib, P. 1967. Sur un mode de glissement des massifs rocheux. *C.R.Acad.Sci.,* **264**, 151-153.

Hayashi, J.N. & Self, S. 1992. A comparison of pyroclastic flow and debris avalanche Mobility. *J. Geophys. Res.,* **97**, 9063 - 9071.

Heim, A. 1932. Bergsturz und Menschenleben. *Beiblatt zur Vierteljahrsschrift der Naturforschenden Gesellschaft in Zurich,* No.20, **77**, 1-217.

Hendron, A.J. & Patton, F.D. 1985. The Vaiont Slide, a geotechnical analysis based on new geologic observations of the failure surface (2 vols). Dept of the Army, US Corps of Engrs, Tech.Rept GL-85-5.

Houghton, B.F., Latter, J.H. & Hackett, W.R. 1987. Volcanic hazard assessment for Ruapehu composite volcano, Taupo Volcanic Zone, New Zealand. *Bull. Volcanol.*, **49**, 737 - 751.

Hsü, K.J. 1975. On sturzstroms - catastrophic debris streams generated by rockfalls. *Geol. Soc. Amer. Bull.*, **86**, 129-140.

Hutchinson, J.N. 1961. A landslide on a thin layer of quick clay at Furre, Central Norway. *Geotechnique*, **11**, 69-94.

Hutchinson, J.N. 1980. Various forms of cliff instability arising from coastal erosion in the UK. *Fjellsprengningsteknikk-Bergmekanikk-Geoteknikk 1979*, 19.1-19.32. Trondheim: Tapir for Norsk Jord-og Fjellteknisk Forbund tilknyttet NIF.

Hutchinson, J.N.1984. An influence line approach to the stabilisation of slopes by cuts and fills. *Can. Geotech. J.*, **21**, 363-370.

Hutchinson, J.N. 1986. A sliding-consolidation model for flow slides. *Can. Geotech. J.*, **23**, 115-126.

Hutchinson, J.N. 1987. Mechanisms producing large displacements in landslides on pre-existing shears. *Mems Geol. Surv. China*, **9**, 175-200.

Hutchinson, J.N. 1988. Morphological and geotechnical parameters of landslides in relation to geology and hydrogeology. *5th Int. Symp.Landslides*, Lausanne, **1**, 3-35.

Hutchinson, J.N.& Bhandari, R.K. 1971. Undrained loading, a fundamental mechanism of mudflows and other mass movements. *Geotechnique*, **21**, 353-358.

Hutchinson, J.N., Prior, D.B. & Stephens, N. 1974. Potentially dangerous surges in an Antrim mudslide. *Q. J. Engng Geol.*, **7**, 363-376.

Jackson, L.E.Jr. 1979. A catastrophic glacial outburst flood (jokulhlaup) mechanism for debris flow generation at the Spiral Tunnels, Kicking Horse River basin, British Columbia. *Can. Geotech. J.*, **16**, 806 - 813.

Janda, R.J., Scott, K.M., Nolan, K.M. & Martinson, H.A. 1981. Lahar movement, effects and deposits. In: The 1980 eruptions of Mount St Helens, Washington (P.R. Lipmann & D.R. Mullineaux, eds), *U.S. Geol. Surv. Prof. Paper.*, **1250**, 461-478.

Johnson, A.M. & Rodine, J.R. 1984. Debris flow, In: *Slope Instability* (D. Brunsden & D.B. Prior, eds), 257 - 361. Chichester; John Wiley & Sons.

Koch, N. & Masch, L. 1992. Formation of Alpine mylonites and pseudotachylytes at the base of the Silvretta nappe, Eastern Alps. *Tectonophysics*, **204**, 289-306.

Kojan, E. & Hutchinson, J.N. 1978. Mayunmarca rockslide and debris flow, Peru. Chap.9 in *Rockslides and Avalanches*, Developments in Geotechnical Engrg **14A** (B. Voight, ed.), 315-361. Amsterdam; Elsevier.

Lemos, L., Skempton, A.W. & Vaughan, P.R. 1985. Earthquake loading of shear surfaces in slopes. *Proc. 11th Conf. Soil Mech. & Foundn Engrg*, San Francisco, **4**, 1955-1958.

Maddock, R.W. 1986. The petrology and geological significance of some fault-generated pseudotachylytes. Ph. D. Thesis, Royal School of Mines, University of London.

Masch, L., Wenk, H.R. & Preuss, E. 1985. Electron microscopy study of hyalo-mylonites ; evidence for frictional melting in landslides. *Tectonophysics*, **115**, 131-160.

Melosh, H.J. 1987. The mechanics of large rock avalanches. *Geol. Soc. Amer. Revs in Engrg Geol.*, **7**, 41-49.

Nasmith, H.W. & Mercer, A.G. 1979. Design of dykes to protect against debris flows at Port Alice, British Columbia. *Can. Geotech. J.*, **16**, 748 - 757.

Nicoletti, P.G. & Sorriso-Valvo, M. 1991. Geomorphic controls of the shape and mobility of rock avalanches. *Geol. Soc. Amer. Bull.*, **103**, 1365 - 1373.

O' Shea, B.E. 1954. Ruapehu and the Tangiwai disaster. *N.Z. J. Science & Technology*, B, **36**, 174 - 189.

Patton, F.D. 1966. Multiple modes of shear failure in rock. *Proc. 1st Int. Cong. Rock Mechs*, Lisbon, **1**, 509-513.

Pierson, T.C., 1980. Erosion and deposition by debris flows at Mt Thomas, North Canterbury, New Zealand. *Earth Surf. Processes*, **5**, 227 - 247.

Pierson, T.C. 1981. Dominant particle support mechanisms in debris flows at Mt Thomas, North Canterbury, New Zealand, and implications for flow mobility. *Sedimentology*, **28**, 49 - 60.

Pierson, T.C. 1992. Rainfall-triggered lahars at Mt Pinatubo, Philippines, following the June 1991 eruption. *Landslide News*, **6**, 6 - 9.

Pierson, T.C., Janda, R.J., Thouret, J-C. & Borrero, C.A. 1990. Perturbation and melting of snow and ice by the 13 November 1985 eruption of Nevada del Ruiz, Colombia, and consequent mobilization, flow and deposition of lahars. *J. Volcanology & Geothermal Res.*, **41**, 17 - 66.

Reid, M.E., Ellen, S.D., Baum, R.L., Fleming, R.W. & Wilson, R.C. 1991. Landslides and debris flows near Honolulu, Hawaii, U.S.A. *Landslide News*, **5**, 28 -30.

Richards, L. 1993. Case examples of rock mechanics principles used in rock engineering. Chap. 28 in *Comprehensive Rock Engineering, Principles, Practice and Projects* (J.A. Hudson, ed. in chief; E.T.Brown, vol.ed.), **1** Fundamentals, 691 - 718. Oxford; Pergamon Press.

Salt, G. 1985. Aspects of landslide mobility. *Proc. 11th Int. Conf. Soil Mech. & Foundn Engrg*, San Francisco, **3**, 1167-1172.

Sassa, K. 1984. The mechanism starting liquefied landslides and debris flows. *4th Int. Symp. Landslides*, Toronto, **2**, 349-354.

Sharp, R.P. & Nobles, L.H. 1953. Mudflow of 1941 at Wrightwood, southern California. *Geol. Soc. Amer. Bull.*, **64**, 547 - 560.

Shreve, R.L. 1968. The Blackhawk Landslide. *Geol. Soc. Amer. Spec. Paper*, No. **108**, 1 - 47.

Sibson, R.H. 1977. Fault rocks and fault mechanisms. *Geol. Soc. Lond. J.*, **133**,191-213.

Skempton, A.W. & Hutchinson, J.N. 1969. Stability of natural slopes and embankment foundations. *Proc. 7th Int. Conf. Soil Mech. & Foundn Engrg*, Mexico, State of the Art Vol., 291-340.

Tika-Vassilikos, T. & Hutchinson, J.N. (in prep.). Rapid ring shear tests on gouge from the Vaiont slip surface.

Varnes, D.J. 1978. Slope movement types and processes. In *Landslides: Analysis and Control* (R.L.Schuster & R.J. Krizek, eds), Special Rept 176, Transportation Research Board, Nat. Acad. of Sciences, Washington, D.C.

Voight, B. & Faust, C. 1982. Frictional heat and strength loss in some rapid landslides. *Geotechnique*, **32**, 43-54.

Voight, B. Janda, R.J., Glicken, H. & Douglass, P.M. 1983. Nature and mechanics of the Mount St Helens rockslide-avalanche of 18 May 1980. *Geotechnique,* **33**, 243-273.

Walton, G. & Atkinson, T.1978. Some geotechnical considerations in the planning of surface coal mines. *Trans. Inst. Mining & Metallurgy,* 87, A147-A171.

Table 1. Possible mechanisms of rapid mass movement on slopes.

A. Triggering mechanisms providing an initial impetus

1. External triggers
   a) Entry of surface water into a slide
   b) Undrained loading of the head of a slide
   c) Undrained unloading of the toe of a slide
   d) Seismic effects, direct and indirect
   e) Magma intrusion and other volcanic phenomena

2. Coalescence of slides

3. Brittle failure within relatively intact, quasi-stable slide mass
   a) Internal shear towards rear of compound slides
   b) Passive shear failure in the toe of translational slides
   c) Buckling in the toe region of translational slides

B. Mechanisms tending to accelerate and sustain movement

4. Slip surface phenomena
   a) Smoothing
   b) Collapse of loose, saturated, metastable structure
   c) Heating
   d) Negative rate effects in rapid shear
   e) Ball- or roller-bearing action

5. Mechanisms within rapidly moving debris
   a) Repeated undrained self-loading
   b) Bagnoldian grain flow
   c) Acoustic fluidisation

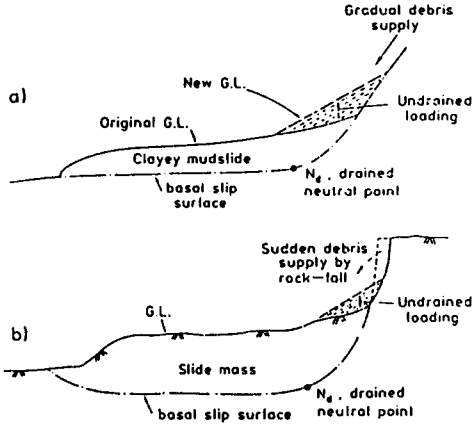

Fig.1 Undrained loading of heads of slides.

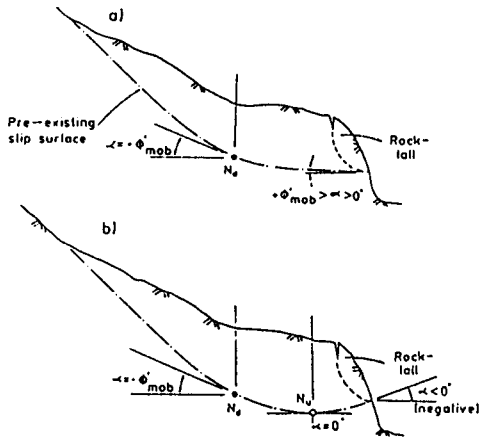

Fig.2 Undrained unloading of toes of deep-seated slides.

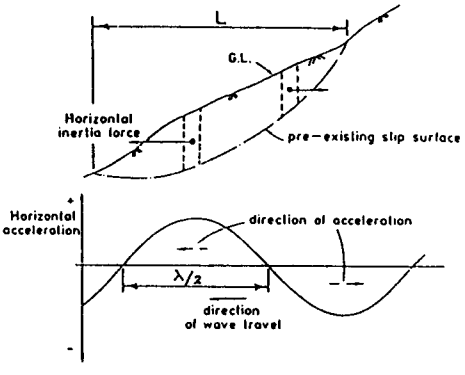

Fig.3 Direct effects of seismic waves on a slide.

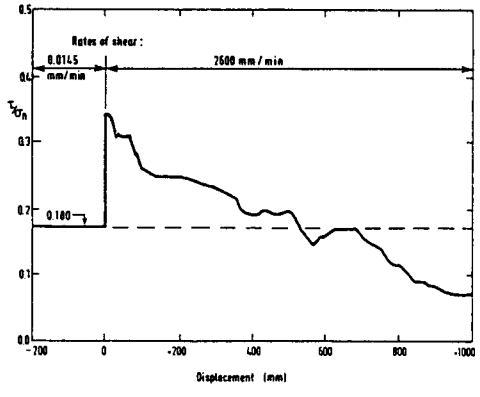

Fig.4 Results of ring shear tests on Vaiont gouge (σ_n = 980kPa).

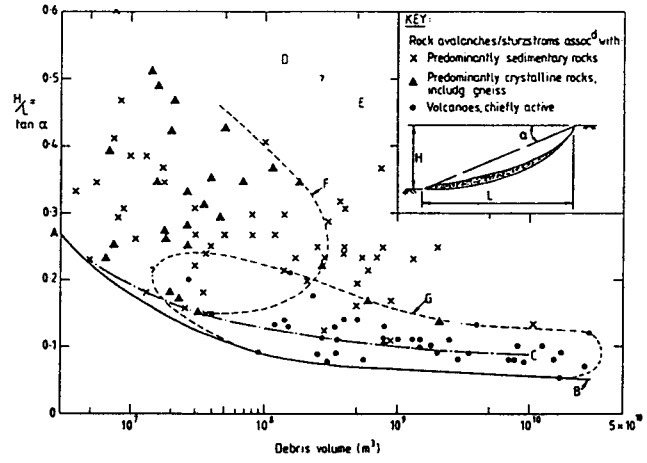

Fig.5 Plot of H/L against log. debris volume, comparing the mobilities of non-volcanic and volcanic rock avalanches/sturzstroms. The former are divided between those involving predominantly sedimentary and predominantly crystalline rocks. Data chiefly from Abele (1974), Cruden (1976), Eisbacher (1979), Heim (1932), Nicoletti & Sorriso-Valvo (1991) & Shreve (1968).

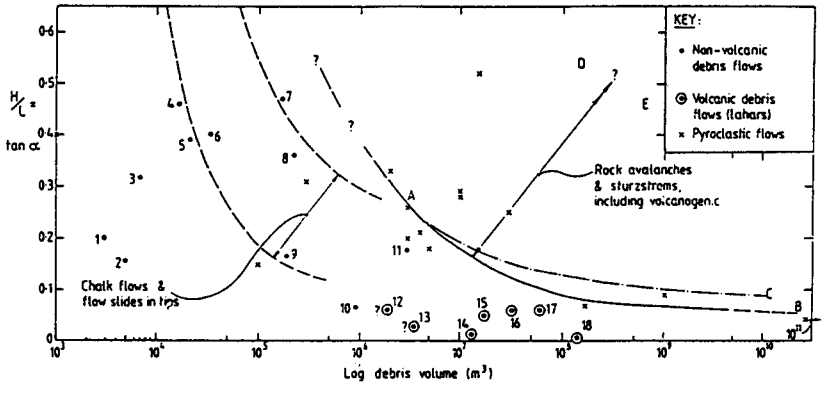

Fig.6 Plot of H/L against log. debris volume, comparing the mobilities of rock avalanches/sturzstroms (from Fig. 5), chalk flows and flow slides from tips of coal-mine waste (Hutchinson, 1988), debris flows (both non-volcanic and volcanic) and pyroclastic flows (after Hayashi & Self, 1992). Sources of the debris flow points, 1 - 18, are: 1 Thompson Creek (Johnson & Rodine, 1984); 2 Port Moody (Eisbacher & Clague, 1981); 3 Newton Canyon (Campbell, 1975); 4 Mayflower Gulch (Curry, 1966); 5 Port Alice, Gully No. 1 (Nasmith & Mercer, 1979); 6 Koulau Mts (Reid *et al.*, 1991); 7 Cathedral Gulch (Jackson, 1979); 8 La Comca (Corominas, pers. comm.); 9 Mt Thomas (Pierson, 1980); 10 Wrightwood (Sharp & Nobles, 1953); 11 Klattasine Creek (Clague *et al.*, 1985); 12 Ruapehu (Houghton *et al.*, 1987; O'Shea, 1954); 13 Mt Pinatubo (Pierson, 1992); 14 South Fork Toutle River, 18 North Fork Toutle River (both Mount St Helens, Cummans,1981; Janda *et al.*, 1981); 15 Rio Guali, 16 Rio Molinos/Quebrada Nereidas, 17 Rio Azufrado/Rio Lagunillas (all Nevado del Ruiz, Pierson *et al.*, 1990).

Rheology and modeling of mass movement deposits

Rhéologie et modélisation des dépôts de mouvements en masse

P.Y. JULIEN*, J.S. O'BRIEN‡

* *Engineering Research Center, Colorado State University*
Fort Collins, CO 80523 -USA
Tel. (1) 303 491 8450 - Fax (1) 303 491 7008

‡ *Principal, FLO Engineering, Inc.*
PO Box 1659, Breckenridge, CO 80424 - USA

Abstract

Fluidized gravitational mass movements typically turn into mud floods, mudflows, and debris flows, depending on the fluidity and granulometric composition of the material. The authors prescribe a classification linked to the governing physical processes. Mud floods contain large concentrations of fine non-cohesive material. Mudflows contain large concentrations of fine cohesive material. Debris flows contain large concentrations of clastic material. Any rheological analysis should recognize four types of shear stresses: 1) yield stress; 2) viscous stress; 3) turbulent stress; and 4) dispersive stress. Dimensionless parameters based on the ratio of these shear stresses are proposed to identify the predominant rheological material characteristic from a quadratic rheological model.
The two-dimensional model FLO-2D has been developed for the simulation of a wide range of non-Newtonian sediment flows based on the quadratic rheological model. The numerical simulation of the Rudd Creek mudflow in Utah is presented as an example of our continuing progress in the physically-based analysis of natural disasters from gravitational mass movements.

Résumé

Les mouvements en masse, gravitaires et fluidisés deviennent des inondations boueuses, des coulées de boues ou de débris selon la fluidité et la granulométrie du matériau. Les auteurs proposent une classification liée aux processus physiques prédominants. Les inondations boueuses contiennent de fortes concentrations de matériaux fins sans cohésion. Les coulées de boue contiennent de fortes concentrations de matériaux fins avec cohésion. Les coulées de débris contiennent de fortes concentrations de matériaux clastiques. Toute analyse rhéologique devrait identifier quatre types de contraintes : 1) seuil de contrainte ; 2) contrainte visqueuse ; 3) contrainte turbulente ; 4) contrainte dispersive. Des paramètres sans dimension basés

sur les rapports entre ces contraintes de cisaillement sont proposés pour identifier les caractéristiques rhéologiques dominantes d'un matériau à partir d'un modèle rhéologique quadratique.
Le modèle à deux dimensions FLO-2D a été développé pour la simulation d'un grand nombre d'écoulements non-newtoniens de sédiments basée sur le modèle rhéologique quadratique. La simulation numérique d'une coulée de boue à Rudd Creek dans l'Utah est présentée comme exemple de notre activité dans l'analyse physique des accidents provenant de mouvements en masse gravitaires.

Introduction

Despite diversified classifications, fluidized gravitational mass movements are similar to hyperconcentrated sediment flows. Hyperconcentrated sediment flows ranging from water floods to debris flows are initiated through excess moisture associated with intense rainfall or snowmelt which may be triggered by hillslope and bank failures as well as landslides. Earthquakes and volcanic activities may also initiate the process of massive mobilization of liquefied soils resulting in mud and debris flows in steep channels and onto alluvial surfaces. For instance, the intensity of rainfall or the hydrograph of the water source can control the type of flow event. The flow properties and runout distances of these flow events are governed by the volumetric concentration and granulometric composition of the material.

Mud floods, or hyperconcentrations of non-cohesive particles, display fluid characteristics at volumetric sediment concentrations $15\%<C_v<40\%$. The sediment concentration becomes rather uniform throughout the flow depth and the increased viscosity of the fluid matrix enhances sediment entrainment. For instance, Woo et al. (1988) provided a detailed analysis of hyperconcentrations of sands.

In mudflows, the concentration of silts and clays is sufficiently high to bond the fluid matrix and to support clastic material. Mudflows behave as a singular fluid mass with lobated deposits where boulders may be rafted along on the surface. Such fluid matrix concentrations generally range from 45-55% depending on the relative proportion of silts and clays. Mudflows exhibit high viscosity and high yield stress, and can travel long distances on mild slopes at slow velocities. A detailed rheological analysis of mudflow properties has been presented by O'Brien and Julien (1988).

Debris flows represent a water-sediment mixture that contains significant quantities of boulders and debris to affect fluid motion. Particle interaction of boulders is a significant mechanism to transfer momentum to the flow boundary. Granular flows constitute a sub-class of debris flows in which the exchange of momentum between the flow core and the boundary occurs almost exclusively through particle collision. The water, which may be present in small quantities does not influence particle collision or lubricate the mass.

Our understanding of sediment particle interaction in flowing water has been evolving from the study of O'Brien and Julien (1985). The definitions involving hyperconcentrated sediment flows should focus on the physical processes of the fluid motion The physical processes of the different hyperconcentrated sediment flows can be explored through a rheological study of sediment hyperconcentrations.

Nomenclature has been formulated around the fluid matrix, which is comprised of silt and clay particles finer than 0.0625 mm.

Rheology of hyperconcentrated sediment flows

The non-Newtonian nature of hyperconcentrations results from several physical processes. Cohesion and bonding of fine sediment particles contribute to the yield shear stress τ_y which must be exceeded to initiate motion. The Mohr-Coulomb shear τ_{mc} is important when considering the stability of steep slopes, while the yield strength exhibited from cohesive particles τ_c primarily contributes to the yield shear stress τ_y during motion of the fluid matrix. The viscous shear stress τ_υ accounts for the increase in Newtonian viscosity. The turbulent shear stress τ_t describes the turbulent nature of hyperconcentrated sediment flows of fine granular material. Energy dissipation through turbulence, large eddies trailing major obstacles like trees and boulders, can be accounted for by considering τ_t. Finally, the dispersive stress τ_d describes the effects of the collision of sediment clasts.
The total shear stress in hyperconcentrated sediment flows includes contributions from each of these five shear stress components:

$$\tau = \tau_{mc} + \tau_c + \tau_\upsilon + \tau_t + \tau_d \tag{1}$$

in which the total shear stress depends on the Mohr-Coulomb shear τ_{mc}, the cohesive yield stress τ_c, the viscous shear stress τ_v, the turbulent shear stress τ_t, and the dispersive shear stress τ_d.
When written in terms of shear rates, or velocity gradient (du/dy), the following quadratic rheological model is obtained:

$$\tau = \tau_y + \eta\frac{du}{dy} + \zeta\left(\frac{du}{dy}\right)^2 \tag{2}$$

where

$$\tau_y = \tau_{mc} + \tau_c$$

$$\zeta = \rho_m l_m^2 + a_i \rho_s \lambda^2 d_s^2$$

in which η is the dynamic viscosity of the mixture; τ_c is the cohesive yield strength; τ_{mc} is the Mohr-Coulomb shear stress $\tau_{mc} = p_s \tan\phi$ depending on the intergranular pressure p_s and the angle of repose ϕ of the material; ζ is the inertial shear stress coefficient depending on the mass density of the mixture ρ_m, the Prandtl mixing length l_m, the sediment size d_s, the volumetric sediment concentration C_v, $a_i \cong 0.01$ and ρ_s is the mass density of sediment. Bagnold defined the linear sediment concentration λ as

$$\frac{1}{\lambda} = \left(\frac{C_m}{C_\upsilon}\right)^{\frac{1}{3}} - 1 \qquad (3)$$

in which the maximum concentration of sediment particles $C_m \cong 0.615$.
It is important to consider that the occurrence of debris flows as prescribed by a dispersive stress relationship alone requires that the following three conditions be simultaneously satisfied: 1) very large sediment concentrations, typically exceeding $C_\upsilon > 0.5$; 2) large velocity gradients typically exceeding $10s^{-1}$; and 3) very large grain sizes typically coarser than gravel.
Julien and Lan (1991) proposed a dimensionless formulation of the quadratic rheological model in the form:

$$\tau^* = 1 + (1 + T_d^*)a_i D_\upsilon^* \qquad (4)$$

in which the three dimensionless parameters τ^*, D_υ^* and T_d^* are defined as:

1. dimensionless excess shear stress *

$$t^* = \frac{\tau - \tau_y}{\eta \frac{du}{dy}}$$

2. dimensionless dispersive-viscous ratio D_υ^*

$$D_\upsilon^* = \frac{\rho_s \lambda^2 d_s^2}{\eta}\left(\frac{du}{dy}\right)$$

3. dimensionless turbulent-dispersive ratio T_d^*

$$T_d^* = \frac{\rho_m l_m^2}{a_i \rho_s \lambda^2 d_s^2}$$

It is suggested to relate the following parametric delineations to the classification of hyperconcentrations: 1) mudflows when yield and viscous stresses are dominant at $D_\upsilon^*<30$; 2) debris flows or granular flows for which the dispersive stress is dominant at $D_\upsilon^*>400$ and $T_d^*<1$; and 3) mud floods when the turbulent shear stress is dominant at $D_\upsilon^*>400$ and $T_d^*>1$. A transition regime may be expected when $30< D_\upsilon^*<400$ for which all the terms of the quadratic equation are not negligible.

Two-dimensional simulation model FLO-2D

Based on the quadratic rheological model, O'Brien et al. (1993) developed the two-dimensional flow routing model FLO-2D for the simulation of fluidized gravitational mass movements. The momentum equation is solved after considering three components of the total friction slope S_f, namely: the yield slope S_y, the viscous slope S_v, and the turbulent-dispersive slope S_{td}. The total friction slope can therefore be rewritten as:

$$S_f = \frac{\tau_y}{\gamma_m h} + \frac{K\eta V}{8\gamma_m h^2} + \frac{n^2 V^2}{h^{\frac{4}{3}}} \qquad (5)$$

in which γ_m is the specific weight of a mixture, h is the flow depth, V is the depth-averaged flow velocity, K=24 for wide-rectangular channels but increases with roughness and irregular cross-section geometry, and n is an equivalent roughness coefficient for the turbulent-dispersive stress. The yield stress τ_y and the dynamic viscosity η increase with the volumetric sediment concentration of the fluid matrix as defined by O'Brien and Julien (1988).

The model serves the dual purpose of delineating hazardous deposit areas as well as determining the principal characteristics of heavily sediment-laden flows. The model is particularly useful to determine the flow depth, the stream flow velocity and the impact force of fast flowing hyperconcentrations. These parameters are essential for the design of appropriate mitigation structures against hazardous natural disasters. The details pertaining to the model FLO-2D are available in O'Brien et al. (1993). Numerous mudflow hazard delineation projects have been completed using the FLO-2D model.

Numerical simulation of Rudd Creek using FLO-2D

An example of numerical simulation using FLO-2D is briefly presented for the case of the 1983 Rudd Creek mudflow in Davis County, Utah. The flood hydrograph and other pertinent data were published by the U.S. Army Corps of Engineers. Available field data from the event included: 1) the area of inundation indicated from photography; 2) a surveyed volume of the mudflow deposit of approximately 64,200 m^3; 3) mudflow frontal velocities on the alluvial fan approximately the speed that a man could walk; and 4) observed mudflow depths that ranged from approximately 3.7 m at the apex of the alluvial fan to 0.6-0.9 m at the debris front.

The mudflow was initiated by a landslide, and therefore a relatively uniform sediment concentration was assumed. Manning n roughness values varied from 0.035 to 0.10 depending on vegetation and flow obstruction. Appropriate values of the yield stress and the viscosity were obtained from O'Brien and Julien (1988). The surrounding houses and buildings influenced the flow path and their effects were modeled by using blocking factors for each grid with man-made structure. A complete time-lapse simulation of the progression of the mudflow deposit over the Rudd Creek alluvial fan is given in O'Brien et al. (1993). Time-sequence flow depths are

written to files for a CAD graphics program plotting contour depths. With the plotting package, the flood hazard delineation is automated. When the viscous flow encounters a street with a favorable slope, it proceeds ahead of the main body of the flow. A three-dimensional graphical display of the time lapse simulation is presented in the above-cited reference, an example is given in Figure 1. These provide a better visualization of the accumulation of mud near the apex of the alluvial fan.

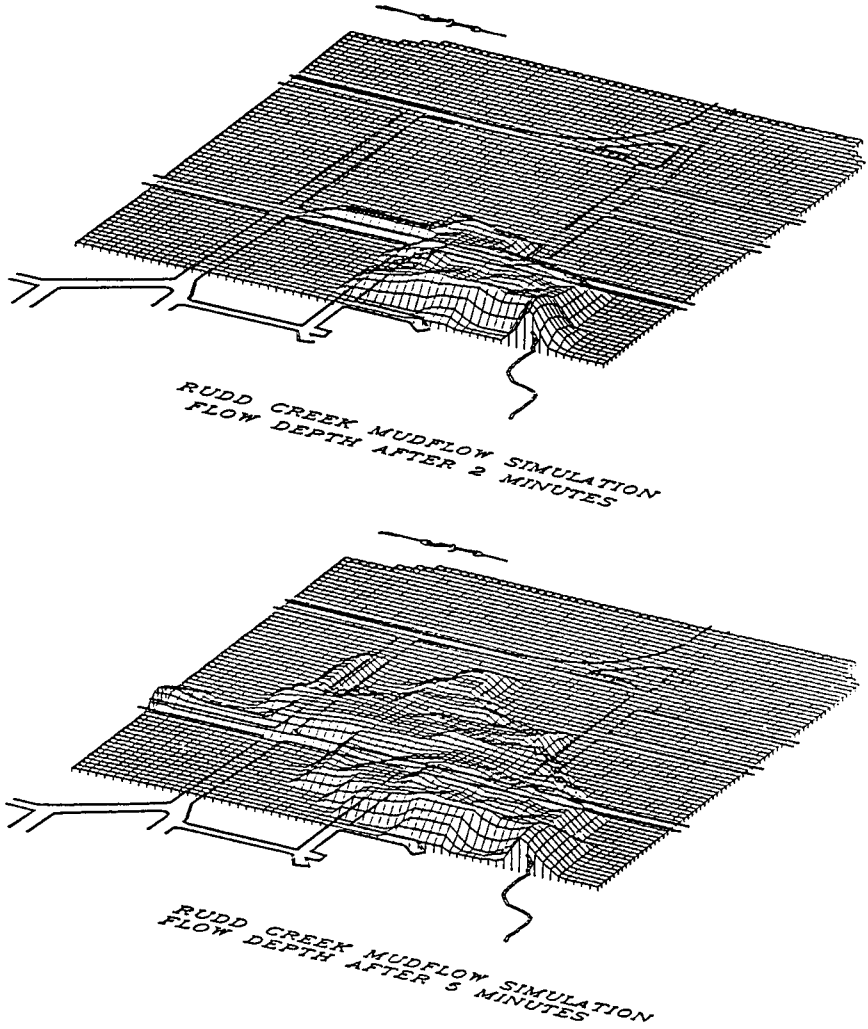

Rudd Creek Mudflow Simulation after 2 and 5 Minutes

Figure 1.

The maximum computed flow depth of 3.6 m downstream of the apex compares well with the 3.7 m observed flow depth. Mudflow velocities predicted on the fan ranged from 0.3 to 1.2 m/s or approximately walking speed as reported. Near the fan apex, the flow velocities were less than 3.0 m/s. Frontal lobe depths ranged from 0.6 to 1.2 m depending on the location on the fan, and correlated well with post-event photos.

Conclusion

The rheology of hyperconcentrations resulting from gravitational mass movements is relatively complex. The proposed quadratic formulation appropriately describes the continuum of flow conditions ranging from mud floods, mudflows and debris flows. The quadratic rheological model enables adequate two-dimensional computer simulations of yield, viscous, turbulent and dispersive stress in hyperconcentrated sediment mixtures.

FLO-2D is a numerical model designed to simulate the motion of non-Newtonian hyperconcentrations in steep channels and on alluvial fans. The Rudd Creek 1983 mudflow triggered by a landslide was properly simulated with the FLO-2D model. The excellent correlation of the simulated results with estimated flow characteristics demonstrates the applicability of the model for the delineation of hazardous areas as well as the determination of key parameters for the structural design of appropriate countermeasures. The analysis stresses the importance of appropriate values of rheologic parameters such as the dynamic viscosity and yield strength.

References

Julien, P.Y. and Y.Q. Lan, 1991. On the Rheology of Hyperconcentrations. J. Hyd. Eng., ASCE, 117(3), 346-353.

O'Brien, J.S., and P.Y. Julien, 1985. Physical Properties and Mechanics of Hyperconcentrated Sediment Flows, Proc. ASCE Hyd. Div. Spec. Conf. on Delineation of Landslides, Flash Flood and Debris Flow Hazards, Logan Utah, June 1984, 260-279.

O'Brien, J.S., and P.Y. Julien, 1988. Laboratory Analysis of Mudflow Properties. J. Hyd. Eng., ASCE, 114(8), 877-887.

O'Brien, J.S., P.Y. Julien and W.T. Fullerton, 1993. Two-dimensional Water Flood and Mudflow Simulation, J. Hyd. Eng., ASCE, 119(2), 244-261.

Woo, H.S., P.Y. Julien, and E.V. Richardson, 1988, Suspension of large concentrations of sands, Hyd. Eng., ASCE, 114(8), 888-898

Seismic mapping of gravitational mass movements on the shielfs and continental margins

Cartes sismiques des mouvements gravitaires en masse sur les plateaux continentaux et leurs marges

A. V. KALININ

Moscow State University
Leninsky Gory, 117-234 Moscou - Russia
Tel. (70) 95 939 43 70 - Fax (70) 95 433 53 47

Abstract

This paper deals with the interest presented by seismic measurements to map and describe submarine gravitational mass movements. After a description of the traditional methods and a few recent improved technics, the main signs of slide masses are listed. The main difficulty is not in the detection of these masses but in the estimation of the velocity of the past movement. Several different types of situations are presented in which structural features of deposits can give an idea of the nature of the movement.

Résumé

Cet article met en évidence l'intérêt des mesures sismiques pour cartographier et décrire des mouvements en masses gravitaires et sous-marins. Après une description des méthodes traditionnelles et de quelques améliorations techniques récentes, les signes principaux des dépôts de mouvements sont énumérés. La difficulté principale n'est pas de détecter ces masses, mais d'estimer la vitesse du mouvement. Plusieurs types différents de situations sont présentés dans lesquelles les caractéristiques structurales des dépôts peuvent donner une idée de la nature du mouvement.

Locations

- The oceans : Pacific, Indian, Atlantic, Artic.
- The seas : Blake, Caspien, Azov, Mediterranean, White, Barents, Okhotsk, Bering, Norway, Baltic.
- The rivers : Volga, Amur, Oka, Ob, Irtish, Moscow-river
- The lakes : Baikal, Sarez, Kuibishev.

Main technic parameters

- Water depth range : 3 m-7000 m
- Frequency band : (30-120), (100-500), (250-1000) cycles

- The technic : one channel continuous seismic profiling with Sparker type source of elastic waves.
- The step of observations along the profile : 1 m - 50 m.

Commonly we use one sparker or array of 3 or 6 sparker with fool energy 5000-30000 joules. Such energy provides us the frequency band of 30-120 cycles or 100-500 cycles, penetration depth through the rocks about 1500 m - 2000 m when water depth doesn't exceed 7000 m. In case of shelf, normal profiling speed doesn't exceed 3 m/s - 4 m/s. The distance between the observation points is 15 - 20 m. The resolution possibility in time changes from 15 ms to 30 ms. For near bottom deposits, it means that the depth resolution Lz is about 12 m - 24 m. The spatial resolution possibility Lsp depends essentially on the depth at which the slide bodies are located and on absorption property of overlayered rocks. Our practice shows that spatial resolution possibility may be evaluated by the following law :

$$Lsp = \sqrt{cH / 2f}$$

where :

c is theelastic wave velocity,
H the distance between the water surface and slide body,
f the central frequency of the reflected wave spectrum.

The value of f depends on the character of concrete source of elastic waves (from the direct pulse shape) and on absorption property of the overlayered rocks.

The evident feature of slide masses mapping is little distance between observation point within the profile and large distance between the profiles. It means that, in most cases, we have the data which present the vertical cross-section along the sediments of our interest. In other words, we have to use two-dimensional images of three-dimensional objects for revealing the slide masses. It is clear that, for this reason, the details of geometric parameters of slide bodies cannot be detected although these parameters often play decisive role in interpretation process.

Some years ago, I offered the technic to overcome the difficulties of such kind. The technic is very simple and consists in combination of seismic research along the straight line profiles and along the circular trajectory of 500 m - 1000 m diameter. Operative control of seismic record during the profiling permits to choose the start point of circular trajectory. After realising the circular profile, the ship continues straight line profile. It is clear that in case of three-dimensional character of studied structures, we will receive possibility to notice some details of buried relief of slide bodies.

The main signs of slide masses

1 Typical morphology of the slide bodies.
2 Geomorphology and paleogeomorphology position of revealed bodies.
3 Irregular structure of the deposits inside indicated bodies.
4 Sudden disappearance of clear stratification within the limited part of observed deposits while, above and beneath that portion of deposits, the stratification is obvious.
5 Unconformity with basic rocks.

Usually there is no problem to detect at the seismic records the slide bodies. The problem consists in determining how rapidly that body moved. Seismic data do not allow to give direct answer to the question. But it is obvious that some structural features of deposits permit to evaluate the speed of movement. For example, clear signs of the ruptures of layers and separated position of body within the general sediment structure may arise only in case of rapid movement of large mass of sediments. Pictures show the cases of undoubted rapid movement of sediments located in the south of the Crimea, in Bulgaria, in the Kuril-Kamchatka trench or in the South of Crimea.

On the contrary, there are cases which may be explained only by slow movement of poor-consolidated sediments along the consolidated rigid rocks in condition of weak slope of the beds.

In one region of the Black Sea, we revealed three levels of slow deformation of poor consolidated rocks which were formed in process of periodic changing of the slope. Rhelogical nature of such phenomena is rather clear and can be observed in the south of Crimea, in the Odessa shelf or in shelf break.

Intermediate position is presented by the bodies of large size which interior structure is irregular and chaotic. Within these bodies there are not clear boundaries or layers. Visually, the picture seems as a section of turbulent flow photographed at some moment of its movement. The geologists approve that the bodies of that kind were formed in sea conditions in process of rapid movement of poor consolidated deposits along the rigid bedrock.

They confirm also that these processes are typical for the time of low sea level, when the transient zone at the shelf is short and the volume of deposits from the land is large. Is it true or not - I do not know being a geophysisist - but our investigations near Crimea and at Bulgarian shelf show that at the same geological time during low sea level similar type of slide bodies was formed (cf. the South of Kerch Straight-Paleo Don, Paleo Kuban, deposits of glacial periods, distribution of the slide bodies in the region to South of Crimea, Bulgarian shelf, the correlation of the slide movements of different type at Bulgarian and Crimea continental edge in geological time - 800000 years - the times of low sea levels).

The modern technic of satellite navigation provide conditions for long-term observation over the selected area of shelf in connection with dynamic problems of gravitational movement. Unfortunately at the time of our active work, we had not such possibility. But in connection with other problems we were realizing long-term observations along the Moscow-river using the combination of high resolution seismic and electrical self potential measuring. Now we have a series of 12 years observations in conditions of precise navigation that permits us to reveal the variations of bottom relieve and self electrical field year by year and to find the correlation between two proceses. We plan to continue these observations in future and, maybe, expand them involving other areas of water.

Anyway, in our time, the high resolution seismic is the only possible technic to reveal the slide masses and, for reliable interpretation of seismic data, it would be very important to use the data of physical and mathematical modeling of rapid slide processes in the sea conditions.

Numerical modelling of debris flow dynamics

Modélisation numérique de la dynamique des coulées de débris

D. LAIGLE, P. COUSSOT

Cemagref / Division Protection Contre les Erosions
BP 76, 38402 Saint-Martin-d'Hères - France
Tel. (33) 76 76 27 66 - Fax (33) 76 38 51 03

Abstract

In order to predict complex transient debris flows, we developed a numerical model based on shallow water equations. We consider only muddy debris flows the behaviour of which is well described by a Herschel-Bulkley model. In laminar regime, the wall friction force is assumed to be equal to the resistance of a steady uniform flow having the same depth and mean velocity. The parameters of this model, directly deduced from the fluid behaviour, are determined independently by rheometrical measurements. The main characteristics of our experimental transient flows, established in a laboratory flume, are in fairly good agreement with the predictions of the numerical model. It should be noticed that these results were obtained without any complementary fitting.

Résumé

Afin de décrire les écoulements transitoires des laves torrentielles, un modèle numérique fondé sur les équations de Saint-Venant a été construit. On s'intéresse uniquement aux laves torrentielles essentiellement boueuses, qui ont une loi de comportement de type Hershel-Bulkley. En régime laminaire, nous faisons l'hypothèse que le frottement à la paroi est égal à celui d'un écoulement permanent uniforme ayant mêmes vitesse moyenne et hauteur. On présente ici la confrontation entre des écoulements transitoires de matériaux modèles en laboratoire et les simulations numériques correspondantes. Les paramètres de la loi de frottement sont déterminés indépendamment par des expériences de rhéométrie. L'adéquation entre simulations et expériences est satisfaisante et d'autant plus prometteuse qu'aucun calage préalable de paramètres n'est effectué.

Introduction

Debris flow differ from other free surface flows [**Johnson and al.** (1984), **Meunier** (1991)] by two main characteristics which are :

- the nature of the flowing material, constituted of a mixture of water, clay and granular materials of different sizes ;

- the nature of the flow itself, which is rapid, transient and includes a steep front mainly constituted of rocks.

In a first time, we neglect phenomena such as : concentration fluctuations, local discontinuities in the strain field due to local fractures, slip at the wall, segregation or sedimentation. In these conditions, the flowing material can be considered as an homogeneous fluid.

Shallow water equations are often used for debris flow modelling [**Takahashi** (1987), **Mizuyama** (1987), **Martinet** (1992-a-b)] and the main point that differs from a numerical model to another is the formulation of the wall friction force deduced from the rheological assumptions. Even if many assumptions have been tested [**Chen** (1987)], most of the time, the rheological models used are :

- Bingham's model for muddy debris flow [**Johnson** (1970)]
- Bagnold's model for granular debris flow [**Takahashi** (1980)]

New developments on clayey concentrated mixtures have established that their behaviour is well represented by a Herschel-Bulkley model [**Major and Pierson** (1992), **Coussot** (1992)]. Using this latter assumption and the fact that many debris flows are laminary, **Coussot** (1993-a-b) has established theoretically a new wall friction expression and has validated it on steady uniform flows in a laboratory flume. This friction expression is here introduced in a numerical model based on the conservative form of shallow water equations [**Vila** (1986) and (1987)] and validated on transient flows in a laboratory flume.

One shall notice that parameters are deduced directly from rheological measurements and therefore no calibration is introduced in this study.

Numerical modelling

In order to represent debris flows, we had to do the choice of equations describing the motion and taking into account the front as well as the material characteristics.

Equations of motion

Shallow-water-equations can be written in a particular form, called "conservative", which is also solution of the hydraulic jump (Rankine-Hugoniot) equations. Associated to special numerical schemes, these equations are the basis of a numerical model able to treat the discontinuity as well as any other point, and to determine its position at any time, giving an overall treatment of the flow with reasonnable complexity and calculation times [**Vila** (1986)].

We consider channelized flows represented by one-dimensional shallow-water-equations which can be written on the following conservative form :

$$\frac{\partial}{\partial t}\begin{pmatrix} S \\ Q \end{pmatrix} + \frac{\partial}{\partial x}\begin{pmatrix} Q \\ \alpha\frac{Q^2}{S} + P(S,x) \end{pmatrix} = \begin{pmatrix} 0 \\ gS\sin(\theta) - Frot + B(S,x) \end{pmatrix}$$

S : cross section area

Q : discharge in this section

α : correcting coefficient ($\alpha = \frac{\overline{u^2}}{\overline{u}^2}$)

Frot : friction force

with $\frac{\partial P(S,x)}{\partial x} - B(S,x) = gS\cos(\theta)\frac{\partial h}{\partial x}$

Numerical scheme

Considering only the left-hand member of shallow water equations, we obtain a non-linear hyperbolic system for which there exists well adapted numerical methods (bearing the existence of discontinuities) such as the Godunov scheme here employed [**Vila** (1986) and (1987)]. The result is then corrected to take into account the right-hand member (gravity, friction, etc.)

Wall friction force

For a problem whose initial conditions, boundary conditions and geometry of the channel are known, the wall friction force remains the only unknown of shallow water equations. This unique expresion enables the introduction of the fluid behaviour into the equations of motion [**Chen** (1987)]. We are interested only in muddy debris flows (clay fraction higher than 10%) for which simple shear stress is well represented by a Herschel-Bulkley model [**Coussot** (1992)] :

$$\tau = \tau_c + K\gamma^n \text{ with } n=1/3$$

τ : shear stress
τ_c : yield stress
γ : velocity gradient
K and n : model parameters

Theoretical considerations on Herschel-Bulkley fluid flows on a wide plane, strengthened and completed by experiments in a laboratory flume have led to establish the following expressions of the wall friction for steady uniform flows in open channels [**Bossan** (1993), **Bossan and al.** (1993), **Coussot** (1993-a)] :

$$\tau p = \tau c(1+a(Hb)^{-0,9}) \qquad Hb = \frac{\tau_c}{K}\left(\frac{h}{U}\right)^{1/3}$$

with :

- infinitely wide channel : a=1,93
- rectangular cross section channel : $a=1,93-0,43\text{arctang}\left((10h/L)^{20}\right)$ for $h/L<1$

The friction force expression introduced in shallow-water-equations is then given by :

$$Frot = \frac{\tau_p}{\rho}Pe \qquad Pe : \text{wet perimeter} \qquad \rho : \text{density (kg.m-3)}$$

The wall friction expression for steady uniform flows taking into account the local mean velocity and depth, we assume that the local resistance for transient flows is equal to the friction force calculated for the same discharge and depth with the

expression previously established for steady uniform flows. The same assumption, made for gradually varying flows has been validated experimentaly [**Bossan** (1993)].

Main assumptions

Shallow-water-equations assume [**Cunge and al.** (1980)] that fluid density is constant and that vertical accelerations (steep waves, large slope variations) and horizontal accelerations (varying width of the flume, centrifugal accelerations, etc.) can be neglected. The front is represented on grid points by discontinuities which verify physical balances but do not express the detailed stucture of the front.

Model validation

In order to validate the model, we compare its predictions to experimental results obtained with water-natural clay mixtures flows in a uniform geometry laboratory flume. These flows are in similarity to natural debris flows. The wall friction force parameters are directly deduced from rheometrical measurements carried out on the materials. Therefore, the comparison introduces no fitting.

Laboratory experiments

We create, in controlled conditions, dam-breack waves in a model fluid and we measure the height of the flow at any time, at different, points of the flume The experimental principle is to create, in controlled conditions, dam-break waves in a model fluid and to measure the flow depth at any time, at different points of the flume and for different slopes, different quantities of material, different initial heights and different fluids. In order to take into account the surging nature of debris flows, we consider two cases :

- a zero initial height to represent the first wave
- a non-zero initial height to represent the following waves

Four materials made of a water-clay mixtures (natural clay from Sinard, Isère, France) with different concentrations are used. Their rheological parameters are given in the following table :

material	density ρ ($kg.m^{-3}$)	yield stress τc (Pa)	K (Herschel-Bulkley's model)
A	1410	19	3,5
B	1422	17	5,6
C	1397	9,5	3,1
D	1330	4,5	1,4

For more details on measurement technics, one can refer to **Coussot** (1993-a).

By adding uncertainties on measurements and rheological model fitting, estimation errors on rheological parameters are estimated to be of the order of magnitude of 20%.

The experimental device (Fig. 1) is constituted of 4 m x 0.6 m flume with a rectangular cross section and a slope varying from 6% to 31%. Its up-stream extremety

is limited by a wall (abscissa x=0). At abscissa x=0.85m is disposed a vertical plate constituting a dam which can be pulled up rapidly. At abscissa 1.65m, 2.75m and 3.85m are installed three ultrasonics sensors bound to a computer recording 33 measurements per second for each sensor and for 10 seconds.
The experimental uncertainties on measurements, bound essentially to the synchronism between dam-break and data acquisition trigerring, to the ultrasonics sensors principle of work or to the dam opening system are estimated to be in the range of 5% to 15% of depths or propagation times measured values.

Fig. 1 : experimental device

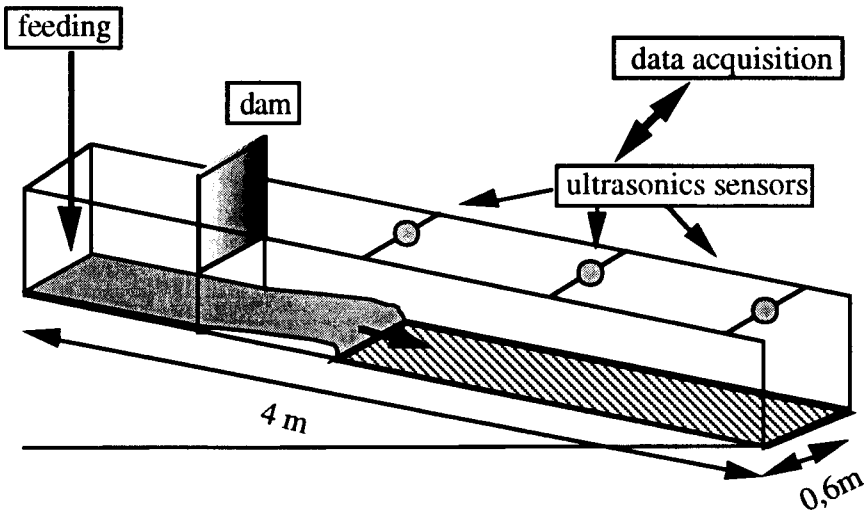

Flows with a zero-initial height

Behaviour and sensibility of the model

In order to estimate a priori the model behaviour and sensibility in the domain of the experiments carried out, its reply in terms of maximum depth and propagation time for a wide domain of variation of parameters, including the experimental conditions tested, has been calculated.
In reference to experimental conditions, we consider flows in a wide channel presenting two main characteristics :

- initial velocity is zero at any point ;
- the initial height is zero in the flume and the material initially stocked behind the dam has got an horizontal free surface.

The initial conditions are then completely given by the height of material initially stocked behind the dam (Hbar)

The non-dimensionnal form of shallow water equations exhibits two non-dimensionnal numbers which completely determine the flow at each point of the channel, in the conditions previously set forth :

$$G'' = \frac{\rho g H_{bar} \sin(\theta)}{\tau_c} \quad H'' = \frac{K}{\tau_c}\left(\frac{g\cos(\theta)}{H_{bar}}\right)^{n/2}$$

Hbar : initial height behind the dam

The experiments take place in a domain of variation from 4 to 70 for the parameter G′ and 0.35 to 0.80 for the parameter H′. This domain is wide enough to include flows in similarity to most real debris flows. For example, the material A in the 4 meters long flume shows at scale 1/30 the behaviour of a natural material (ρ=2200 kg.m-3, τc=900 Pa, K=290) in a 120m long flume.

Fig. 2 : sensibility on maximum depths (H''=0,684)

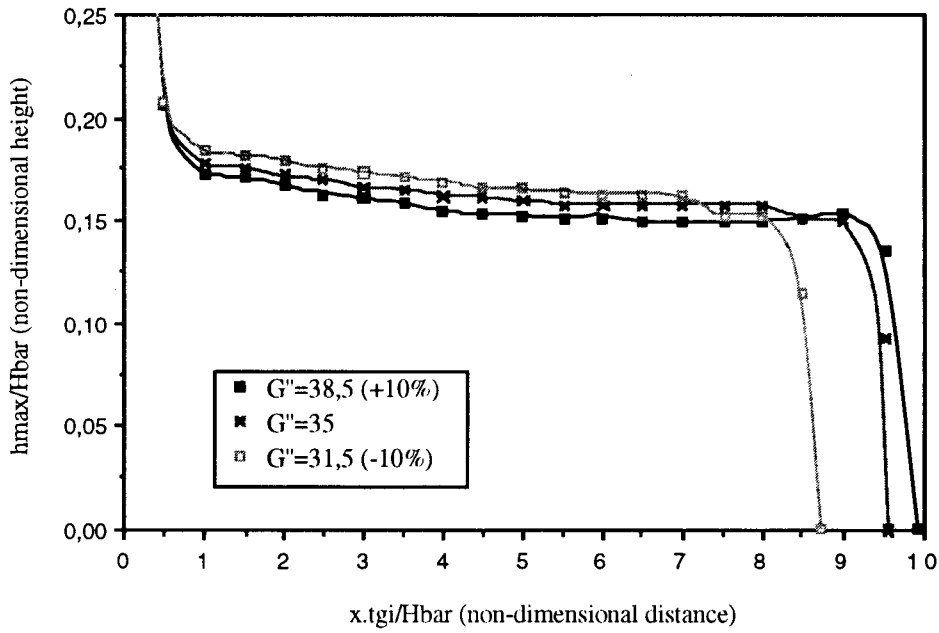

For a fully developed flow, after a fast decrease observed during the starting phase, maximum heights tend asymptotically towards a quasi-constant value (Fig. 2 and 3). The front velocity is quite constant during these two first phases (Fig. 3). The stopping phase is expressed by a fast decrease of maximum heights and propagation velocities. The sensibility to any variation of parameter values is generally weak, except during the stoppage (Fig. 2 and 3). These results, established for a variation of G′, remain qualitatively significant for a variation of H′. For a fully developed flow, the sensibility decreases for a decrease on H′ or an increase on G′.

Comparison between experiments and simulations

Gradually varying flows

Comparisons carried out on gradually varying flows show a very good agreement between flow curves established numerically or directly deduced from the friction expression. These latter are also able to describe experimental data with uncertainties less than 25%.

Transient flows

Qualitatively, simulations and measurements are in good agreement (Fig. 4). The general form of hydrograms is well represented, the order of magnitude of depths and propagation times is consistent with the measurements.

Fig. 3 : sensibility on propagation times (H''=0,684)

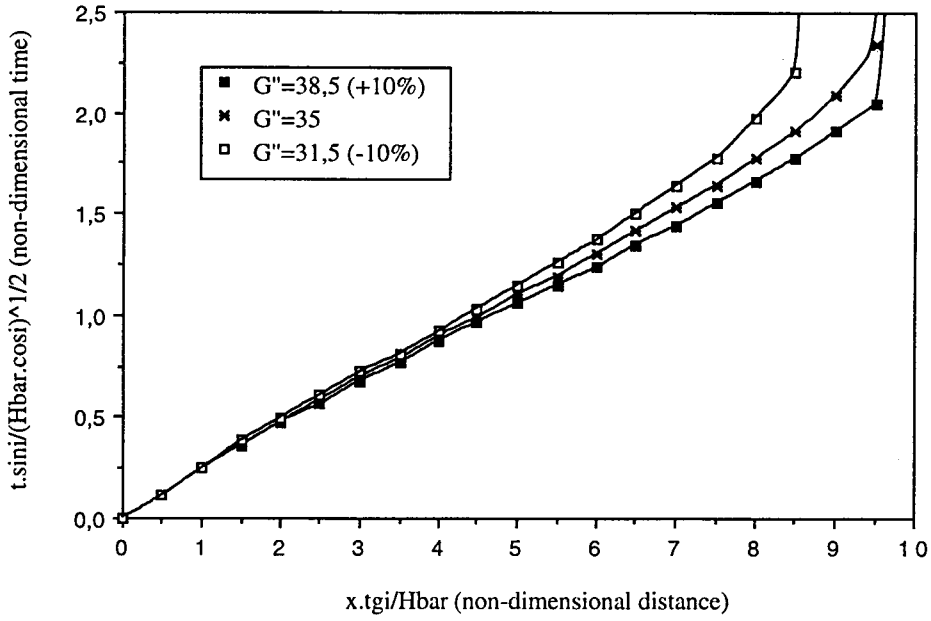

The differences concern :

- an interval between maximum depths of about 20% of measured values (Fig. 5) for which sensibility is high ; only 12% of calculated values are outside this range, some of them corresponding to stopping phases ;
- an interval between propagation times of about -20% to 10% of measured values (Fig. 6), except in the case of stopping flows (high sensibility) ;
- an interval between depths at the end of the experiment (at t=10 seconds) of about +10% to +15% of measured values ;
- an interval between stopping distances of about ±25% of measured values.

Fig. 4 : example of comparison simulations/measurements (zero initial height)

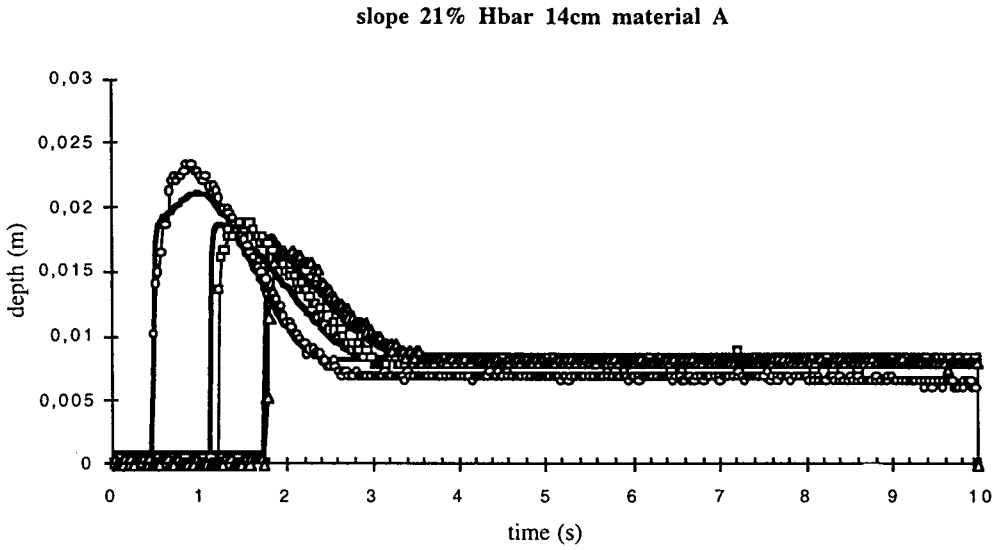

Fig. 5 : comparison simulations/measurements on maximum depths

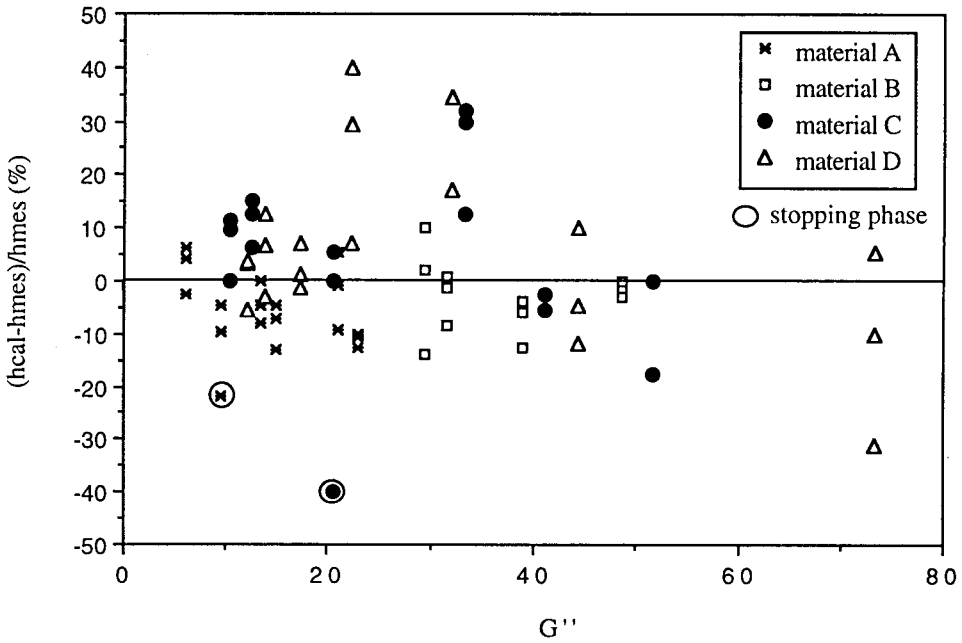

Fig 6 : comparison simulations/measurements on propagation times

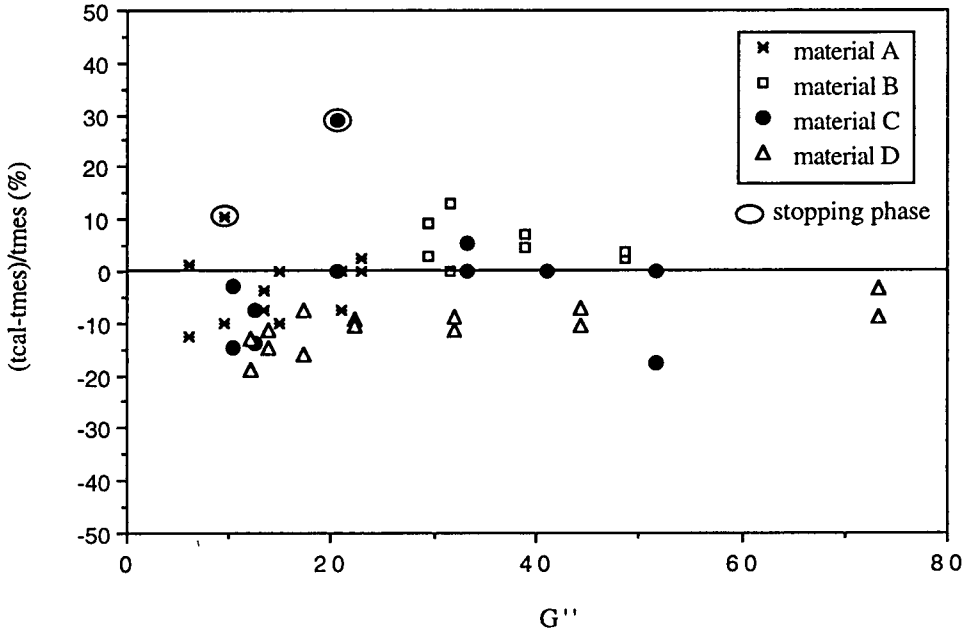

Fig.7 : example of comparison simulations/measurements (non-zero initial height)

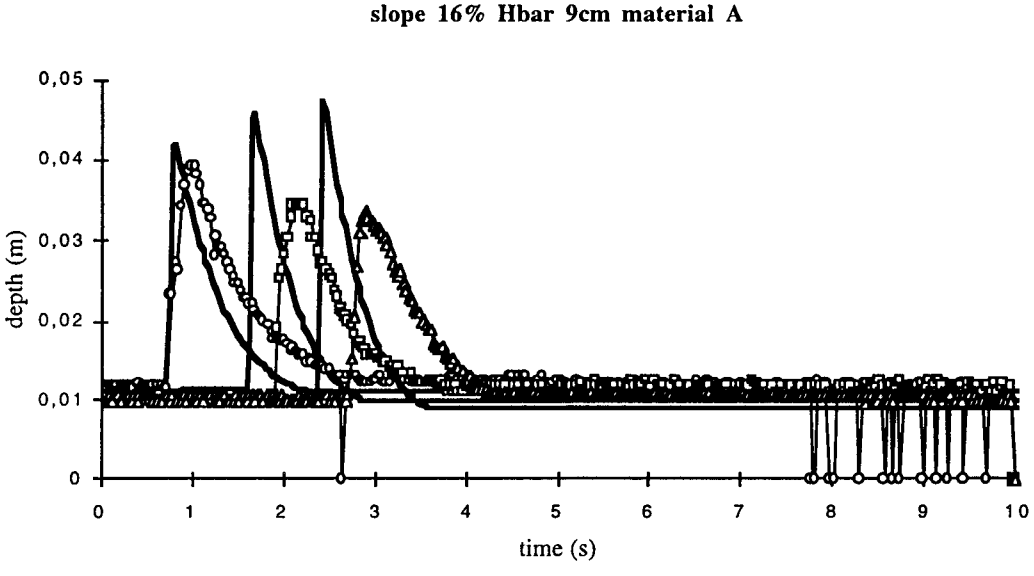

The analysis of results doesn't exhibit any link between estimation errors and non-dimensional parameters (G' or H') as well as geometrical scale. The main uncertainties appear for the material D whose rheometrical parameters have been difficult to obtain. Most observed discrepancies are in the range of precision one can reasonnably admit for the measurements. The experimental uncertainties, generally speaking, and particularly rheometrical errors are important enough to explain these differences and to hide the inaccuracies of the model itself.

Transient flows with a non-zero initial height

The calculated waves are steeper, faster, with a higher spike and a shorter lowering phase than measured waves (Fig. 7). The magnitude of errors can reach +70% on maximum depths and -35% on propagation times and is clearly related to the wave amplitude (Fig. 8).

Fig. 8 : comparison simulations/measurements on maximum depths and propagation times

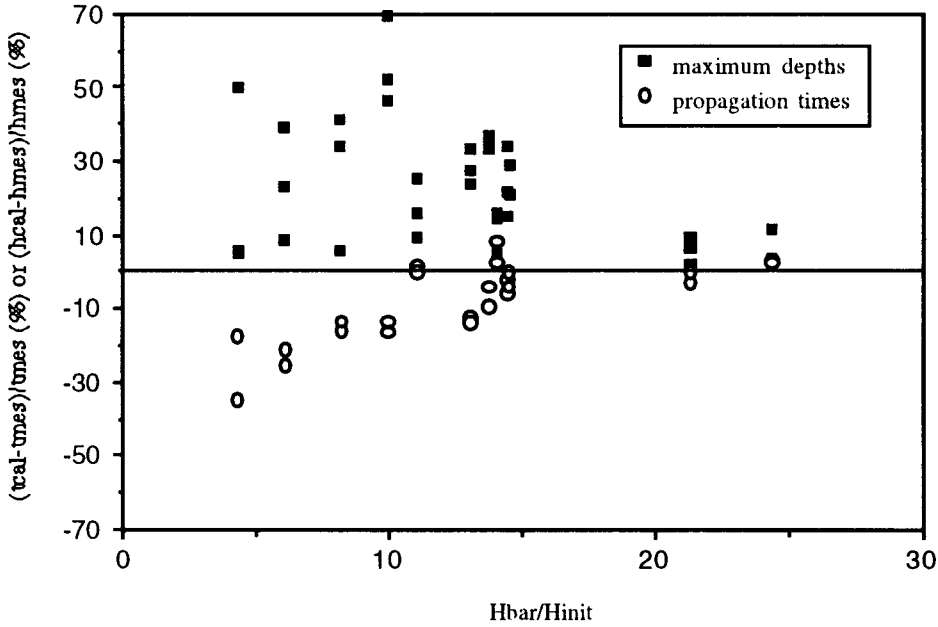

The dam height to initial height ratio is a good criterion for distinguishing cases of good or bad agreement between simulations and measurements. This criterion takes here the place of parameter G' which has been established for zero initial height flows, its significance is physically very close. A possible explenation of this difference is linked to the incapability of the model to represent some types of waves with important vertical accelerations [**Stoker** (1957)] which cannot be considered as the displacement of a front. This is for example the case of solitary or sine waves

[Naaim (1991)]. A second possible explanation is the difficulty to represent correctly the transient effects and modifications of the velocity profile (compared with the model assumptions) due to the integration into the flow of the material initially present in the flume.

Conclusion

The presented modelling shows good capabilities to predict flows of the studied water-clay mixtures. The wall friction force expression has been validated for transient flows. Inside the domain of validity established here (Hbar-to-Hinit ratio higher than about 20), the model seems to introduce errors weak enough to be occulted by the amplitude of experimental errors (particularly the estimation of rheometrical parameters).

Currently, further work remains to be done on physical phenomena, their description and quantification. The model described here is a good tool for this kind of investigation.

The proposed model must be developed now in the sense of a better agreement with field conditions (complex geometry, take into account a rocky front or more granular materials). Even if a systematic use of this model as an engineering tool can't be intended yet, it can be used for testing physical assumptions on transient flows. A two-dimensional model able to describe the spreading-out of non-channelized debris-flows is now being developed.

References

Bossan, E., (1993), "Expériences d'écoulements de laves torrentielles sur modèle réduit" DEA de mécanique, INPG, Grenoble, France.

Bossan, E., Krage, J.-U., et Tiberghien, G., (1993), "Hydraulique des laves torrentielles - Expériences d'écoulement à surface libre en canal ouvert-", Projet de fin d'études de l'ENSHMG, 100p.

Chen, C. L., (1987), "Comprehensive review of debris flow modeling concepts in Japan", Geological Society of America, Reviews in Engineering Geology, vol. VII, pp. 13-29.

Coussot, P., (1992), "Rhéologie des laves torrentielles", thèse de Doctorat de l'Institut National Polytechnique de Grenoble, Grenoble, France, 420p.

Coussot, P., (1993-a), "Lois d'écoulement des laves torrentielles", Colloque SHF-Transport solide en eaux continentales et littorales - 17 et 18 novembre 1993, Paris.

Coussot, P., (1993-b), "Steady, laminar, flow of concentrated mud suspensions in open channel - I theory - ", submitted to Journal of Hydraulic Research.

Coussot, P., (1993-c), "Steady, laminar, flow of concentrated mud suspensions in open channel - II experiments and comparison with theory : uniform flows - ", submitted to Journal of Hydraulic Research.

Cunge, J.A., Holly, F.M., Verwey, A., (1980), "Practical Aspects of Computational River Hydraulics", Pitman,.London, England.

Davies, T.R., Phillips, C.J., Pearce, A.J., Zhang Xin Bao, (1991), "New aspects of debris flow behaviour", Japan-U.S. Symposium on Snow Avalanche, Landslide, Debris Flow Prediction and Control.

Johnson, A.M., (1970), "Physical processes in Geology", W.H. Freeman, San Francisco, 577p.

Johnson, A.M., and Rodine, J.R., (1984), "Debris flows", in : "Slope Instability", (D. Brunsden and D.B. Prior Editors), chapter 8, John Wiley and sons, New-York.

Major, J.J. and Pierson, T.C., (1992), "Debris flow rheology : experimental analysis of fine-grained slurries", Water Ressources Research, vol. 28, n°3, pp. 841-857.

Martinet, G., (1992-a), "Contribution à la modélisation des avalanches de neige dense et des laves torrentielles", thèse de Doctorat de l'Université Joseph Fourier, Grenoble, France, 218p.

Martinet, G., (1992-b), "Modélisation tridimensionnelle des laves torrentielles - Application à un cas réel : Utilisation du code bidimensionnel LAVE1D-", Colloque INTERPRAEVENT 1992, Berne, Suisse, vol. II, pp. 331-342.

Meunier, M., (1991), "Eléments d'hydraulique torrentielle", Cemagref, Collection Etudes, série Montagne n°1, 274p.

Mizuyama, T. and Yazawa, T., (1987), "Computer simulation of debris flow depositional processes", Erosion and sedimentation in the Pacific Rim (Proceedings of the Corvallis Symposium), IAHS n°165, pp. 179-190.

Naaim, M., (1991), "Modélisation numérique des effets hydrodynamiques provoqués par un glissement solide dans une retenue", thèse de Doctorat de l'Université Joseph Fourier, Grenoble, France, 157p.

Stoker, J.J., (1957), "Water waves", Interscience, New York.

Takahashi, T., (1980), "Debris flow on prismatic open channel", Journal of the Hydraulics Division, 106(HY3), pp. 381-396.

Takahashi, T., Nakagawa, H. et Kuang, S., (1987), "Estimation of debris flow hydrograph on varied slope bed", Erosion and sedimentation in the Pacific Rim (Proceedings of the Corvallis Symposium), IAHS n°165, pp. 167-177.

Vila, J.P., (1986), "Sur la théorie et l'approximation numérique de problèmes hyperboliques non linéaires, applications aux équations de Saint Venant et à la modélisation des avalanches de neige dense", thèse de Doctorat de l'Université Paris VI, Paris, France, 481p.

Vila, J.P., (1987), "Schémas numériques en hydraulique des écoulements avec discontinuités", Actes du colloque AIRH, Lausanne, Suisse.

Evidence of Rapid Gravitational Mass Movement on the Submerged Flanks of the Hawaiian Islands

Mise en évidence de mouvements gravitaires rapides sur les flancs immergés des îles Hawaii

H. J. LEE

U.S. Geological Survey
Menlo Park, CA 94025 -USA
Tel. (1) 415 354 30 38 - Fax (1) 415 354 31 91

Abstract

This paper deals with differents types of gravitational mass movements which take place on the submerged flanks of the Hawaiian Islands : debris avalanches, giant slumps and volcaniclastic flows.
After a description of the measurement methods used to map mass movement features, the author presents each of these three phenomena. Different examples are given. In conclusion, the issue of the mechanisms at work in giant debris avalanches is discussed as well as their modelling. The relations between these phenomena are finally detailed.

Résumé

Cet article traite de différents types de mouvements gravitaires en masse qui ont eu lieu sur les flancs immergés des îles Hawaï : avalanches de débris, glissements géants et écoulements de roches volcaniques clastiques.
Après une description des méthodes de mesure utilisées pour cartographier les dépôts liés à ces mouvements en masse, l'auteur présente chacun de ces trois phénomènes. Différents exemples sont donnés. En conclusion, les mécanismes à l'oeuvre dans les gigantesques avalanches de débris sont discutés ainsi que leur modélisation. Les relations entre ces phénomènes sont finalement détaillées.

Introduction

Recent investigations of the submerged flanks of the Hawaiian Islands have disclosed three types of mass movement processes that may be unique to active mid-plate volcanic islands. These types of processes are: (1) Debris avalanches that may be among the largest on earth, (2) giant slow-moving slumps that can encompass a third or more of the total area (subaerial and submarine) of the major shield volcanoes and can produce earthquakes of magnitude 7.0 or greater, and (3) volcaniclastic flows that involve possibly rapid downslope movement of coarse sand-size material generated as lava enters the sea. Knowledge of the existence and

extent of deposits resulting from these processes has been made possible through the development of modern sidescan sonar and swath bathymetry systems. The critical quantitative factors describing the initiation, movement, and deposition of these landslides have not been evaluated except in a very approximate way.

Methods

The advent of acoustic survey methods that ensonify swaths of the seafloor (sidescan sonar and swath bathymetry) rather than only penetrating the bottom beneath ship's tracks has greatly expanded our ability to map marine geologic features. In few locations has this improved ability been proven more useful than on the submerged flanks of the Hawaiian Islands. As part of a program to map the U.S. Exclusive Economic Zone, a complete sidescan sonar mosaic of the seafloor from the Hawaiian coast to a distance of 370 km offshore has been constructed using the GLORIA (Geologic Long-Range Inclined Asdic) system (Somers et al., 1987). To obtain information for such a mosaic, the GLORIA system projects sound to as much as 22.5 km to each side of the ships track. The amplitude of sound returned varies as a function of bottom slope, bottom roughness, and bottom lithology, as well as geometric and depth factors. The data are processed to yield images that appear somewhat similar to aerial or satellite photographs.

In addition to GLORIA imagery more detailed images have been obtained in some areas using mid-range sidescan sonar systems, such as SeaMARC II. Another fairly new technology is swath bathymetry in which water depths at numerous points to each side of the ship are measured acoustically and the results are processed to yield a detailed, continuous bathymetric chart. Swath bathymetry using the SeaBeam system is systematically being obtained around the Hawaiian Islands. Older technologies such as high-resolution subbottom profiling, dredging, box and gravity coring, scuba diving, and bottom still and video photography have also been employed to investigate mass movement features off Hawaii.

Debris Avalanches

The most remarkable result of GLORIA mapping of the Hawaiian exclusive economic zone has been the discovery of slump and debris avalanche deposits that cover about 100,000 km^2, an area more than 5 times the land area of the islands. Some of the individual debris avalanche deposits are more than 200 km long and about 5000 km^3 in volume, making them among the largest on earth. The existence of a few of these giant landslides was speculated upon earlier (Moore, 1964) but was controversial and unproven until the GLORIA mosaic showed dramatically both that the deposits exist and that much of the seafloor around the islands is covered by them (Lipman et al., 1988, Moore et al., 1989, Normark et al., 1993).

The debris avalanche deposits can be recognized by their distinctive pattern on the sidescan imagery. The upper parts of the features are indicated by well-developed amphitheaters that, in the case of many of the landslides, are expressed subaerially by high coastal cliffs or palis. The mid-sections are broken into large blocks, the largest of which is the Tuscaloosa seamount northeast of Oahu, a feature that measures 30 km long by 17 km wide. The blocks are easily recognized on the mosaic

and range in size down to talus below the resolution of GLORIA (100 m). The distal aprons of the landslide deposits are shown by a distinctive hummocky terrain that may contain blocks up to 1 km across. The thickness of the deposits may range up to 2 km.

The Hawaiian Islands are surrounded by a topographic low called the Hawaiian Deep, a result of downwarping of the oceanic crust under the load of the islands. Some of the debris avalanches crossed the axis of the Hawaiian Deep and moved uphill a considerable distance on the other side. The best example of this behavior is the Nuuanu Debris Avalanche, which resulted from the disintegration of the northeast portion of the island of Oahu. The Nuuanu debris avalanche is about 230 km long, as measured from its headwall at the Nuuanu Pali on Oahu to its toe half way up the southwest flank of the Hawaiian Arch, the rise that lies beyond the Hawaiian Deep. After crossing the axis of the Hawaiian Deep, the avalanche moved uphill a distance of about 140 km from a depth of at least 4600 m in the deep to its terminus at about 4300 m on the arch. These geometric constraints show that the avalanches were truly catastrophic with landslide blocks attaining velocities of 100 m/s or more as they crossed the axis of the deep.

Differences between the longitudinal profiles of the landslides and those of their unfailed margins shows roughly the volumes of the deposits and their source areas. Comparing these profiles also shows roughly the maximum depth of failure within the source area. This latter comparison for two of the largest debris avalanches, the Nuuanu and Wailau, shows failure extending to somewhat more than 3000 m below present sea level. The failed debris then collapsed at least 1500 m into the Hawaiian Deep before riding up the other side.

The submerged scars of the landslides are incised by many submarine canyons, which appear to have initially been carved subaerially, before the islands subsided. In fact, submarine canyons in the vicinity of the Hawaiian Islands appear to be found almost exclusively in the scars of giant landslides.

The debris avalanches were almost certainly tsunamigenic, given their large volumes and high speeds. As one measure of the size of tsunami that can be produced, Moore and Moore (1988) identified a marine gravel at the 326 meter level on the island of Lanai. Evidence indicates that this gravel and similar deposits on nearby islands were emplaced by a giant wave generated by a submarine landslide south of Lanai. This 105,000 year old deposit may have resulted from the Alika Debris Avalanche, west of the island of Hawaii, which appears to be one of the youngest debris avalanches mapped by GLORIA.

By virtue of the fact that large parts of individual islands can catastrophically collapse into the sea and that 300-m-high sea waves can result, the Hawaiian debris avalanches are clearly a potential hazard both to the state of Hawaii and to the entire Pacific coast. Estimating their recurrence interval is then a critical factor in evaluating the extent of this hazard. According to Normark et al. (1993), the best control on debris avalanche recurrence interval is provided by volcano growth rates. The islands grow at 0.1 km^3 per year; hence, 10,000 years is required to produce the 1,000 km^3 of the average large debris avalanche. However, only about 10% of the island material ultimately becomes involved in debris avalanches. Accordingly, a

best estimate of the recurrence interval of the large debris avalanches is 100,000 years. Judging by the large size of this time period, these types of failure most likely do not present a serious hazard for the near future. A more serious hazard might be presented by smaller scale but more frequent landslide events.
Although the above discussion focuses on the Hawaiian Islands, similar giant debris avalanche deposits have also been found on the flanks of many other oceanic volcanoes (Holcomb and Searle, 1991).

Slumps

The GLORIA mosaic and other evidence also show the existence of giant mass movement features with strikingly different morphologies. These features, termed slumps, have a steep scarp at their toe, are cut by transverse faults into a few large blocks, and commonly lack a well-developed amphitheater at their head. At least one of these features, the Hilina Slump on the southeast flank of Kilauea Volcano on the island of Hawaii, is presently active, moves episodically, and generates earthquakes as it moves. The 1975, magnitude 7.2 earthquake was caused by movement of the Hilina Slump and resulted in subsidence of up to 3.5 m of a 60-km-long section of the island's coast. The hypocenter of the 1975 shock, and most aftershocks, were about 10 km deep, near the boundary between island volcanic rock and the prevolcanic seafloor. Moore et al. (1989) suggested that the sole of the landslide was likely contained within poorly consolidated volcanic rubble and pelagic sediment that had been emplaced directly on oceanic crust.
In addition to the Hilina slump, at least three other giant slumps are located off the Hawaiian Islands. Some of the features are associated with comparatively small debris avalanches that are spawned by the oversteepened fronts of the slump toes. The complete conversion of one of these giant slumps into a massive debris avalanche seems unlikely given the very deep (10 km) seated nature of the slumps relative to the comparatively shallow (1-2 km) debris avalanches. A catastrophic failure of the surface of the giant slump blocks, leading to a debris avalanche, is possible and could be generated by one of the earthquakes caused by the slump movement.

Volcaniclastic Flows on Flanks of Active Volcanoes

As hot lava enters the sea, it cools and fractures, yielding huge quantities of volcanic sand, which accumulates in beaches and nearshore deposits. New lava flows solidify atop these deposits forming lava deltas. During earthquakes or sometimes during aseismic periods, these lava deltas fail catastrophically, with major slippage occurring within the volcanic sands. Divers caught up in these failures of delta fronts (Tribble, 1991) report that much water is entrained, creating a strong downward current.
The GLORIA mosaic and recent SeaBeam bathymetry shows that a 40-km-long section of the upper 2500 m of the submerged flank of Kilauea volcano is extremely smooth in relation to other slopes off the Hawaiian Islands. Recent (1991) camera and coring work on this slope shows it to be completely covered with coarse, angular volcanic sand deposits whose surfaces are modified into current ripples suggestive of downslope water motion.

Analytic and Modelling Questions

These three varieties of volcanic islands landslides have only been identified in recent years. Much work remains to determine the details of their initiation and to model their motion and fate.

Perhaps most intriguing are the giant debris avalanches. If the estimates of recurrence interval are correct, the islands are stable with respect to these types of failure for up to 100,000 years. Then, some critical point is reached and a large part of an island disintegrates into huge blocks and other debris and the failed mass moves up to 200 km with enough momentum to slide upslope, under water, for up to 140 km. The parameters that describe this critical point have not been identified, although evidently the failures culminate near the end of subaerial shield building (Moore et al., 1989). An examination of the influence of island geometry on the overall downslope shear stress field might yield insight into the reasons that the largest failures occur at this point. Magnitudes of magma pressure in the primary rift zones of the active volcano are likely also important parameters, as evaluated in a preliminary sense by Iverson (in press). Pore water pressures are almost certainly not a major factor (Iverson, in press).

Once initiated, the debris avalanches are extremely rapid. Although no published models of their movement are available, any model would need to account for the high velocity and long moveout of giant blocks of rock moving through water. Enough is known about the source region, block size, path geometry, and deposit geometry to allow the beginning of such a modelling effort.

The giant slumps appear to move relatively small distances (a few meters) during an earthquake event and then remain still until the next event. Over a long time period such motion might appear almost continuous. Not well understood is the relation between this type of movement and that of debris avalanches that might be initiated at the toes of these slumps or within their surficial 1-2 km.

The lava delta failures are much smaller in scale than the other two types of landslides. However, they may be much more common and represent a more immediate hazard. Their motion and the relation of sand flow and water mass movement have not been modelled although considerable descriptive information is available. Also, the resulting sand deposits may be present at a number of locations deep within the volcanic islands. Perhaps these loose sands could serve as planes of weakness along which giant debris avalanches and slumps might develop.

References

Holcomb, R.T. and Searle, R.C., 1991. Large landslides from oceanic volcanoes, Marine Geotechnology, v. 10, p. 19-32.

Iverson, R.E., in press. Can magma-injection and groundwater forces cause massive landslides on Hawaiian volcanoes? Volcanology and Geothermal Processes.

Lipman, P.W., Normark, W.R., Moore, J.G., Wilson, J.B., and Gutmacher, C.E., 1988. The giant Alika debris slide, Mauna Loa, Hawaii, Jour. of Geophys. Res., v. 93, p. 4279-4299.

Moore, J.G., 2964. Giant submarine landslides on the Hawaiian Ridge. U.S. Geological Survey Professional paper 501-D, p. D95-D98.

Moore, J.G., Clague, D.A., Holcomb, R.T., Lipman, P.W., Normark, W.R., and Torresan, M.E., 1989. Prodigious submarine landslides on the Hawaiian Ridge, J. of Geophys. Res., vol. 94, p. 17465-17484.

Moore, J.G. and Moore, G.W., 1988. Deposit from a giant wave on the island of Lanai, Hawaii, Science, v. 226, p. 1312-1315.

Normark, W.R., Moore, J.G., and Torresan, M.E., 1993. Giant volcano-related landslides and the development of the Hawaiian Islands, U.S. Geological Survey Bulletin 2002, p. 184-196.

Somers, M.L., Carson, R.M., Revie, J.A., Edge, R.H., Barrow, B.J., and Andress, A.G., 1978. GLORIA II-an improved long range sidescan sonar, Proceedings, IEEE/IERE Subconference on Ocean Instruments and Communication, Oceanology International, London, B.P.S. Publications Limited, p. 16-24.

Tribble, G.W., 1991 Underwater observations of active lava flows from Kilauea volcano, Hawaii, Geology, v. 19, p. 633-636

Fra fjell til fjord : Considerations on viscous flows

Fra fjell til fjord : quelques considérations sur les écoulements visqueux

J. LOCAT

GREGI - Department of Geology and Geological Engineering
University Laval, Sainte-Foy, Québec - Canada, G1K 7P4
Tel. (1) 418 656 2193 - Fax (1) 418 656 2603

Abstract

This paper gives some considerations on physics and modelling of rapid mass movements. First, the viscoplastic approach which has been selected is presented. A short comparison between a previously developed model, SKRED, and a currently written one, LAVAL, is then discussed. The three components of the research work are listed : field, laboratory and numerical modelling. The "grey areas" are described. They concern the material rheological properties, the role played by ground water in the starting zone, the geometry of the failing mass and the mechanisms at work in the run out and terminal zones.

Résumé

Cet article présente quelques considérations sur les mécanismes physiques et la modélisation de mouvements en masse rapides. Tout d'abord, l'approche viscoplastique qui a été retenue est décrite. Une courte comparaison entre un modèle déjà écrit, SKRED, et un autre actuellement en développement, LAVAL, est détaillée. Les trois composantes du travail de recherche sont repris: le terrain, le laboratoire et la modélisation numérique. Les zones sur lesquelles les efforts doivent porter sont identifiées et précisées. Il s'agit des propriétés rhéologiques des matériaux, du rôle joué par l'eau du sous-sol, la géométrie de la masse mise en mouvement et les mécanismes à l'œuvre sur les zones de propagation et d'arrêt.

Introduction

A free translation of *Fra Fjell til Fjord* could sound like: from the high mountains to the deep waters. One could note that both Norwegian words *fjell* and *fjord* have the same root, i.e. starts with the same two letters may be suggesting that both words form a continuous medium. Moreover, it characterises the various environments into which we are actively looking at rapid mass movements: rock avalanches in the Rockies and in the Alps, debris flows in sensitive clays and submarine slides in the Saguenay Fjord. The Norwegian terms also underline that the onset of our research on the dynamics of mass movements resulted from a very fruitful collaboration with the

Norwegian Geotechnical Institute, and particularly with H. Norem who, in collaboration with P. Beghin, guided our initiation into this very interesting field.

The following discussion will be preceeded by an illustration of the type of mass movements that we are investigating (not described in this text) and then I will present some considerations on the physics and the modelling of these rapid mass movements. I hope that my presentation will underline the necessity for increase collaboration in this field where the terms "viscoplastic flows" clearly indicate the diversified approaches needed to study this sort of "continuum dynamics" (a way to paraphrase continuum mechanics !). I would also recommand the reading of report from a workshop held at Nainville les Roches (France) in 1991 which adressed the topic of large mass movements (see Antoine 1992; Durville 1992 for examples).

Physical approach selected

Many types of mass movements can occur which could be represented by various constitutive equations. We have opted for a viscoplastic approach as it can be applied to many types of mass movements who must still meet the following criteria: continuity, homogeneity and mass conservation. Moreover, it only applies to cases were the moving mass is always in contact with the flow surface and where friction generated heat has no influence on material properties and flow characteristics.

The constitutive equation that we have adopted is the following:

$$\tau = \tau_c + \sigma(1 - r_u) \tan \varphi + \rho m \left(\frac{dv}{dy}\right)^r + D \qquad (1)$$

where τ is the resistance to flow, τ_c the yield strength, σ the total stress, r_u the pore pressure ratio, φ the dynamic friction angle, ρ the density, m the dynamic viscosity relative to water, (dv/dy) the velocity gradient in the y direction, and D is the drag coefficient (to be considered only for submarine slides). The exponent "r" tends towards unity for macro viscous flows and towards 2 for inertia flows. The second term of [1] represents the plasticity and the other ones the viscous component. The effective stress component, which is part of the plasticity term, is included in the pore pressure ratio ($r_u = u/\gamma h$) where u is the pore pressure, γ the total specific weight of the soil mixture and h the flow height.

SKRED is the name of the numerical model initially developed by Irgens (1988) for snow avalanches and later adapted to analyse submarine slides (Norem *et al.* 1990) and rock avalanches (Locat *et al.* 1993). It is a finite difference pseudo 2D model (vertical velocity profile is assumed), does not take into account yield strength and pore pressure. The plasticity is assumed to be controlled by the apparent friction angle which is assumed constant during the flow.

A modified version of SKRED model has been worked on at University Laval (the reason for the name !) which uses a finite elements approach, takes into accounts

dynamic friction angle and pore pressure changes, yield strength and drag friction on the upper surface (Moutte *et al.* 1992; Locat 1992).

Our main objective is to develop a physical and a numerical model that will take into account viscoplastic flows with an explicit integration of the material properties and pore pressures in a pseudo 3D system (or even a full 3D). The pseudo 3D system will then have to assume the velocity profiles in all directions so that the flow path could have various shapes (*e.g.* Pandominium Creek avalanche; Evans *et al.* 1989). The physical model is actually been develop for applications in the study of submarine slides. If we succeed, then the model could be easily applied to subaerial flows were the friction in the upper part can be neglected.

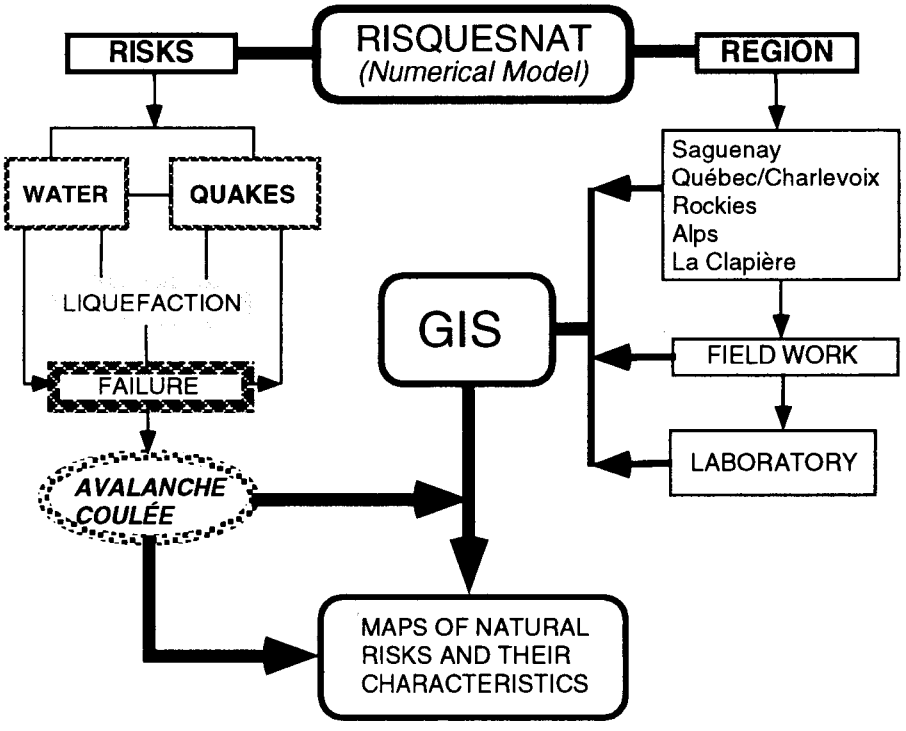

Figure 1. Overall integration of the numerical modelling work into risk mapping

Research approach

Our research is based on three components: field, laboratory and numerical. It may not look very original but I think that it is essential to have interaction between field, laboratory, and numerical analyses. As a first step, the field work is focus on the selection and study of sites well suited for numerical modelling so that the geology, morphological conditions before and after the slide, and structure can be

easily understood. Such sites are: La Clapière (France), Pandominium Creek Avalanche and Frank Slide (both in Canada), St.-Jean Vianney Slide and North Arm submarine slides (Québec, Canada). Other sites are being selected in collaboration with S. Evans (Canada) et G. Colas (France).

The laboratory program is mostly centered on measuring viscous flow properties so as to limit the amount of unknowns related to this component of the flow. So far, most of our research was devoted to macro viscous flows but we are in the process of building a large rheometre (like the one of Coussot 1992) which would be fully instrumented (pore pressures, density profiles, etc...).

The ultimate goal of this research project is to integrate the field surveys to regional data bases so that risk maps could be established which would take into account aerial extent of flows and other characteristics (Figure 1). This type of product would be used by government agencies, oil companies (offshore platform), and many consulting firms involved in environmental engineering.

Grey areas

In the course of developing a numerical model we have found some aspects that are still poorly understood or for which the mechanics is not clear. Follows some considerations on various aspects of the dynamic of mass movements: material properties; the starting zone, the run out zone and the terminal zone.

Material Properties

Material properties are mostly difficult to obtain for very coarse material (*e.g.* boulders). Recent work by Takahashi (1992) has shown the relevance of physical model testing of debris flows to investigate flow behaviour. Coussot (1993) has concentrated his efforts on material properties of debris flow materials. Most people agree to consider that the flowing material behave as a Bingham fluid but one could question whether or not velocity gradients in the field are coherent with a Bingham fluid. If the soils has a constant viscosity, then the velocity gradient in the flowing mass must be fairly linear and curved if it behaves as a Casson fluid. As for the dispersive pressure, we have little direct measurements and therefore a limited possibility for correlation with other elements of the flow.

When one tries to model flow behaviour he is not always equipped to evaluate the various parameters. Therefore, there is a need to produce overall relationships that would make possible the first approximation of material properties from index properties (*e.g.* Locat and Demers 1988, Locat 1992, and Figure 2).

To achieve this, we should encourage physical model experiments like those carried by Iverson (Vancouver, U.S.A.) and Takahashi in Japan. At Laval, we are planning to build a large rheometre similar to the one developed by Coussot (1992) but able to provide profiles of pore pressures and density (using acoustic profiling) and capable to carry tests at either constant height or constant total vertical stress.

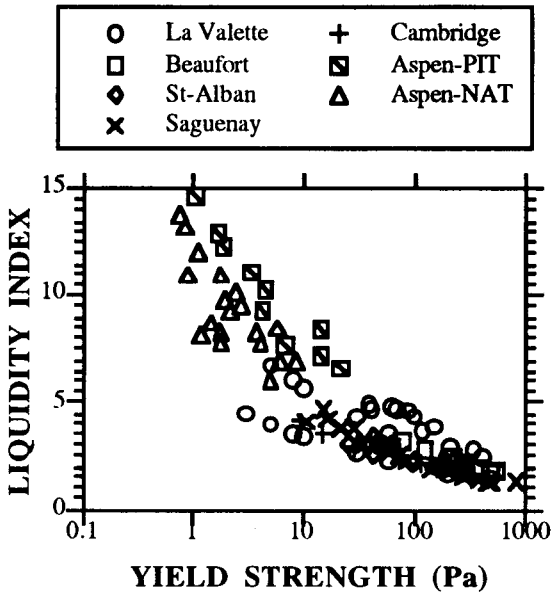

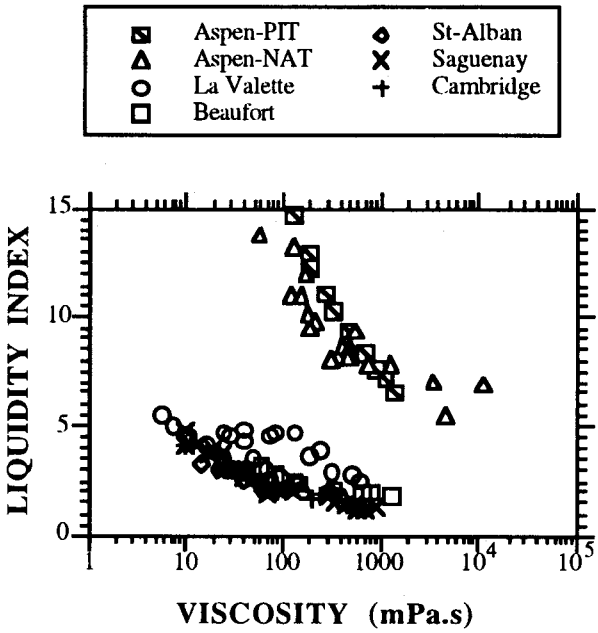

Figure 2. Correlations of viscosity and yield strength with liquidity index for some clayyey and silty material (Locat 1992).

The Starting Zone

One of the major unknown in the case of rapid mass movements, as for the case of non-rapid movements, is the ground water. There are only very few cases were ground water conditions at the time of failure are well known so as to be able to postulate the initial conditions. This information is crucial in the case of "wet" mass movements. If, for example, we look at the case of La Clapière, it is very difficult to make sound hypothesis on the pore pressure conditions within the failing mass. No water seepage is apparent on the slope face but a clear connection has been established between movements of the failing mass and stream discharge fluctuations (Gervreau 1991).

There is a need to address more clearly the nature of ground water flow in large mountains even if this is often very complicated in the sector were failure is taking place (Antoine 1992). It is important to know whether or not the failing mass has to be considered "wet" or "dry".

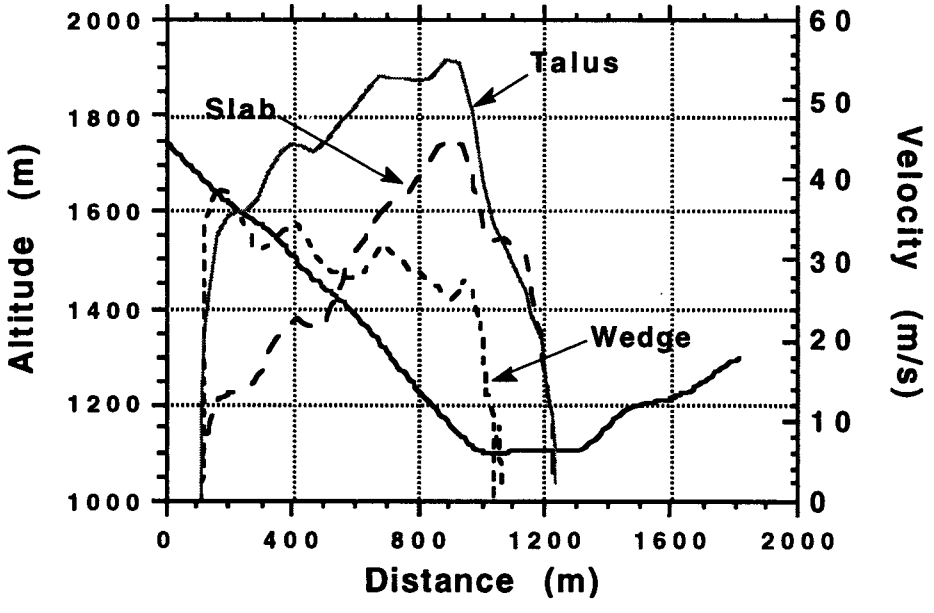

Figure 3. Effect of failing mass geometry on frontal velocity, simulated at La Clapière.

In using SKRED to analyse some aspects of La Clapière Slide, we tried to evaluate the effect of the shape of the failing mass in the starting zone on the flow behaviour by looking at three types of morphology: slab, wedge and talus (Locat *et al.* 1993). It was very interesting to found that both the velocity profile, run out distance and average flow depth were greatly affected by the shape of the failing mass in the

starting zone (Figures 3 and 4). It indicates the great importance of knowing as precisely as possible the site conditions just prior to the slide if one wishes to properly ascertain the flow dynamics. This is also a good example of the potential use of numerical models for parametric studies.

Other considerations about the starting zone that can be mentioned are:

- how do develop velocity vectors in a mass that evolves from stability to instability and then to flow.
- how does the grain size (or block size) initially evolves during the onset of the flow.

The Run Out Zone

In the run out zone the pore pressure also plays a great role in influencing the mobility of viscoplastic flows. In the case of rapid macro viscous flow, it can be understood that the evolution of pore pressure is not very important as the dissipation mechanism would take much more time then the flow event itself. However, as for the case of slow macro viscous flows and for inertia flows, pore pressure changes during flow are critical.

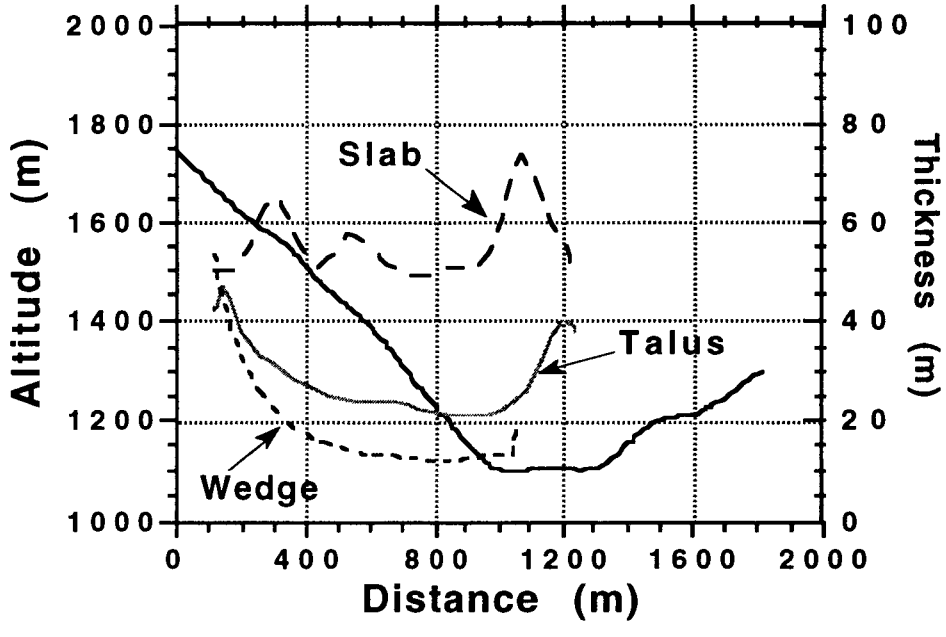

Figure 4. Effect of failing mass geometry on average flow depth, as tested at La Clapière.

Hutchinson (1986) has proposed a sliding consolidation model which mostly considers the dissipation of pore pressure and the resulting increase in shear strength

of the mass as the mechanism controlling the flow. In a sense, it assumes the movement is that of a plug flow without considerations of shear in the flow and the resulting development of a velocity profile. Sassa (1988) on the other hand have shown that pore pressure could develop during the flow as a result of shearing. These two mechanisms could play an important role in a debris flow were a plug could exist in the upper part. But what could be the relative importance of these to phenomena is not clear yet. This is a critical point as in many numerical models where the plasticity term is taken as an apparent friction angle considered constant during the flow (as it is for SKRED) thus considering a constant pore pressure. In the case of the LAVAL model, being developed, we have formulated explicit values for the friction angle and included the pore pressure ratio which, at this time, is assume to decay with time (Figure 5) according more or less to the coefficient of volumetric compressibility (c_v). This aspect of flow mechanism will required much more laboratory work in the future.

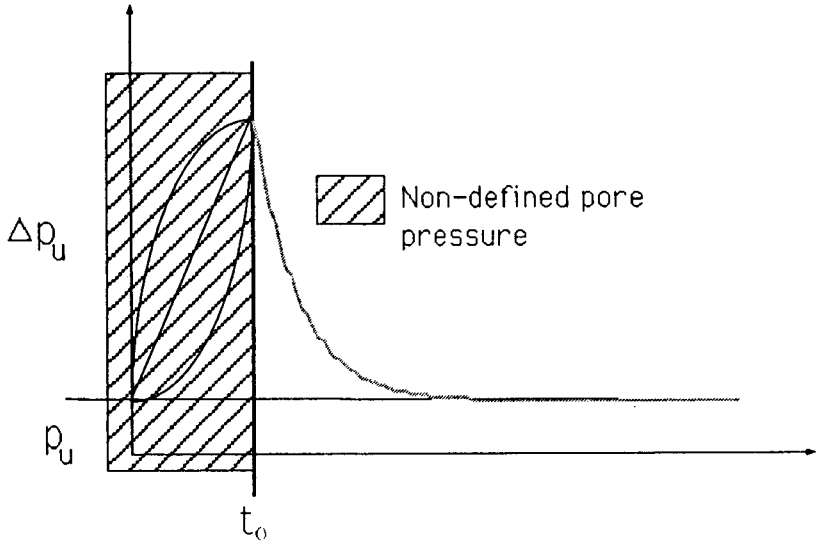

Figure 5. Pore pressure dissipation from time initiation of flow (Moutte *et al.* 1992)

For the case of submarine slides, one has to take into account the shear stresses in the upper part of the flow. We normally should be looking at all stresses operating on the upper surface in a manner similar to that proposed by Schlichting (1958). So far, we have decided to take this into account by working on the velocity profile (Figure 6) so as to add an arbitrary parameter that would "bend" the velocity profile to simulate the friction effect on the upper surface. This resistance to flow shall be included in the term "D" of equation [1]. This will be very important in the study of the generation of turbidity current from a submarine debris flow.

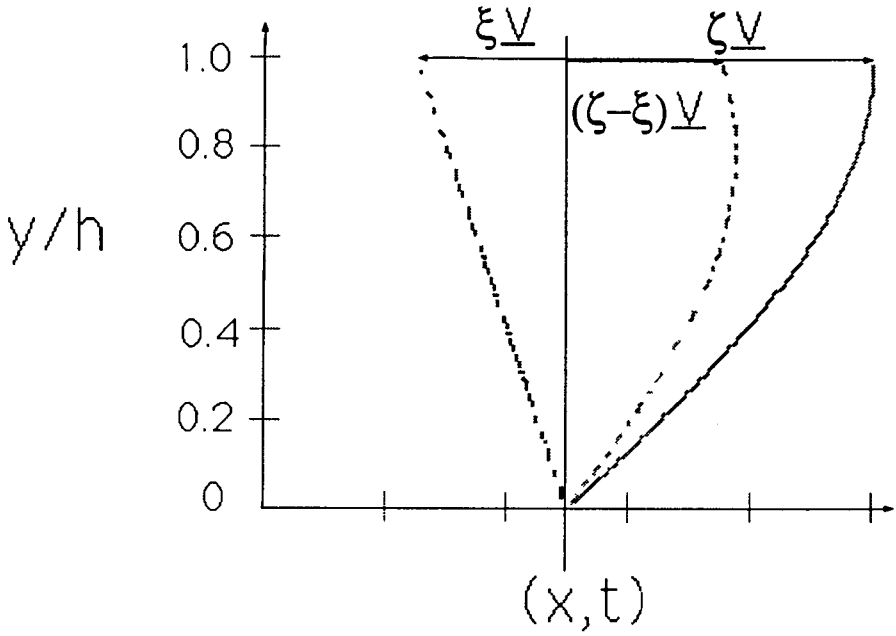

Figure 6. Velocity profile correction to take into account friction on the upper surface (from Moutte *et al.* 1992)

The Terminal Zone

The terminal zone is the most well known part of the process of rapid mass movements. With the event of 2D numerical models this morphological information becomes a crucial component to test the validity of the models. On the other hand, since our models so far assumes conservation of mass, there could be cases were the back analysis of the terminal zone could not be adequately performed.

Conclusion

The above discussion has underlined some aspects of the research that need particular attention. A common denominator to all this is that the field of mass movement dynamics is so diversified that it is almost impossible to work all the various aspects of the problem alone. Any strategy to investigate these phenomena will require to look at the geology, the geomorphology, soil and rock mechanics, hydraulics and physics. Our actual modelling tools are far more simple than the actual phenomena that we are studying. For example, we have not yet been able to take into account erosion and deposition of material, non conservation of mass, inhomogeneous materials and internal computation of the velocity of each element. There is still a lot to be done.

As the need to produce risk maps to reduce loss of life and property intensifies, I think that we should take the opportunity of the International Decade for Natural

Disaster Reduction (IDNDR) to initiate co-operative research projects were efforts could be maximised.

Acknowledgements

I would like to thank those from whom, over the last few years, I benefited of their comments and generous advises, namely: H. Norem, S. Evans, O. Hungr, G. Colas, P. Beghin and G. Brugnot. I would also like to thank the National Science and Engineering Research Council of Canada for supporting this research and particularly the work of R. Couture and S. Gharbi, graduate students at Laval.

References

Antoine, P., 1992. Les problèmes causés par l'instabilité des versants de grande ampleur: aspects géologiques. IAEG Bulletin, 45:9-24.

Evans, S.G., Clague, J.J. Woodsworth, G.J., and Hungr, O., 1989. The Pandominium Creek rock avalanche, British Columbia. Canadian Geotechnical Journal, 26: 427-446.

Coussot, P., 1992. Rhéologie des laves torrentielles: étude des dispersions et suspensions concentrées. Thèse de doctorat, Institut National de Polytechnique de Grenoble; Études du Cemagref, série Montagne No. 5, 415 p.

Durville, J.-L., 1992. Mécanismes et modèles de comportement des grands mouvements de versants. IAEG Bulletin, 45: 25-42.

Gervreau, E., 1991. Étude de l'évolution des versants naturels en mouvement: prévoir, alerter.Thèse, Paris, 244 p.

Hutchinson, J.N., 1986. A sliding consolidation model for flow slides. Canadian Geotechnical Journal, 23: 115-126.

Irgens, F., 1988. A continuum model of granular media and simulation of snow avalanche flow in run-out zones. Presented at the 17th ICTAM, Grenoble.

Locat, J., 1992. Viscosity, yield strength, and mudflow mobility for sensitive clays and other fine sediments. Proceedings of Geotechnique and Natural Hazards, Vancouver, pp.: 389-396.

Locat, J., and Demers, D., 1988. Viscosity, yield stress, remolded shear strength, and liquidity index relationships for sensitive clays. Canadian Geotechnical Journal, 27: 799-806.

Locat, J., Norem, H., and Therrien, P., 1993. An approach to rock avalanche dynamics. Presented at the 1990 symposium of Mass Movements in the Canadian Rockies (Vancouver 1990), modified and submitted to the Canadian Geotechnical Journal.

Moutte, F., Locat, J., and Therrien, P., 1992. Numerical modelling of physical aspects of submarine debris flows. Proceedings of Geotechnique and Natural Hazards, Vancouver, pp.: 381-388.

Norem, H., Locat, J., and Schieldrop, B., 1990. An approach to the physics and modelling of submarine flowslides. Marine Geotechnology, 9: 93-111.

Sassa, K., 1988. Geotechnical models for the motion of landslides. In Proceedings of the 5th International Symposium on Landslides, Lausanne, C. Bonnard, ed., vol. 1, pp.: 37-56.

Schlichting, H., 1958. Boundary layer theory. New York, Mc Graw Hill, 523 p.
Takahashi, T., 1992. Debris flows. IAHR Monograph, Balkema, 165 p.

Rheological Characteristics of Snow Flows

Caractéristiques rhéologiques des écoulements de neige

N. MAENO

Institute of Low Temperature Science, Hokkaido University
Sapporo 060 - Japan
Fax (81) 11 716 5698

Abstract

Rheological characteristics of snow flows were discussed in special reference to the friction and viscosity of snow. The general constitutive relation of snow flow or fluidized snow is described by three components; first component is a velocity independent friction term characterized by a dry friction coefficient of snow μ_s, which increases with rising temperature mainly due to adhesion. The second component is a viscosity term increasing linearly with velocity or shear rate. Ranges of viscosity coefficient and kinematic viscosity were found 10^{-4}-1 Ns/m^2 and 10^{-6}-10^{-3} m^2/s respectively depending on the degree of fluidization and density of snow. The third component is a turbulent and snow plowing term increasing with the square of shear rate, which becomes predominant at velocities roughly above 15 m/s. Based on the estimated small friction coefficients in natural large-scale avalanches a regime of Mohr-Coulomb relation with smaller μ_s was suggested to exist at larger normal stresses than about 10 kPa.

Résumé

Les caractéristiques rhéologiques des écoulements de neige sont analysées en insistant particulièrement sur le frottement et la viscosité de la neige. La loi de comportement d'un écoulement de neige ou de la neige fluidisée comprend trois termes.
Le premier est un terme de frottement indépendant de la vitesse qui est caractérisée par le coefficient de frottement solide de la neige. Il augmente avec la température à cause de phénomènes d'adhésion. Le second terme est le terme de viscosité qui augmente de façon linéaire avec la vitesse ou avec le taux de cisaillement. Les domaines des valeurs possibles pour le coefficient de viscosité et pour la viscosité cinématique s'étendent respectivement entre 10 et 1 et entre 10 et 10 m2/s. Ils dépendent du degré de fluidisation et de la densité de la neige. Le troisième terme est un terme qui correspond à la turbulence et à l'entraînement. Il augmente avec le carré du taux de cisaillement et devient prépondérant au-delà de 15 m/s. On suggère un régime avec une relation de Mohn-Coulomb avec une valeur du coefficient plus faible pour les cas où la contrainte normale dépasse 10 kPa. Cette solution est fondée sur les faibles valeurs de coefficient de frottement observées dans des avalanches naturelles de grande ampleur.

Introduction

Main resistance forces to suppress snow avalanche motion originate from friction at the base, air drag at the front and sides, entertainment of air and snow, and viscous forces at the base and in the interior of the avalanche. Among the above four kinds of forces, the friction and viscosity are most important and fundamental because they continue to produce effects just after the initiation of motion and roughly determine the scale and magnitude of avalanches. In this paper our rheological interest is focused on the friction and viscosity characteristics of snow.

A typical slab snow avalanche just set in motion is considered as a sliding snow cover with a finite dimension along a specific slide plane. As the increase in the sliding speed it disintegrates into several blocks, and finally becomes a continuous flow composed of various sizes of snow blocks and particles, which may be adequately called a mixed-phase snow flow or fluidized snow. Accordingly the initial interaction between the avalanche and slide plane is the friction of snow block and then that of fluidized snow, or viscosity.

It has been known, however, that even at small speeds just after the initiation of motion the bonding structure of snow in the bottom region of snow slab is continuously broken and the friction or viscous interaction of fluidized snow is essential. Even in a laboratory-scale experiment of snow block sliding the pulverization and fluidization can be easily observed. With the sliding speed the degree of pulverization and fluidization increases and the friction and viscosity of fluidized snow becomes more important.

Friction coefficient of a snow avalanche (μ_a)

The friction coefficient of a snow avalanche, μa, can be defined as the ratio of the tangential and normal components of the force acting on the avalanche bottom without regards to the physical structure and mechanism acting in the avalanche interior. Reported values of μ_a are summarized in the following (Fig. 1):

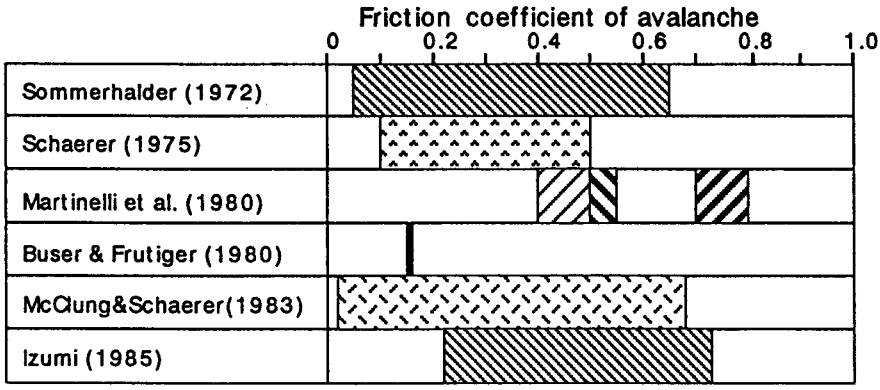

Fig. 1 Variously estimated friction coefficients of avalanches (μ_a).

(1) μ_a of natural snow avalanches was estimated by Sommerhalder (1972), who measured shear (τ) and normal (σ) stresses caused by avalanches flowing over snowsheds in the Swiss Alps by installing mechanical devices over the breadth of gallery roofs. From maximum values recorded in several winters, μ_a was computed as τ/σ, ranging from 0.05 to 0.65 with a mean of 0.27 for the breadth of the gallery. It should be noted that a value as small as 0.05 has been measured.

(2) μ_a can also be estimated as the ratio of the total height difference and horizontal running distance, that is the total length of the running distance projected on a horizontal plane. The physical meaning of the friction coefficient thus calculated is that all the potential energy of an avalanche of a finite mass is dissipated by friction at the bottom. Izumi (1985) analyzed 17 avalanches, which took place in Japan, and obtained μ_a = 0.22 - 0.73. The mean of μ_a for avalanches with smaller volumes than about 10^4 m^3 is about 0.63, but it decreased with the increase in the avalanche volume for larger avalanches, that is the friction resistance for avalanches decreases resulting in the increase in the running distance. Such large-scale avalanches are mostly dry snow avalanches.

(3) μ_a can be computed from movie films of running avalanches. In the case an equation for the avalanche motion must be assumed to get a friction coefficient by fitting measured velocity data. Schaerer (1975) applied the well known Voellmy's equation, which includes two parameters, friction and turbulent coefficients, to many avalanches observed on slopes 10 to 25 degrees and obtained the following relation,

$$\mu_a = 5/u \qquad (1)$$

where u is the speed in m/s. As the equation was obtained in a speed range from 10 to 50 m/s, the range of the friction coefficients observed is 0.1 - 0.5.
Martinelli et al. (1980) used a two-dimensional finite-difference computer program based on the Navier-Stokes equations to determine two parameters involved. Obtained values of μ_a are 0.5 - 0.55 for midwinter dry snow, 0.7 - 0.8 for hard slab, and 0.4 - 0.5 for fresh soft slab. They report that though Eq. (1) could give satisfactory results when the Voellmy's equation is used, friction coefficient values of 0.15 or lower are needed to duplicate some of field data.
McClung and Schaerer (1983) used a center-of-mass equation developed by Perla et al. (1983), which, just like the Voellmy's equation, contains two parameters, one related to the bottom friction and the other to turbulent friction and mass, and analyzed data by breaking running paths into several segments. Obtained values of μ_a ranged from 0.02 to 0.68, but they write that many of the values of μ_a are very high. The arithmetic mean of the thirty data given in their paper is 0.41.

(4) Buser and Frutiger (1980) selected ten avalanches with extremely long run-out distances from past Swiss avalanche records. They used a modified Voellmy's equation, and gave μ_a = 0.155 - 0.157. Based on the result they recommended in calculations of avalanche zoning to use a friction coefficient as small as 0.16 for extreme flowing avalanches such as newly fallen snow and soft slabs.

The above results as summarized in Fig. 1 show that μ_a ranges from 0.02 to 0.8, depending on snow type, temperature, velocity, method of estimate, and so on. Larger values of μ_a above about 0.5 should be attributed to the turbulent and snow ploughing resistance as discussed in the next sections, and cannot be regarded as a Newtonian friction in a strict physical sense. An important point is that μ_a as small as 0.02 was found for natural avalanches which are usually large-scale with long running distances.

Friction coefficient of snow (μ_s)

A number of measurements have been carried out on friction coefficients of snow as summarized in Lang and Dent (1982) and Colbeck (1992). However most of them were made on friction between snow and other materials including ski, roofs, and other structures. The friction between snow and snow was only measured by Inaho (1941), Bucher and Roch (1946), Japan National Railways (1961), and Casassa et al. (1989, 1991). They obtained the friction coefficient of snow by measuring the force acting on a snow block sliding on a snow surface.

Inaho (1941) allowed blocks of granular snow to slide at speeds up to 4 m/s over a slope covered with similar snow at temperatures near 0°C. He showed that the friction coefficient of snow (μ_s) can be expressed as

$$\mu_s = \mu_c + aS/W \qquad (2)$$

where μ_c is the Coulomb friction coefficient, a is the adhesion coefficient (adhesion force per unit contact area), S and W are respectively the surface contact area and normal force acting on the surface. Measured values of μ_s ranged from 0.45 to 0.65, from which μ_c was estimated as 0.42 - 0.62 and a as 12 - 85 Pa.

Bucher and Roch (1946) pulled wet granular snow blocks over a similar snow surface at speeds 0.2 to 0.85 m/s, and obtained values of μ_s as 0.23-0.85 (mean 0.47).

Similar μ_s measurements to Inaho's were conducted by Japan National Railways (1961) and Casassa et al. (1989). Japan National Railways obtained mean values of μ_s of 0.71 for compact snow and 0.69 for granular snow at speeds up to 20 m/s. In the snow block sliding measurement at speeds from 1.4 to 7.0 m/s and temperatures from -2 to -10°C, Casassa et al. obtained μ_s ranging from 0.57 to 0.86 for snow of density 100

to 340 kg/m^3, which gave the mean Coulomb friction coefficient μ_c = 0.62 and adhesion coefficient a = 20 Pa.

All the above measurements were conducted in natural snow fields, so that enough accuracy could not be attained in controlling the measurement condition such as snow types, temperatures, sliding velocities and so on. We have carried out a laboratory investigation to obtain the friction coefficient of snow as a function of snow type, temperature, sliding velocity and applied load; details of the measurement are given in Casassa et al. (1991). We give here the new result of reanalyses and consideration. The friction coefficient of snow was obtained by measuring a steady-state torque exerted to a fixed annular snow plate (120 and 180 mm in inner and outer diameters respectively and 20 mm in thickness) when its surface is in contact with that of another similar rotating annular snow plate.

Fig. 2 gives one of the typical results, which shows the measured apparent or total friction coefficient (μ_t) of snow (density 390 kg/m^3), that is the measured torque force divided by normal load applied, plotted against the velocity. It was shown that μ_t could be described by a parabolic function in the velocity range studied (0 - 25 m/s):

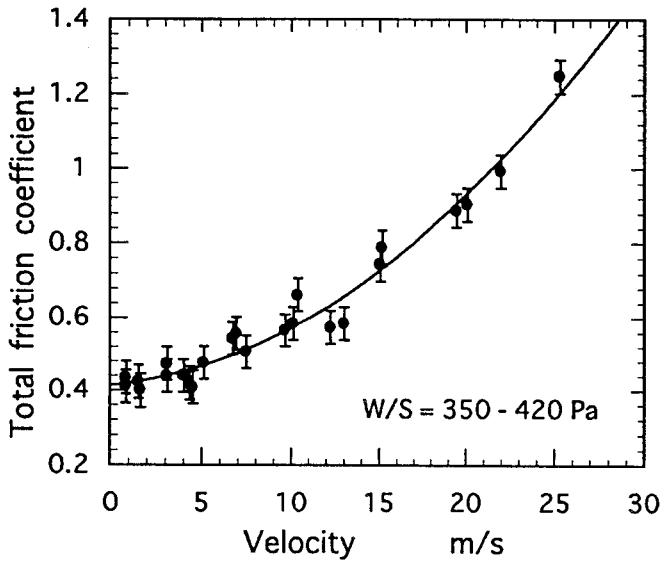

Fig. 2 Total friction coefficient (μ_t) of snow (density 333 kg/m^3) plotted against velocity. Temperature is -10 °C and normal pressure applied is 350 - 420 kPa.

$$\mu_t = \mu_s + Bu + Cu^2 \qquad (3)$$

where μ_s is the friction coefficient of snow, or dry friction term independent of velocity, and B and C are constants. The terms Bu and Cu^2 are related respectively to

viscosity and turbulence (ploughing) of snow as discussed later, and the latter becomes predominant at velocities larger than about 15 m/s.
Values of μ_t measured at velocities lower than 10 m/s are given in Fig. 3 as a function of velocity and temperature (snow density is 333 kg/m^3). Linear relations correspond to the first two terms in Eq. (3). Values of μ_s are estimated by linear extrapolation to zero velocity and plotted in Fig. 4. The relation between μ_s and temperature (θ in °C) is as follows:

$$\mu_s = 0.47 + 0.01\theta \tag{4}$$

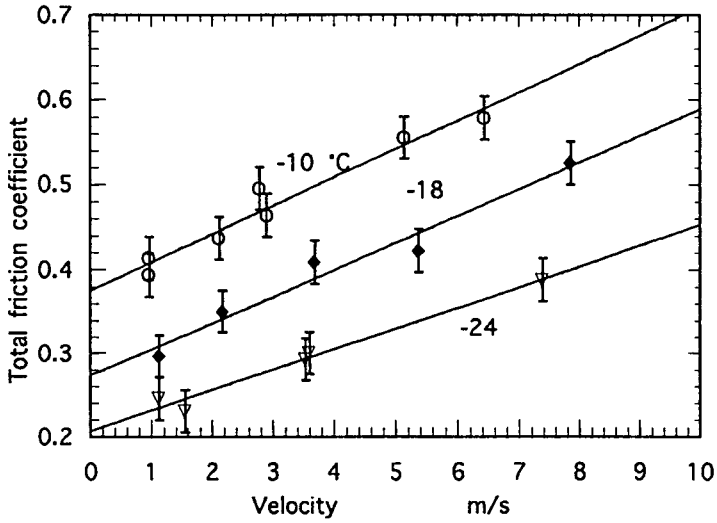

Fig. 3 Total friction coefficient (μ_t) of snow (density 333 kg/m^3) at velocities below 10 m/s. Temperature is -10, -18, and -24 °C and normal pressure applied is 300 - 400 kPa.

The strong dependence of μ_s on temperature is mainly attributable to adhesion and characteristic of the unique friction property of snow at lower velocities.
The above measurement was conducted by applying normal stresses of 300-400 Pa. Fig. 5 shows an example of the relation between the measured shear stress (τ) and applied normal stress (σ) in a velocity range 3.5-6.5 m/s. At each temperature the following Mohr-Coulomb relation is satisfied:

$$\tau = \mu\sigma + F \tag{5}$$

where μ is the internal friction coefficient (=tanϕ, ϕ: friction angle) and F is a constant related to adhesion. Strictly speaking μ should be μ_c but is roughly equal to μ_s in this case. F values are small, a few tens Pa, and included in experimental errors

in Fig. 5. It should be noted that Eq. (5) is identical to Eq. (2) if it is rewritten as $\mu_s W/S = \mu_c W/S + a$.

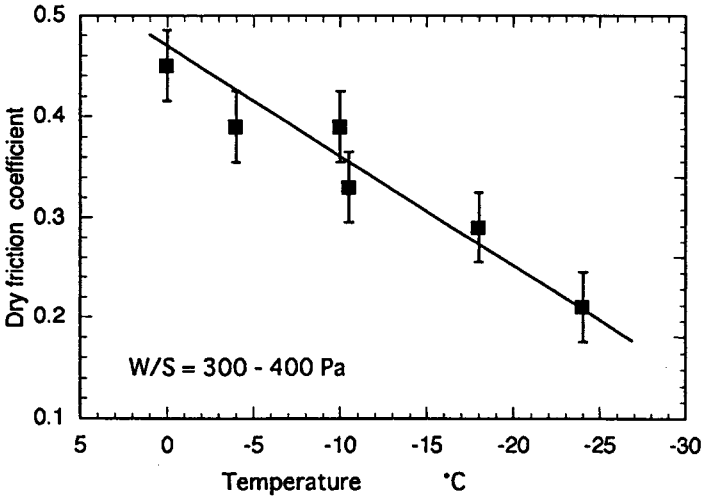

Fig. 4 Fiction coefficient of snow (μ_s), or dry friction coefficient plotted against temperature. Normal pressure applied is 300 - 400 Pa.

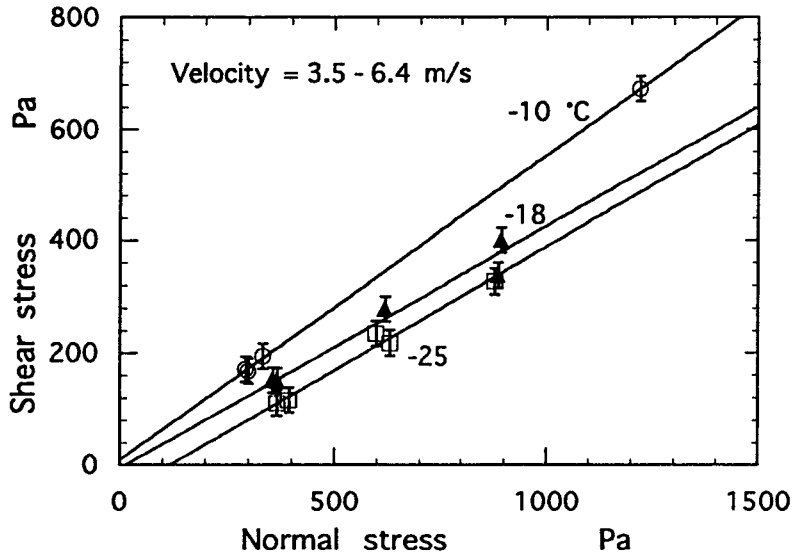

Fig. 5 Shear stress plotted against normal stress at temperatures -10, -18 and -25 °C. Snow density and velocity are 333 kg/m^3 and 3.5 - 6.4 m/s respectively.

Viscosity coefficient of fluidized snow (η)

It was noted in Fig. 3 that the total friction coefficient increases linearly with velocity, which implies the contribution of viscosity due to fluidized snow produced in the friction layer. The viscosity coefficient of fluidized snow, η, can be estimated from slopes of straight lines in Fig. 3 because B in Eq.(3) can be written as

$$B = \eta S / \delta \tag{6}$$

where S and δ are the area and thickness of fluidized snow respectively. As δ was estimated as about 2 mm, if the density of the fluidized layer is assumed to be that of original snow (333 kg/m^3), the three lines give η=(3.85-5.71)x10^{-3} Ns/m^2 at temperatures -10 to -24 °C, which corresponds to the kinematic viscosity $\nu = \eta/\rho$ =(1.58-1.71)x10^{-5} m^2/s. The values of η and ν are plotted against temperature in Fig. 6 together with similar results obtained for snow of density 390 kg/m^3. Constant values of η and ν in the temperature range are reasonable because temperature dependent adhesive properties of ice are only expected to contribute to the first friction term in Eq. (3).

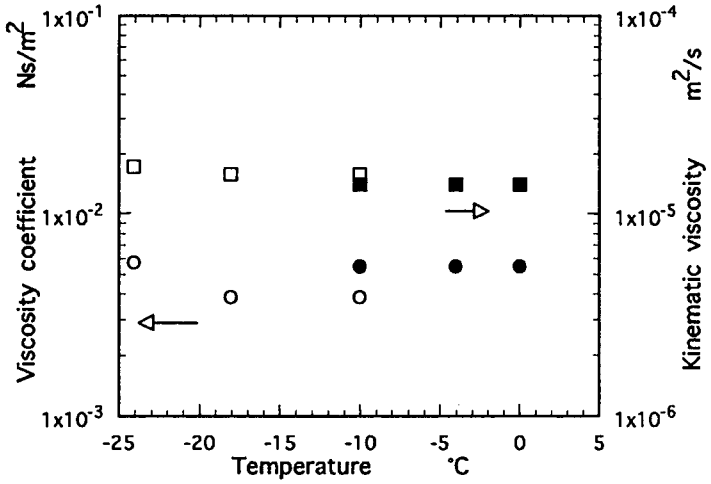

Fig. 6 Viscosity coefficient (η, circles) and kinematic viscosity (ν, squares) of fluidized snow plotted against temperature. Open and solid symbols refer to snow of density 333 and 390 kg/m^3 respectively.

More precise estimate of viscosity coefficients can be made by measuring directly shear or torque forces caused by viscous motion of fluidized snow (Maeno and Nishimura, 1979; Maeno et al., 1980). A recent result by Nishimura (1990) is shown in Fig. 7, which gives viscosity coefficients of fluidized snow (mean particle diameter 0.59 mm) measured by use of two kinds of rotation viscometer. Although data are much scattered an exponential increase of η with density is clear:

$$\eta = 1.62\text{x}10^{-6}\exp(0.0255\rho) \tag{7}$$

Were the units of η and ρ are Ns/m^2 and kg/m^3 respectively. The result roughly agrees with that obtained in the friction experiment shown in Fig. 6 (solid dots in Fig. 7). It should be noted, however, that the shear rate is much different in the two measurements; about 1-10 s^{-1} in the rotation viscometer measurement and roughly 200-2000 s^{-1} in the friction measurement.
Nishimura (1990) showed that apparent viscosity coefficients obtained by applying a Bingham model to observed vertical velocity profiles in a chute flow experiment of snow are erroneous because shear stress exerted on the flow bottom was measured to increase with the square of shear rate; the rheological characteristics should be described by non-Newtonian models including the third square term in Eq. (3). The same reasoning applies to the apparently large values of μ_a estimated for natural avalanches summarized in Fig. 1.

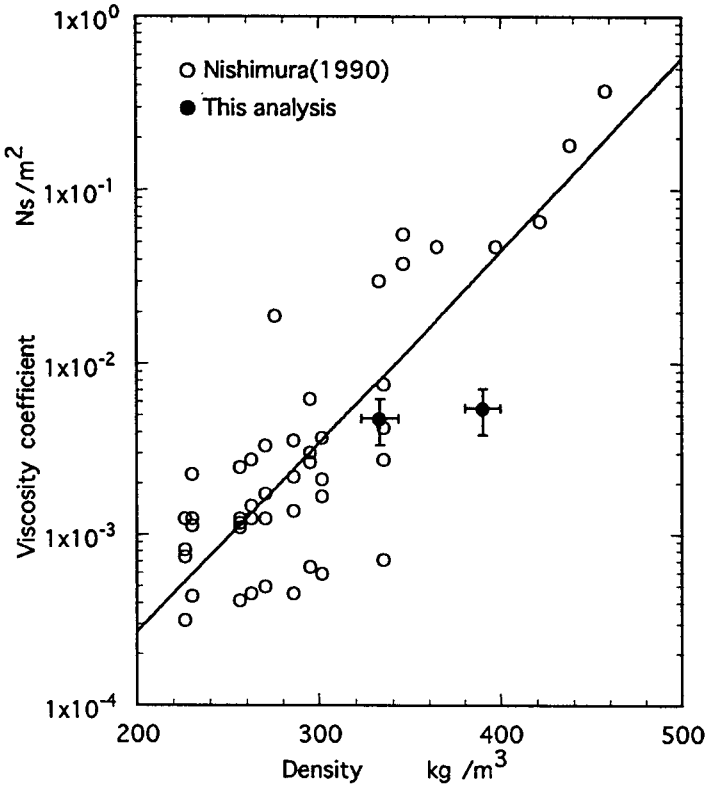

Fig. 7 Viscosity coefficient of fluidized snow (η) plotted against density measured by Nishimura (1990). Two solid dots give viscosity coefficients estimated in the present paper.

Discussions and conclusions

As shown above the snow friction coefficient decreases sharply with lowering temperature, but this cannot explain the small friction coefficient 0.02-0.2 as estimated for natural large-scale avalanches. Furthermore while smaller friction coefficients are usually expected for hard snow in laboratory and field experiments, these small values have been often obtained for soft new snow or powder snow avalanches.

At present we do not have a clear answer to the above contradiction appearing in the magnitude of friction coefficients estimated in snow experiments and avalanche observations. But the following consideration leads to a significant hypothesis about friction at larger normal stresses. It was shown that with increase in the scale of a snow avalanche its fluidity increases and friction coefficient decreases, which would be closely related to the complex phenomena of pulverization and fluidization of snow taking place at the avalanche bottom. The effective pressure at the bottom of a natural avalanche has never been measured, but if it is approximated as ρgh where ρ and h are the density and height of the avalanche and g is the acceleration of gravity, it is roughly 20-400 kPa when ρ is 200-400 kg/m^3 and h is 10-100 m, which is by 20 to 2000 times larger than that in our snow experiment.

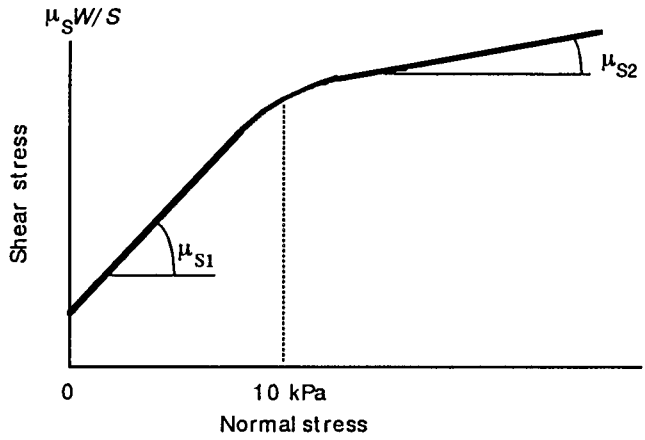

Fig. 8 Schematic relation between shear stress and normal stress in a wide range of stresses.

Then a possibility of the existence of a smaller friction regime at higher stresses is suggested; Fig. 8 gives a hypothetical example which shows two friction regimes divided by a critical normal stress around 10 kPa; in each regime the Mohr-Coulomb relation, Eqs. 2 and 5, with a pair of μs and a is satisfied. The existence of such multi-friction-regimes should be examined by snow experiments in future.

Acknowledgments

The author would like to express his sincere thanks to Drs. H. Narita and K. Nishimura of the Institute of Low Temperature Science, Hokkaido University and Dr. G. Casassa of Ohio State University for their contribution in the friction and viscosity experiments. The study was supported in part by the special fund for Scientific Research of the Ministry of Education, Science and Culture, Japan.

References

Buser, O. and H. Frutiger (1980) J. Glaciology, 26(94), 121-130.
Casassa, G., H. Narita and N. Maeno (1991) J. Appl. Phys., 69(6), 3745-3756.
Colbeck, S.C (1992) U.S. Army CRREL Monograph, 92-2, 1-40.
Inaho, Y. (1941) Seppyo, 3, 303-307 (in Japanese).
Izumi, K. (1985) Ann. Rep. Saigai-ken, Niigata Univ., 7, 187-194 (in Japanese).
Lang, T.E. and J.D. Dent (1982) Rev. Geophys. Space Phys., 20(1), 21-37.
Maeno, N. and K. Nishimura (1979) Cold Regions Sci. Tech., 1, 109-120.
Maeno, N., K. Nishimura and Y. Kaneda (1980) J. Glaciology, 26(94), 263-274.
Martinelli, M., T.E.Lang and A.I.Mears (1980) J. Glaciology, 26(94), 109-119.
McClung, D.M. and P.A.Schaerer (1983) Annals of Glaciology, 4, 170-173.
Nishimura, K. (1990) Contr. Inst. Low Temp. Sci., A37, 1-55.
Perla, R., T.T.Chen and D.M.McClung (1980) J. Glaciology, 26(94), 197-207.
Schaerer, P. (1975) IAHS-AISH Publ., 114, 425-432.
Sommerhalder, E. (1972) Genssenschaft der Bundnerischen Holzproduzentan, 9, 155-169 (in German).

Snow Avalanches : Classification and modelisation

Avalanches de neige : classification et modélisation

O. MARCO

Cemagref / Division Nivologie
BP 76, 38402 Saint-Martin d'Hères - France
Tel. (33) 76 76 27 93 - Fax (33) 76 51 38 03

Abstract

After a reminder of the International Avalanche Classification, this paper presents different kinds of avalanche flow models. If there is a consensus on physic explanations for the dynamic of powder snow avalanches among laboratories, it is not the case for dense avalanches. Experimental field data are still lacking. Presently, the most reliable models are finally the simplest ones, referred to as empirical models. With their frequent use by practitioners, their different parameters are statistically analysed.

Résumé

Après un rappel de la Classification Internationale des Avalanches, cet article présente les différents modèles d'écoulements avalancheux. Si l'explication physique des avalanches aérosols trouve aujourd'hui un consensus entre les laboratoires étudiant ces phénomènes, il n'en est pas de même des écoulements denses. Les données expérimentales de terrain manquent et les modèles les plus fiables sont finalement les plus simples, qualifiés d'empiriques. Grâce à leur utilisation fréquente par les praticiens, ils bénéficient, de fait, d'une analyse statistique de leurs différents paramètres.

Introduction

Snow avalanche is a natural phenomenon which groups a large number of different flows. Each kind has a usual name. But it may be not the same for every one, mountain people, engineers or scientists for example. Or, information from observations must be exchanged. It is essential that every one uses the same classification. So, we are going to recall the basic rules of the international avalanche classification [1]

Snow avalanche is also a natural hazard we must fight. To do it, several ways exist. One of them is understanding the avalanche mechanics and establishing a physical model. But the phenomenon is so complex that it doesn't exist, today, a model accepted by every-one. We will list the main ones and will try to indicate their limits.

Avalanche classification

The international classification [1] has two basic subclassifications. One is based on direct avalanche observation : It is the morphological classification. The other one is focused on processes which induce avalanche situations : It is the genetic classification.

The morphological classification is mostly used when we rather study the motion of an avalanche than its forecasting. It is concentrated on the avalanching snow, its properties and its appearance. It also includes the morphology of movement.

Avalanches are classified according to criteria to be encountered in the zone of origin, transition or deposit (see table 1).

Zone	Criterion	Alternative characteristics and denominations	
Zone of origin	*A*. Manner of starting	*A1* starting from a point (loose snow avalanche)	*A2* starting from a line (slab avalanche) *A3* soft *A4* hard
	B Position of sliding surface	*B1* within snow cover (surface layer avalanche) *B2* new snow fracture | *B3* old snow fracture	*B4* on the ground (full-depth avalanche)
	C Liquid water in snow	*C1* absent (dry snow)	*C2* present (wet snow)
Zone of transition	*D* Form of path	*D1* path on open slope (unconfined avalanche)	*D2* path in gully or channel (channelled avalanche)
	E Form of movement	*E1* snow dust cloud (powder avalanche)	*E2* flowing along the ground (flow avalanche)
Zonof deposit	*F* Surface roughness of deposit	*F1* coarse (coarse deposit) *F2* angular blocks | *F3* rounded blocks	*F4* fine (fine deposit)
	G Liquid water in snow debris at time of deposition	*G1* absent (dry avalanche deposit)	*G2* Present (wet avalanche deposit)
	H Contamination of deposit	*H1* no apparent contamination (clean avalanche)	*H2* contamination present (contaminated avalanche) *H3* rock debris, soil | *H4* branches, trees

Table 1 Morphological classification of the international classification

This classification was not drawn up to study avalanche mechanics. It doesn't imply knowledge or theories. For example, the criterion of liquid water in snow is not specified to have an idea of the snow rheological properties but to recall it is "an important fact for rescue work and avalanche clearing" ([1], page 394).

But it shows how an avalanche flow may be complex. A dry sliding slab may become a powder avalanche or a wet snow flow, removing or not deposited snow along its

path. Strong assumptions must be done to simplify the issue and to develop a physical model.
Such a model, often far from physical reality, needs the knowledge of initial conditions which may change according to different goals (mapping, building.). An avalanche model is only a way for an expert, a help for a decision.
From this basic remark, avalanche models can be classified according to their physical assumptions but also to their final uses. Of course, these ones depend of their physical assumptions but also of the way they have been fitted to observations and experiments on the field.

Empirical models

We call empirical models whose reliability is based more on the quality of their fit than on the realism of the physical assumptions. We find in this group these which regard the avalanche as a solid [2], or assume that the motion of the avalanche is the same as the motion of the centre of mass (Voellmy's model [3]). The resistance force expression is :

$$F_{resist} = \mu g \cos\psi + bV^2 \qquad (1)$$

μ : coefficient of solid friction, is function of the snow quality
ψ : angle of the slope
V : speed of the avalanche
b : constant coefficient. (Its meaning changes with the basic physical assumptions)
μ an b are estimated from observations and experiments on the field.

These models are used for all kinds of avalanche (slab, powder or flow avalanche). As they are unidimensional, they give the maximal speed which can be reached by an avalanche along a section of its track, and its run-out distance. Depths of the flow and of the avalanche deposit are estimated from empirical laws.
Voellmy's model was improved by Salm and Gubler [4] Now, the speed may be estimated at each point of the track and the beginning of the zone of deposit is clearly defined. They also introduce the notion of statistical depth of snow in the zone of origin. This parameter, given for a return period, is a function of the slope, the altitude and the wind. This notion is very useful for people in charge of avalanche protection. Because, without it, it is often more efficient to estimate the largest run-out distance with a stereophoto-interpretation of the field than with a physical model. But two remarks may be made :

- The relation between the return period of an avalanche and this of the depth of snow in the starting zone is certainly not very simple. For example, snow properties may be very different with a same depth.
- Sometimes, the most disastrous avalanche is not the largest but the most unexpected one. Some unusual meteorologic conditions (rain, wind direction, for example) may modify the snow cover in the starting zone and then modify the path of the avalanche. But it is difficult for a unidimensional model to take this fact into account.

With their basic physical assumptions, these models can't describe the avalanche motion around of an obstacle (avalanche damp, braking teeth...). Forces on obstacles are estimated from hydraulic theory with empirical coefficients.

Even if they seem too simple, these models, and more especially, the V.S.G.'s one (Voellmy, Salm, Gubler's model) are today the most convenient and reliable if they are used in their domain of application, because they have been adjusted with a large number of avalanches. They remain the best tool for engineers.

The fluid models

These models regard the avalanche body as a gas for the dust cloud [5], [6] a viscous fluid ([7], [8], [9], [10]) or a granular fluid ([11], [12]) for the flowing component of the avalanche. The main assumptions are :

- These models are deterministic
- The avalanche body is a continuous medium.

The last assumption is obvious for a gas or a viscous fluid. It seems be right for a granular medium if its depth is more large than fifty times the diameter of a particle. So, the theory of continuous medium mechanics may be used and a rheological law must be found. But these models can't be used for all kinds of avalanche.

The dust cloud of a powder avalanche is studied as a turbidity current. First, the coefficients of this model (air friction coefficient, coefficients of growth of the cloud) were estimated from experiments into a water tank [5], [6]. For a few years, a numerical model has been developed [13], [6 ; 2]. Its fit to experiments and observations on the field is in progress [14].

But, most often, the avalanche is lead by its flowing component. Granular models [11], assume that the dust cloud stay some meters behind the front of the dense flow. In this case, mass transfer between dense component and cloud is neglected. The cloud may leave the dense flow if this one is strongly braked (a turn of the track for example) or if its mass is large enough, and takes its own dynamic.

The flowing component of the avalanche is usually regarded as a viscous or granular fluid. Evolution of assumptions from Newtonian to binghamian and finally to granular flow may be explain as followed :

If the assumption of a Newtonian fluid is made [8], [9]. a solid friction force is always introduced to get a term in the expression of the resistance force independent of the speed. This term can explain the fact that an avalanche may stop on a slope, impossible for a Newtonian fluid. To remove this assumption, the fluid may be regarded as a binghamian or biviscous one [10], [11]. A critical shear stress takes the place of the solid friction.

Then, experiments have shown that the resistance force has certainly a term proportional to V^2. To explain it, the notion of turbulent flow is introduced into most of viscous fluid models. This was made, first, by Voellmy who assumed that the flow is turbulent when the speed passes 1m/s. It is right in free surface hydraulic theory. But it is not based for very viscous or Binghamian fluid. Experiments and observations show that, most often, the flow is laminar for snow avalanche [11] or

debris flow [15]. And to find a criterion as the Reynolds's number to know when these fluids may have a turbulent flow is not easy [16]. This assumption can not be acceptable for every kind of snow flow and specially for wet snow one. If the avalanche is regarded as a granular fluid, the rheological law introduces this term proportional to V^2, without the assumption that the flow is turbulent.
These models seems more close to the physical reality than the empirical ones. In fact, the progress would be real if it was possible to measure the different coefficients of the rheological law (viscosity, critical shear stress,.) [17] of the avalanche body. But, today, theses coefficients are not known for each kind of deposited snow. And they may be very different of these of moved medium formed by snow clods and air [18]. So, the resistance force is written as :

$$F_{resist} = a+bV +cV^2 \qquad (2)$$

and coefficients a, b, c must be estimated from observations and experiments on the field. We have the same issue than with the empirical models.

The main advantages of these models are :

- Their numerical solution which allows a study in two or three dimensions and so makes it easier to take the topographical reality of the track into account. The trouble may come from the precision of the topographic data and the sensitivity of the model, specially in the zone of deposit where the avalanche speed is low.
- Their ability to take new physical knowledge into account, if it becomes necessary (snow compressibility, removed snow, front...) For example, these models could be used to study forces on bodies in avalanches (pressure, friction drag coefficient) when we shall have more information about the fluid compressibility and the kind of flow (laminar or turbulent).

Today, fluid models can't be used easily. First, they are not fitted to a large number of avalanches. Tables of coefficients don't exist. Second, they usualy need heavy computer means.
They are only used for complex studies, for example when a mapping of pressure field is asked. But, most often, the empirical models are satisfactory.
They will become more useful (and it may be soon the case for the AVL model of the powder snow avalanche) when they will be able to explain the effect of a protective construction on an avalanche flow.

The probability models (for dense flow avalanche)

These models, for dense flow avalanches, should be not determinist and should view the avalanche body as a non continuous medium.
Today, they don't exist. But some ideas are already suggested. In 1984, Perla [19] spoke about an additional random force due to collisions between particles. In 1989, Gubler [20] described a PF model (partly fluidized flow model) with retardation forces due to collisions (elastic between ice grains, non-elastic between snow balls) and granulation. On our experimental field, we are trying to verify if a wet snow avalanche can be regarded as a continuous medium [21].

These assumptions seem close to the physical reality. But, parameters of such models may become very numerous. An advantage is it could be easier to know which ones depend on snow properties and which ones on field data. But it is difficult to fit such models. Before, we must verify if the fluid models will be able to give satisfactory results in all cases, and more specially to study forces on bodies in an avalanche flow.

Conclusion

The international morphological avalanche classification shows how this natural phenomenon can be complex. To study it, different approaches are possible. If we want to cartography the largest avalanche which existed, the stereophoto-interpretation is a good way. To have an idea about the return period of an avalanche, it's better to use a statistical model [22].To get information about the path, the volume, the speed of an avalanche, physical models are used. Of course, initial conditions must be known. These models can be reliable only if they are used by experts. It is the reason of the development of expert knowledge integration in models [23]. For simple studies (when the track is exactly known and when only run-out distance, and maximum speed are asked) the empirical models as VSG'one are the most efficient. If we want a mapping of pressure field, or a rate of flow function of the time, fluid models must be used.
Today, to estimate forces on bodies in an avalanche flow, we have only empirical formula and no way to study the effects of protective construction (damp, braking teeth) on dense flow avalanches,(the precision of topographic data being about 10 meters). A lot of experiments on the field must be done to improve these models, to know if it is useful to look for a larger precision for topographical data and perhaps to verify when the basic assumptions of these models are too strong. In that case, it might be useful to develop new models as probability ones.

References

Quervin de M., Crecy de L., Lachapelle E.R., Losev K. and Shoda M.,(1973) "Avalanche Classification" proposal of the Working Group on Avalanche Classification of the International Commission on Snow and Ice hydrological Sciences Bulletin XVIII 4

Kozik S.M. (1962), "Raschet dvizheniia snezhnykh lavin" Leningrad, Gidrometizdat, set by Eglit M.E. in "Soviet avalanche research" Glaciological data 1984, report GD 16 pp 63-116

Voellmy A. (1955) "Uber die Zerstörungskraft von Lawinen, sonderdruck aus der Schweiz" Bauzeitung, 73 Jahrg. Hefte 12, 15, 17 19 und 37

Salm B., Burkard A. and Gubler H. (1990) " Calcul des avalanches : Une méthode didactique pour le calcul pratique" rapport de l' E.I.S.L. n° 47 traduit par Ancey.

Beghin P. and Olagne X. (1991) "Experimental and theoretical study of the dynamics of powder snow avalanches" Cold Regions Science and Technology vol.19 pp 317-326

Hermann F., Hermann J. and Hutter K. (1985) " Laboratory experiments on the dynamics of powder snow avalanches" IAHS Publ. n°162, pp 431-440

Hermann F., Issler D. and keller S. (1993) "numerical simulations of powder-snow avalanches and Laboratory Experiments on Turbidity currents" "Pierre Beghin " International Workshop on Rapid Gravitational Mass Movements

Brugnot G. et Pochat R. (1981) "Numerical simulation study of avalanches" Journal of Glaciology, Vol. 27, n°95 pp 77-88

Cheng T.T. and perla R. (1979) " Numerical computation of Avalanche motion" NHRI, Paper n° 5

Martinet G. (1992) "Contribution à la modélisation numérique des avalanches de neige dense et des laves torrentielles" Thèse de Doctorat en Mécanique de l'Université Joseph Fourier

Dent, J. D. (1982) "A biviscous modified bingham model of snow avalanche motion" U M I Dissertation Information Service

Norem H., Irgens F. and Schieldrop B. (1986)"A continuum model for calculating snow avalanche velocities" IAHS publication n° 162 pp 363-380

Norem H. (1992,) " Simulation of snow - avalanche flow by a continuum granular model " notes du NGI Norway

Hutter K., Savage S.B. and Nohguchi Y. (1989) "Numerical analytical and laboratory experimental studies of granular avalanche flow" Annals of Glaciology, vol. 13, pp 109-116

Sampl P. (1993) "Current status of the AVL avalanche simulation model" "Pierre Beghin " International Workshop on Rapid Gravitational Mass Movements

Schaffhauser H. (1993) "The verification of the AVL powder-avalanche model based on data of avalanche disasters in Austria"

Coussot P. (1992) "Rhéologie des boues et laves torrentielles. Etude de dispersions et suspensions concentrées" Cemagref, Etudes Montagne n° 5 pp 390 -391

Nishimura K. (1990) "Studies on the fluidized snow dynamics " Report of the I.L.T.S. Hokkaido University

Runich A.V. and Zalikhanov M.Ch.(1972) "Structure and mechanical properties of the avalanche snow" Papers of the Highmountain Geophysical Institute, Leningrad

Perla R., Lied K. and Kristensen K. (1984) "Particle simulation of snow avalanche otion " Cold Regions Science and Technology, vol. 9 pp 191 -202

Gubler H. (1989) " Comparison of three models of avalanche dynamics" Annals of glaciology, vol.13 pp 82 - 89

Marco O. "Instrumentation d'un site avalancheux pour l'étude de la dynamique des avalanches denses" Phd in preparation (1994)

Lied K. and Toppe R. (1989) "Calculation of maximum snow - avalanche run-out distance by use of digital terrain models" Annals of Glaciology, vol. 13, pp 164-169

Buisson L. and Charlier C. (1989) "Avalanche starting-zone analysis by use of a knowledge-based system" Annals of Glaciology, vol. 13, pp 27-30

Le Praticien RTM est-il un médecin généraliste ?

Is the RTM field engineer a general practitioner ?

R. MARIE

Service de Restauration des Terrains en Montagne
3, Bd des Diables Bleus, 38000 Grenoble - France
Tel. (33) 76 46 92 03 - Fax (33) 76 87 48 53

Abstract

This paper presents the personal point of view of a field practitioner in charge of natural hazard protection. After a description of his work through a comparison with a general practitioner, the author lists the main question he must answer. He then analyses the methods and tools available to help him in his work. He concludes by a call for new models.

Résumé

Cet article présente le point de vue personnel d'un praticien de terrain responsable de la protection contre des risques naturels. Après une description de son travail à travers une comparaison avec celui d'un médecin généraliste, l'auteur énumère les principales questions auxquelles il doit répondre. Il analyse ensuite les méthodes et les outils disponibles qui peuvent l'aider dans son travail. Il conclut en réclamant de nouveaux modèles.

Définition du praticien (Petit Robert)

1/ personne qui connaît la pratique d'un art, d'une technique
2/ médecin qui exerce, soigne les malades.

La manière dont les praticiens des services de Restauration des Terrains en Montagne exercent leur activité, s'identifie pleinement à la seconde définition. En effet, les fléaux sont les phénomènes naturels, les malades sont les populations concernés (depuis l'habitant d'un bâtiment menacé jusqu'au conseil municipal), les ordonnances médicales s'apparentent aux rapports préconisant les principes de protection.
La comparaison peut aller plus loin : les remboursements de la sécurité sociale peuvent s'assimiler aux subventions accordées pour les travaux de protection, et le mode d'intervention des "médecins-géologues" est également comparable : Interventions urgentes, de type SAMU, ou prophylaxie et médecine préventive.
Une différence cependant en matière de prévention : Là ou le médecin est généralement bien accueilli, les géologues, dans leur action de zonage du risque, avec leurs instruments réglementaires : PER, R-III-3... sont davantage ressentis comme des empêcheurs d'aménager...

Les personnels techniques chargés d'afficher le risque sont placés en fait à 2 interfaces différentes :

1- L'interface entre les phénomènes naturels et les habitants,
2- L'interface entre les théories et la traduction sous forme de documents (rapport, zonage, principes de protection) directement applicables.

1°) La première interface concerne en fait la traduction d'une situation de menace par un phénomène naturel, en termes suffisamment compréhensibles pour que les populations menacées soient bien informées.
Lors d'interventions urgentes, la demande des populations se résume en 2 questions
- pourquoi et comment ce phénomène s'est-il produit ?
- quelle est son évolution et quel est le danger résiduel ?
Au cours d'opérations d'affichage du risque (PER, R-III-3, POS...) il faut au préalable convaincre les habitants (les élus du conseil municipal en particulier) de l'existence de risques naturels : c'est parfois difficile mais les riches archives des services RTM ou des municipalités s'avèrent alors très utiles.
Les réponses aux demandes justifiées de la population, nécessitent d'appréhender correctement le mécanisme du phénomène et ses conditions de déclenchement et pour ce faire, la 2è interface s'avère indispensable.

2°) Elle permet, d'une part lorsque le phénomène est complexe (écroulement rocheux par exemple) de cerner au mieux les différents mécanismes, d'affiner le volume des masses en mouvement et de proposer éventuellement des investigations géotechniques adaptées.
A l'inverse, lorsque les mécanismes semblent simples, les applications pratiques des théories trouvent alors leur finalité en proposant des modèles représentatifs du phénomène. Cela permet en particulier des prévisions (extension du phénomène) et des protections (dimensionnement et emplacement des dispositifs de protection).
Les modèles les plus utilisés par les géologues, concernant les phénomènes de chutes de blocs isolés (avec ou non fragmentation).
Pour les cas plus complexe (écroulements rocheux), mettant en jeu des interactions entre blocs, actuellement, seules les observations de terrain et les comparaisons avec d'autres écroulements anciens ou similaires permettent de se faire une idée du comportement d'un tel phénomène. D'où un manque évident d'optimisation des zonages de danger (vision souvent trop pessimiste...) et donc des systèmes de protection (mal adaptés, trop couteux, etc)... Messieurs les théoriciens à vos modèles !

Classification of stream flows

Classification des écoulements torrentiels

M. MEUNIER

Cemagref / Division Protection contre les Erosions
BP 76, 38402 Saint-Martin d'Hères - France
Tel. (33) 76 76 27 68- Fax (33) 76 51 38 03

Abstract

Classifications of stream flows are useful only if they use two criteria. Since the existing classifications of this type are based on quantitative variables as the velocity or the relative submersion, they are rather difficult to use in practice. In this paper, we present a new classification based on the solid concentration on one hand, and the nature of the solid material on the other hand. We explain the reasons of that choice and the different behaviour types of the flowing fluid in each class. The final diagram allows to synthetise the mass movements and the stream flows which occur in a mountain catchment.

Résumé

Pour être utilisables, les classifications des écoulements torrentiels doivent comporter deux critères. Les classifications de ce type qu'on trouve dans la littérature nécessitent une connaissance de certains paramètres de l'écoulement (vitesse, submersion relative), elles sont donc difficiles à utiliser. On présente ici une autre classification, plutôt qualitative, basée sur la nature du matériau solide d'une part et sur la concentration en matériau solide d'autre part. L'article présente les raisons de ce choix et explicite les différences de comportement des fluides qui permettent de justifier l'existence de ces classes. Le graphique obtenu en synthèse permet de présenter de manière unifiée les mouvements de masse et les écoulements torrentiels se produisant sur un bassin versant de montagne.

Introduction

Many classifications of the different kinds of torrential flows exist. They separate sediment laden flows, concentrated flows, debris flows, mudflows, hyperconcentrated flows, slurry flows, etc. Usually, only one criterion, the solid concentration, is used to establish a classification. But there is no agreement on one of them (Bradley, 1986, in Rickenmann, 1990).

It is necessary to use at least two variables to obtain a useful classification ; for instance, Pierson T.C. and Costa J.E. (1987) used the solid concentration and the flow velocity, to separate the different flow types, according to their behaviour. One problem is to recognize this fluid behaviour, since for the same velocity and the same

solid concentration, it is possible to have different kinds of rheological behaviour, according to the solid material mineralogy and grain size distribution. Another classification was proposed by Takahashi T. (1991), who used the relative submersion on one hand, and the slope on the other hand. This classification is very interesting, as it allows to choose between the different tools which are usable in the field of torrential hydraulics, according to Takahashi's views. But, as these classifications need the knowledge of quantified parameters, the velocity with Pierson and Costa's classification, the relative submersion with Takahashi's classification, it is necessary to have a previous idea of the fluid fluid we are dealing with, in order to use the right tools to compute these parameters

A qualitative classification

In order to get this previous idea, I proposed (Meunier M., 1991) a qualitative classification, which is based on the fact that the behaviour of the flows depends on the nature of the solid material. This separation is coherent with the already known phenomenons : at low concentrations, fluvial hydraulic distinguishes between suspension and bed-load transport. At very high concentrations, the behaviour of debris flows is also different whether the fluid is mainly carrying clayey or coarse particules. In the field of mass movements also, the phenomena are distinguished according to their granulometric composition, with landslides for soil mass movements and rockslides and rockfalls for the rocks and coarse material movements.

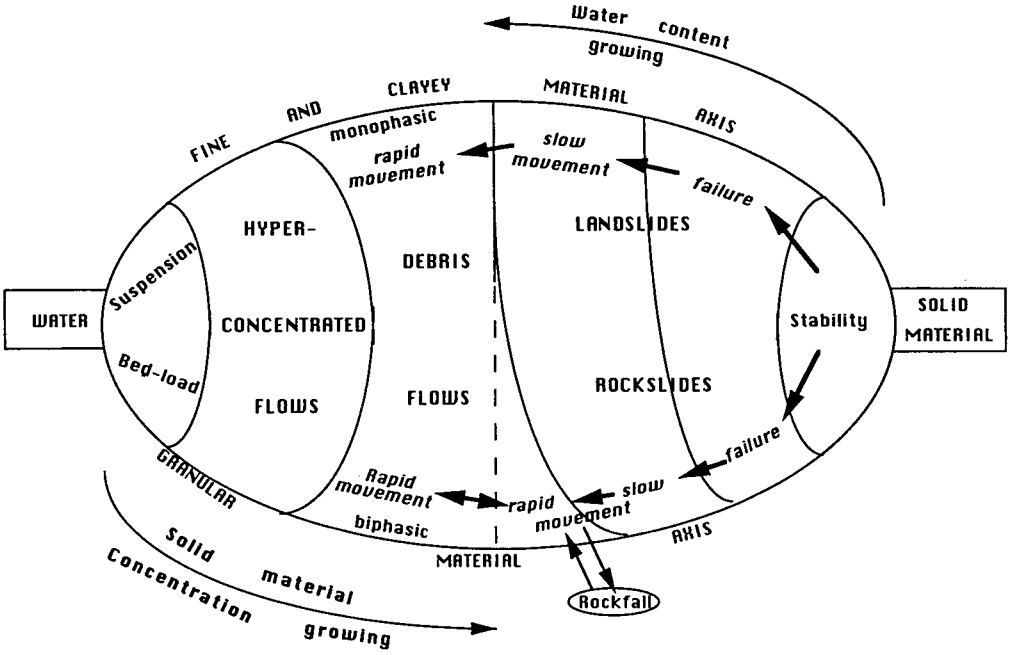

Figure 1 : Classification of torrential flows and mass movements

The other parameter used in this classification is roughly the solid concentration, as in the Pierson and Costa's one, which is always strongly correlated to the slope, being so coherent with the Takahashi's classification. In fact, on this axis the transitions between the different fields depend also of the mineralogy and the sieve curve

This separation between two axis according to the nature of solid transport, leads to the figure 1, where we can see the different fields of torrential flows which lie between the classical fluvial hydraulics and the field of mass movements.

The field of mass movements is mainly studied by geologists ; in this field the displacements are always small (some cm/day), and there is no need to study them by the use of the momentum equation. But, when there is an acceleration of the movement (up to velocity which are measured in m/s), we enter the fluid mechanics field as the basic structure of the landslide or the rockslide, is destroyed, and the kinetic energy may no longer be neglected. We enter then the field of debris flows, i-e mudflows, when the main responsible of the rheological behaviour of the flow is clay or argileous component, or stone debris flows, when there is only non cohesive coarse material. These two fields for debrisflows correspond to different rheological behaviours, for which many authors proposed various solutions.

As everybody knows, debris flows are intermittent flows ; sometimes, the physical reason of this behaviour is internal : instabilities grow and generate roll-waves ; but, sometimes the reason is simply external, this intermittent behaviour is explained by the rupture of temporary dams which are made by the flow, generally at singularities of the channel.

According to this transient regime of debrisflows, there is evidence for the necessity of the separation between debris flows and hyperconcentrated flows ; on the contrary, it does not seem so evident that we have to put a limit between the classical fluvial hydraulic and the field of hyperconcentrated flows ; but many observations in the field of hyperconcentrated flows with coarse material, indicate that this separation is necessary :

- In fluvial hydraulic, to compute the water level, we are allowed to suppose that the streambed is fixed ; in hyperconcentrated flows, when solid transport is very high, the variations of the stream bed during the floods are more rapid than the variations of liquid discharge. Then it becomes the most important phenomenon and can't be neglected, especially in alluvial channel.
- At high slopes (>7-9%), especially with constrained channels, the flow level is induced by the solid discharge as well as by the liquid discharge (Smart G.M., Jaeggi M., 1986), as we can see on the figure No 2, which compares the measured height of hyperconcentrated flows to the one which is computed with Manning formula with the liquid discharge.

Near the axis of cohesive and fine sediments, there is also a need to separate the field of hyperconcentrated flows from the classical suspension field ; the flows which are studied in China, both in the field and in the lab, prove that an important amount of suspension attenuates the turbulency, and makes free a new

quantity of energy ; consequently, the discharge becomes higher for the same level. Furthermore, the work of Fei (in Quian Ning and Wan Zhaohui, 1986) shows that the flow behaviour is no longer newtonian, as appears a yield stress when the volumic concentration increases.

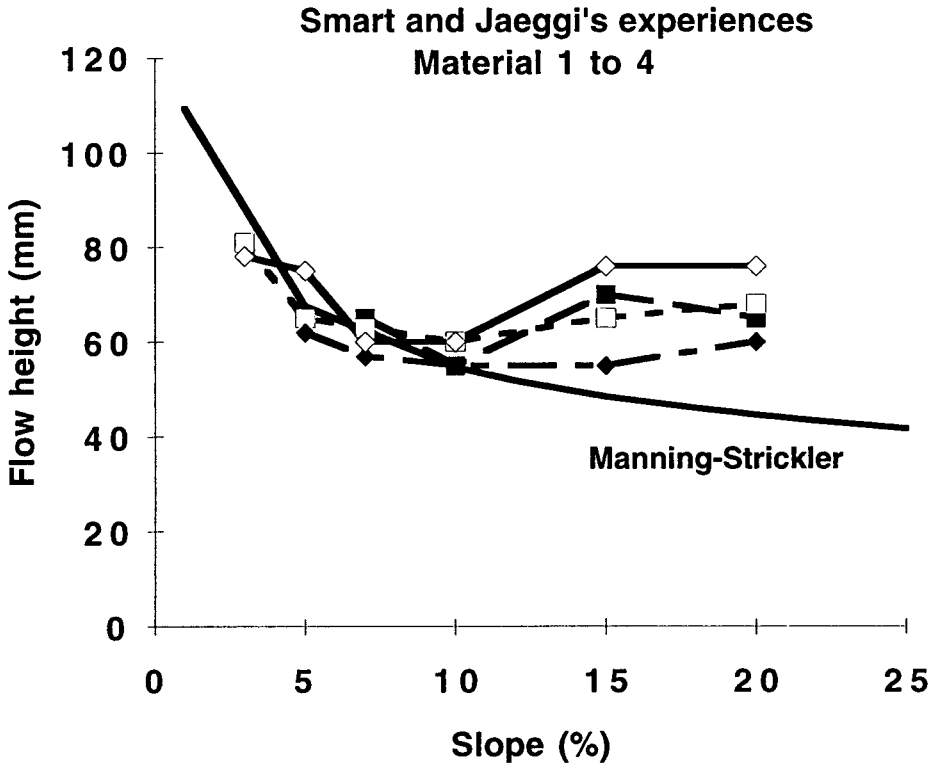

Figure 2 : Heigth of hyperconcentrated flows with the same liquid discharge (20 l/sec)compared to the height given by Manning formula

Different parameters to measure the solid concentration

The different values of the solid concentration show very clearly the differences between the different fields : in the field of debris flows, the parameter which is mainly used is the volumic concentration Cv. It varies from .45 to .75. Let us see what occurs in the field of hyperconcentrated flows.

As we already said, the transition from hyperconcentrated flows to debris flows is very evident, from a phenomenologic point of view. Is the transition also clear with the solid concentration ?

On the coarse material axis, for hyperconcentrated flows, the parameter which is the most adequate, is the ratio C of the solid to the liquid discharge. It varies from some % to 35 or 40%. If we transform these values into the equivalent values of Cv,

we get only 1 to 25%. It means that there is a gap between the two fields, not only in the phenomena, but also in the solid concentration.
On the cohesive and fine material axis, the parameter the most frequently used is the solid concentration, counted in Kg/m3, or g/l. For hyperconcentrated flows, we may have from 100 to 800 g/l, according to chinese values. This corresponds to values of Cv from 3.7 to 30% ; there is also a gap with the values commonly said for mudflows. In fact, it would be necessary to know the behaviour of the fluid for which such high values of concentration where measured.
If we look now at the transition between fluvial flows and hyperconcentrated flows, it seems that the point where we should put the limit is not strongly assessed, as the transition is progressive. For instance many formulas which give the maximum transport capacity on the coarse material axis, are valid for the two fields. On the cohesive and fine material axis, as it is shown with the Fei's work, the same formulas can't be used on the total range of the possible concentrations ; but the phenomenons are modified in a progressive way, from the fluvial suspension to the hyperconcentrated flows, when the concentration increases. Nethertheless, the values of the solid concentration are very different in the fluvial flows : it is counted only in mg/l for suspension, and for bed load, the solid transport is used by itself, (in m3/s or Kg/s) without any ratio with liquid discharge, as this ratio would be too small.

Conclusion

A classification of stream flows is proposed, which includes mass movements and distinguishes debris flows, and hyperconcentrated flows from the usual fluvial flows. It is based on the distinction of the different phenomena occuring in these flows. The differences depend mainly of the granulometry and the slope. The different criteria used in this classification are explained, and the values of the solid transport are quantified for each kind of flow.

References

BRADLEY J.B., 1986. *"Hydraulics and bed material transport at high fine suspended sediment concentrations"*, Ph.D. Dissertation, Colorado State University, Fort Collins, Colorado (in Rickenmann D.,1990)

MEUNIER M., 1991. *"Eléments d'hydraulique torrentielle."* Cemagref Série Etudes Montagne No 1. 278 pages.

PIERSON T.C et COSTA J.E., 1987. *"A rheological classification of subaerial sediment-water flows."* Engineering Geology, Vol VII

QUIAN NING, WAN ZHAOHUI. 1986. *"A critical review of the research on the hyperconcentrated flows in China."* IRTCES. Beijing China. 43 p.

RICKENMANN D.,1990. *"Bedload transport capacity of slurry flows at steep slopes"*. Versuchsanstalt für Wasserbau,Hydrologie und Glaziologie der Eidgenössischen Technischen Hochschule, Zürich. 249 p.

TAKAHASHI T., 1991. *"Debris flow."* Monograph Series. AIRH. Balkema. Rotterdam. 165 p.

SMART G.M., JAEGGI M.,1983. *"Sediment transport on steep slopes"*. Zurich. Mitteilungen der Versuchsanstalt fur Wasserbau, Hydrologie und Glaziologie, ETH No 64. 191 p.

Ideas on a phase diagram for granular materials

Quelques idées sur un diagramme de phase pour les matériaux granulaires

H. NOREM

Norwegian Geotechnical Institute
PO Box 3930, Ulleval, Hageby, 0806 Oslo - Norway
Tel. (47) 22 23 03 88 - Fax (47) 22 23 04 48

Abstract

This paper gives some ideas on rheology and energy dissipation in natural avalanches. In a first part, common characteristics of avalanches are described. In a second part and after a presentation of the assumption that consideres the granular material as a continuum, a phase diagram is proposed to classify the behaviour types of these materials. For each phase, the processus which explain this behaviour are developed.

Résumé

Cet article donne quelques idées sur la rhéologie et la dissipation d'énergie dans les avalanches. Dans une première partie, des caractéristiques communes aux différents types d'avalanches sont décrites. Dans une seconde partie, après la présentation d'une hypothèse qui assimile le matériau granulaire à un milieu continu, un diagramme de phase est proposé pour classer les comportements de ces matériau.x Pour chaque phase, les processus qui expliquent ces comportements sont développés.

Introduction

Natural avalanches are found in the nature in a great variety of types, both related to the materials involved and the type of flow behaviour. The avalanche types are often characterized as either a debris flow type (high volumetric density) or a turbidity current type (low volumetric density). Full scale experiments have shown that some avalanches consist of at least two flow types, and probably there also exist transitional flow types.

The scope of this paper is to present ideas on the rheology for the different flow types. Special attention has been paid on the effects that cause energy dissipation and the physical requirements for a granular material to reduce its volumetric concentration.

The present paper is to a great extent based on the discussions and the cooperation the author had with Pierre Beghin the spring 1992, thanks to a Cemagref fellowship. The author feel honored to be given the opportunity to present the

results of this cooperation in the workshop dedicated to the memory of Pierre Beghin.

Characteristics of avalanches

All known avalanche types consist of particles surrounded by an interstitial fluid, water or air. Snow avalanches, submarine slides, and to some extent, rockslides are the only avalanches that are pure two-phase flows, as both the ambient fluid and the interstitial fluid is the same. The other types consist of a mixture of particles and water with air as the ambient fluid.
Full scale experiments on snow avalanches carried out the last 10 years clearly show that the snow avalanches most often consists of both a dense part close to the bed and a turbidity part above that, Norem et al. (1990). Probably there is also a transition zone between these two layers.
Seismic investigations of a submarine slide area in northern Norway have also indicated a similar behaviour for submarine slides, Norem et al. (1990).
Natural avalanches having water as the interstitial fluid and air above the flow will never generate a turbidity layer. An important exception is what Takahashi (1991) calls "immature debris flows", with a dense part close tot eh bed and particles transported as suspended particles above that.

Presentation of the phase diagram

All known avalanches starts as a solid material, but within a short time, the material obtains a liquefied or vaporized behaviour. The main problem to understand the physics of avalanches, and to simulate their flow is to investigate the transitions in flow behaviour during the avalanche event.
Short time after the release of an avalanche the solid material disintegrate into smaller particles and a reduction of the volumetric density takes place. The modelling of an avalanches may thus either be treated as a flow of a sample of individual particles, or as a continuum where the particles and the fluid form a mixture. This presentation is based on the assumption that the flow height compared to the particle diameter is sufficient high to assume the behavior of the granular material to be more close to a continuum than to the flow of individual particles.
The reduction of the particle volumetric concentration when the particles are in motion has to be explained by excessive normal stresses necessary to keep the particles apart and which are not found when the particles are in rest. The physical effects that may cause a reduction of the volumetric concentrations are:

- Uplift of the particles due to friction (dilatans).
- Dispersive pressures due to collisional effects.
- Uplift of the particles caused by turbulence in the interstitial fluid.

The behavior of the granular material is dependent on which of these effects that are dominant and that the behavior may be divided in three phases, according to

classical theories for continuum. The three phases are solid, liquid and vapor, and each of the phases are characterized by, Fig. 1.

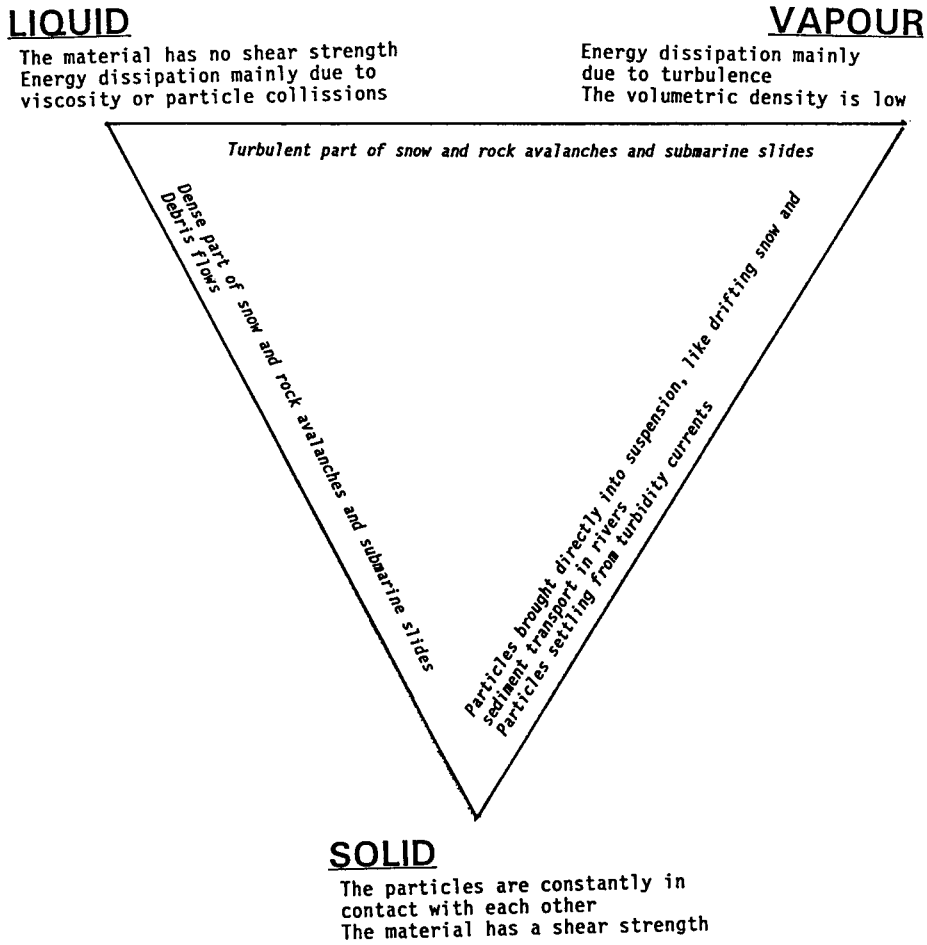

Fig. 1 : Phase diagram for granular materials

The solid phase

In the solid phase the particles are in steady and close contact with each other. The solid phase of a granular material is usually well described by a Mohr-Coulomb behaviour. The main parameters that define the shear strength of a solid granular material is:

- cohesion
- Coulomb-friction coefficient
- normal stresses
- pore pressure

The liquid phase

The liquid phase is defined as a state where the granular material has none or only minor shear strength. The particles collide frequently in the liquid phase, and the volumetric concentration must thus be fairly high. The main physical effects to keep the particles apart are frictional forces and particle collisions, and the energy dissipation is dominated by fluid viscosity or particle collisions.

The pioneering work to understand and quantify the behaviour of liquefied granular materials was made by Bagnold (1954). He performed shear cell experiments with wax spheres in a liquid having the same density as the particles, thus avoiding the effects of effective stresses and shear strength of the material.

According to Bagnold the behaviour of granular materials exposed to velocity gradients can be divided in three regimes:

- *The macro-viscous regime* where the main energy dissipation is caused by the effect of fluid viscosity modified by the presence of the particles.
- *The inertia regime* where particle collisions are the dominant effect due to energy dissipation.
- *The transition zone* where both collisions and viscosity play an important role.

The inertia regime is the one best studied and explained by Bagnold (1954). In his ring shear experiments with a constant distance between the two disks, Bagnold recorded both an increase in the shear and normal stresses, which were dependent on; density of particles, volumetric density, particle diameter and velocity gradient. The ratio shear stress to normal stress was approximately constant for all velocity gradients. This ratio is probably a material property defined mainly by the elasticity of the particles, the particle shape and the volumetric concentration.

The Bagnold (1954) - experiments indicated that the viscosity of a particle-fluid mixture in the macro-viscous regime depends both on the viscosity of the fluid and the volumetric concentration. To some surprise Bagnold did not present any experimental results for the normal stresses, but probably there are some dilatans at high concentrations, which one should be able to record as excessive shear stresses in a ring shear cell. Such relationships for the normal stresses is important to establish for modelling avalanches flowing in the macro viscous regime.

The vapour phase

The main energy dissipation and the physical effect to keep the particles apart is turbulence in the interstitual fluid. The particles are seldom involved in collisiions and the volumetric concentration thus must be small. Bagnold (1954) assumes 9% concentration to be the upper limit to exclude the effects of particle collisions.

The vapour phase can only exist by a continous energy input into the interstitual fluid causing turbulence. For a granular material only exposed to gravity as external forces, the turbulence has to be generated at the boundaries.

The capacity to keep heavy particles in suspension is dependent on the local turbulence, and for all kinds of granular flow distinct particle concentration gradients are normally found. This is the case both where the flow of the fluid generate the turbulence as in drifting snow and sediment transport in rivers as well as in pure turbidity currents.

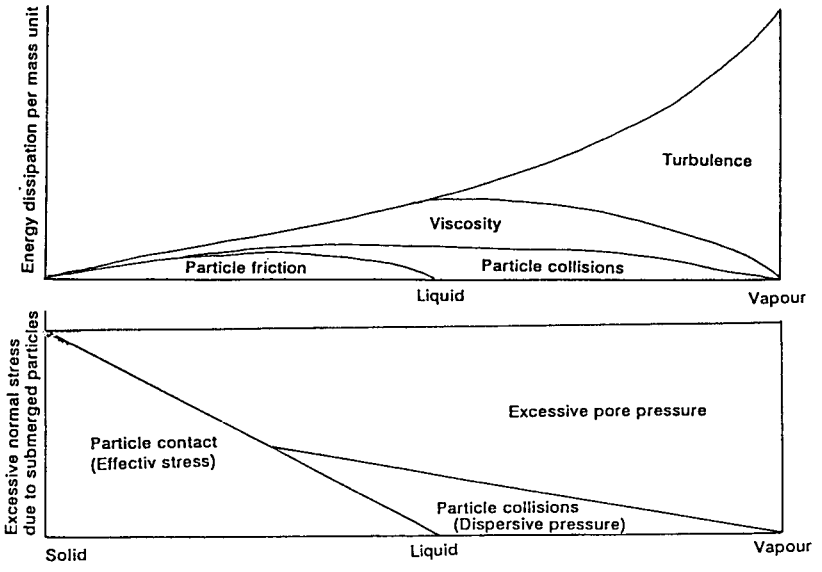

Energy dissipation and excessive normal stresses in a granular material submerged in an incompressible fluid and developing from the solid to the vapour phase

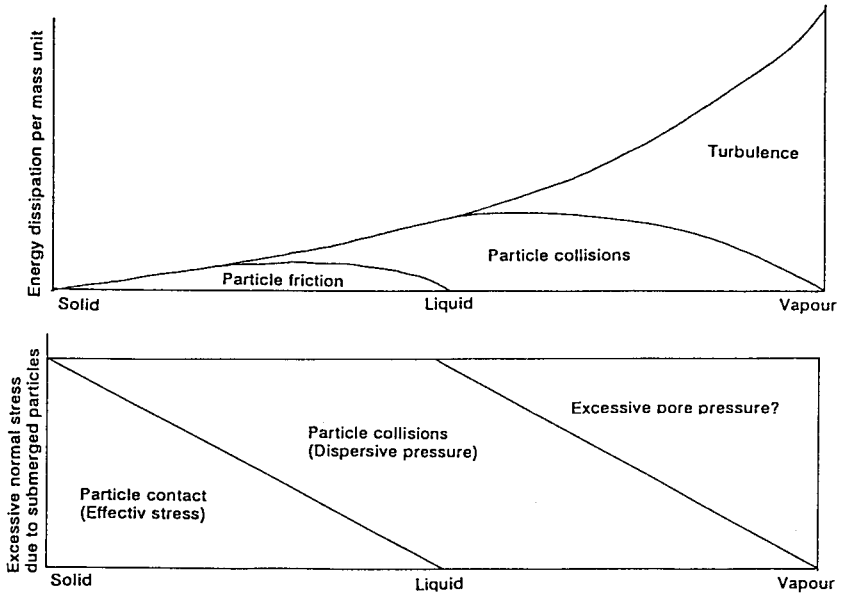

Energy dissipation and excessive normal stresses in a granular material submerged in a compressible fluid and developing from the solid to the vapour phase

Fig. 2 : Assumed diagrams for energy dissipation and excessive normal pressures for a granulat material developing from the solid phase to the liquid phase.

The transition zones

Solid to liquid phase

The behaviour of the avalanching material and the resulting energy dissipation and the excessive normal pressures are indicated in Fig. 2.
The figure presents the behaviour separately for avalanches having water or air as the interstitual fluid. For each case, two diagrams are presented, one for the develepment of normal pressures, and one presenting the physical effects causing energy disspation.
In the transition zone between the solid phase to the liquid phase when air is the interstitual fluid, the energy dissipation is first caused by Coulomb friction and then more and more dominated by particle collisions as the velocity gradients increase. The dispersive pressures caused by the particle collisions are in this case the main excessive normal pressure to keep the particles diluted. On the other hand, when water is the interstitual fluid, the energy disspation is mainly caused by viscosity and Coulomb friction, and the particles are kept apart by the generation of excessive pore pressures.

Liquid to vapour phase

The dispersive pressures caused by Coulomb friction (dilatans) and particle collisions are both dependent on the volumetric dansity, and dedrease rapidly with reduced dansity. The volumetric density must therefore be relatively high in the liquefied phase, whatever the interstitual fluid will be. A further dilution can probably only be explained by the existence of turbulens in the interstitual fluid.
Fig. 2 shows that, when either water or air is the interstitual fluid, turbulens becomes the main physical effect for the energy dissipation, and to keep the particles apart, when the degree of vapourization increases.

Acknowledgement

The ideas presented are results of longtime research and consulting work on avalanches, theoretical work on granular materials, and fruitful discussions with collegues. I would like to thank prof. J.D. Goddard ofr presenting me the idea of a phase diagram on the back-page of an airticket in 1985, and espacially to my collaborators for the theoretical studies, Fridjov Irgens and Bonsak Schieldrop. A special tank also goes to Pierre Beghin, who I sheared office with for two months, and then helped me a lot to clarify the presented ideas. Our collaboration was made possible due to financial support from French-Norwegian Foundation for scientific research, Cemagref and Norwegian Geotechnical Institute.

References

Bagnold, R.A., 1954. Experiments on a gravity-free dispersion of large solid spheres in a Newtonian fluid under shear. Proc. of the Royal Soc. of London. Series A 225:49-63.

Norem, H., Locat, J. and Schieldrop, B., 1990. An approach to the physics and the modelling of submarine flowslides. Marine Geotechnology., Vol. 9, 93-111.

Takahashi, T., 1991. Debris flow. IAHR Monograph Series. Balkema, Rotterdam.

Rapid Mass Movements in the Bavarian Alps and some Special Aspects of their "Impact" on the Valley Floor

Mouvements en masse rapides dans les Alpes Bavaroises et quelques problèmes liés à leur impact dans les fonds de vallée

A. VON POSCHINGER

Bayerisches Geologisches Landesamt
Hesstr. 128 D-80797 München - Deutschland
Tel. (49) 89 12 000 002 - Fax (49) 89 12 000 647

Abstract

After an introduction about the geological framework of mass movements in Germany and, specially, in Bavaria, this paper presents 3 examples of mass movements : the Rubihorn rockfall which occurred in 1987, the Marquartstein Landslide, and the Altenau Landslide. The last two events are assumed to be prehistoric but post-glacial.
Mass deposits are particulary described. The interpretation of these field observations deals with the part played by pore pressure in the movement and in the reduction of the friction. However, this theory cannot explain the existence of radial fingerlike ridges in the deposition.

Résumé

Après une introduction relative au contexte geologique des mouvements en masse en Allemagne et, plus spécialement en Bavière, cet article présente trois exemples de mouvements en masse ; l'écroulement rocheux de Rubihorn qui s'est produit en 1987 et les glissements de terrain de Marquartstein et d'Altenau. Ces deux derniers sont supposés être préhistoriques, mais post-glaciaires. Les dépôts sont plus particulièrement décrits.
L'interprétation de ces observations de terrain porte sur le rôle joué par la pression interstitielle dans le mouvement et dans la réduction du frottement. Cependant, cette théorie ne peut expliquer l'existence, dans le dépôt, d'une série d'arêtes radiales, formant une digitation.

Rapid Mass Movements in Germany

The Bavarian Geological Survey is concerned with mass movements in the German part of the Alps. One of his tasks is to investigate and to register mass movements and related endangered areas in the Bavarian Alps.
Apart from the Alps fast mass movements as rock falls and rock slides are to be expected in many parts of Germany. Among the most endangered areas are the

"Rheinisches Schiefergebirge" and the steep outcrops of the Malm-plate in Franconia and Swabia of southern Germany. In these regions because of the morphological situation rapid mass movements do not attain such dimensions, as they are found at Alpine accidents.
The largest part of the Bavarian Alps is built up by the tectonic unit of the Northern Limestone Alps. Apart from that the flysch zone has the largest extension. About 30% of the surface of the Alpine region are covered by quarternary deposits. The Northern Limestone Alps are a lithologically inhomogeneous rock complex and are characterised by a sedimentary change of limestones and clayey to marly sediments. But also an intensive tectonic slicing took place, mostly along the front of the tectonic nappes.
This geological frame explains the special kind of the problems concerning mass movements. Most of the slope movements belong to the category of "slow" movements. The occurrance of slow landslides, mudstreams and creeping features in the clayey and marly sediments is common and the main cause for destruction and loss by slope movements. The risk is very often aggravated by the transition from a gravitational slope movement to a debris flow. This can cause the transport of the masses from the sliding site over a long distance to built up areas.
But also the variability of the geological conditions is a common cause for rapid mass movements. The succession of formations with hard limestones on top of more or less plastically reacting clays and marls represents a classical instable situation. The rigid overlying plate breaks as a result of tensile stresses due to the plastic reaction of the underlying layer to the heavy overburden. Water can enter through these cracks and thus further weathering. The underlying layer will weaken more and more and the overlying limestones have to disintegrate subsequently, until a part of the slope will move downwards.
Recent rockfalls are relatively rare, so the interpretation of the moving acts must essentially rely on the interpretation of older events. Only the interpretation of these "large-scale-experiments of nature" helps to evaluate and to predict future mass movements. As settlements in alpine regions are intruding more and more in areas endangered by mass movements, the prediction of slope movements will be the most important task of mass movement investigations.

Field examples

At first a typical example of a rapid mass movement shall be described. Thereafter some special cases will be reported. They are presented to the auditory for discussion.

The Rubihorn rockfall

At the Rubihorn northeast of Oberstdorf im Allgäu in may 1987 a rockfall occurred. Even though there are no reports on former events in historical times, the existence of a clear cone in the deposition area of the latest rockfall hints at the occurrence of numerous previous events.
The Rubihorn forms in this area the front of the nappe of the Northern Limestone Alps (fig. 1) tectonically overthrust on flysch sediments. At the northern foot of the Rubihorn between these two tectonic units a thin slice of "Arosa-nappe" is found.

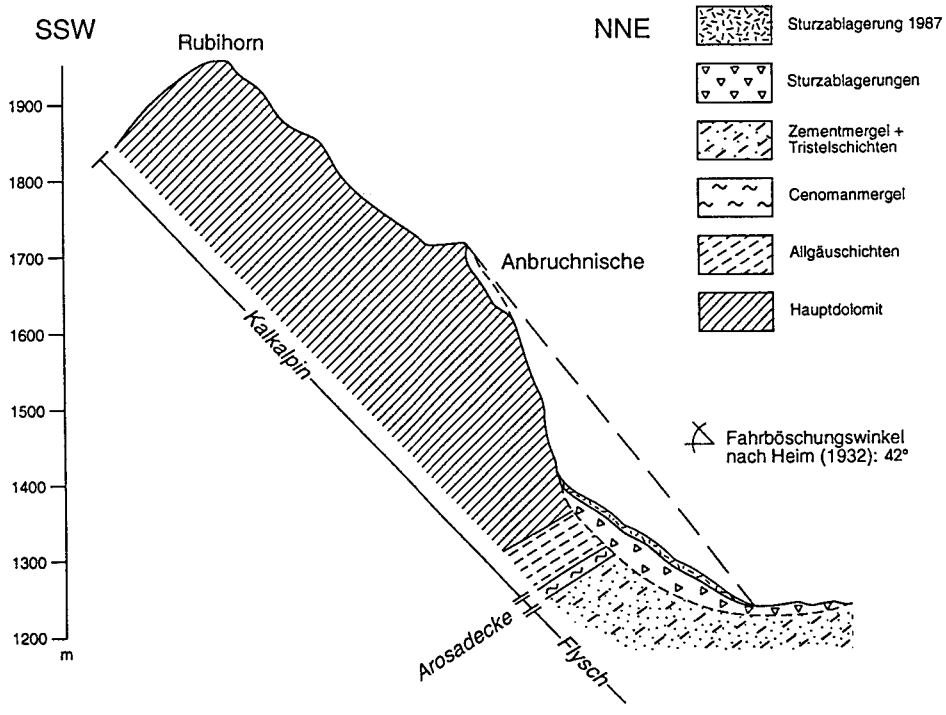

Fig. 1: Cross section of the Rubihorn rockfall area

The flysch here is built up mostly by marlstones and sandstones. The tectonically heavily crushed series of the Arosadecke is mechanically dominated by the occurrence of Cenomanian marlstones. The succession in the Limestone Alps starts at the bottom partly with intercalated marlstones of the upper Triassic and the Liassic, partly directly with Norian dolomites. The top of the mountain finally is entirely built up by layered, south dipping dolomites.

The cross-section (fig. 1) shows a typical picture of a potentially instable pile. The rigid dolomites react on deformation in the weaker, underlying marlstones.

The rockfall with a volume of about 50.000 m^3 happened in several consecutive events. The rock material was situated in a scar, limited by intersecting joints at an altitude of 1.630 to 1.700 m a.s.l. The way from the scar to the foot of the slope must have been traversed by the rockmass more or less by falling. On the cone the way was continued in rolling and jumping downwards.

The reach of the rockmass was extremly small. The mass came to a standstill within the area of the cone. The toe of the cone advanced only insignificantly. The fahrböschung of the rock mass according to HEIM (1932) can be calculated to be 42°, which means a very steep inclination. The cause for such a small range is to be seen in the fact that the event occurred in the form of several sub-events during some days. In that sense it was a continued blockfall rather than a single rockfall.

In 1993 some subsequent rockfalls occurred. Behind the landslide scar many open crevasses are found, signaling the future break-down of a further slice of the mountain. Even if the danger of a new rockfall is high, the risk can be evaluated to be low. Within the potential reach of a further - even bigger - rockfall there are no potentially endangered objects. Even the brook at the toe of the cone will probably not be blocked.

The Marquartstein Landslide

Near the village of Marquartstein the deposition of one of the largest landslides in Bavaria had taken place. Its volume was estimated up to now to be about 50 mio. m^3 (ABELE 1974). The landslide scar is found at the east side of the valley at the 1600 m a.s.l. high Hochgern mountain. The age of the landslide is unknown; it is assumed to be prehistoric but postglacial.

The geological situation within the scar is characterised by a intensely folded sequence of Triassic and Jurassic sediments concerning mostly limestones and dolomites. The main fracture occurred perpendicular to the fold axis so various lithological series are affected. The cause for the instability might be - apart from the glacial erosion of the toe of the hill - the existence of plastically reacting and water impermeable marlstones of the "Kössener Schichten" beneath the sliding plane.

In the deposits a clear separation of the material can be recognized. The "Kössener" limestones outcropping in the southern part of the scar are found as blocks in the southern area of the deposition and dolomites from the north of the scar are found in the northern part of the deposition. Hence the movement probably was not very turbulent but rather laminar.

The horizontal range of the landslide is 3.450 m at an altitude difference of 950 m. The inclination of the "fahrböschung" according to HEIM (1932) therefore can be calculated to be only 15°. According to ABELE (1974) that means, with regard to the volume, a comparatively great travel distance.

To this point a "normal" landslide accident similar to a "sturzstrom" as introduced by HEIM (1932) has been described, but field evidence showed some peculiarities worth reporting:

For a long time the morphology of the depositions was considered to be of no special interest. There are landslide-typical hills within a plain protruding up to a height of 70 m. Nevertheless a closer view shows a special arrangement of the hills. All the hills are more or less long ridges directed radially and concentrically around the landslide scar. In that way their morphology resembles the spread fingers of a hand, the wrist being the landslide scar. Between the fingers the morphology is more or less plain. Up to now it had been assumed that the hills had been partly buried by a later sedimentation and only the tops of the hills were standing out of the plain. Geophysical investigations as well as borings proved that this is not correct. There is no connection between the ridges beneath the plain. They are isolated within a mass of lacustrine clays and, in the deeper underground, in gravel. The block masses continue only several meters beneath the land surface into the valley deposits. The formerly estimated volume therefore must be adjusted to the new knowledge and reduced to about 40 mio m^3.

Another peculiarity is the steepness of the ridges in cross section. The lateral slopes reach inclinations of up to 42°, an angle which is very steep considering these loose, unconsolidated masses.
A fact important for the interpretation given below is the existence of well rounded gravel on the top of the sliding mass in the distal area. They are found in an elevated position in an area where a fluvial deposition after the landslide event could not have been possible.

The Altenau landslide

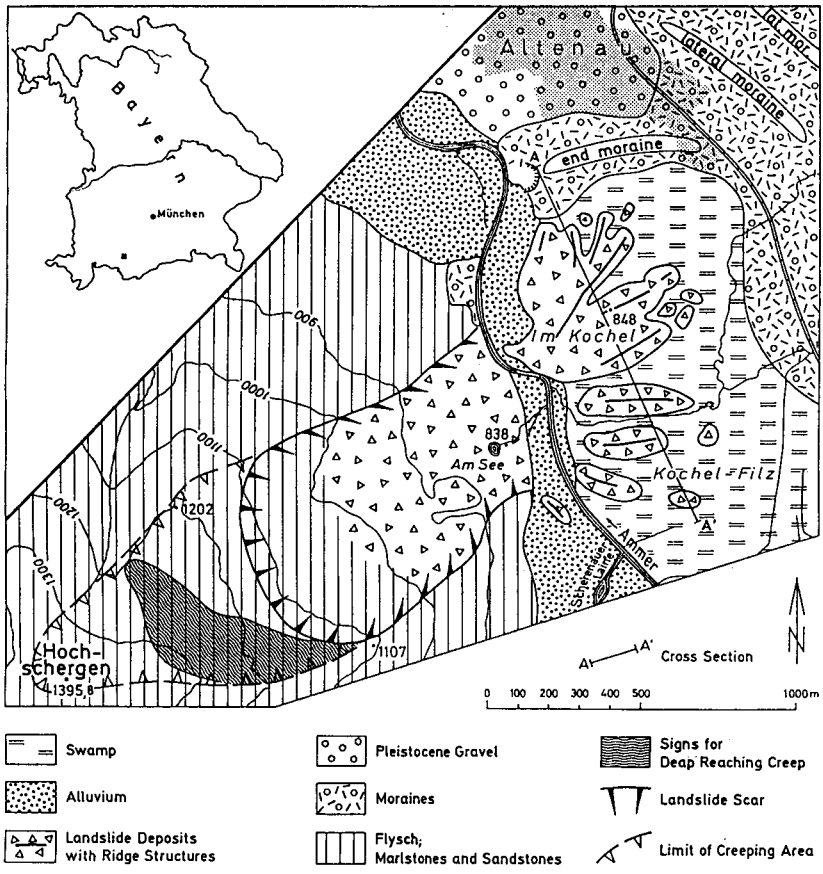

Fig. 2: Geological scetch of the Altenau landslide area.

South of the village of Altenau near Oberammergau (s. fig. 2) some hills exist within an aluvial plain which has been interpreted in literature for a long time to be glacial deposits. This opinion was based on the fact that these hills are in the vicinity of a clear moraine circle of the late wurmian. But according to our own investigations, these "hills" are a deposition of a prehistoric but postglacial mass movement from the 1359 m a.s.l. high Hochschergen mountain in the west. There clearly a landslide scar can be observed. Behind the scar many large crevasses

indicate that the whole mountain ridge of the Hochschergen underwent a deep seated, creeping movement.
The Hochschergen area is built up of flysch sediments forming a smooth syncline with fold axes dipping towards the valley. The landslide removed the marly sandstones, the filling of the syncline, the layering serving as gliding plane.
The slope movement attained a difference in elevation of 370 m at a longitudinal distance of 1.720 m. The inclination of the fahrböschung according to HEIM (1932) is to be calculated at 13°. This value is considered to be very low regarding the volume of only about 4 mio m^3.
The peculiarity of the Altenau depositions is certainly their morphology. Similar to the Marquartstein landslide, but more intensely expressed, there are ridges in a radial concentric arrangement. Their crests reach a height up to 40 m above the surrounding swampy plain. The course of the crests is more or less straight. The cross section (s. fig. 3) of the ridges again shows steep flanks with slope inclinations of up to nearly 40°. Some of the ridges are interrupted in their course by a deep incision, continuing at the same height and direction after a gap of 20 to 50 meters. Whereas the "spreading" of the "fingers" in Marquartstein included an angle of about 90°, in Altenau the angle between the most external ridges totals 160°!

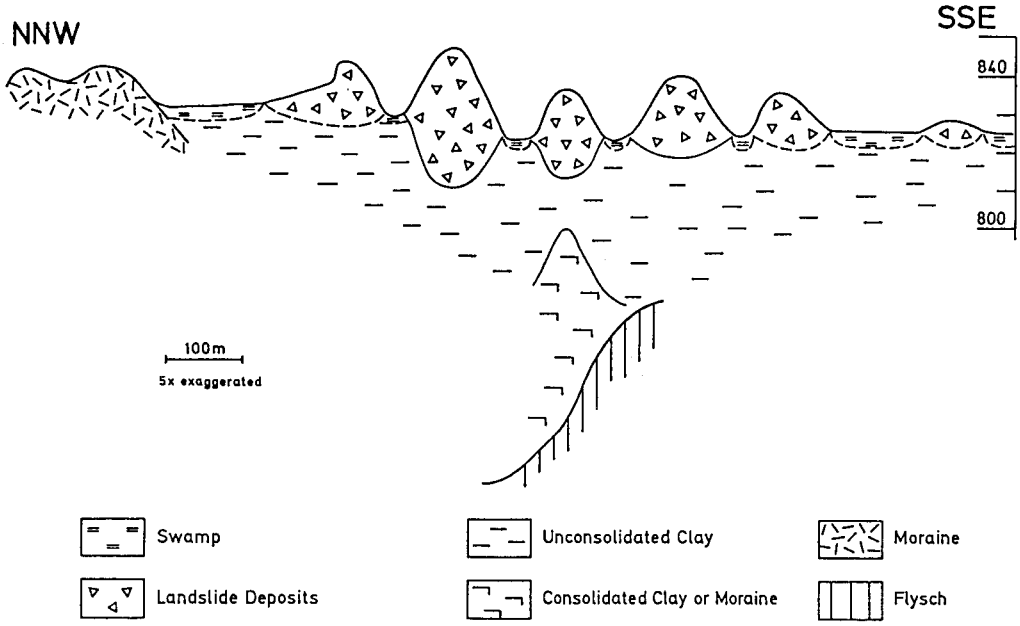

Fig. 3: Cross section through the Altenau landslide deposits. Indications about the deeper underground are made according to geophysical invetigations.

Also here the "fingers" have no underground connection beneath the lacustrine sediments. According to borings and geophysical investigations it has to be assumed that the sliding masses were deposited in or above the clays continuing only a few meters beneath the old plain surface.

It must be mentioned that in a digging about 50 m away from one ridge, lacustrine clays had been found with layers dipping nearly vertically downwards!

Interpretation of the field observations

The field observations in Marquartstein and in Altenau show some analogies concerning the depositions of the masses. Whereas a typical landslide will produce normally a more or less coherent pile, here radial concentric fingerlike ridges without any connection in the underground are found.
It can be assumed that the depositions are the product of a rapid mass movement. The masses moving downhill must have hit an easily displaceable ground surface at the valley floor. In Marquartstein the plain is made up by lacustrine clays which according to geophysical investigations are sedimented partly above consolidated clays or moraines, or partly above gravels. In Altenau the sediments forming the surrounding plain are composed of unconsolidated lacustrine clays. The landslide masses obviously pushed these sediments partly apart and intruded them like a snow-plough. The sudden load on the water saturated materials might have caused an excess porewater pressure reducing the friction to nearly zero.
This displacement theory can explain the steep dip of the layering found in lacustrine clays near the Altenau deposits and also the existence of gravel on top of the sliding mass in Marquartstein.
Nevertheless this theory can not sufficiently explain the special morphology with radial concentric ridges around the landslide scar. It does not seem conceivable that a fast mass movement diverges at the toe of the hill in such a way that the most exterior ridges are deposited nearly in opposite directions. Also the phenomenon of the interruption of the ridges does not have a plausible explanation. The steep cross sections may be explained by the "snow-plough" mechanism, but the surrounding sediments should still show some morphological signs of a ridge-parallel accumulation. In the field there are no signs of such an accumulation.

Outlook

Much research is done on mechanics and reach of rapid mass movements but only little attention is payed to the aspect of the "landing strip". As this might have a decisive influence on rapid mass movements there is important need of further research on that point. The described examples favour the theory that the special mechanical properties of the loose sediments on the valley floor can produce the described features can originate. It is not known whether such phenomena have been seen being created nowadays. If the pore pressure is be responsible for a reduction of the friction almost to zero, this would be an important factor not to be neglected at future reach estimations.
To approach to a solution of the "finger deposition problem" a physical model will be built. It will be tried to reproduce the phenomena by variation of the mechanical properties of a sliding mass as well as of a mass simulating the lacustrine sediments on the valley floor.
The problem of the impact of a landslide on water saturated sediments was recently also reported in different circumstances and morphological manifestations by ABELE

(1991). He had found characteristical sediments in the surroundings of some large rapid landslides caused by the displacement of gravel by the landslide-impact. The completely unstratified sediments are made up of sandy clay with gravel components showing a distinct upward grading. ABELE found such sediments at Flims, at Köfels and at Tschirgant. For the latter it is assumed that the landslide hit the water saturated sediments of the river Inn valley wrapping these sediments partly into the sliding masses. Here also the excess porewater pressure might have been responsible for the reduction of the friction. That means the general problem seems to be not as rare as the morphological phenomena reported before. As far as is known up to now nobody has described similar morphological manifestations or even a recent deposition of this kind.

References

ABELE, G. (1974): Bergstürze in den Alpen.- Wiss. Alpenvereinshefte, **25**, 165 S., München.

ABELE, G. (1991): Durch Bergstürze mobilisierte Muren und durch Muren transportierte Bergsturzmassen.- Jahresber. 1989/90 d. Österr. Geogr. Ges., Zweigverein Innsbruck, 33-39, Innsbruck.

HEIM, A. (1932): Bergsturz und Menschenleben.- Vjschr. Naturforsch. Ges. in Zürich, 77, Beibl. 20, 1-218, Zürich.

Gravitational Mass Movements and Resedimentation in Applied and Fundamental Geology

Mouvements en masse gravitaires et ressédimentation en géologie appliquée et fondamentale

C. RAVENNE, C. PONSOT-JACQUIN

IFP
BP 311, 92506 Rueil-Malmaison - France
Tel. (33) 1 47 52 66 47 - Fax (33) 1 47 52 70 67

Abstract

After a description of works dedicated to gravitational deposits and experiments modeling gravitational processes, this paper emphasizes resedimentation aspects. Then the authors review new techniques available for the observation of gravitational phenomena. Different processes involved in these phenomena are listed.
New needs in fondamental and applied geology are discussed and the environments where gravitational movements take place are presented. Four examples are mentioned and, finally, the authors pay attention to the remaining problems.

Résumé

Après une description de travaux consacrés aux dépôts gravitaires et d'expériences de modélisation de processus gravitaires, cet article met en évidence les aspects liés à la ressédimentation. Les auteurs traitent des nouvelles techniques disponibles pour l'observation de phénomènes gravitaires. Différents processus impliqués dans ces phénomènes sont passés en revue. De nouveaux besoins en géologie fondamentale et appliquée sont détaillés et les environnements dans lesquels les mouvements gravitaires apparaissent sont présentés. Quatre exemples sont mentionnés et, finalement, les auteurs insistent sur les problèmes qu'il reste à résoudre.

Present Stage

Gravitational Mass Movements occur in all the geological environments from continental (mountains, lacustrine, fluvial) to shallow marine, shelf, slope and deep marine settings in both passive and active margins.

a) Around the 60-70's, a lot of works have been done concerning the **Descriptive Aspects** of gravitational deposits and especially about facies classification and types of systems by numerous authors such as Bouma A.H., Mutti E., Walker R.G., Normark W.R..

These descriptive papers concerned mostly the resulting redeposited units. The 80's were a time for using and testing these classifications. Today, some of them are improved or questionned and new papers are coming out on this subject (Guibaudo G., Kolla V., Mutti E., Pickering K.T., Stow D.A.V., Walker R.G.).
Significant studies were also leading in the 70 -80's on **Experiments** recreating gravitational processes (Middleton G.V., Walker R.G., Mc Cave I.N., Beghin P., Ravenne C.). These studies allowed the different types of gravitational transports to be characterize (debris flow, mass flow, turbidity current, and slumping). For each of these categories, stages and subdivisions were described from the experiments, helping to a better understanding of the deep water sediments organization.

b) Improvements on the understanding of the gravitational processes are still **needed**, not only from an academic point of view, but mostly for economical reasons: numerous oil fields were discovered and will be discovered within turbidites. From the environmental side, it is important to understand for instance slidings which could occur close to coastal towns (such as the recent sliding close to the Nice airport).

c) The **important points** for the sedimentologists and the oil industry are the **resedimentation aspects**. Numerous points need to be explicited such as the characteristics and differences between turbidites, contourites, even storm deposits; the recognition of the initial depositional profile; and the geometries of the sedimentary bodies. The knowledge of these criteria is fundamental in order to understand and determine the **traps**, whatever they are oil, gas or water traps, of stratigraphic or structural origin. The flow motions zones, the lateral heterogeneity processes within the deep water context are of prime importance for the geologist and the reservoir engineer.

New Data

a) Considerable progresses in the knowledge of gravitational movements and deposits appear now in relation with the **big improvement of** the used **techniques**: The improvement of processings allows better resolution of observation and brings to the recognition of bodies, morphological changes, density surges... that were not even suspected before (multifold, high resolution (3,5 kHz) seismic, 3D imaging, deep tow Sonar...).

b) Significant external and internal **Factors** influence the gravitational mass movements and the resulting sedimentary units (Figure 1):

- **Tectonic** effect is certainly one of the major of them, tectonic at a global scale as well as a local scale by diapirism, tilting and subsidence. It acts on different ways such as : -the erosional processes at the source, -the starting of the motions, -the available space for the sediments to accumulate, -the initial depositional profile of the receiving basin.
- The **Sea-Level** variations certainly have a big influence, even if it is not a quantified one; it appears for most of the geologists that the turbidites and deep water sediments occur mostly during lowstand periods.

- The **Climate** influences strongly the *environmental* conditions by modifications of the supply amount and the equilibrium profile, and by its role on the erosional processes. Climate seems also to play a major role on the *cyclicity* of the events (such as turbidites pulsations) as well on the continent, the platform, the shelf, as on the deep water environments. The sequence stratigraphy tool allows the recognition of several orders of cyclicity and the climate would be of prime importance especially for the lower ones (cf. Milankovitch theory on the orbital cycles).
- The quantity and type of **supply** have also to be taken into account, even if they are strongly related to the three above factors. The quantity and induration of the removed materials, the distance from the source, the type of source, the type of "feeding" (canyon, delta, slumping...) are as much influencing supply features.
- The **morphological** criteria of the transitory and receiving areas should not be neglected. The equilibrium profile and its potential breaks depend in particular of the plateform width, gradient and stability, of the slope gradient,and of the size and shape of the basin.

As previously mentionned, the **sequence stratigraphy** use leads to a new approach in the reconstitution of the depositional events especially by bringing the notion of cyclicity.
Tectonic and climatic constraints, rates of influx, modification of base level... are as much causes of these cycles. These factors act at different time scales, in a very simplified way, it could be said that global tectonics and sea level changes would overprint the higher orders, climate and supply the lower's; but an interaction of all has always to be kept in mind.
The next step in the understanding of the causes is the recognition of the **allocyclic** (internal) versus **autocyclic** (external) events. Until now, the focus was mostly on the autocyclicity such as lobes migration, avulsion, abandonment.

c) The use of these new data already results in a **new way** of considering the mass movements sediments.
Several examples of these new approaches can be given :

- Even if they are preferentially deposited during lowstand periods, turbidites may also occur during ravinement period in **transgressive** phase (Kolla V., 1993).
- Some **tidal** influences may overprint the last stages of redeposition of some fine grained turbidites.
- The **carbonate** bioclastics turbidites can develop geometries similar to their siliciclastic counterparts (Jacquin T. *et al.*, 1991).
- Because of these new data and techniques, the differentiation between **storm deposits** versus turbidites will certainly be improved as well as the differences between turbidites and **contourites**.

Needs

The needs are investigated by advanced research in applied and fundamental geology.

The **Quantification** aspects are of two types :

1) **descriptive** such as the size, shape i.e. the *geometry* of the sedimentary units as well as the *facies* characteristics, classification and organization.
2) quantification of the **parameters** by experiments ; the parameters can be either dynamic or of external constraints.

The **Modeling** approach concerns mostly the Reservoir and can also be of two types :

1) **deterministic** i.e. many complex processes lead to one end.
2) **stochastic** i.e. a set of circumstances may lead to different outcomes which have a same probability of occurence.

In a **fundamental research** point of view, the modeling will be mostly a tool for the recognition, quantification and effects of the constraints.

In an **applied approach**, the modeling will concern the reservoir characteristics such as bodies geometry and connectivity, permability barriers, facies heterogeneity repartition. The principal technique in reservoir modeling is the use of geostatistical tools.

All types of reservoirs will gain from the use of modeling; the petroleum industry, of course, and more specifically the production aspect of oil & gas, but also the environmental domains for aquifer reservoirs or for underground storages.

Modeling is really a nowadays subject of studies and numerous teams especially petroleum related teams, are actually working on modeling oil fields. A new effect is that the reservoir engineer has to work in close relation with the geologist because the interconnectivity and the complementarity of the two sciences are now recognized.

Concerned depositional environments

The **Continent** : the mass movements on land concern mostly the nature of the supplies, the erosional features, and the transport processes. But some mass deposits also occur on land by avalanches, by sliding, within lakes, even in relation with earthquarkes.

The erosional and transport processes of mass moved materials continue on the **shallow marine** environment, with differentiation between periods of high and low relative sea level. The lowstand would be for instance the time of shelf erosion with creation of canyons, the highstand a time when clastics will be trapped by building thick shelfal units.

Some relatively deep lakes can also be considered as shallow marine environment with deposition of sediments by mass movement events.

During late lowstand and transgressive systems tracts, turbidites can be deposited by ravinement on the shelf and as shingled turbidites on the toes of some prograding clinoforms.

The **slope** zone is of course one of the main area for mass movements effects. The slope breaks can be multiple on either passive and active margins and they can be considered as as much hydraulic jumps.

Slope areas can be a transitional zone for the materials that will be resedimented downdip. They would present in that case mostly erosional features : canyons, scars, slumps.
Some materials can also be deposited in such environment, for instance during highstand periods, muddy sediments will fill the canyons (ex : the subactual Indus canyon).
The base of the slope is a significant zone for deposition of mass moved sediments : it is frequent to find there debris flows, mass flows, slumps, even so-called ponded lobes (Nelson C.H.).
The **rise** and **proximal abyssal plains** are a privileged zone for gravitational materials to sediment. They will be deposited either on the proximal zone close to the slope toe or they can reach significant distances on the abyssal plains in relation with the (sequence stratigraphy) timing of deposition and the amount and types of supplies (example of the quaternary Indus deep sea fan reaching 3000 km in length).

Cases studies

We will illustrate the transport and redeposition processes with three seismic and one outcrop case studies.
On a margin passive context, the **Indus Fan** displays clearly the influence of relative sea level changes at a very large scale.
The french **Cap Ferret** example illustrates a case of very complex morphology (multiple plateform) with both longitudinal and transversal influxes. Huge mass gravitational events and different orders of remobilization have been there observed.
In a context of carbonate turbidites, the **Eleuthera Fan** is an example for multiple feedings by both a canyon and great mass slidings affecting the Bahamas escarpment. Megaturbidites have been observed and seem to be very similar to the silisiclastic Pyrenean ones (Labaume et al., 1985).
The **Annot Sandstones** is an outcrop example which could display allocyclic deposits. The experiments carried out by P. Beghin have served to explain the typical Annot deposits, the so-called "granules" bars. (Figure 2).

Remaining Problems

Numerous cases studies need to be **reinterpreted in a sequence stratigraphy framework**. The units have to be reconsidered as sedimentary bodies and not only as isofacies units, they have to be positionned within the sequential orders and the different phases of relative sea level variations. The goal of such reinterpretation is also very applied: the knowledge of the organization of the different lithofacies within a potential reservoir body will greatly help for the permeability - porosity variabilities; the deduced potential geometry of the reservoir bodies by sequence stratigraphy analysis will be of prime importance for the knowledge of the extension of the reservoir, the connectivity of the bodies and the permeability barriers.
Direct measurements are still insufficient, very few collectors such as turbidimeters or currentometers are permanently installed.

More studies should **focus on the quantification and modeling** aspects of the mass movements processes and deposits. Field work itself should be reconsider in order to quantify the observed data. Some experiments are still needed, especially concerning the large scale deposits in deep water conditions.
Autocyclic versus allocyclic events are still to be differentiated in relation with the different sequential orders.
Gravitational mass movements knowledges are a very actual **subject in full evolution** and improvement.

References

Beghin P.1992, Modelisation physique et simulation numérique de l'experience BADFEX - Rapport d'Etude pour IFP, Cemagref, confidential, Janv.1992.

Beghin P.1988, co-author with Laval A., Cremer M., Ravenne C. Density Surges : two dimensional experiments - Sedimentology (1988), vol. 35, pp. 73-84.

Bouma A.H., 1962, Sedimentology of some flysh deposits: a graphic approach to facies interpretation. Elsevier.

Bouma A.H., 1972, Recent and ncient turbidites and contourites. Trans. Gulf Coast Ass. Geol. Soc. vol. 22, pp. 205-221.

Guibaudo G. 1992, Subaqueous sediment gravity flow deposits: practical criteria for their description and classification - Sedimentology (1992), vol.39, pp. 423-454.

Haldorsen H. H. & Damsleth E., 1990 : Stochastic Modeling, JPT, April 1990, pp. 404-412.

Jacquin Th, Vail P. & Ravenne Ch. 1991, Systems tracts and depositional sequences in a carbonate setting: study of continuous outcrops from plateform to basin at the scale of seimic sections - Mar. Petrol. Geol. vol. 8, pp. 122-139.

Kolla V. 1993, Lowstand deep water siliciclatic depositional systems: characteristics and terminologies in sequence stratigraphy and sedimentology - Bull. Cent. Rech. Expl. Prod. ELF- Aquit., vol. 17, n° 1, pp. 67-78.

Kolla V. & Perlmutter M.A. 1993, Timing of turbidite sedimentation - Mississippi Fan - AAPG. Bull. vol. 17, n° 7.

Labaume P., Mutti E. & Seguret M. 1985, Megaturbidites : a depositional model from the Eocene of the SW Pyrenean foreland basin, Spain - Geo-Marine Letters vol. 7, pp. 91-101.

Mac Cave I.N. 1982, Erosion and deposition by currents on submarine slopes - Bull. Inst. Geol. Bassin d'Aquitaine, vol. 31, pp. 47-55.

Middleton G.V. 1966, Experiments on density and turbidity currents - Can. J. Earth Sci., vol. 3, pp. 523-546 & 627-637.

Milankovitch M. 1941, Kannon der Erdberstrahlung und seine anwendung auf das eiszeitenproblem - Royal Serb. Acad. Spec. Pub 133, pp. 1-633.

Mutti E. & Ricci Lucchi F. 1975, Turbidites facies and facies associations - IX Congress Int. Assoc. Sedimentologists, Guidebook, Nice, France.

Mutti E. et al., 1985 - Stratigraphy and Facies characteristics of the Eocene Hecho group turbidite systems, south central Pyrenees, VI European meeting of the Int. Assoc. Sedimentologists, Guidebook, Lleida, Spain.

Nelson et al. 1978, Thin bedded turbidites in modern submarine canyons and fans - in Sedimentation in submarine canyons, fans and trenches, Stanley & Kelling eds.

Normark W.R.1978, Fans valleys, channels and depositional lobes on modern submarine fans: characters for recognition of sandy turbidite environments - Bull. Assoc. Petr. Geol., vol. 62, pp. 9212-931.

Normark W.R. & Piper D.J.W. 1984, Navy Fan, California borderland: growth pattern and depositional processes - Geo-Marine Letters, vol. 3, pp. 101-108.

Pickering K.T., Hiscott R.N. & Hein F.J. 1989, Deep marine environments, Unwin Hyman.

Ravenne C. & Beghin P. Apport des Expériences en canal à l'interprétation sédimentologique des dépôts de cônes détritiques sous-marins - Revue de l'IFP, vol. 38, n°3, Mai-Juin 1983. pp. 279-297.

Stow D.A.V. & Piper D.J.W. 1984, (eds) Fine-grained sediments : deep water processes and facies - Geol, Soc. sp. pub. 15, Blackwell.

Walker R.G. 1975, Generalized facies model for resedimented conglomerates of turbidite association - Bull. Geol. Soc. Am., vol. 86, pp. 737-748.

Estimating debris flow parameters

Estimation des paramètres dans les coulées de débris

D. RICKENMANN

Swiss Federal Institute for Forest, Snow and Landscape Research
CH-8903 Birmensdorf - Switzerland
Tel. (41) 1 739 21 11 - Fax (41) 1 739 24 88

Abstract

A number of theoretical approaches have been proposed to treat the debris flow process. In view of the scarce field data available on debris flows, a simple avalanche model is presented to estimate the flow velocity, and it is applied to some debris flows that occurred in Switzerland in 1987. The model is based on two friction components. With observed runout distances and velocity estimates from field evidence, possible combinations of the two parameters are determined which best describe the actual field event. The results are compared with other data on debris flows and similar processes. Finally, an empirical formula is proposed to estimate the magnitude of a debris flow event.

Résumé

Un certain nombre d'approches théoriques ont été proposés pour prendre en compte les mécanismes des laves torrentielles. Compte tenu du peu de données de terrain disponibles, un modèle simple permettant d'estimer la vitesse des avalanches est présenté. Il est appliqué à quelques laves torrentielles qui se sont produites en Suisse en 1987. Le modèle repose sur deux coefficients de frottement. Différentes combinaisons possibles des deux paramètres sont déterminées de telle sorte qu'elles correspondent le mieux aux évènements réels qui sont décrits à l'aide des distances d'arrêt observées et des vitesses estimées d'après des indices de terrain. Les résultats sont comparés avec d'autres données sur les laves torrentielles et sur des phénomènes similaires.
Enfin, une formule empirique est proposée pour estimer l'ampleur d'une lave torrentielle.

Introduction

Debris flows are an important process of massive sediment transport in mountain torrents. Particularly the fast moving fronts may be destructive along the river course or in the fan area. Therefore it is important to estimate the peak discharge and the velocity of the largest debris flow pulses (Rickenmann, 1993). Although there are a number of theoretical approaches to describe the behaviour fo debris flows, practical methods are still rather limited (Costa, 1984; Meunier, 1991; Takahashi, 1981).

A simple avalanche model is applied to some of the numerous debris flow events of the summer 1987 in Switzerland (Haeberli et al., 1991). The model allows to determine the velocities along the flow path and to estimate the runout distance. To delineate the deposition zones of debris material on the fan, knowledge of the event magnitude is essential (Rickenmann, 1993). An empirical formula is developed to estimate a maximum possible magnitude of a debris flow event.

Model for debris flow velocity

Takahashi (1981) proposed a theoretical method to estimate the runout distance of a debris flow, based on energy or momentum conservation. A similar model had earlier been developed for snow avalanches (Salm, 1966). These models may be used when there is a fairly well defined change in slope from the transportation reach to the deposition zone. Based on a similar approach, Körner (1980) presented a model to compute the velocity development along the whole avalanche path. As in earlier works on snow avalanches (Salm, 1966), it is assumed that the motion is mainly governed by two frictional components: A sliding friction coefficient and a turbulent friction slope that is determined by a Chezy-type relation. This allows to account for both solid-to-solid and fluid like shear stresses. The resulting equation gives the velocity v_{i+1} at the end of a segement of constant slope, if the input velocity v_i from the previous segement is known:

$$v_{i+1} = [v_{ei}^2 - (v_{ei}^2 - v_i^2) \exp(-2\, \Delta s_i / k_2)]^{1/2} \qquad (1)$$

with :

$$v_e = [H\, C^2 (\sin\theta - \mu \cos\theta)]^{1/2} \qquad (2)$$

$$k_2 = HC^2/g \qquad (3)$$

where v_e: maximum velocity on a path of constant slope, Δs: length of the segment, H: flow depth, C: Chezy friction coefficient $[m^{1/2}/s]$, θ: slope angle, μ: sliding friction coefficient, g:gravitational acceleration, and the parameter k_2[m] accounts for turbulent friction effects.

Theoretically, the two parameters $\mu$and $k_2$can assume different values for each segment. However, since there is not enough detailed data available, they are generally taken as constant over the whole flow path. Perla et al. (1980), using the same model, interpret the parameter k_2 as mass-to-drag ratio, and they discuss the effects of these two components on the value of k_2.At concave transitions in slope, Perla et al. (1980) introduced a momentum correction, which is also applied in our case (Rickenmann, 1990).

The model is applied here to 8 debris flow events that occurred in the summmer 1987 in Switzerland. To determine possible combinations of the two friction parameters μ and k_2, two different criteria are used: Either there were velocity estimates at several cross sections, or the stopping point is well defined, if the flow deposited all the material without any major obstructions in the depositional area. From

superelevation measurements in the field the velocity could be estimated for three events (cases no. 1, 3 and 4 in Fig. 1); in one case (no. 2) the velocity head was used to obtain velocity estimates. For all the other events (cases no. 5 to 8) the stopping point (where v = 0) was selected as criterion two compute the appropriate model parameters.

In principle, there are many possible combinations of μ and k_2 that satisfy the relatively poor field data. For given flow conditions, for example, the same runout distance can be obtained by different combinations of μ and k_2; the choice of a larger μ value generally requires an increase in k_2, resulting in higher flow velocities. An additional restriction is therefore introduced by limiting the maximum velocity to 30 m/s. Values for debris flows reported in the literature range up to about 20 m/s, but they were obtained at slopes below about 20° (Costa, 1984). The results of the model computations for the Swiss debris flow events are tabulated in Rickenmann (1990).

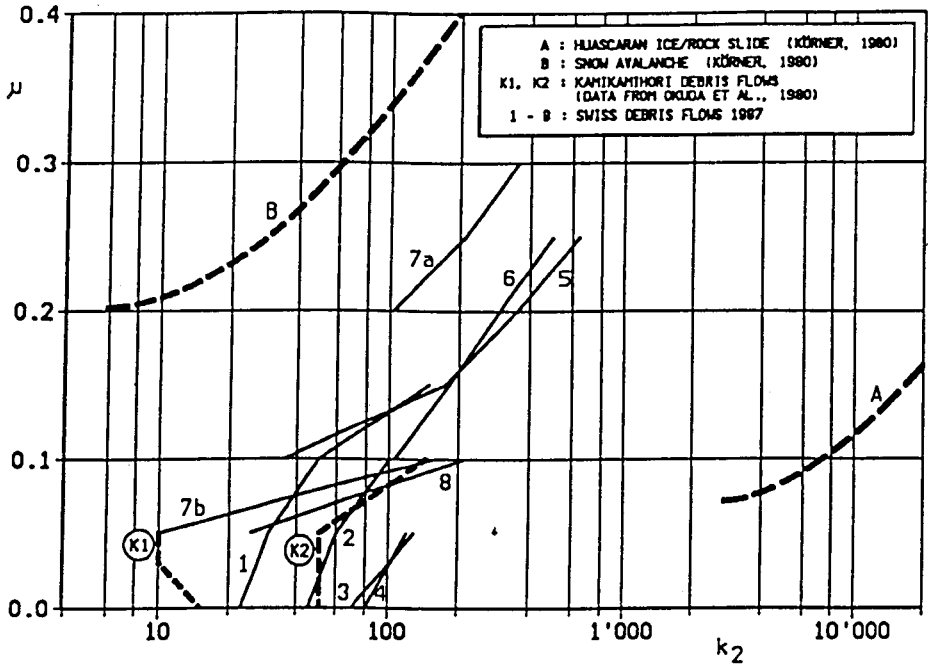

Fig. 1: Resulting combinations of the model parameters m and k_2, for the Swiss events (no. 1 to 8) and other data on derbis flows and similar processes.

The resulting parameter combinations are plotted in Fig.1, together with data from other events. Line A represents data for the 1970 ice/rock slide of Mount Huascaran (Peru), and line B gives possible parameter combinations for a snow avalanche with measured velocities (both lines taken from Körner, 1980). The lines K1 and K2 were determined from data of a japanese debris flow observation station. In a study of Okuda et al. (1980) velocity measurements are given together with the longitudinal

profile for two debris flows of Aug 14, 1976 (K1) and July 19, 1976 (K2). Using this information, parameter combinations for K1 and K2 were backcalculated with the model. As an example, the observed velocity of the Kamikamihori debris flow of July 19, 1976 is shown in Fig. 2 together with model velocities calculated for different parameter combinations.

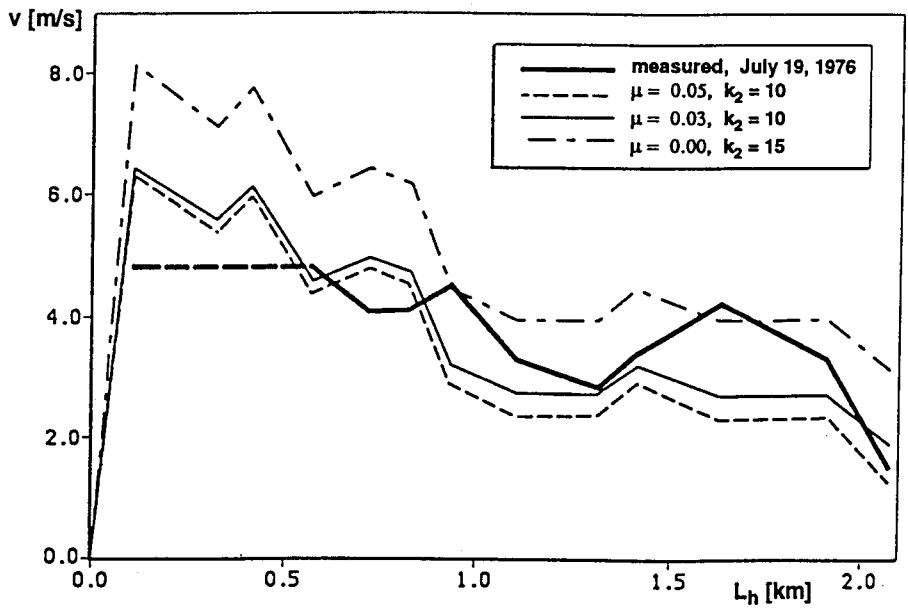

Fig. 2: Calculated development of debris flow velocity in Kamikamihori valley in Japan, in comparison with field data of Okuda et al. (1980). Calculated parameters correspond to line K2 in Fig. 1.

It is interesting that the lines K1 and K2 plot within the same region in Fig. 1 as is indicated by the lines representing the Swiss data. With these events, the volumes involved in one single debris surge was of the order of 1'000 to several 10'000 m^3. The Huascaran slide (line A) was much larger (volume of about $5*10^7$ m^3) and had an estimated flow depth of about 100 m (Körner, 1980); although the debris stream contained some (melting) ice, the material composition is in principle similar to a debris flow. The volume of the snow avalanche (line B) was about 10'000 m^3; in this case the different material density and friction characteristics must be be the reason, why the parameters lie away from the region for the debris flow events.
Considering the Swiss events only, there is a tendency for flows with a larger catchment area at the point of initiation (cases no. 1, 2, 3, 4, 7b and 8) to require smaller μ values than the events with smaller catchment areas (no. 5, 6 and 7a). This fact may be explained with larger amounts of water available in the main channel to dilute the grain mixture of the debris flow. A dilution will change the rheological

properties of the grain-water mixture, reducing its shear strength (Costa, 1984). In the presented model, the parameter μ could partly account for the shear strength characteristic of debris flows.
Alean (1984) determined possible parameter combinations for 19 ice avalanches in the Alps. His best-fit parameters are generally larger (μ up to 0.7, k_2 up to 100'000) than for the debris flows. He found that both μ and the mean slope tend to decrease with increasing ice volumes. A similar conclusion results from the analysis of the numerous Swiss debris flow events (Zimmermann, 1990). Thus it appears that smaller μ values are associated with smaller mean slopes and probably with larger volumes of debris flow material. A similar dependence is also observed for rock slides (Scheidegger, 1973).
It should be pointed out that the runout distance can only be modeled if the μ value is larger than the actual deposition slope. If μ approaches this slope the computed runout distance is very sensitive to small changes in m. With the events no. 1 - 4, the main objective was to model the velocity development; therefore also μ values equal to zero were used.

Magnitude of debris flow events

For hazard mitigation, a serious problem is the delineation of dangerous zones on the fan which may be impacted by debris flow deposits. For the evaluation of the most important debris flow parameters it is essential to estimate a possible event magnitude (Rickenmann, 1993). As a function of the event nagnitude, a value for the peak discharge may then be estimated (Mizuyama et al., 1992).

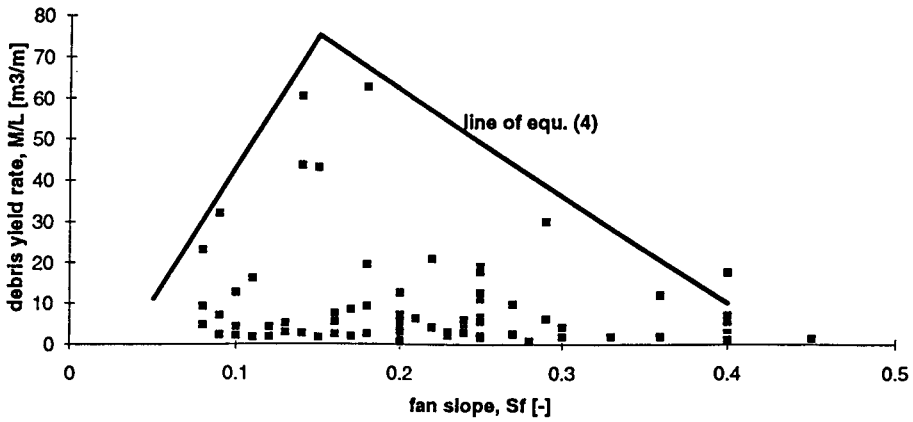

Fig. 3: Debris yield rates for Swiss debris flow events of 1987, plotted against fan slope.

Based on data of 80 debris flow events that occurred in the Swiss Alps in 1987, the following empirical formula has been developed to estimate an upper limit of the expected event magnitude:

$$M = (640\, S_f - 21)\, L \qquad 0.05 < S_f <= 0.15 \qquad (4a)$$

$$M = (110 - 250\, S_f)\, L \qquad 0.15 < S_f <= 0.40 \qquad (4b)$$

where M is the possible maximum event magnitude in [m^3], S_f is the fan slope, and L in [m] is the channel length of the expected debris flow path.
The basis for the derivation of equ. (4) is shown in Fig. 3. For fan slopes increasing up to 15%, the increasing maximum debris yield rates, M/L, represent increasing specific erosion volumes that are responsible for building up steep fans. With fan slopes above 15%, however, the decreasing catchment size seems to become more dominant; smaller volumes of surface and subsurface water may be the reason for decreasing maximum debris yield rates in this case.

Conclusions

A simple model originally developed for snow avalanches has been applied to Swiss debris flows. The resulting parameter combinations are in agreement with data from measured velocities of two Japanese debris flows. A prediction of the runout distance is only possible if μ is larger than the deposition slope. For a practical application of the model more precise information on the values of the two parameters is needed. Hydraulic model tests could be performed to examine how the parameters depend on material characteristics and bed roughness.
An empirical formula has been proposed to estimate the debris flow event magnitude in terms of the mean fan slope and the length of the active debris flow path.

References

Alean, J. (1984): Untersuchungen über Entstehungsbedingungen und Reichweiten von Eislawinen. Mitt. der Versuchsanstalt für Wasserbau, Hydrologie und Glaziologie, ETH Zürich, Nr. 74, 217p.

Costa, J.E. (1984): Physical geomorphology of debris flows. In Developments and applications of geomorphology, eds. Costa and Fleisher, Springer-Verlag, Berlin and Heidelberg, p.268-317.

Haeberli, W., Rickenmann, D., Rösli, U., Zimmermann, M. (1991): Murgänge. Ursachenanalyse der Hochwasser 1987, Ergebnisse der Untersuchungen. Mitt. des Bundesamtes für Wasserwirtschaft, Bern, Nr. 4 = Mitt. der Landeshydrologie und -geologie, Bern, Nr. 14, p.77-88.

Körner, H.J. (1980): Modelle zur Berechnung der Bergsturz- und Lawinenbewegung. Proc. Int. Symposium Interpraevent, Bad Ischl, A, p.15-55.

Meunier, M. (1991): Eléments d'hydraulique torrentielle. Cemagref, Etudes Montagne no. 1, Grenoble, France, 278p.

Mizuyama, T., Kobashi, S., Ou, G., 1992: Prediction of debris flow peak discharge. Proc. Int. Symp. Interpraevent, Bern, Bd. 4, p.99-108.

Okuda, S., Suwa, H., Okunishi, K., Yokoyama, K., Nakano, M. (1980): Observations on the motion of a debris flow and its geomorphological effects. Z. Geomorphol., Suppl. Bd. 35, p.142-163.

Perla, R., Cheng, T.T., McClung, D.M. (1980): A two-parameter-model of snow avalanche motion. J. Glaciol., 26 (94), p.197-207.

Rickenmann, D. (1990): Debris flows 1987 in Switzerland: modelling and fluvial sediment transport. Proc. Int. Conf. on Water Resources in Mountainous Regions, IAHS Publ. no. 194, p. 371-378.

Rickenmann, D. (1993): Beurteilung von Murgängen. Herbstkurs Wildbäche, Forstl. Arbeitsgruppe für Naturgefahren, unveröff. Kursunterlagen, 12p.

Salm, B. (1966): Contribution to avalanche dynamics. Proc. Int. Symp. on Scientific Aspects of Snow and Ice Avalanches, Christchurch, N.Z., IAHS Publ. No. 69, p.199-214.

Scheidegger, E.A. (1973): On the prediction of the reach and velocity of catastrophic landslides. Rock Mechanics, 5, p.231-236.

Takahashi, T. (1981): Estimation of potential debris flows and their hazardous zones; soft countermeasures for a disaster. J. Natural Disaster Science, 3(1), p.57-89.

Zimmermann, M. (1990): Debris flows 1987 in Switzerland: Geomorphological aspects and meteorological conditions. Proc. Int. Conf. on Water Resources in Mountainous Regions, IAHS Publ. no. 194, p. 387-393.

Current Status of the AVL Avalanche Simulation Model - Numerical Simulation of Dry Snow Avalanches

Etat actuel du modèle AVL de simulation des avalanches - Simulation numérique des avalanches de neige sèche

P. SAMPL

AVL List GmbH
Kleiststrasse 48, Graz - Austria
Tel. (43) 316 987 563 - Fax (43) 316 987 777

Abstract

This paper gives a short summary of the underlying physics, mathematical formulation and numerical treatment of a snow avalanche model developed at AVL, Graz, in co-operation with the Federal Service for Avalanche and Torrent control of Austria. A dense flow- and an aerosol part of the avalanche are distinguished. For each part a separate model has been established. The application of these models and the comparison of the results with observations are described as well as the intended coupling and further development of the models.

Résumé

Cet article présente de façon succincte les fondements physiques, la formulation systématique et le traitement numérique d'un modèle d'avalanche développé par AVL, à Gradz, en coopération avec le Service Fédéral Autrichien de Protection contre les Avalanches et les Torrents. Les parties dense et aérosol de l'écoulement de l'avalanche sont traitées de façon distincte. Pour chacune, un modèle spécifique a été développé. L'application de ces modèles et la comparaison des résultats avec des observations sont décrits ainsi que le couplage projeté et le développement futur des modèles.

Introduction

As alpine regions in Austria encounter more and more touristical and economical use, additional attention has to be paid to snow avalanches. Numerical simulations may be used to help the responsible authorities with hazard zoning and the design of defence structures. The most severe damages in Austria are caused by "dry" avalanches, as they attain high speeds and affect large areas. Therefore the described models were developed to simulate dry avalanches.

Physics of Snow Avalanches

Three different types of avalanches may be distinguished according to the following table:

Avalanche Type	wet	moist	dry
Snow Cover	soft	soft	hard
Particles	none, fluid	big, soft balls, cohesive forces	small, hard, pulverised particles, no cohesion
Motion	viscous flow	rolling, sliding	colliding particles
Distance between Particles	-	small, permanent contact	comparable to particle size
Interaction with Air	none	none	air drag leads to suspension - aerosol (Powder Avalanche)

For the dry avalanche the following sketch shows two different flow regimes: the 'dense flow regime': a system of dense packed, colliding particles near the ground; and the 'powder regime': particles suspended in air (aerosol) above the dense part of the avalanche.

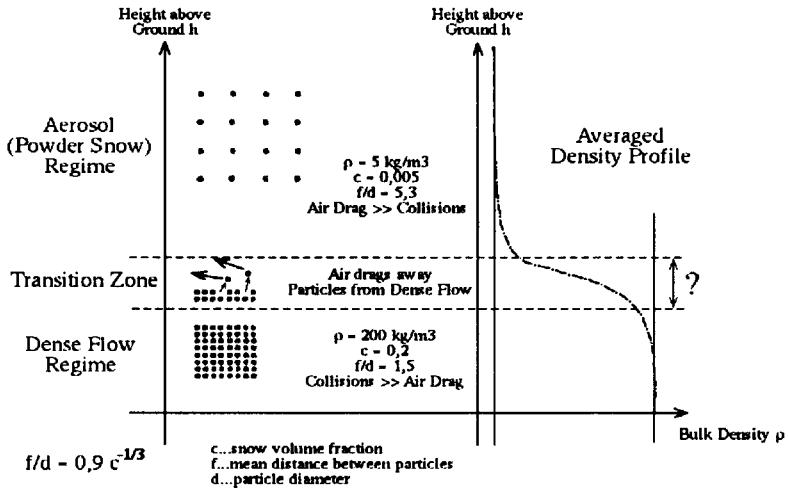

In the dense flow regime one can neglect the effect of air between the particles, the motion is mainly dependent on the collisions between the particles. These collisions lead to a highly fluctuating motion of the particles containing 'turbulent' energy.
The motion of the aerosol is governed by the turbulent motion of the air and the drag between the particles and the air. Gravitation is the motor of the motion in either regime.
In the 'transition zone' between these regimes effects of air drag and particle collisions are of the same order of magnitude. Particles pushed out of the dense packed region will be suspended because of speed differences between air and dense flow and because of air turbulence. Not much is known about this transition zone, so a 'dense flow model' and a 'powder snow model' have been developed separately as a first step towards a complete dry avalanche model.

Mathematical formulation

Dense flow model

Following the ideas of *Savage and Hutter (1991)*, a depth averaged formulation was used to describe the behaviour of the dense flow dry avalanche. It results from applying the mass and momentum balances on a granular material with Coulomb like both bed and internal friction. So the effect of particle collisions is represented by friction coefficients. Several assumptions simplify the problem: the density is taken to be constant, the stream wise velocity is uniform over the depth and the shear stress is linearly distributed over the depth. *Savage and Hutter* also drop some terms that are relatively small as the avalanche depth is small compared to its length. The resulting independent variables are the avalanche depth h and velocity u tangential to the surface. The following equations are a simple extension of the equations used by *Savage and Hutter (1991)* to two spatial dimensions:

t.....time
x_i.....terrain following co-ordinates (i=1, 2)
u_i.....velocity (i=1, 2)
h.....flow depth
n_z .....sine of inclination angle
n_i.....cosine of inclination angle in direction i
ρ.....avalanche density
g.....gravitational constant
τ_{wi}.....wall shear stress component
p_w .....static pressure at bottom
μ.....friction coefficient
κ_u .....surface curvature in direction of velocity

Conservation of Mass

$$\text{Euler:} \quad \frac{\partial h}{\partial t} + \frac{\partial (u_j h)}{\partial x_j} = 0$$

$$\text{Lagrange} \quad \frac{dh}{dt} = -h\frac{\partial u_j}{\partial x_j}$$

Conservation of Momentum

$$\rho\frac{\partial (hu_i)}{\partial t} + \rho\frac{\partial (hu_i u_j)}{\partial x_j} = \rho h\frac{du_i}{dt} = -\rho g h n_z \cdot \frac{\partial h}{\partial x_i} + \rho g h n_i + \tau_{wi}$$

$$\tau_{wi} = -p_w \cdot \mu\frac{u_i}{|u|}$$

$$p_w = \rho g h n_z + u_j u_j \kappa_u \rho h$$

The Lagrangian formulation is also given because it is used for the numerical simulation. The lateral shear stress is not yet included in this equations. In addition,

the internal friction coefficient is taken to be the same as the basal friction coefficient.

Powder avalanche model

The AVL powder snow model is based on the three-dimensional Reynolds-averaged Navier-Stokes equations for the turbulent flow of a air-snow suspension. The density of the suspension is calculated via the snow volume fraction c. Separate mass balances for the snow fraction and the suspension are used but only one momentum balance for the total air snow suspension. This implies that the two phases do not move relatively to each other. (This assumption is only valid if the slip velocity between the two phases is small, which may not be the case e.g. at strong streamline curvature.) The turbulent diffusion terms are modelled using the second-order k-ε-closure scheme *(Rodi, 1980)*.

t ..... time
x_i ..... co-ordinates (i=1,2,3)
u_i ..... velocity (i=1,2,3)
p ..... pressure
ρ ..... density
τ_{ij} ..... stress tensor (i,j=1,2,3)
η ..... viscosity
c ..... snow volume fraction
η_t ..... turbulent viscosity
k ..... turbulent energy (from k-equation)

overbar indicates averaged quantities,
primed quantities represent turbulent fluctuation parts;
indices: 1=air, 2=snow

Bulk Continuity

$$\frac{\partial \bar{\rho}}{\partial t} + \frac{\partial (\bar{\rho}\bar{u}_j)}{\partial x_j} = 0$$

Conservation of Snow Fraction

$$\frac{\partial (\rho_2 \bar{c})}{\partial t} + \frac{\partial (\rho_2 \bar{c}\bar{u}_j)}{\partial x_j} = \frac{\partial (\rho_2 \overline{c'u_j'})}{\partial x_j}$$

Bulk Momentum

$$\frac{\partial (\bar{\rho}\bar{u}_i)}{\partial t} + \frac{\partial}{\partial x_j}(\bar{\rho}\bar{u}_i\bar{u}_j) = -\frac{\partial \bar{p}}{\partial x_i} + \frac{\partial}{\partial x_j}(\bar{\tau}_{ij} - \bar{\rho}\overline{u_i'u_j'}) + \bar{\rho} g_i$$

$$\bar{\tau}_{ij} = \eta\left(\frac{\partial \bar{u}_i}{\partial x_j} + \frac{\partial \bar{u}_j}{\partial x_i}\right) - \frac{2}{3}\eta \frac{\partial \bar{u}_k}{\partial x_k}\delta_{ij}$$

Bulk Density

$$\bar{\rho} = (1-\bar{c}) \cdot \rho_1 + \bar{c} \cdot \rho_2$$

Eddy Viscosity Concept

$$-\bar{\rho}\overline{u_i' u_j'} = \eta_t \left(\frac{\partial \overline{u_i}}{\partial x_j} + \frac{\partial \overline{u_j}}{\partial x_i}\right) - \frac{2}{3}\left(\bar{\rho} k + \eta_t \frac{\partial \overline{u_k}}{\partial x_k}\right)\delta_{ij}$$

Eddy Diffusity Concept

$$-\rho_2 \overline{c' u_i'} = \frac{\rho_2}{\bar{\rho}} \frac{\eta_t}{\sigma_f} \frac{\partial \bar{c}}{\partial x_i}$$

The remaining equations of the turbulence model will be found in *Brandstätter et al. 1992)*. This model is valid strictly for the flow of two perfectly mixing fluids of different densities. Many experiments concerning powder snow avalanches are based on assuming similarity of such a flow with the flow of the air-snow suspension. So are the water tank experiments of *Beghin and Olagne (1991)*. They studied the flow of a dense salt solution down an inclined plane in a water tank. A comparison of their observations with results of the described model gave good agreement (see below; see also *Brandstätter et al. 1992*).

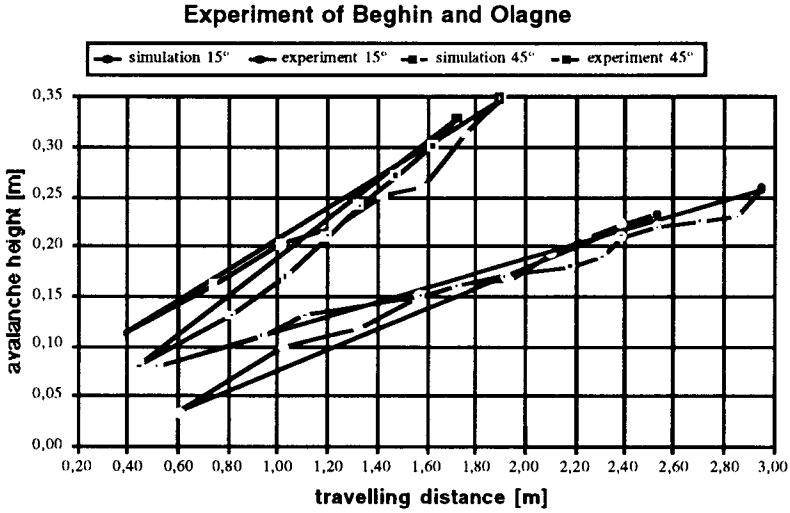

Numerical solution procedures

Dense flow model

A Particle-in-Cell method (PIC, *Potter, 1980*) is used to solve the two dimensional depth-averaged dense flow equations. Mass and momentum of the flow are represented by a large number of fluid particles. The movement of the particles is

prescribed by the Lagrangian dense flow equations given above. Avalanche depth and the terms on the right hand side of the equations are calculated using a triangular surface grid. The mass and momentum of each particle will be distributed to the neighbouring grid nodes. So each node is assigned an area, avalanche mass and momentum, as well as a resulting flow depth. The advantage of this method is that the information is found where the avalanche mass is located and that no numerical diffusion occurs which might be the case when using only a fixed Eulerian grid. A simulation using 10000 particles will take in the order of an hour on an IBM RS6000/580 workstation.

Powder snow model

The equations for the air-snow suspension are solved using a fixed 3D Eulerian grid and a procedure based on the SIMPLE algorithm (*Patankar, 1980*). A general co-ordinate transformation fits the grid to the surface. Linear equation systems are solved using a conjugate gradient method *(Bachler et al., 1991)*. A simulation involving 60000 grid cells and 1000 time steps will take about 40 hours on an IBM RS6000 workstation.

Application of the models

In 1984 a large dry avalanche hit the village of Ischgl, Tyrol, and killed one person. Figure 1 shows the observed area of avalanche impact. This avalanche event was simulated using both dense and powder avalanche models. In the 'pre-processing' of the simulation the geometry of the surface and the release area and the snow mass have to be specified. The geometry for all parts of Austria is available on disc from governmental authorities on a 50m x 50m rectangular grid. Where this grid was too coarse, data from maps were additionally digitised. The release area was determined by local avalanche experts, the released mass of the avalanche was approximately 60.000 tons. Two extreme cases were considered: taking the whole mass as dense flow avalanche and taking half of the mass as suspended powder avalanche. Snow entrainment was not considered. The bed friction coefficient for the dense avalanche simulation run was set to a value of 0,4 corresponding to a friction angle of 21,8 degrees. Figure 2 shows the avalanche deposition area as calculated with the dense avalanche model. Figure 3 shows the peak dynamic pressure resulting from the powder avalanche calculation. A short comparison of the observed and the calculated impact areas shows

(1) for the case of the dense flow simulation:

the dense flow avalanche track is reproduced correctly and the velocities (not shown here) agree well with observations *(Hufnagel, 1986)*. The area of deposition (Fig.3) does not correspond exactly to the observed area (Fig.1). The runout distance is highly dependent on the dry friction coefficient. Adjusting the friction coefficient according to the surface roughness may improve the result;

(2) for the case of the powder snow simulation:

at the last turn of the avalanche track a separation of the dense and the aerosol part was observed. The simulated powder snow avalanche follows completely the observed aerosol part. The observed dynamic pressure in the runout (Fig.3) is in the

same order as the observed pressure near location 'Parkgarage' *(Hufnagel, 1986)*. The powder snow avalanche doesn't stop but looses momentum very rapidly in the runout. The velocity is higher (up to 80m/s) and the density very much lower than for the dense flow avalanche.
One should expect a good qualitative and quantitative behaviour of the models if they are coupled and the constitutive law for the dense flow is improved. Anyhow, extensive testing has still to be done.

Conclusions and further development

Further development of the model will comprise the following steps:

(1) The use of spatially varying surface friction coefficients depending on the surface roughness, snow entrainment and, if necessary, 'filling' of the surface roughness as the dense flow avalanche passes.

(2) The use of refined constitutive laws for the dense avalanche flow. That may require the calculation of 'turbulent energy' of the fluid particles to calculate bottom and internal shear stress. Also the density of the dense flow will be a function of turbulence.

(3) The coupling of the dense and powder avalanche models. A formulation for the mass transfer from the dense to the suspended phase will be needed. This mass transfer is likely to be a function of turbulence in both dense flow and suspended flow, of the velocity difference between the two parts and the vertical snow fraction gradient in the suspension at the dense flow surface.

(4) To find the relationships between velocity, turbulent energy, surface roughness, flow depth and density for the dense flow avalanche, experimental results would be highly welcomed, but very hard to get. An other way could be the 'direct simulation' of a small part of the dense avalanche as a system of hard, nearly elastic, colliding snow grains (comparable to 'Molecular Dynamics Simulations'). It must be examined, however, whether this task is computationally achievable.

References

Bachler, G., Brandstätter, W., Ennemoser, A., Ennemoser, C., Mayer, R., Pachler, K., Steffan, H. und Wieser, K., FIRE Instruction Manual Version 3.3, AVL-List GmbH., Graz, 1991.

Beghin, P., Olagne, X., Experimental and theoretical study of the dynamics of powder snow avalanches, Cold.Reg.Sci.Technol. 19, pp 317-326, 1991.

Brandstätter, W., Hagen, F., Sampl, P., Schaffhauser, H., Dreidimensionale Simulation von Staublawinen unter Berücksichtigung realer Geländeformen, Zeitschrift der Wildbach- und Lawinenverbauung Österreichs 120, pp 107-137, Oktober 1992.

Hufnagel, H., Diplomarbeit, WLV Imst, 1986.

Patankar, S., V., Numerical Heat Transfer and Fluid Flow, McGraw-Hill Book Company, New York, 1980.

Potter, D., Computational Physics, Wiley, New York, 1980.

Rodi W., Turbulence Models and their Application in Hydraulics, Int.Assoc.for Hydraulic Research (IAHR), Delft, 1980.

Savage, S., B., Hutter, K., The dynamics of avalanches of granular materials from initiation to runout. Part I: Analysis, Acta Mechanica 86, 201-223, 1991.

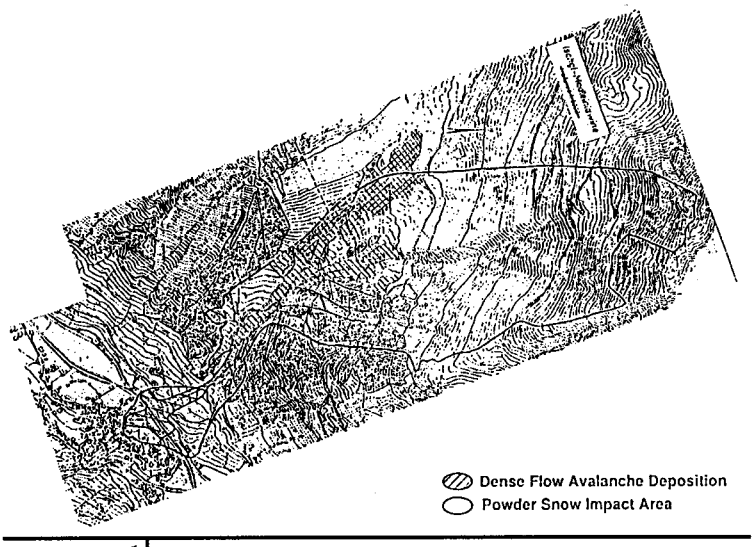

Madlein Avalanche, 1984
Observations (Hufnagel 1986)

Figure 1

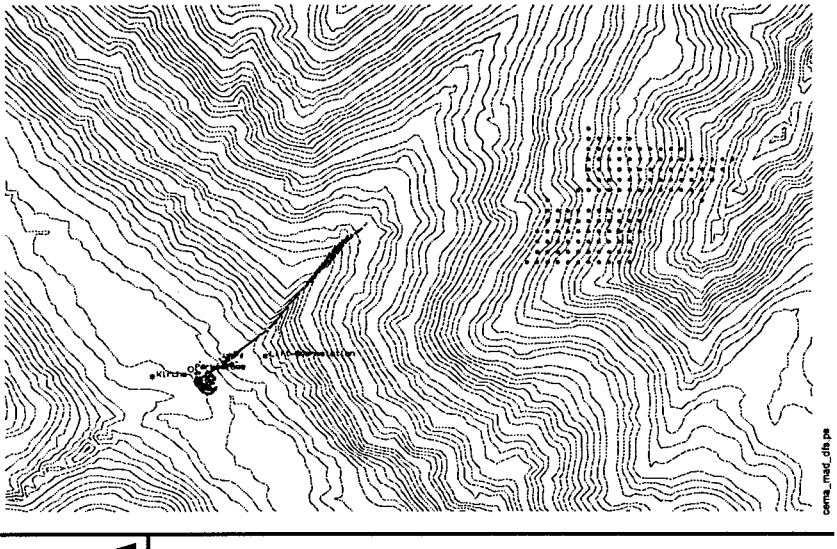

Madlein Avalanche, Dense Flow Simulation
Deposition Area

Figure 2

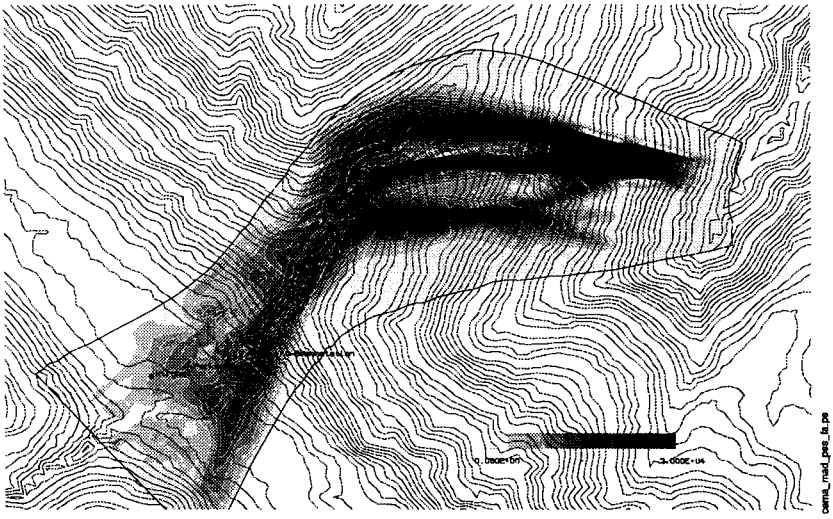

Madlein Avalanche, Powder Snow Simulation
Peak Dynamic Pressure [0 - 20.000 Pa]

Figure 3

Simulation of powder avalanches by FIRE ; Verification of results on example of Wolfsgruben avalanche (march 1988), in St Anton, Tyrol, Austria

Simulation d'avalanche poudreuse par FIRE ; etude des résultats sur l'exemple de l'avalanche de Wolfsgruben (mars 1988) à St Anton dans le Tyrol autrichien

P. SAMPL*, H. SCHAFFHAUSER‡

* *AVL List GmbH*
Kleiststrasse 48, Graz - Austria
Tel. (43) 316 987 563 - Fax (43) 316 987 777

‡ *Austrian avalanche reserach institute*
Rennweg 1, 6020 Innsbruck - Austria
Tel. (43) 512 573 933 - Fax (43) 512 572 820

Abstract

The application of the AVL-powder-avalanche model, the comparison between the results of this numerical model an the mapped damages are demonstrated to the Wolfsgruben avalanche (photo 1) disaster in St. Anton (March 1988) in Tyrol/Austria.

Résumé

L'application du modèle AVL d'avalanche poudreuse et la comparaison entre les résultats obtenus par ce modèle numérique et les dégâts cartographiés sont présentés dans le cas particulier de l'accident de l'avalanche de Wolfsgruben (photo 1), à Saint Anton dans le Tyrol, en Autriche.

Introduction

The rapid increase of the recreation-areas in the wake of economical growth in the alpine countries and their periphery was called for a effective tool for hazard zoning. In this respect, the konwledge about the dynamic behaviour of powder avalanches-a lot of catastrophic avalanches are flowing avalanches with a high powder component- in the run out zone is of enormous importance for practize in avalanche control and hazard zoning.
Meanwhile in Austria the calculation of the flowing part of avalanches bases on method of A. VOELLMY 1955, Salm B., Burkard A. and Gubler H. 1990 respectively

on the method of Hagen G. (1991)-Schaerer P. (1975). Before 1993 existed no model, which can be used to simulate the dynamics of powder avalanches.
For the simulation of powder avalanches are considered as a mixture from air and snow. For Calculating powder avalanches by FIRE there are USER-function applied. The snow-concentration is represented using the passive scalar and the local density is calculated via a USRDEN-function depending on the passive scalar. The motion of the mixture is caused by the interaction of gravitation and the density differences. With a density of (10) 30 kg/m3 in a USRINI-function is the avalanche started
At the bottom a fixed wall-boundary condition with wall-roughness is used. For the other forces (top, lateral) of the computational domain is set constant to 1 bar (= pstat + pdyn).
The three-dimensional AVL-powder avalanche model based on the fundamental differential equation-system, which governs the conservation of mass, momentum, snow concentration and the effects of turbulence are taken into a two equation turbulence model (Brandstätter W., Hagen F., Sampl P., Schaffhauser H., 1992).

Description of observations

The length of fracture line and fracture width was determined by terrestrial photogrammetry combined with a equilazation of concentrate beam block of the program "Orient" (Hagen F., Otepka G., 1988) with an exactness within the meter range alonge the fracture line, relating to the fracture thickness within the one decimeter range. In the case of the Wolfsgruben-avalanche the mean value of thickness was governed by this method with 1.37 m.
The release-zone with an areal of 37,40 hectar is situated 800 m above the bottom ot the Stanzer-valley (1320 m).
The geometrical boundary conditions (slope-morphology model) was manually created by digitazing the contour-lines of a map, scaled 1:5000.
Currently the model is only applicable to the motion of powder snow avalanches, the starting point for the calculation is this moment from that time the avalanche was enough scattered as dust. The avalanche is initiated with a mean density of ρ_S = 10 kg/m^3. The calculation-grid was filled up with 37.800 mesh-cells, the calculation was timed in time-steps of 0,20 seconds. For 250 time-steps the IBM-RS 16.000-350 workstation calculated about eight hours.

Results-comparison of the observations

With effect from pressure along a theoretical infinite hindrance vertical to the avalanche path is caused by turn round of the flow and is calculated with ρv^2.
Avalanche pressures of more than 25 kPa are indicated as so called RED ZONE of the hazard zone map - buildings and infrastructures are in this case not officially approved. The YELLOW ZONE covers areas with reduced forces below 25 kPA till 2 kPa.
Figures 1 and 2 show the avalanche in vertical cut plane 40 seconds after the starting point. The head of the powder avalanche reaches the locality Nasserein on the

eastend of St. Anton. The height of the powder avalanche amounted a height till 200 m.
In the run-out zone the avalanche is strong rarefied. The max. density amounts 3 kg/m3, also the velocities till 65 m/sec. nearly the bottom are yet considerable (Fig. 1,2).
The figures number 3 and 4 showing likewise the distribution of velocities and densities in the lower part of the slope (transition zone between track- and run-out zone) 40 seconds after the moment of starting. A big part of the avalanche streams through the slope center changing over into the shallow area extending very strong to the width. But a considerable part of the powder, a snow mass streams certainly over the ridge on the time the avalanche reaches belated the bottom of the valley. The canalization-effect of the channel is very limited. Figure number five outlines the observed impacts of the Wolfsgruben-avalanche after assessment b. Klenkhart (1988, avalanche-control, section Tyrol). The dissolved degrees of grey represent the calculated distribution of dynamic pressure 40 seconds after the moment of starting with a maximum pressure of 13.5 kPa. TSCHOM H. (1988) civil engineere for static calculated on observed damaged buildings (photo 2) the impact pressure. On the occasion could on the example of the destroyed house "Zangerle" - near point 1 in figure 5 - a pressure in the range between 13 kPA and 17 kPa determines. The computed results with 13kPa near point one in figure 5 bring into a good line with the calculated results.

Conclusions

The application of the AVL-model to the Wolfsgruben avalanche disaster is demonstrated and delivers in this case reassuming results, as for as they could compared with the observed reality. On the example of furhter-fourteen mapped avalanche disaster the results of AVL-Powder avalanche model will be compared in the next future. In parallel to these investigations in view of the developing of a dense flow-avalanche model by AVL in collaboration with the Austrian Torrent- and Avalanche Control and the Austrian Avalanche-Research Institute will came out for the verification measurements of avalanche-velocities by a pulsed C-band radar.

References

BRANDSTÄTTER, W., WIESER, K. SCHAFFHAUSER, H. (1992): Three-dimensional Simulation of Powder Avalanches, Paper presented at the 2nd Conference on Snow Engineering, Santa Barbara, California.

HAGEN, G., OTEPKA, G. (1986): Die Bestimmung der mittleren Anrißmächtigkeit von Lawinen mit Hilfe photogrammetischer Verfahren, Zeitschrift WLV, Juli 1988.

BRANDSTÄTTER, W., HAGEN, F., SAMPL, P. SCHAFFHAUSER, H.: Three dimensional simulation of powder snow avalanches in complex terrain, Zeitschrift des Vereins der Diplomingenieure der WLV Österreichs, Heft 120, Oktober 1992.

HAGEN, G. (1991): Proceedings of a Workshop on avalanche dynamics. Mittlg. EISLF Nr. 48 Ed. by H. U. Gubler.

Skizze nach KLENKHART, 1988, zur Verfügung gestellt vom Institut für Lawinenkunde, Innsbruck

TSCHOM, H. (1988): Lawinenabgang "Wolfsgrubenlawine" im Gemeindegebiet St.Anton-Nassrein, Berechnung der "Statischen Lawinenlast", 1988, zur Verfügung gestellt von der Gebietsbauleitung Oberes Inntal der Wildbach- und Lawinenverbauung, Imst.

SALM, B. BURKHARD, A., GUBLER, H.U. (1990). Berechnung von Fließlawinen. EISLF Nr. 47, Davos 1990.

VOELLMY, A. (1955): Über die Zerstörkraft von Lawinen, Schweiz. Bauzeitung 73, 1955

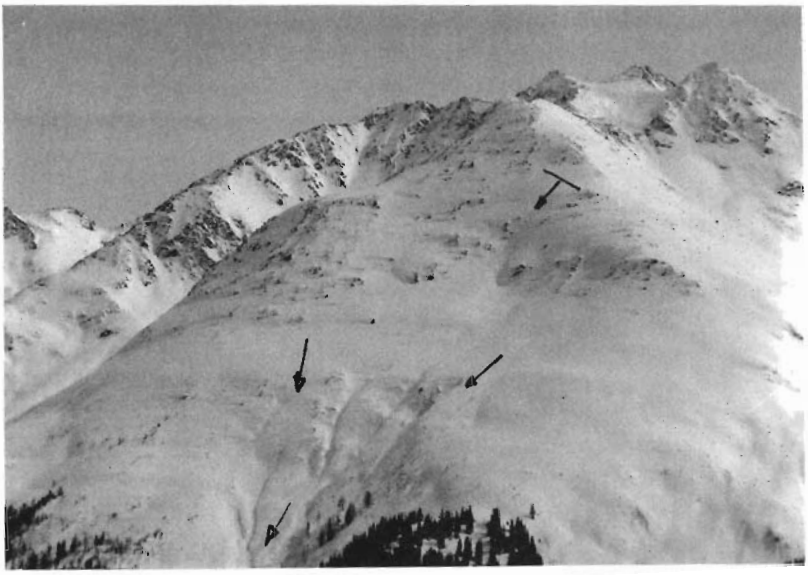

Photo 1: Release area of Wolfsgruben-Avalanche
(H. Schaffhauser, 1988).

Photo 2: Destroyed buildings in the run-out zone of
Wolfsgruben-Avalanche
(H. Schaffhauser, 1988).

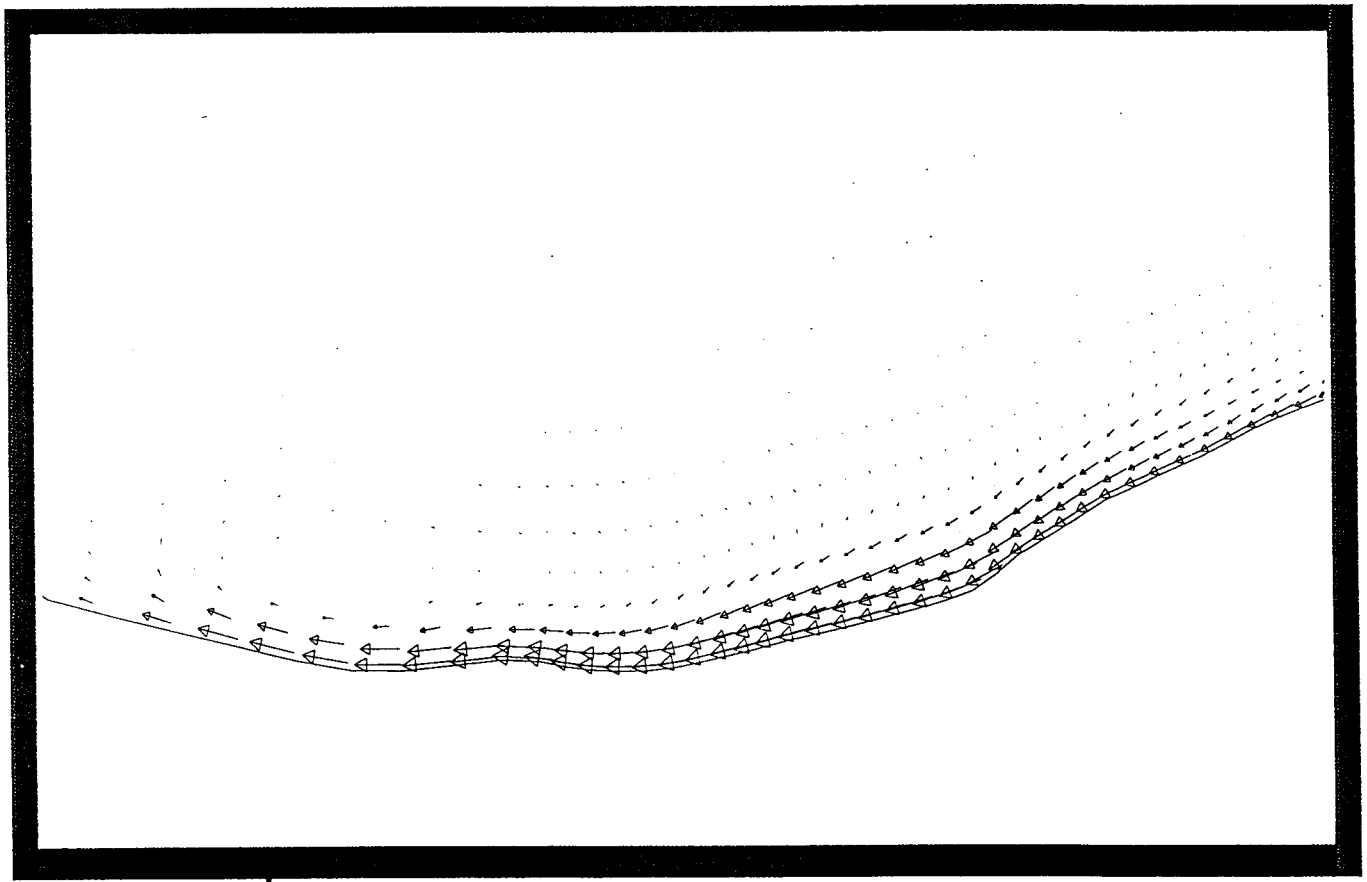

FIRE AVL

Wolfsgrube

Time = 40 sec: Velocity, v_max = 64 m/s

Fig. 1

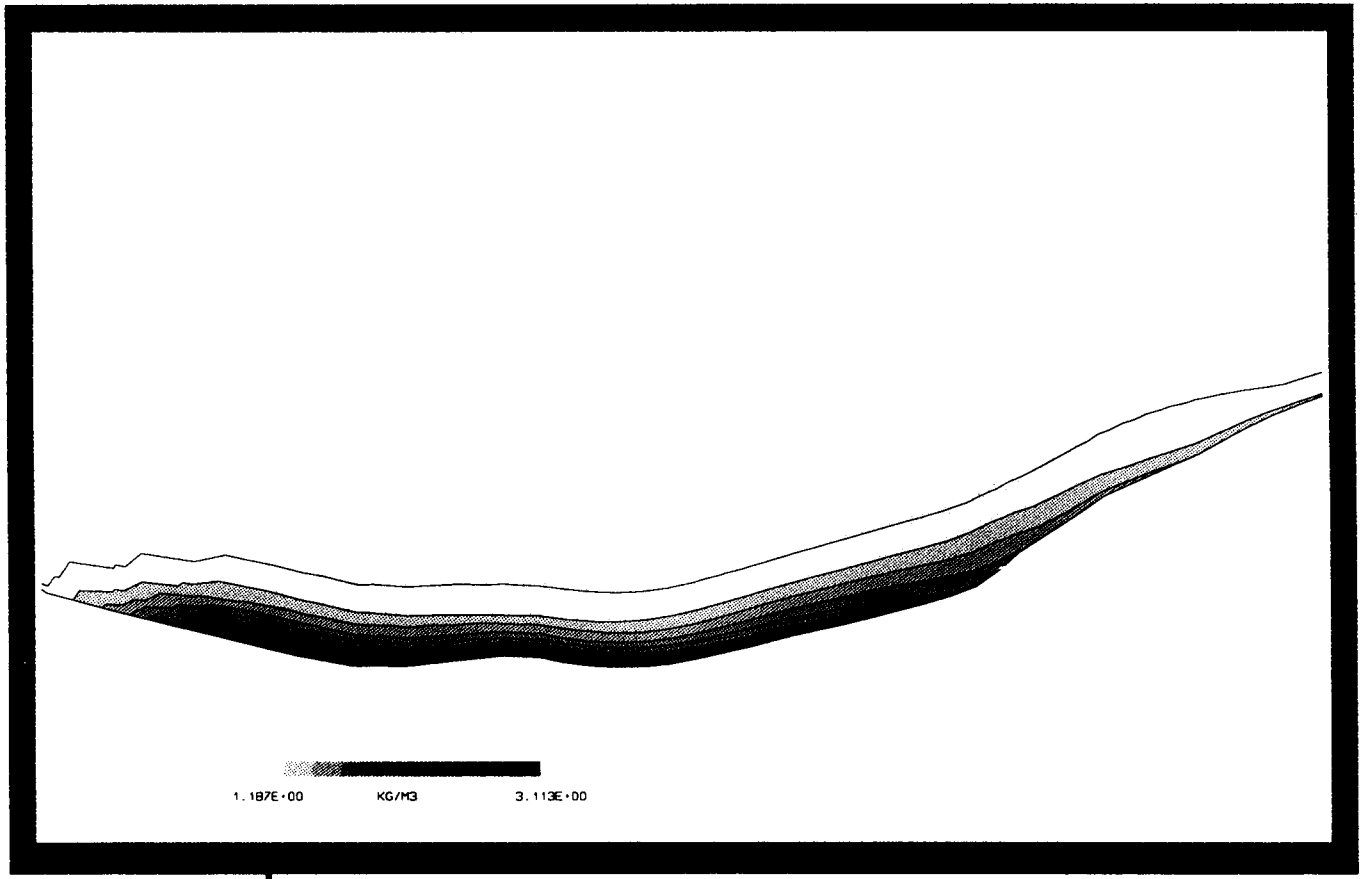

FIRE AVL

Wolfsgrube
Time = 40 sec: Density

Fig. 2

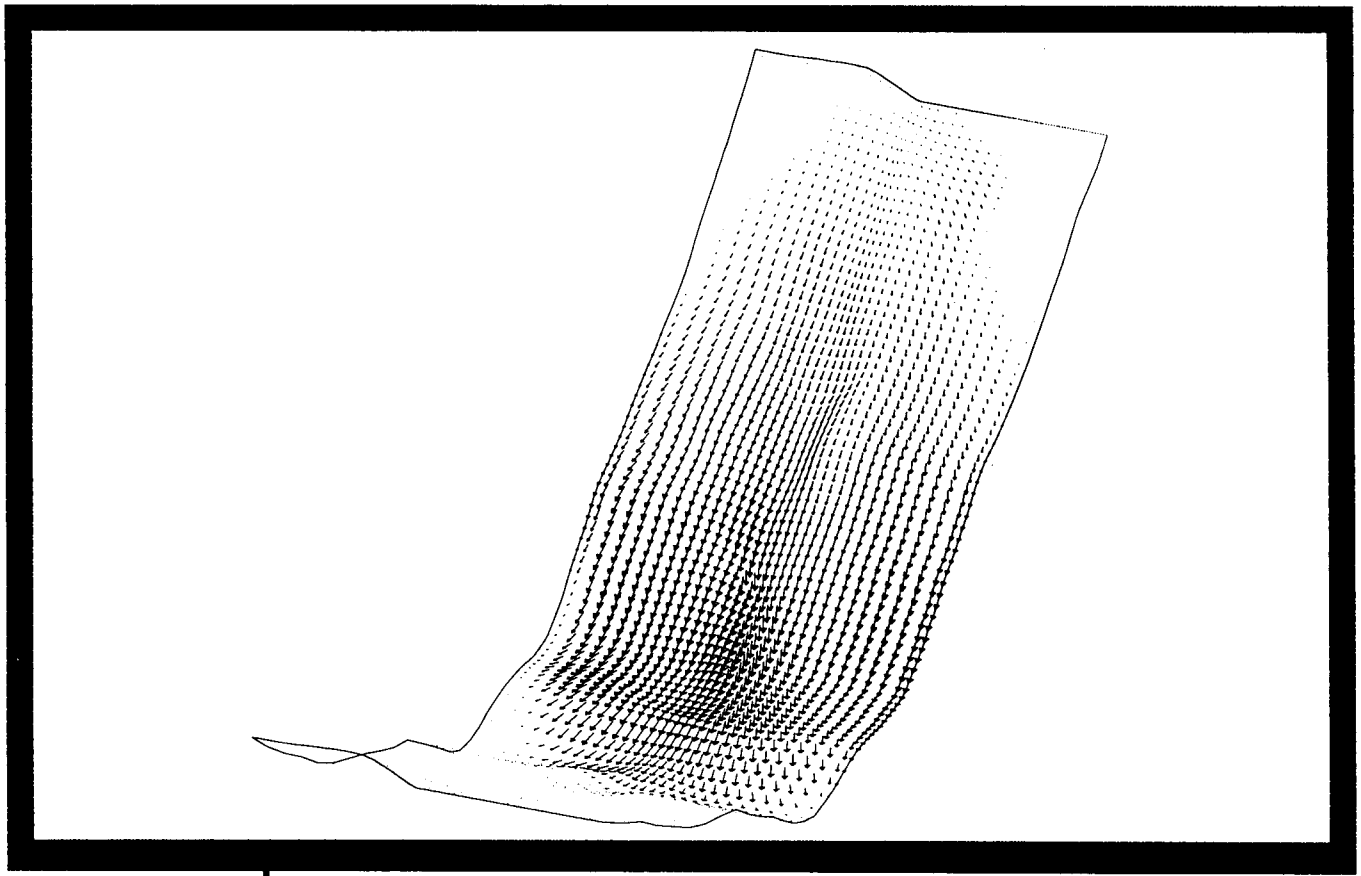

FIRE AVL

Wolfsgrube

Time = 40 sec: Velocity, v_max = 64 m/s

Fig. 3

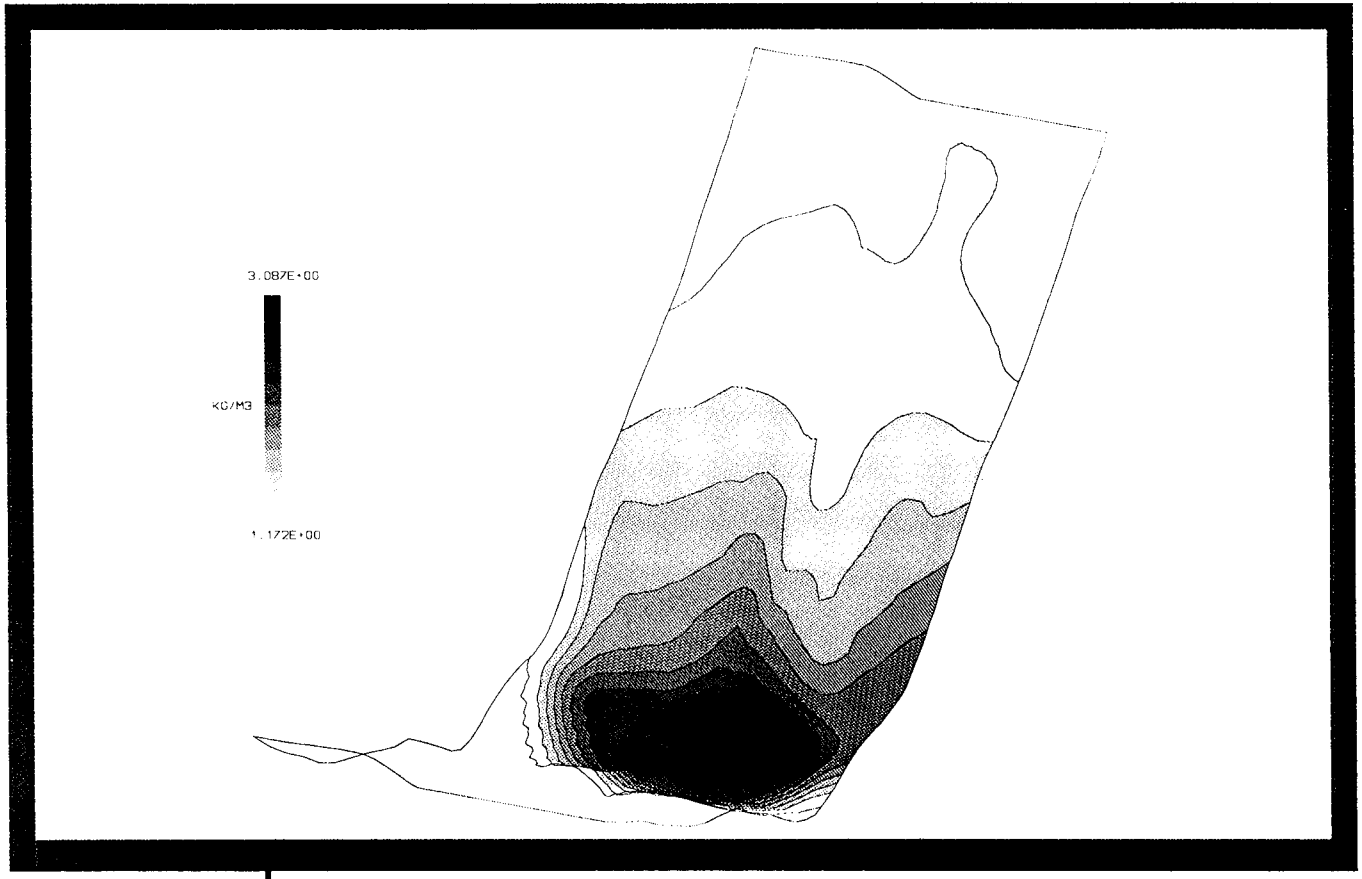

FIRE AVL

Wolfsgrube
Time = 40 sec: Density

Fig. 4

Fig. 5

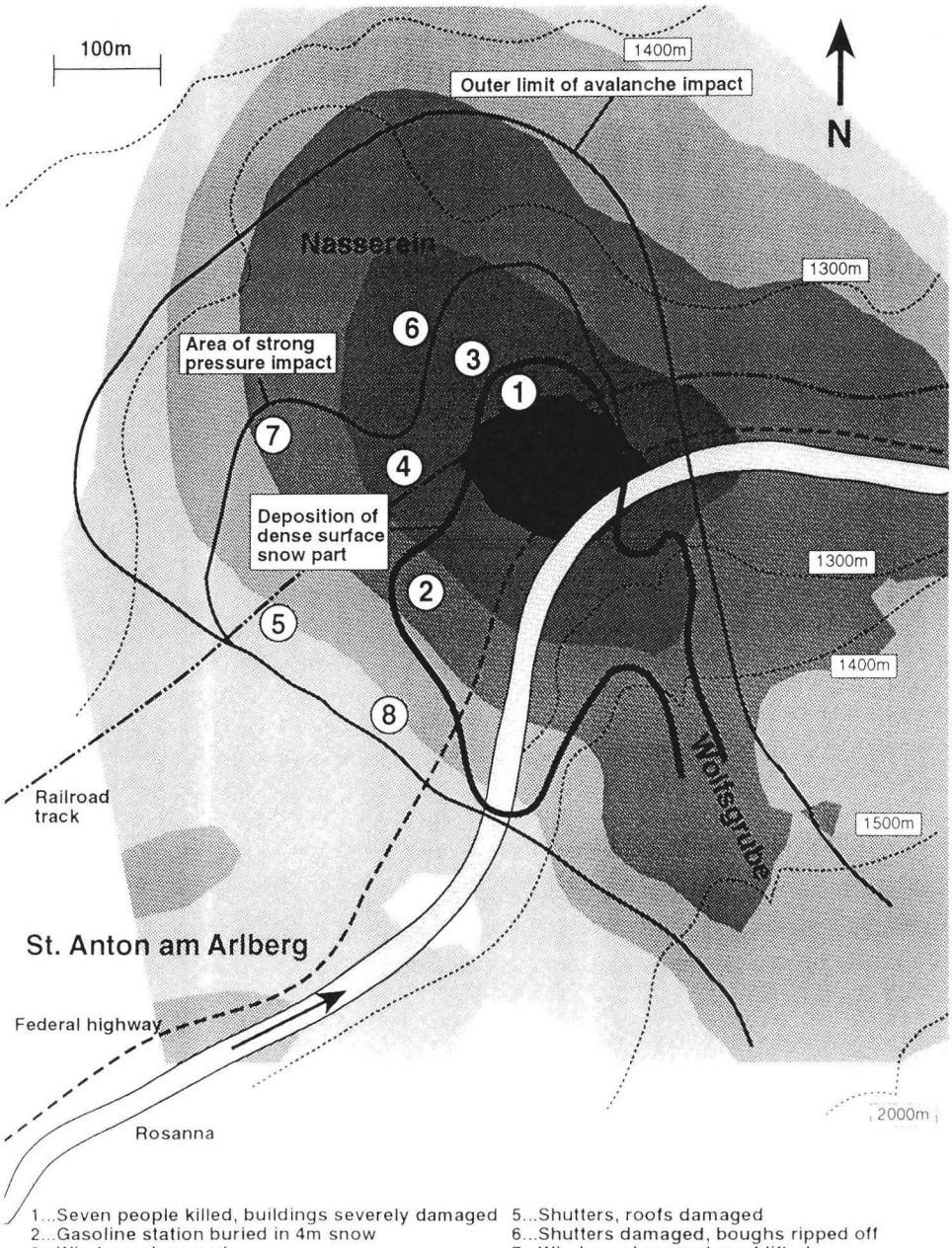

1...Seven people killed, buildings severely damaged
2...Gasoline station buried in 4m snow
3...Windows damaged
4...Windows damaged
5...Shutters, roofs damaged
6...Shutters damaged, boughs ripped off
7...Windows damaged, roof lifted
8...Pine tree with boughs ripped off

Sketch of observed damages of the 1988 Wolfsgrube avalanche (WLV Klenkhart, 1988)

Prediction of Landslide Motion ; Measurement of the apparent friction angle under undrained loading condition and the computer simulation

Prévision du mouvement d'un glissement de terrain ; mesures de l'angle de frottement apparent dans des conditions de chargement sans drainage et simulation informatique

K. SASSA

Disaster Prevention Research Institute, Kyoto University
611 Kyoto - Japan
Tel. (81) 774 32 07 89 - Fax (81) 774 32 55 97

Abstract

A statistical correlation ship between the lower value of the apparent friction angle and the greater volume of landslides have been noticed by Scheidegger (1973), Hsü (1975), Li (1983), and Okuda (1984). This presentation gives a theoretical explanation to this relationship based on the measured values of the apparent friction angle of the samples taken from a long traveling landslide in China. This research is a progress in the measurement of apparent friction angle from the geotechnical model for the motion of landslides proposed by Sassa, 1988, and the key concept is the undrained loading onto the alluvial deposits.

Résumé

Un lien de corrélation statistique entre la valeur basse de l'angle de frottement apparent et le volume des glissements de terrain ont été mis en évidence par Scheidegger (1973), Hsü (1975), Li (1983) et Okuda (1984). Cette communication donne à cette relation une explication théorique basée sur les valeurs mesurées d'angles de frottement apparent d'échantillons prélevés le long d'un grand glissement de terrain en Chine.
Ces travaux de recherche constituent un progrès dans la mesure de l'angle de frottement apparent utilisé dans le modèle géotechnique du mouvement des glissements de terrain proposé par Sassa (1988). Le concept clé est celui du chargement sans drainage de dépôts alluvionnaires.

Relationship between the ratio H/L and the apparent friction angles mobilized in the traveling path.

The apparent friction angle mobilized during the motion of landslides is decided mostly by the effective friction angle and pore pressure on the sliding surface during the motion of landslide and possibly also by other factors such as the energy loess due to collision. When the energy loss other than friction is not so high, we can approximately the apparent friction angle as follows (Sassa, 1985, 1988, Sassa et al, 1985).

$$\tan\phi_a = \frac{\sigma - u}{\sigma}\tan\phi_m \qquad (1)$$

Here, ϕm : effective friction angle during motion
ϕa : apparent friction angle during motion
σ : normal stress u : pore pressure.

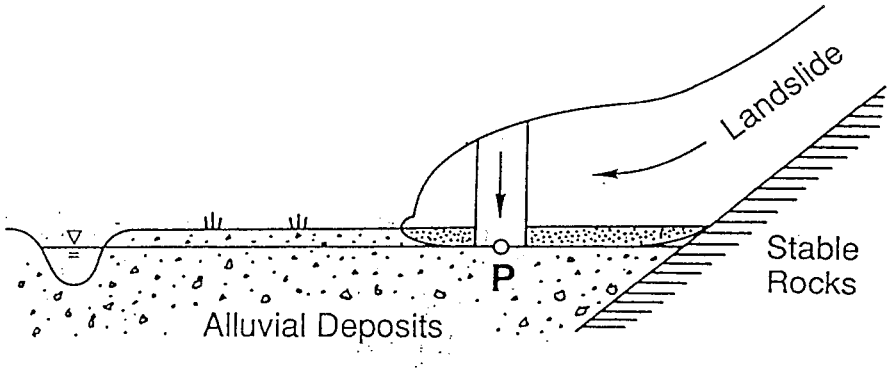

Fig.1 Schematic profile of a landslide onto the alluvial deposit

Large scale landslides usually move on alluvial deposits in the toe of slopes as schematically shown in Fig.1. The alluvial deposits were formed by rivers, so the ground water table should usually exist in the relatively shallow depth. When a large scale landslide moves on the alluvial deposit, pore pressure should be generated in the saturated soil layer due to the rapid (usually undrained) loading, so the apparent friction angle mobilized in the alluvial deposit can be much smaller than the effective friction angle of the materials. In this case, the sliding surface will be formed on the saturated layer, and the landslide mass can travel long.

To express the average apparent friction mobilized in the motion of landslides, the ratio of total height difference (H) and horizontal distance (L) between the initial point and the toe of deposit is often used as the equivalent coefficient of friction or the average coefficient of friction. The apparent friction angle defined in Equation (1) is different in places. Referring Fig.1, the apparent friction angle during the moving path can be approximately divided in two parts, namely fa1 in the

slope(drained shear in unsaturated soils, and undrained shear in the case of saturated and low permeable soils) and fa2 in the alluvial deposit (undrained loading and undrained shear).

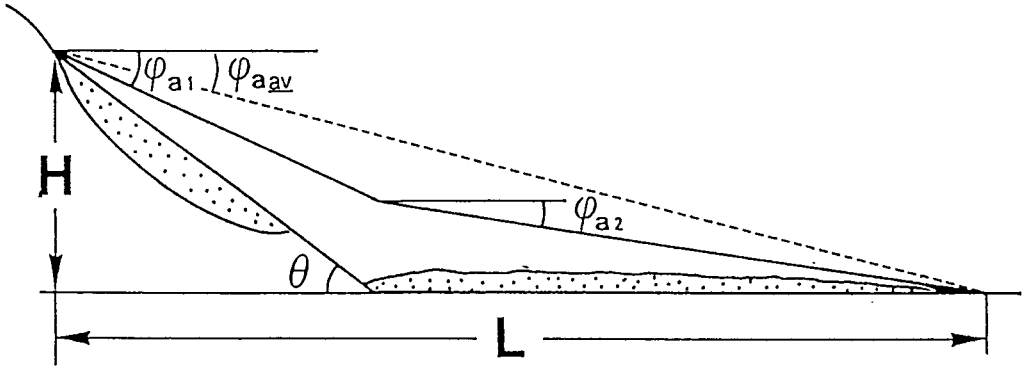

Fig.2 Apparent friction angles in the simplified geometry of landslides

Regarding the alluvial deposit to be horizontal, Equation (2) is obtained from the geometry shown in Fig.2.

$$H/L = \tan\phi_{aay} = \frac{\tan\phi_{a2}}{1 - \cot\theta\,(\tan\phi_{a1} - \tan\phi_{a2})} \qquad (2)$$

We can predict the value of H/L, if we can measure the apparent friction angles ($\phi a1$, $\phi a2$) by the soil mechanical tests before the initiation of landslide in consideration.

A new undrained cyclic loading ring shear apparatus

The cyclic loading ring shear apparatus was developed by Sassa 1992. The shear box and the pore pressure measurement system has been recently improved. Then, undrained dynamic and cyclic loading tests and successful pore pressure measurement during shear is now possible.

Fig.3 shows its schematic diagram of the apparatus. In the figure, the sample (I) is loaded by the loading plate (H) and the air piston (B). The loaded normal stress is measured by the load cell (C2). The sum of the friction between the sample and the upper shear box and the contact pressure (100 kgf) of rubber edge in the gap (right figure) is measured by the load cell (C6). The real normal force acting on the shear surface is obtained as the difference of values measured by two load cells (C2 and C6). This value is sent to the servo-amplifier as the feed back signal. Then, the normal stress on the shear surface is automatically controlled so as to be the same with the control signal given by the computer. The contact pressure of rubber edge is automatically controlled by the servo motor (N) using the feed back signal obtained

from the gap sensor (C8) in the precision of 2/1000 mm. The shear stress is supplied by the torque control servo motor (Q). The loaded torque is measured by the torque transducer (C7).

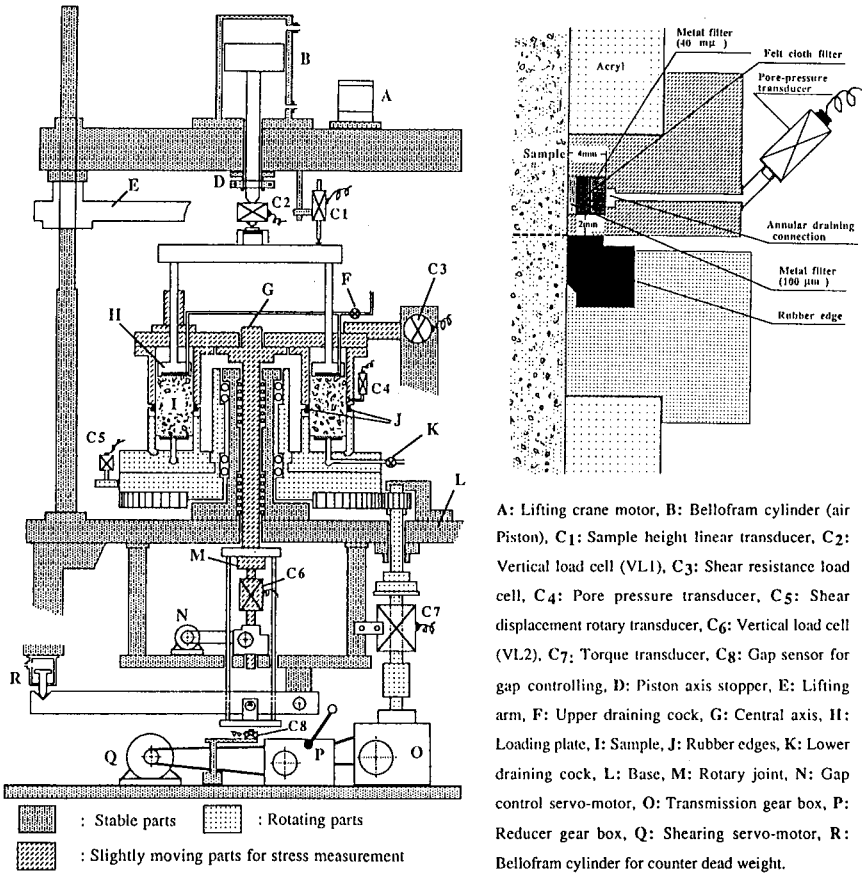

Fig.3 Schematic diagram of the undrained dynamic loading ring shear apparatus

Using the monitored value of C7 as the feed back signal, the loaded shear stress is automatically controlled by servo amplifier and servo motor so as to be the same with the predecided value given by computer. The shear resistance acting on the shear surface is monitored by the load cell (C3) retraining the upper half of the shear box from rotation.

Pore pressure is measured by pore pressure transducer (C4) which is connected to Pthe gutter (4x4mm) along the whole circumference of the outer and upper edge. The gutter is located at 2 mm above the shear surface and it is covered with two metal filters and a felt cloth between them. The needle type pore pressure measurement system used in Sassa,1992-1 was broken during shear and it is not effective for low permeable

soils because the area facing to samples is not enough. However, a new system was very successful.
The undrained state was well kept during shear. In the test of pure water in place of sample, no leakage did not take place under 3.0 kgf/cm^2 during 54 m of shearing at 30 cm/sec velocity.

Measurement of the apparent fiction angles in the 1983 Sale landslide, China

A large scale landslide (volume:3.5x107 m3)took place in Gansu, China in 1983. It moved about 1 km over the alluvial deposits at 13-14 m/sec velocity and killed 227 persons (Zhang and Sassa 1992). Sassa et al investigated this landslide as a large scale long traveling landslide and measured the apparent friction angles fa1, fa2 in this landslide.

Fig.4 is the central section of the Sale landslide which was re drawn from the geological map made by the Gansu Geological Bureau, 1986. The Bureau investigated the area including 23 bore holes and estimated the geological sections.
We took two samples, namely Sample No.1 (Tertiary sandy mudstone) from the sliding surface for fa1 and Sample No.2 from the alluvial deposit for fa2 as shown in Fig.4.

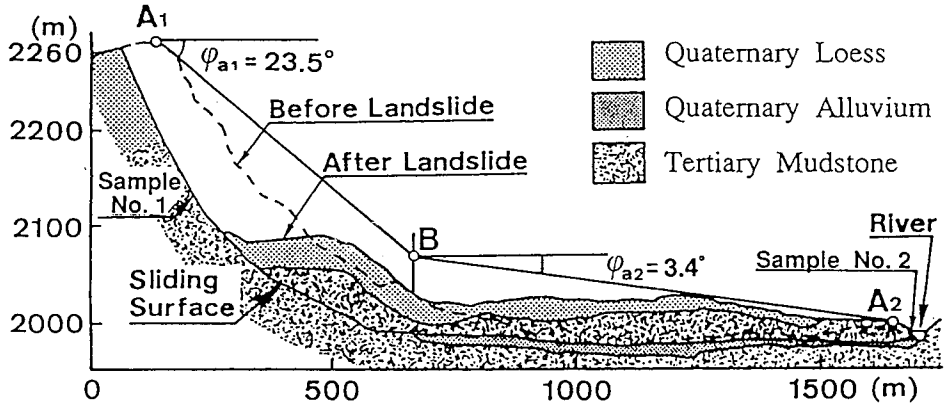

Fig.4 Section of the 1983 Sale landslide, China (from the geological map by the Gansu Geological Bureau)

A crack appeared in the top of mountain in a rainy year (649.5 mm, 1.6 times of the average annual rainfall) of 1979. The slope gradually creeped and finally failed in March 1983. The period before failure was almost no rainfall for two months and no earthquake at the time. The sliding surface was estimated to be not saturated. So the apparent friction angle (ϕa1) mobilized on the sliding surface is estimated to be

around its residual friction angle of the partially saturated state. Fig.5 is the result of speed control ring shear test (0.005 cm/sec velocity) of Sample No.1 at the degree of saturation of 73 %. It indicates that the residual friction angle (almost equal to $\phi a1$ in this case) is 23.5 degrees, because the rate effect is not considerable in granular materials (Fukuoka, 1991, Sassa, 1988).

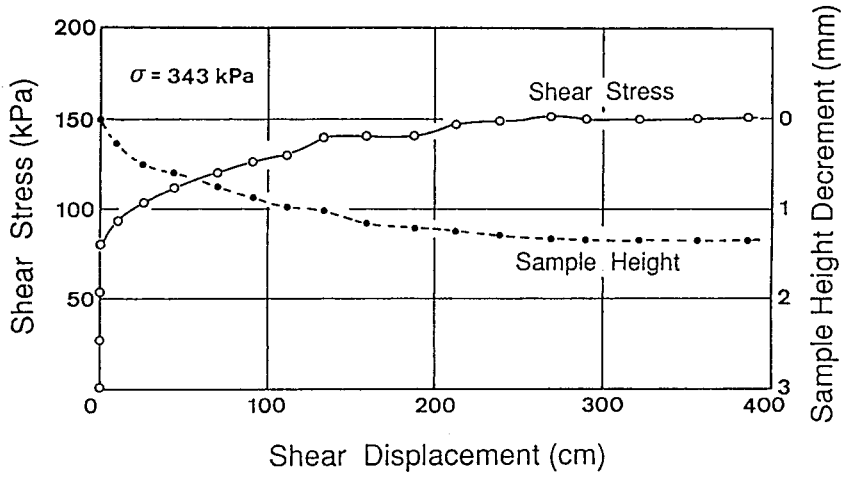

Fig. 5 Measurement of the apparent friction angle ($\phi a1$) mobilized in the slope using the sample No.1.

The alluvial deposit area was used as paddy fields, and water was taken in the fields, so the alluvial deposit was estimated to be saturated in a few meters below the ground surface. Then, the sample was well mixed with water until the slurry state and consolidated at 42 kPa in the shear box which will correspond to the initial stress on the potential sliding surface as point P illustrated in Fig.1. The pore pressure parameter in the direct shear state (BD) was 0.98. BD is defined by Sassa, 1985, 1986 together with another pore pressure parameter AD. BD value is the same with the pore pressure parameters in one dimensional compression. Then, shearing of 0.014 cm/sec was given in the drained state in order to obtain the shear strength before the undrained loading. Thereafter, the shear box was changed to the undrained state by closing two drainage cocks (F, K in Fig.3). The normal stress was increased up to 366 kPa in 50 sec during shearing at 8.8 cm/sec. The stress point moved from A to B in the total stress, and A to B′ in the effective stress as found in Fig.6. The apparent friction angle ($\phi a2$) after the undrained loading is 5.2 degrees. To obtain the effective friction angle, the shear box was changed to the drained state and slow shearing of 0.014 cm/sec was given until full dissipation of pore pressure. The stress path during this process is shown as B-C in the total stress and B′-C in the effective stress. Both stress path met on the point C. Then, the effective friction angle is 30.1

degrees, the deviation of effective stress path from the estimated failure line may be due to a low permeability (2.9x10-6 cm/sec) of this soils.

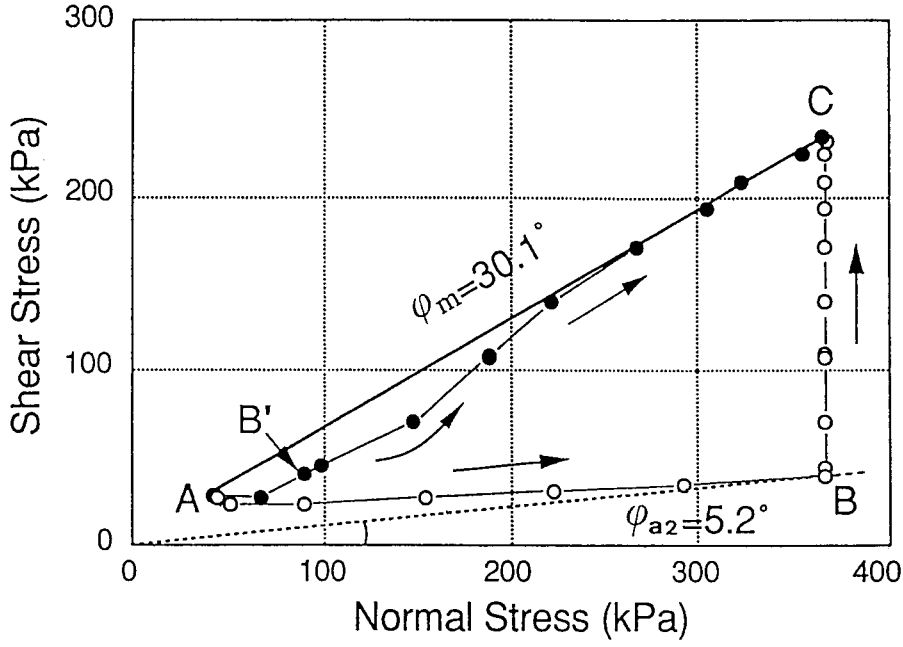

Fig. 6 Measurment of the apparent friction angle Φιγ. 62) mobilized in the alluvial deposit using the sample No.2

In the case of the Sale landslide, the height of moving landslide mass was 40 m, it corresponds to 680 kPa in the case of 17 KN/m^3. So the apparent friction angle $\phi a2$ in this landslide is estimated as 4.3 degrees by extending the line A-B for further 680 kPa. Drawing the energy line from the top of the landslide mass (A1) in the inclination of $\phi a1$ (23.5 degrees) until the border to the alluvial deposit, the point B is obtained. Drawing a line from the point B to the highest point of the toe of landslide (A2), the apparent friction angle of 3.4 degrees is obtained. This value is almost same with the value estimated from the test result of the alluvial deposit. Therefore, it is said from the sled model that the measured apparent friction angles well agreed with the motion of Sale landslide.

Theoretical interpretation of the relationship between the landslide volume and the apparent friction angle

It is imagined from the undrained loading stress path A-B and the apparent friction angle $\phi a2$ in Fig.6 that, if the loaded normal stress is smaller than the case of Fig.6, the apparent friction angle $\phi a2$ should be greater. On the contrary, if the loaded normal stress will be greater, the apparent friction angle must be smaller. Assuming the undrained loading stress path to be linear, the relationship between the loaded normal stress and the apparent friction angle is obtained as Equation (3).

$$\tan\phi a2 = (\tau 0 + \alpha\,\Delta\sigma)/(\sigma 0 + \Delta\sigma) \quad (3)$$

$\sigma 0$: initial normal stress
$\tau 0$: shear strength at $\sigma 0$
$\Delta\sigma$: loaded normal stress
α : gradient of the undrained stress path in the total stress

The loaded normal stress by a moving landslide mass must be in proportion to the volume of the landslide. Assuming the ratio of length and width (L/W) as 2.0 (Okuda, 1984), the total unit weight of a landslide mass as 16.7 kN/m^3, and using the relationship of $L=9.98V^{0.32}$ proposed by Davies (1982), Equation (4) is obtained (Sassa, 1992).

$$V=19.8\,\sigma^{2.78} \quad (4)$$

σ : normal stress on the base of landslide (kPa)
V : landslide volume (m^3)

σ in Equation (4) corresponds to the normal stress increment ($\Delta\sigma$) in Equation (3). The average apparent friction angle ($\phi a\underline{av}$) is obtained from Equations (2), (3), and (4).

In the Sale landslide, the apparent friction angle in the slope ($\phi a1$) was 23.5 degrees because the soil layer was estimated to be unsaturated. However, in the 1994 Ontake landslide in Japan, it was estimated that the pumice layer including the sliding surface was saturated and the shearing took place in the undrained situation because it was triggered by an earthquake. Probably, the case of Ontake landslide will present one of the lowest values of the apparent friction angle ($\phi a1$) mobilized in the slope. Fig.7 is the effective stress path of undrained cyclic loading ring shear tests. At first the initial stress before earthquake was loaded to the normally consolidated and fully saturated pumice (BD=0.96) in the drained state. Then, the increasing amplitude of cyclic stress was loaded in the undrained state.

The direction of loaded cyclic stress was so as to simulate a horizontal seismic stress to the slope of 30 degrees. In the stress diagram, the loaded stress direction was cataclinal to the failure line, but the effective cyclic stress path became anaclinal to the failure line due to the negative pore pressure generation before failure as shown in Fig.7 (Shoaei and Sassa, 1994). In the figure, (I) is the initial stress point before cyclic loading, (F) is the stress point at failure, and (M) is the stress point during motion. The positive pore pressure generation took place after failure because of crushing of the pumice skeleton. Accordingly, the apparent friction angle during motion in the slope ($\phi a1$) was small as 4.8 degrees. Probably this value shows one of the minimum value of $\phi a1$. The maximum value will be around the residual friction angle of sandy materials, namely 30-37 degrees.
Fig. 8 shows the relationship between the landslide volume and the average apparent friction angle and the ratio H/L which are obtained from Equation (2), (3), (4). Here, θ=35 degrees, parameters in Equation (3) is of the rapid loading ring shear test in the case of Sale landslide (Sassa, 1992), and three lines of 5, 25, 30 degrees in

$\phi a1$ are drawn in the figure. Plots of landslides are by Hsü (1975), Okuda(1984), Sassa(1988) and others. These three lines almost cover those plots; this seems to well represent the tendency of higher mobility in larger landslides. The case of Ontake is below the line of 5°; it can be explained by the fact that the alluvial (torrent) deposit was not so flat as assumed in Fig. 2.

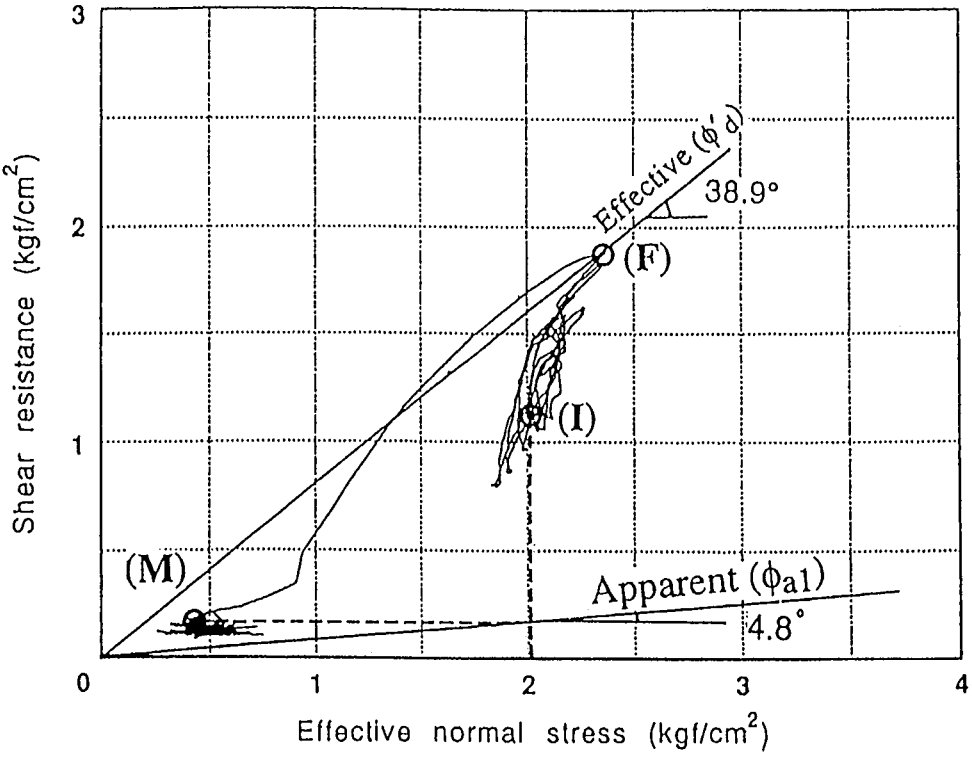

Fig. 7 Measurement of the apparent friction angle ($\phi a1$) in the saturated pumice (BD=0.96)

Two cases for the apparent friction angle (30°, 35°) which are the same in the slope and also in the alluvial deposit are drawn for reference. This case corresponds to no pore pressure generation in the alluvial deposit as well as in the slope.

Computer simulation of the Sale landslide

Sassa (1988) proposed the geotechnical model for the motion of landslides. Fig.9 shows its concept, and Equation (5) presents its basic concept for the equilibrium equation of a vertical column in the landslide mass.

$$a \cdot m = W_p + \frac{\partial P_x}{\partial x} + \frac{\partial P_y}{\partial y} + R \qquad (5)$$

Here, Wn + N = 0

a: Vector of acceleration, m: Mass of a soil column
R: Shear force at the bottom of a soil column
N: Normal Stress on the slope
W: Weight of a soil column
Wp, Wn: Components parallel and normal to slope of W
Px, Py: Lateral pressure in x-direction and y-direction

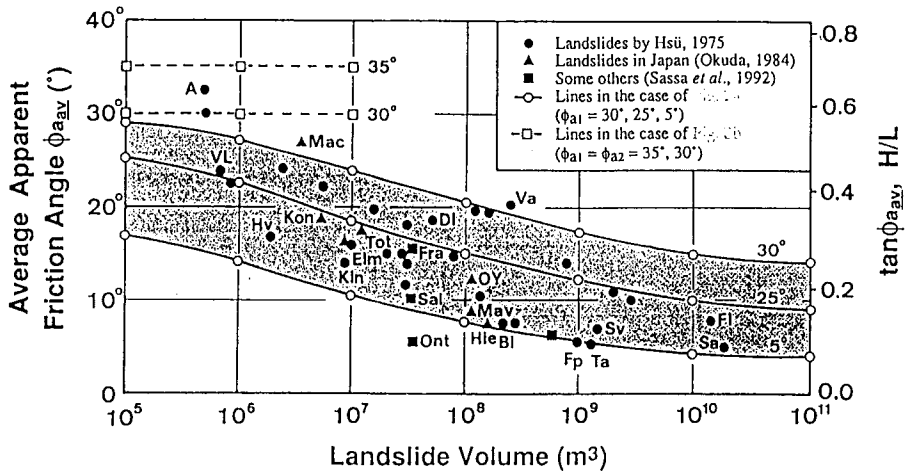

Fig. 8 Relationship between landslide volume and the average apparent friction angle

In Equation (5), the apparent friction angles in the slope and in the alluvial deposit control the value of R. The lateral pressure is controlled by the lateral pressure ratio k as well as the height of soil column and the soil density. The apparent friction angle regulates the travel distance of the landslide mass, and the lateral pressure ratio regulates the magnitude of spreading of the landslide mass. The value of k is 1.0 in the liquid, 0 in the rigid body. In soils, assuming that the Jaky Equation is effective during motion, Equation (6) is obtained.

$$k=1 - \sin\phi_{ia} \tag{6}$$

Here,

$$\tan\phi_{ia} = \frac{\sigma - u}{\sigma}\tan\phi'_i$$

ϕ'_i : effective friction angle inside the landslide mass
ϕ_{ia} : apparent friction angle inside the landslide mass.

The value of ϕ_{ia} is 0 in the liquefied state, and same with ϕ'_i in the no pore pressure state, and it is usually between 0.4 for no pore pressure inside the sandy landslide mass and 0.8 for high pore pressure inside the landslide mass, though it can be close to 1.0 in the case similar to debris flows. In the case of Sale landslide, the landslide mass was rather dry because of arid climate and almost no rainfall for 2 months before the landslide. Then, k=0.4 was adopted in this simulation.
To check this value, a speed control ring shear test on less saturated (29.3%) state of the Tertiary sandy mud stone (Sample No.1) which composed a major part of the moving mass was performed(Zhang and Sassa 1992). The peak friction angle was 39.5 degrees and the residual friction angle was 33.7 degrees. These friction angles corresponded to k=0.36 and 0.45 respectively.

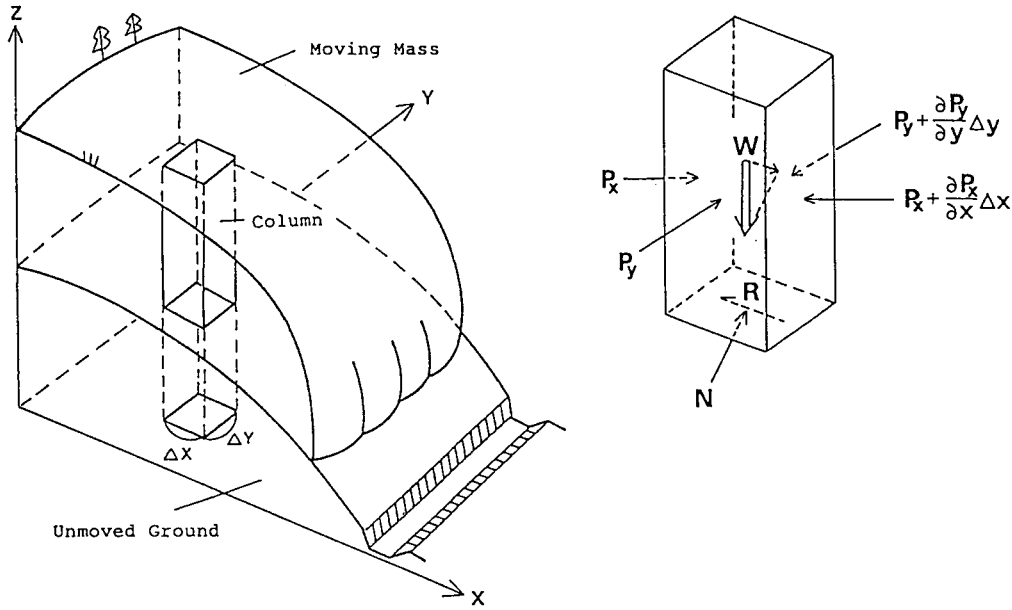

Fig.9 A moving landslide mass and forces acting on a column in it.

Fig.10 shows A) plan of the Sale landslide and the location of meshes for simulation, B) distribution of apparent friction (tan ϕa) used in simulation(Zhang and Sassa, 1992-2). Fig.11 is the initial soil depth distribution and the final soil depth distribution after motion. The result of computer simulation of

Acknowledgement

The author thanks Assistant Professor Dr. H. Fukuoka, and also post graduate students Mr. D. X. Zhang, Mr. J. H. Lee, Mr. Z. Shoaei from China, Korea and Iran of the Landslide Section, Disaster Prevention Research Institute, Kyoto University for their active ooperation.

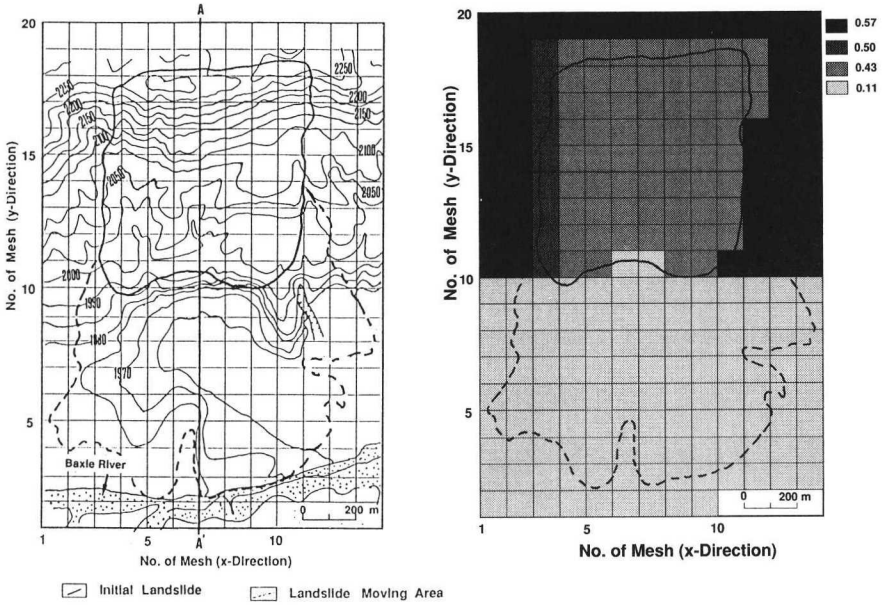

Fig. 10 Topography and the apparent friction angle used in the computer simulation of the Sale landslide
A) Plan of the landslide and the location of mesh and the central section A-A′ in Fig;4.
B) Distribution of apparent friction

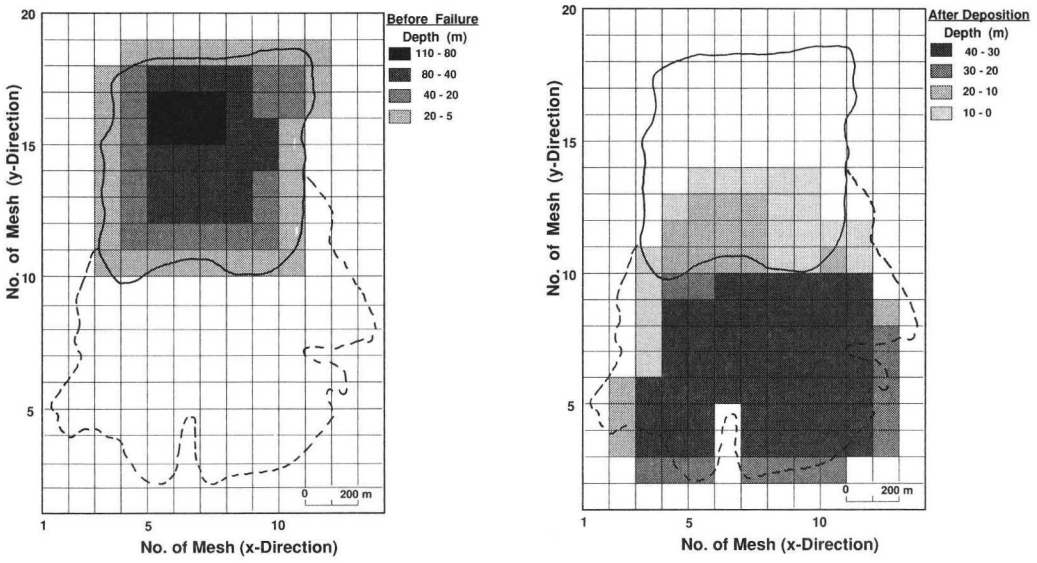

Fig.11 Results of computer simulation of the Sale landslide (Zhang and Sassa, 1992-2) A) Soil depth distribution before motionB) Calculated soil depth distribution after motion

References

Davies, T. (1982): Spreading of rock avalanche debris by mechanical fluidization, Rock Mechanics, Vol. 15, p.9-24.

Fukuoka, H. (1991): Variation of the friction angle of granular materials in the high-speed high-stress ring shear apparatus -Influence of reorientation, alignment and crushing of grains during shear-. Bulletin of the Disaster Prevention Research Institute, Kyoto University, Vol.41, Part 4, pp.243-279.

Gansu Geological Bureau (1986): Geological maps on the Sale landslide.

Hsü, K. (1975): Catastrophic debris streams(sturzstroms) generated by rock falls, Bull. of Geological Society of America, Vol. 86, p.129-140.

Li, T. (1983): A mathematical model for predicting the extent of a major rockfall, Zeitschrift für Geomorphologie, Bd. 27, Heft 24, p.473-482.

Okuda, S. (1984): Features of debris deposits of large slope failures investigated from historical records, Annals of DPRI, Kyoto Univ., No. 27B-1, p.353-368 (in Japanese).

Sassa, K., M. Kaibori and N. Kitera (1985): Liquefaction and undrained shear of torrent deposits as the cause of debris flows. Proc. International Symposium on Erosion, Debris Flows and Disaster Prevention, Tsukuba, pp.231-236.

Sassa, K.(1985): Rapid landslides and debris flows. Theme lecture for Discussion Session 3A "Motion of Landslides and Debris Flows", 11th ICSMFE, 33 pages.

Sassa, K. (1988): Geotechnical model for the motion of landslides, Special lecture, 5th Int. Symp. on Landslides, "Landslides," Balkema, Vol. 1, p.37-55.

Sassa, K. (1992-1): Access to the dynamics of landslides during earthquakes by a new cyclic loading high-speed ring shear apparatus, Theme address, 6th Int. Symp. on Landslides, In: "Landslides," Balkema, Vol. 3, 20 pages (in print)

Sassa, K. (1992-2): Landslide volume-apparent friction relationship in the case of rapid loading on alluvial deposits. International Newsletter "Landslide News", No.6, pp.16-19.

Scheidegger, A. (1973): On the prediction of the reach and velocity of catastrophic landslides, Rock Mechanics, Vol. 5, p.231-236.

Shoaei, Z. and K. Sassa (1994): Basic study on the shear behavior of landslides during earthquakes -Excess pore pressure generation in the undrained cyclic loading ring shear tests- . in contribution to the Bulletin of the Disaster Prevention Research Institute, Kyoto University, Vol.44.

Zhang D. and K. Sassa (1992-1) : The mechanism of the Sale landslide, China. Annuals of the Disaster Prevention Research Institute, Kyoto University, No.35 B-1, pp.95-112. (in Japanese)

Zhang D. and K. Sassa (1992-2) : The mechanism of the Sale landslide (China, 1983) and its computer simulation, Proc. 32nd Annual Conference of the Japan Landslide Society, pp.267-270. (in Japanese)

Appendix: Photos of the apparatus

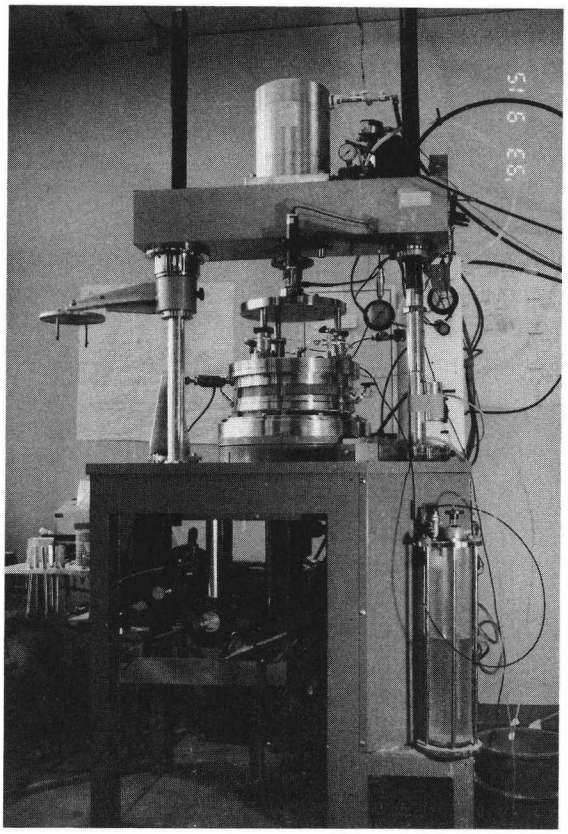

Photo 1. Frontal view of the apparatus. Comparing with Fig.3 in the text, the outline of structure is found. The transparent plastic tank in the right side is for de-aired water to saturate samples. The main servo-motor Q and the gear box P in Fig. 3 are not seen, they are in the back side of apparatus

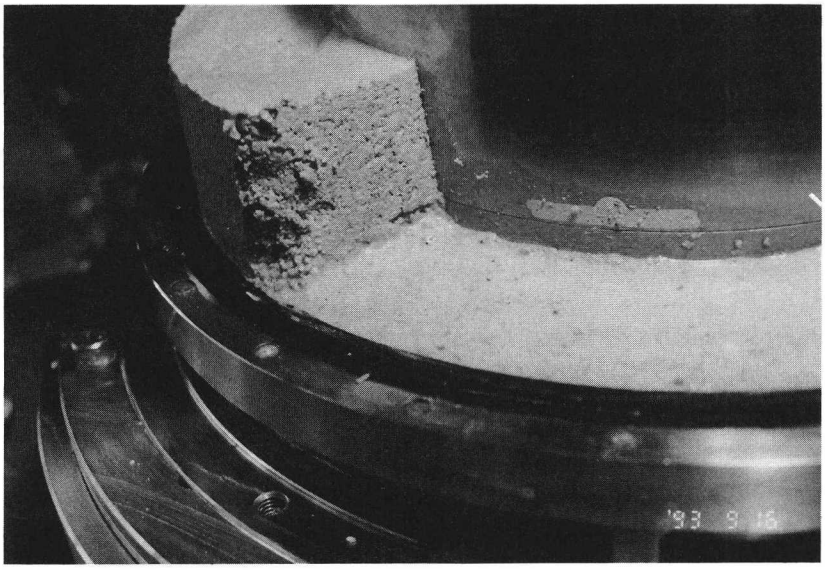

Photo.2 Ontake pumice sample after undrained cyclic loading test. The shear plane was very thin because of no consolidation due to grain crushing, though a relatively wide shear zone including crushed grains was found in drained tests.

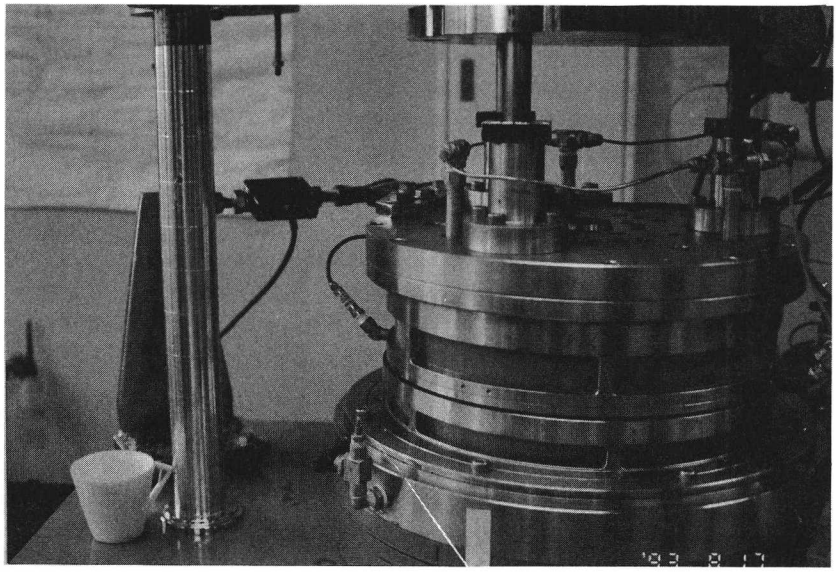

Photo.3 Outside view of shear box The lower half of shear box is rotated. The upper half is retained from rotation through the shear load cell (C3) to the stable stand. C3 is seen between a pillar and the shear box. The pore pressure transducer (C4) is found at the left side of the upper shear box. L-shape cock attached to the lower shear box is for supplying de-aired water into the shear.

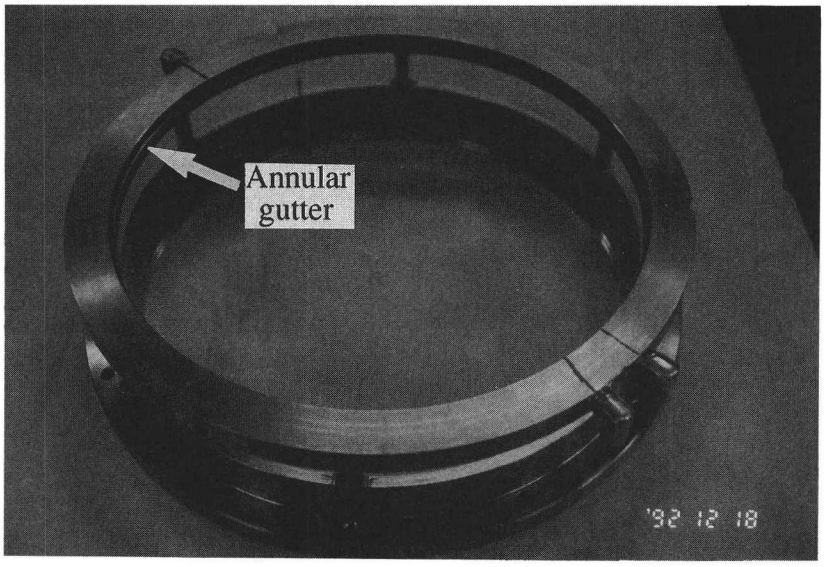

Photo 4 Outside wall of the upper shear boxIt was put in the upside-down position to show the annular gutter along the whole cercumference of the outside for masurement of pore pressure as shown in the right-up of Fig.3. This annular gutter is connected to the pore pressure transducer in Photo 3.

Qualification de la chasse ancienne	Qualification de la chasse actuelle	Auteurs du récit	Qualification de l'évolution de la chasse	Qualification du chasseur actuel
respectueuse des populations animales	respectueuse	des chasseurs	dépréciation du savoir des chasseurs locaux	victime (brimé, méprisé)
respectueuse	irrespectueuse	des naturalistes et des gardes-moniteurs	décadence de la chasse	décadent
irrespectueuse	toujours irrespectueuse	des naturalistes et des gardes-moniteurs	absence d'évolution	égal à lui-même
irrespectueuse	respectueuse	des chasseurs	importance et difficulté de la mutation accomplie par les chasseurs	rationnel
irrespectueuse	encore irrespectueuse	des chasseurs	importance et difficulté de la mutation demandée aux chasseurs	perfectible

La question de l'éthique de la chasse ancienne a permis de repérer plusieurs registres de récits[1]. Deux d'entre eux peuvent être considérés comme de simples variantes. Ceux qui considèrent les chasseurs comme constamment mauvais au fil du temps se rapprochent en effet de ceux qui les disent décadents. Quant aux récits qui présentent le chasseur actuel comme « perfectible », ils se laissent assez aisément rattacher aux récits de rationalisation. On peut donc, en définitive, distinguer trois registres principaux, qui insistent soit sur la décadence des contemporains, soit sur leur rationalisation, soit sur les injustices dont ils sont victimes.

On retrouve ces trois grands registres dans la plupart des passages relatifs à l'évolution des pratiques, qu'ils concernent la chasse, le pastoralisme ovin ou la protection de la faune sauvage. Quels éléments exploitent-ils d'un côté et délaissent-ils de l'autre ?

1. Un autre registre existe : celui de la disculpation. Mais, pour se disculper, on recourt moins à un récit qu'à un discours. Prenons à nouveau l'exemple de la chasse. D'une part, les chasseurs s'efforcent de reporter sur d'autres les torts dont ils se pensent accusés : les actes de braconnage sont toujours commis par les chasseurs des départements ou des pays voisins ; l'état insatisfaisant des populations est à imputer aux promeneurs, aux protecteurs, aux maladies, etc. D'autre part, ils essaient d'établir qu'ils ne sont pas responsables des actes qu'ils commettent (le goût pour la chasse est qualifié de virus ou de drogue), que la chasse s'accompagne de grandes souffrances qui méritent bien de petites compensations, ou encore qu'ils réparent par un grand bienfait les petits méfaits qu'ils ont pu commettre. Se reporter aux analyses éclairantes de Dalla Bernadina sur la « comédie de l'innocence », notamment dans Dalla Bernadina (1996).

Qualification de la chasse ancienne	Qualification de la chasse actuelle	Auteurs du récit	Qualification de l'évolution de la chasse	Qualification du chasseur actuel
respectueuse des populations animales	respectueuse	des chasseurs	dépréciation du savoir des chasseurs locaux	victime (brimé, méprisé)
respectueuse	irrespectueuse	des naturalistes et des gardes-moniteurs	décadence de la chasse	décadent
irrespectueuse	toujours irrespectueuse	des naturalistes et des gardes-moniteurs	absence d'évolution	égal à lui-même
irrespectueuse	respectueuse	des chasseurs	importance et difficulté de la mutation accomplie par les chasseurs	rationnel
irrespectueuse	encore irrespectueuse	des chasseurs	importance et difficulté de la mutation demandée aux chasseurs	perfectible

La question de l'éthique de la chasse ancienne a permis de repérer plusieurs registres de récits[1]. Deux d'entre eux peuvent être considérés comme de simples variantes. Ceux qui considèrent les chasseurs comme constamment mauvais au fil du temps se rapprochent en effet de ceux qui les disent décadents. Quant aux récits qui présentent le chasseur actuel comme « perfectible », ils se laissent assez aisément rattacher aux récits de rationalisation. On peut donc, en définitive, distinguer trois registres principaux, qui insistent soit sur la décadence des contemporains, soit sur leur rationalisation, soit sur les injustices dont ils sont victimes.

On retrouve ces trois grands registres dans la plupart des passages relatifs à l'évolution des pratiques, qu'ils concernent la chasse, le pastoralisme ovin ou la protection de la faune sauvage. Quels éléments exploitent-ils d'un côté et délaissent-ils de l'autre ?

1. Un autre registre existe : celui de la disculpation. Mais, pour se disculper, on recourt moins à un récit qu'à un discours. Prenons à nouveau l'exemple de la chasse. D'une part, les chasseurs s'efforcent de reporter sur d'autres les torts dont ils se pensent accusés : les actes de braconnage sont toujours commis par les chasseurs des départements ou des pays voisins ; l'état insatisfaisant des populations est à imputer aux promeneurs, aux protecteurs, aux maladies, etc. D'autre part, ils essaient d'établir qu'ils ne sont pas responsables des actes qu'ils commettent (le goût pour la chasse est qualifié de virus ou de drogue), que la chasse s'accompagne de grandes souffrances qui méritent bien de petites compensations, ou encore qu'ils réparent par un grand bienfait les petits méfaits qu'ils ont pu commettre. Se reporter aux analyses éclairantes de Dalla Bernadina sur la « comédie de l'innocence », notamment dans Dalla Bernadina (1996).

Numerical simulation of basin sedimentation affected by slope failure and debris flow runout

Simulation numérique de la sédimentation dans un bassin concerné par des instabilités de pente et des laves torrentielles

J. P.M. SYVITSKI, J. M. ALCOTT

Geological Survey of Canada, Bedford Institute of Oceanography
Box 1006, Dartmouth, NS. - Canada, B2Y 4A2
Tel. (1) 902 426 6867 - Fax (1) 902 426 4104

Abstract

This paper deals with the integration of two numerical models DELTA5 and SKRED, dedicated to two different phenomena : basin sedimentation for DELTA5 and viscoplastic debris flows for SKRED. The aim of this integration is to simulate basin sedimentation affected by slope failure and debris flow runout. After a description of these two finite difference models, the authors present different issues related to the factor of safety, the pore pressure and the earthquarte loading effect. Integration problems linked to bin size are discussed.

Résumé

Cet article est consacré à l'intégration de deux modèles numériques, DELTA5 et SKRED, destiné à la simulation de deux phénomènes : la sédimentation pour DELTA5 et les laves torrentielles viscoplastiques pour SKRED. L'objectif de cette intégration est de simuler des bassins sédimentaires affectés par des ruptures de pente et des coulées de débris. Après une description de ces deux modèles aux différences finies, les auteurs envisagent différents problèmes relatifs au facteur de sécurité, à la pression interstitielle et aux effets sismiques. Les problèmes d'intégration liés à la discrétisation de l'espace sont discutés.

DELTA6

DELTA6 is an advanced basin sedimentation model that combines the advantages of the finite difference numerical models DELTA5 and SKRED. DELTA5 is a unified 2-D process-response model that simulates the progradation of a river delta and the resultant fill of one or more marine basins (Syvitski, 1989; Syvitski and Daughney, 1992). The model simulates four mechanisms that affect the rate and style of basin-filling: (1) hemipelagic sedimentation of particles carried seaward by river plumes; (2) delta-front progradation as affected by bedload deposition at the river

mouth; (3) proximal slope bypassing, primarily by turbidity currents; and (4) downslope diffusive processes that work to smear previously deposited sediment into deeper water. Four size fractions in the mud size range: coarse silt, medium silt, fine silt and clay are initially distributed spatially using: (1) the velocity distribution developed from a buoyancy-dominated, free, two-dimensional jet flowing into a highly-stratified marine basin; and (2) a particle-scavenging model that takes into account the biogeochemical affects of settling of particles in a marine environment (i.e. flocculation). This hemipelagic component is predicted either seasonally (four times a year) or daily, and is based on fluctuations in river velocity and river mouth shape, and on the suspended load discharged into the sea. Sand deposition is predicted from the seasonal rate of turbidity current generation from delta front failure, and is directly affected by the bedload carried by the river.

Sediment accumulation is predicted spatially from a parabolic partial differential equation that combines these four mechanisms for depositing sediment within a basin. The final numerical solution employs a finite difference approximation solved by an explicit method. DELTA provides an opportunity to examine details of sedimentation events over time periods less than 10^5 years. Input parameters may vary over a number of user-defined time intervals. The accuracy of model predictions depends directly on the accuracy of the initial input parameters and the suitability of the model assumptions (cf. Syvitski et al., 1988, for model verification). The numerical approach was developed initially to understand Quaternary sedimentation in fjord-like basins (Syvitski, Smith, Calabrese and Boudreau, 1988; Andrews and Syvitski, in press), and later applied to the petroleum industry (Syvitski and Farrow, 1989; Ross et al., in press). It has since been used to understand the affects of near-future climate change scenarios on the hydrology and sedimentation within arctic basins (Syvitski and Andrews, in press). Development of equations used in DELTA and its sister programs GRAIN and RIVER are described elsewhere (Syvitski and Daughney, 1992; Syvitski and Alcott, 1993; Syvitski and Alcott, in prep.).

SKRED was developed for the Norwegian Geotechnical Institute by Fridtjov Irgens of the Institute of Mechanics at the Norwegian Institute of Technology, Trondheim. SKRED is a 2-D numerical model that simulates the movement of a viscoplastic debris flow with simulation of the flow stresses (effective, normal and shear), velocities, height and volume at regular time intervals. The physical approach is based on classical soil mechanics and the dynamics of granular material. The constitutive equations are based on a modified CEF fluid (Criminale, Ericksen and Filbey, 1958) where the plasticity part is represented by the generally accepted plasticity theories and the CEF fluid represents the viscoplastic part. The model, although developed to simulate the behaviour of snow avalanches has been successfully used to simulate the Sokkelvik flowslide in Norway. Development of equations used in SKRED are described elsewhere (Norem et al., 1987, 1989, 1990).

To introduce the action of debris flows through SKRED into the basin fill simulations of DELTA, a number of new subroutines were developed. One subroutine checks the seafloor profile at specified time intervals, identifies all peaks and plateaus and then checks whether a minimum horizontal distance for generating a failure surface exists. Another subroutine generates all possible failure planes on each potential surface using a fitted quarter-ellipse profile. A third subroutine calculates the minmium factor of safety for each surface based on a modified Janbu Method of slope stability analysis, which ignores inter-slice forces. The factor of safety for each element is calculated and Newton-Raphson iterations are performed until a convergence of 0.0001 is achieved.
The factor of safety, F, is given as :

$$F = \frac{f\sum(b\, s \sec^2\alpha)}{\sum W \tan\alpha}$$

where

$$s = \frac{c + (\frac{W}{b} - \Delta u)\tan\phi}{1 + \frac{\tan\alpha \tan\phi}{F}}$$

and f is the correction factor, b is the slice width, is slope angle, W is weight, c is cohesion, is the internal friction angle set to 30° in DELTA6 (H. Lee, personal communication), and Δu is the excess pore pressure. The equations are not valid for cases where (1 + tanatan/F) ≥ 0.2. The modified Janbu is quite accurate for long flat failure surfaces, but requires the correction factor to account for other surfaces. The correction factor, f, (after Morganstern and Price, 1965), is based on the ratio of the maximum depth perpendicular to the slope over the length of the failure plane along the slope (for the cases $c \neq 0$ and $f \neq 0$ and $c = 0$). The case $f = 0$ has been ignored, as it is largely an unrealistic laboratory state and does not occur naturally.

DELTA6 refers to pore pressure (Δu) as that in excess of the hydrostatic pressure (the difference between the pore pressure at the base of the slice and the external water level to which seepage is occurring). Gibson (1958) describes pore pressure as a function of sedimentation rate. For cases where the base is impermeable and x, γ', h, t and c_v are known, pore pressure is given as :

$$\Delta u = \gamma' mt - \gamma'(\pi c_v t)^{-0.5} e^{-\frac{x^2}{4c_v t}} \int \xi \tanh \frac{m\xi}{2c_v} \cosh\left(\frac{x\xi}{2c_v t}\right) e^{-\frac{\xi^2}{4c_v t}} d\xi$$

Where γ' is the submerged unit weight ($\gamma_{sat} - \gamma_w$), m is h/t or sedimentation rate, t is time, c_v is the coefficient of consolidation (10^{-4} cm²/sec), x is the horizontal distance from bedrock to the base of the element, $x = x/h(t)$, and h is height of the sediment

column. Gibson developed a design chart solution to the above equation, from which the regions $1 \leq x/h \leq 0.6$ can be approximated as linear. Each curve on the chart is defined by a time term, T $(m^2/c_v t)$. The linear portion of these curves can be represented by the equation:
$x = (y - 1.0)/(dy/dx)$ and family of curves developed for dy/dx and T as:

$$dy/dx = 6.4\,(1 - T/16)^{17} + 1.0$$

based on the maximum values $T_{max} = 16$ and $dy/dx_{max} = 6.4$. Pore pressures may then be determined for any value of T from zero to infinity. Where $x/h < .6$ the equation is not valid. This generally occurs in a deep basin where the total height of the sediment column is small. Pore pressure can be assumed to be zero except for the following cases : 1) underconsolidation due to rapid sedimentation; 2) gas generation; 3) 'artesian' gas or water pressures in lower formations; 4) external loading, wave and earthquake (Saxov and Nieuwenhuis, 1982). DELTA does not presently allow for consolidation and dewatering. Sediments are assumed to be saturated and underconsolidated (condition 1 for excess pore pressure applies).

Earthquake loading effects as developed for the case of an infinite slope account for the reduction of the factor of safety:

$$F = \frac{c' + \gamma' z \cos^2\alpha \tan\phi'}{\gamma' z \sin\alpha \cos\alpha + K \gamma z \cos\alpha}$$

where c' is the effective cohesion, ' is the effective friction angle, is the slope of the seafloor, ' is the submerged unit weight, is the saturated unit weight of sediment, $_w$ is the unit weight of water, z is sediment thickness, and K is the peak horizontal earthquake acceleration (as a percent of the acceleration due to gravity). In order to easily incorporate this effect into the Janbu method we handle earthquake acceleration as a function of excess pore pressure such that:

$$K = c\Delta u$$

where c is a constant greater than 1.

Once a failure site is identified, the failure surface and the dimensions of the discretized sediment mass are passed to our modified SKRED subroutine. The user is required to supply the following variables: shear viscosity; bed friction; and normal stress viscosities. As long as the debris flow's velocity is non-zero the subroutine will continue to calculate flow height, slip and slide velocities. The number of iterations is dependent on the time step. We employ a small time step (0.1 sec) to preserve resolution.
Runout distances from the model of kilometers are common with the debris flow material spread out over several bins (0.5 to 2 km). Deposition often occurs in flatter sections of the basin; with short basin floor lengths, some runup onto the opposite margin is common. The bin lengths used in DELTA6 are generally 30 -100 m. These are considerably larger than the 1 to 10 m bin length used with SKRED. To determine the

effects of the variation of bin length on runout distance and front velocity a sensitivity analysis was performed. The only parameter varied was the number of elements along the flow path. For small numbers of elements (1 to 8) the runout values and front velocity values fluctuated wildly. As the number of elements increased there was always a convergence of runout distance and front velocity. This suggests that the correct number of elements are necessary for SKRED to provide stable and reproducible runout distances.

One implication for DELTA6 is that the original single bin size (DELTA5) was too large for easy inclusion of SKRED. The existing bins describing a failure surface were thus split into smaller bins and reassembled later into their original bin lengths by averaging the points on either side of the original bin position. A few problems still remain in terms of swapping errors. Once these are resolved, DELTA6 will offer earth scientists the possibility of creating realistic sedimentary sequences and then evaluating their slope failure potential in terms of steady state and non-steady (i.e earthquakes) conditions. The effect of episodic debris flow deposits on the subsequent path of bottom currents such as turbidity currents could then be evaluated.

References

Almagor, G., and Wiseman, G. 1982. Submarine slumping and mass movements on the continental slope of Israel. In: Saxov S., Nieuwenhuis J.K. (eds.) Marine Slides And Other Mass Movements, Nato Conference Series IV: Marine Sciences 6: 95-128.

Andrews, J.T., and Syvitski, J.P.M., in press. Sediment fluxes along high latitude glaciated continental margins: Northeast Canada and Eastern Greenland. In: M. Meybeck and W. Hay (eds.) *Global Sedimentary Geofluxes.* National Academy of Sciences Press, Washington.

Chowdhury, R.N. 1978. Slope Analysis. Developments in Geotechnical Engineering 22: 143-144.

Criminale, W.O., Jr., Ericksen, J.L., and Filbey, G.L. 1958. Steady shear flow of non-Newtonian fluids. Archive for Rationale Mechanics and Analysis 1: 410-417.

Gibson, R.E. 1958. The progress of consolidation in a clay layer increasing in thickness with time. Géotechnique 8: 171-182.

Morganstern, N.R., and Price, V.E., 1965. The analysis of stability by general slip surface. Géotechnique 15: 79-93.

Norem, H., Locat, J., and Schieldrop, B., 1990, An approach to the physics and the modeling of submarine flowslides: Marine Geotechnology, v. 9, p. 93-111.

Norem, H., Locat, J., and Schieldrop, B., 1989. Simulation of snow avalanche flow in run-out zones. Annals of Glaciology no. 13, 218-225.

Norem, H., Locat, J., and Schieldrop, B., 1987. A continuum model for calculating snow avalanche velocities. Proceedings of Avalanche Formation, Movements and Effects, Davos, 1986, IAHS Publication 162: 363-379.

Ross, W. C., Halliwell, B. A., May, J. A., Watts, D. E., and Syvitski, J. P. M. in press. The Slope Readjustment Model: A New Model for the Development of Submarine Fan/Apron Deposits. Geology.

Saxov S., Nieuwenhuis J.K., 1982, Marine Slides And Other Mass Movements, Nato Conference Series IV: Marine Sciences 6: 353 p.

Syvitski, J.P.M., 1989, Modelling the sedimentary fill of basins, *in* Agterberg, F.P., and Bonham-Carter, G.F., eds., Statistical Applications in the Earth Sciences: Geological Survey of Canada, Paper 89-9, p. 509-515.

Syvitski, J.P.M., and Andrews, J.T. in press. Global change: numerical modelling of sedimentation and coastal processes, eastern canadian arctic. Arctic and Alpine Res.

Syvitski, J.P.M., and Alcott, J.M. (In Prep.) RIVER3: Simulation of water and sediment river discharge from climate and drainage basin variables. Computers and Geoscience.

Syvitski, J.P.M., and Alcott, J.M. 1993. GRAIN2: Predictions of particle size seaward of river mouths. *Computers & Geoscience* 19(3): 399 - 446.

Syvitski, J.P.M., and Daughney, S., 1992, DELTA2: Delta progradation and basin filling, Computers and Geosciences 18(7): 839-897.

Syvitski, J.P.M., and Farrow, G.E., 1989, Fjord sedimentation as an analogue for small hydrocarbon-bearing fan deltas, *in* Whateley, M.K.G., and Pickering, K.T., eds., Deltas: Sites and Traps for Fossil Fuels: Geological Society of London, Special Publication No. 41, p. 21-43.

Syvitski, J.P.M., Smith, J.N., Calabrese, E.A., and Boudreau, B.P., 1988, Basin sedimentation and the growth of prograding deltas, Journal of Geophysical Research, v. 93, p. 6895 - 6908.

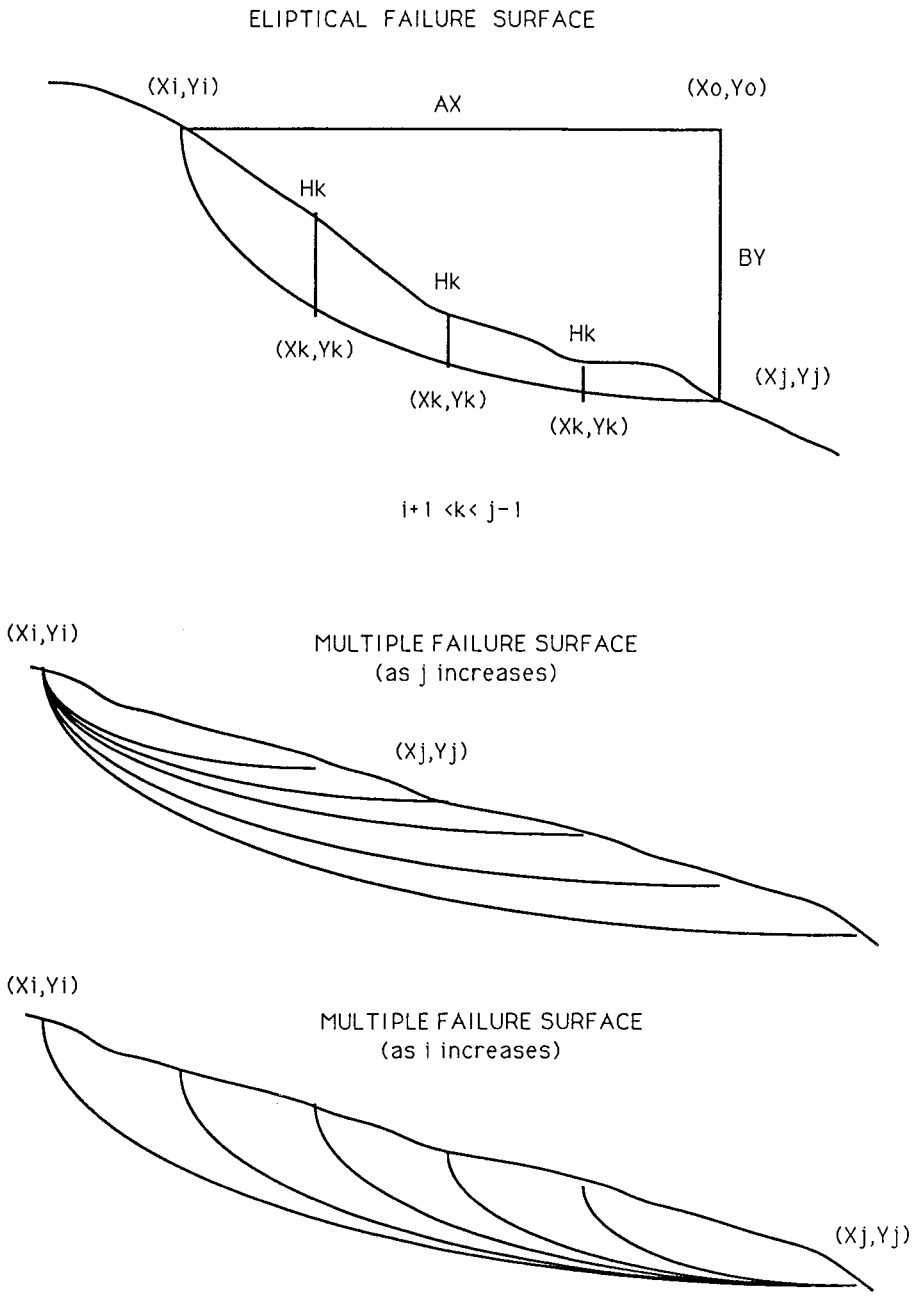

Figure 1. Cartoon representing the initial failure surface, that of a quarter of an ellipse, and the search for the largest failure surface above and below the initial failure surface in increments of i and j.

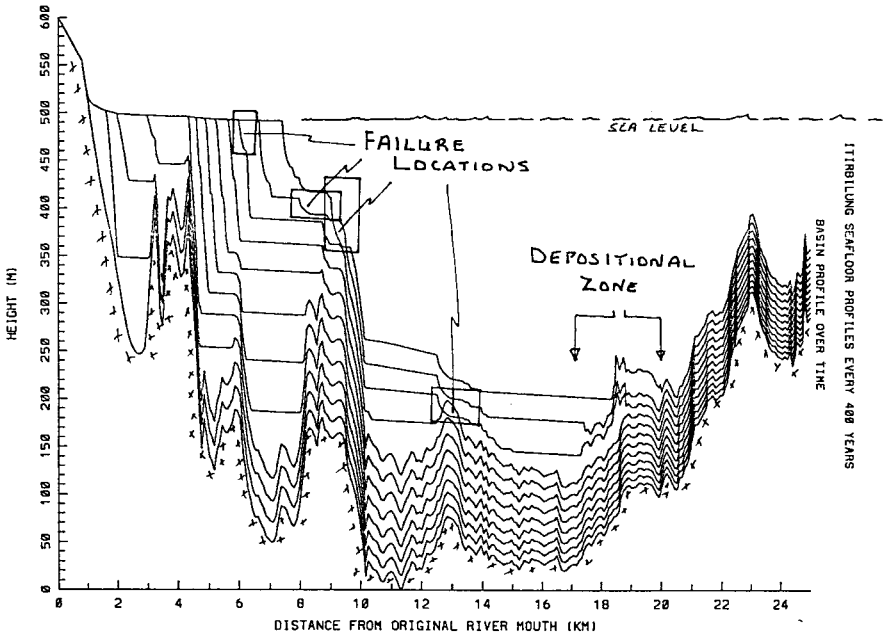

Figure 2. The seafloor within an arctic basin (Itirbilung Fjord, Baffin Island) through time and according to a DELTA6 simulation. The seafloor is adjusted due to sediment input 4 times a year. Shown is the seafloor at intervals of 400 years. The initial bedload is trapped at the delta and within the shallow water "perched basins" as turbidites; the outer fjord is mantled conformably with hemipelagic deposits from the fallout of river plumes. At year 3399, two initial failures occurred. The first with a volume of 5,833 m^3/m width occurred along a failure length of 0.21 km, at a position 5.94 km from the origin, with an initial maximum height of 31.3 m at its mid-section. The second of volume 18,639 m^3/m width occurred along a failure length of 0.76 km, at a positon 12.56 km from the origin, with an initial maximum height of 33.7 m at its mid-section. These debris flows moved at average velocities at their upper boundaries of 73 and 34 m/s, respectively. The flows travelled 12.7 km and 5.2 km, respectively, before deposition occurred. At year 3799, an initial failure volume of 12,404 m^3/m width occurred along a failure length of 0.84 km, at a position 9.06 km from the origin, with an initial maximum height of 19.4 m at its tail. The debris flow moved at an average velocity at its upper boundary of 17.7 m/s. The flow travelled 8.6 km before deposition occurred. At year 4199, an initial failure volume of 24,204 m^3/m width occurred along a failure length of 0.55 km, at a position 9.06 km from the origin with an initial maximum height of 46.7 m near its mid-section. The debris flow moved at an average velocity at its upper boundary of 66.0 m/s. The flow travelled 10.4 km before deposition occurred.

Fluid Mechanical Modelling of the Viscous Debris Flow

Modélisation en mécanique des fluides d'une lave torrentielle visqueuse

T. TAKAHASHI

Disaster Prevention Research Institute, Kyoto University
611 Kyoto - Japan
Tel. (81) 774 32 31 11 - Fax (81) 774 32 60 39

Abstract

After an analysis of the differences between stony inertial flows and viscous debris flows the emphasis is laid on the particle sustaining mechanism which takes place in a viscous debris flow. Critical particle concentrations corresponding to different types of interaction between particles are defined. The sustaining mechanism might be the squeezing flow expelled from the void between approaching particles. The constitutive equations for viscous debris flows is given under an assumption on the origin of particle sustaining dispersive pressure and shear stress. The characteristics of flow are deduced. If the material is a well graded mixture, the flow can transport a much larger solid concentration. A hierarchic buoyancy increment effect is suggested as a possible cause for the high competence to transport particles.

Résumé

Après une analyse des différences entre les écoulements inertiels pierreux et les laves torrentielles visqueuses, l'accent est mis sur le mécanisme de transport de particules dans ces coulées. Des concentrations critiques en particules correspondant à différents types d'interaction entre particules sont définies. Le mécanisme de transport peut être lié à un flot d'expulsion de vide situé entre des particules qui se rapprochent. Les lois de comportement des laves torrentielles sont données à partir d'une hypothèse sur l'origine de la pression dispersive qui soutient les particules et de la contrainte de cisaillement. Les caractéristiques de l'écoulement sont déduites. Si le matériau est un mélange avec un granulométrie étalée, l'écoulement peut transporter une concentration solide plus importante. Un effet d'augmentation de poussée est proposée comme cause possible d'une grande capacité à transporter des particules.

Introduction

It seems to exist two distinct regimes in the debris flows; one is the stony inertial debris flow and the other is the viscous debris flow. The front part of the stony debris flow is mainly comprised of big boulders, stones and water, and the depth of the flow may be at most a few ten times of the mean diameter of the solids phase. It often stops even in a steep gully and generally by running out to a place flatter than 4 or 3

degree it ceases themotion. The constitutive relations for such a flow including the water devoiding granular flow have been extensively discussed stemming from Bagnold's conceptof the dispersive pressure due to collision of particles, and the variouscharacteristic behaviors of the stony inertial debris flows have been explained using those constitutive equations (Takahashi 1991). Therefore, the main particle sustaining force in the flow, when the local particle volume concentrationis less than about 0.5, seems to be attributable to the repulsion on the frequent particle encounter.

The viscous debris flow, on the other hand, contains sufficiently high concentration of very fine materials such as clay and silt and the dominant coarse particles are usually smaller than a few ten centimeters in diameter. Accumulation of big particles in the front part is not conspicuous and sometimes it is highly turbulent. The rear part is, however, laminar with very placid surface. It can sometimes flow in a fantastic speed even in the gully flatter than 3 degree. The constitutive relations of such a flow was also suggested by Bagnold (1954), but since then attentions have been focused on either the rheological characteristics of the interstitial slurry or the back analyses of the parameters appeared in the assumed constitutive equations using the observed data of the debris flows. So far many investigations have attributed the high competence of the viscous debris flow to freight large particles to the yield strength of the interstitial slurry. In this concept, the larger the particles to be freighted, the larger the yield strength should be. This, in turn, meets with a difficulty that theoretically the flow cannot exists on a gentle slope where the viscous debris flows are often observed. Thus, discussions on the coarse particle upholding mechanism in the viscous debris flow are wanting.

Particle sustaining mechanism in a viscous debris flow

The linear concentration, λ, defined by Bagnold (1954) is the ratio of the particle diameter to the mean free distance between the particles and it is given by the following equation.

$$\lambda = \left\{ \left(\frac{c_{*0}}{c} \right)^{1/3} - 1 \right\}^{-1} \tag{1}$$

When a granular material comprised of uniform spheres is most densely packed, the theoretical volume concentration of the solids in it, c, is as much as 0.741 ($c=c_{*0}$) and the λ at the maximum possible concentration is, therefore, infinitive. The most sparse cannon ball packing is possible at $c_*=0.605$ ($\lambda \cong 14$), and the solids concentration in the most sparse square packing is attained at $c_*=0.523$ ($\lambda \cong 8$). At a solids concentration larger than λ_2 ($\cong 17$), particles can not dislocate each other by interlocking. General shearing of the granular material becomes possible when $\lambda<17$, but if $\lambda > \lambda_3$ ($\cong 14$), particles are always in touch with each other and the applying shear must overcome the resisting stress due to the internal friction and the yield strength of the interstitial fluid if any. When $\lambda < \lambda_3$, in some arrangements of particles, and when $\lambda <8$, in any arrangement of particles, any particle is, on the

average, free from other particles. The resistance to shearing in such a substance devoiding any skeleton structure should only originate from the resistance in the interstitial fluid (the viscous stress and yield strength if any).
Those critical concentrations for the well graded mixture are not clear yet, but fine particles can enter into the void among the coarse particles and incidentally those concentrations may shift to larger values. For example,Rodine and Johnson (1976) suggests by their theoretical analysis that 89 to more than 95 vol.% debris can be clastic materials without significant particle interlocking, and the samples obtained at the Jiangjia Gully in China showed c^*_0=0.61~0.73,whereas the very fast debris flows passed through the channel whose slope was only about 3° with the concentrations c=0.61~0.72 (Wu et al. 1990).
Under the action of gravity, however, the particles heavier than the surrounding sheared fluid (no strength exists in the fluid under shear) cannot maintain their neutral positions but settle down to the bed. This means to keep the heavy particles dispersed in the entire depth, some particle supporting forces which balance with the submerged weight should act. A candidate of cause of such force in a slow viscous flow might be the squeezing flow expelled from the void between the approaching particles. This squeezing flow would dissipate energy and the excess shear stress would be produced.
Content of very fine materials (smaller than about 0.05mm) may be important in determining the mechanics of debris flow, because they are not only effective to increase the apparent density of the interstitial fluid; thereby increasing buoyancy so that reducing the necessary particle sustaining force, but also increase the viscosity of the fluid and influence the resistance to flow as well as particle dispersion pressure.

Constitutive relations of the viscous debris flow

Consider the case in which the volume concentration of large uniform spherical particles c in the slurry is less than 0.51, which means the individual large particles are, on the average, not in contact with one another. Even if the stationary slurry has a certain strength to sustain the large particles, once it is sheared and under continuous deformation, the skeleton structure in the slurry is already disappeared and no matrix strength remains. The source of the dispersive force to be able to sustain particles in such a flow should be attributed to the dynamic structure of the flow.
Consider a particle i is moving with a relative velocity δu over a layer of particles as shown in Fig.1, where the particles are immersed in the static viscous fluid. When the particle i approaches the particle j in the lower layer, fluid in between the two particles is expelled and a flow around the particle is generated. The access speed between the two particles in the direction of the line connecting the centers is $\delta u \sin\psi$, and so the fluid dynamic force applying opposite to the access direction on the i particle is $6\pi\mu_f a^2 \delta u \sin\psi / s$, where μ_f is the fluid viscosity, a is the particle radius, ψ is the angle of the line of centers to the vertical direction at a certain time and s is the free distance between the particles [Davis et al. 1986]. The upward fluid dynamic force, F, acting on the i particle is then :

$$F = 6\pi \mu_f a^2 \frac{b \sin\psi \cos^2\psi}{b - \cos\psi} \frac{du}{dz} \tag{2}$$

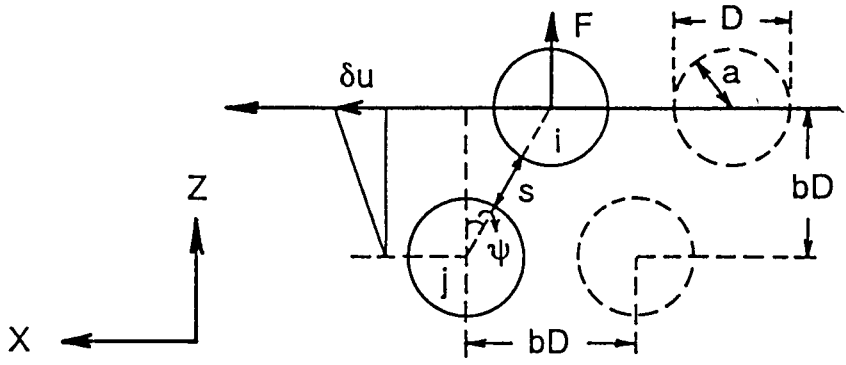

Fig.1 Definition sketch of sheared granular material

The i particle may exist at any position in the area of $4a^2b^2$, so that, the dispersive pressure applying to this area may be written as

$$p = \frac{3}{2}\left[\frac{1}{b}\frac{\sin\psi \cos^2\psi}{b - \cos\psi}\right]_{av} \mu_f \frac{du}{dz} \tag{3}$$

where $[\ ]_{av}$ means the mean value in the bracket in the process of approaching. As the particle i approaches to the j particle, the pressure increases, and at a certain ψ it becomes maximum and then decreases to zero at the top of the j particle, where $\psi = 0$. The mean value in the blacket during the total approaching process is larger, the smaller the b value; i.e.,the larger the λ, the larger the dispersing pressure. This implies that to be capable to sustain a particle under a relative velocity, the distance between the particles should be smaller than a certain value; i.e., the concentration of the particles should be larger than a certain value. As the i particle moves apart, a negative pressure may result by the backward flow to fill the gap between the particles. But this may not be as large as that in the approaching process due to weak return flow from larger area around the particle (The gap in between the two particles has become smaller than the average distance while in approaching, so that the remaining space around the i particle while in departing should be larger than the average.). The actual phenomena in the granular material should be more complicated, because the i particle is nothing but a randomly chosen one in the same layer it belongs to. Namely, the effects of assemblage of particles such as obstruction to the expelled flow due to narrowness of the gap and the change of the gap space due to deceleration and acceleration motion in the processes of approaching and departing are neglected; when the i particle is going apart from the j particle, it is, at the same time, approaching the one standing in a line downstream of the j particle; and moreover, the particles in a layer do not form a straight line

and the trace of the i particle approaching from lower position will form a curve around the j particle. Nevertheless, the dispersive pressure may be a function of solids concentration. Consequently, herein, the following formula is assumed.

$$p = g(\lambda)\,\mu_f \frac{du}{dz} = k\,\lambda^2\,\mu_f \frac{du}{dz} \tag{4}$$

where k is a numerical constant.
The shearing stress would be the sum of the viscous stresses due to deformation of the interstitial fluid and that produced by the expelled flow. Then,

$$\tau = \mu_T \frac{du}{dz} = f(\lambda)\,\mu_f \frac{du}{dz} + \Phi\, g(\lambda)\,\mu_f \frac{du}{dz} \tag{5}$$

where μ_T is the apparent viscosity of the flow and Φ is a numerical constant.
Because the particles cannot be deformed, the shear strain concentrates in the decreased space among particles, and this reduction of shearing space affects to increase the apparent viscosity of the interstitial fluid. If energy losses in the unit volume with and without particles are assumed equal, $f(\lambda)$ may be written as

$$f(\lambda) = 1 + \lambda \tag{6}$$

Then,

$$\mu_T = (1 + \lambda + \Phi k \lambda^2)\mu_f \tag{7}$$

$$\frac{\tau}{p}(\equiv \Psi) = \frac{1 + \lambda + \Phi k \lambda^2}{k\lambda^2} \tag{8}$$

Bagnold (1954) gave the following formulae according to his own theory and experiments.

$$\mu_T = (1 + 1.5\,\lambda + 0.5\,\lambda^2)\mu_f \tag{9}$$

$$\Psi = 0.77 \tag{10}$$

The above mentioned discussions focused on the case where individual particles in the flow are not in touch with one another, and therefore, no direct stress transmission among the particles exists. When the solids concentration is large (for uniform particle case; c >0.51), the effect of the particle contact becomes important. Even in such a case, if one watches a particular particle's motion, it would move in contact with other particles for a while and become free in another time. In this process, the total pressure in excess of the buoyancy p may be the sum of that directly transmitted between the particles, p′, and the dispersive pressure produced by the

expelled flow among particles. Consequently, it may be possible to flow on a flatter slope on which the quasi-static regime flow cannot exist.

Characteristics of flow

Consider a steady uniform flow in a rectangular channel, which is composed of highly viscous liquid and uniform particles and the solids concentration is less than 0.51. The pressure and the shearing stress balance equations are, respectively, from (4) and (5)

$$k\lambda^2\mu_f\frac{du}{dz} = (\sigma - \rho)\, g\cos\theta \int_z^h c\,dz \tag{11}$$

$$\mu_T\frac{du}{dz} = \frac{R}{h}\left\{(\sigma - \rho)\, g\sin\theta \int_z^h c\,dz + \rho g\sin\theta\,(h - z)\right\} \tag{12}$$

where R is the hydraulic radius and the shearing stress is assumed to distribute evenly on the bed as well as on the side walls.
Making some approximations and assuming Ψ = const., the distribution of the solids concentration under the boundary condition; at z=0, $c=c_b$, is obtained from (11) and (12) as

$$\left|\frac{c - c_\infty}{c}\right| = \left|\frac{c_b - c_\infty}{c_b}\right|\left(1 - \frac{z}{h}\right)^{3k\{(h/R)\Psi - \tan\theta\}} \tag{13}$$

where

$$c_\infty = \frac{\rho\tan\theta}{\{(h/R)\sigma - \rho\}(\Psi - \tan\theta)} \tag{14}$$

Equation (13) implies that if $c_b=c_\infty$, $c=c_\infty$ for the entire depth, if $c_b>c_\infty$, c decreases upward and at the surface $c=c_\infty$, and if$c_b<c_\infty$, the maximum concentration c_∞ appears at the surface and the concentration decreases downward. The experiments using a rigid bottom flume (Takahashi and Kobayashi 1993), however, show that flow without deposition can exist when the average particle concentration in the supplied flow, c_s, is smaller than or equal to c_∞ and the particles distribute in the entire flow depth only when c_s is between a certain critical concentration c_c and c_∞.
When c_s is smaller than c_c particles can occupy only the lower part of the flow. In any case, particles distribute nearly uniformly throughout the particle mixture layer. In this context, Ψ in (14) is important and the experimental data suggest it is around 0.5. The value of c_c would be a function of μf, D, σ/ρ, du/dz, etc. and in the experiments it was about 0.3.
When particles distribute uniformly througout the depth, the velocity distribution is obtained from (12) as following:

$$\frac{u}{u_*} = \frac{u_* h}{\mu_T}\{(\sigma - \rho)c + \rho\}\left\{\frac{z}{h} - \frac{1}{2}\left(\frac{z}{h}\right)^2\right\} \tag{15}$$

where

$$u_* = \sqrt{gR\sin\theta}.$$

This is nothing but the parabolic velocity distribution for a laminar flow.
Fig.2 is an example of comparison of experimental velocity distribution with (15). The experiment was conducted in a rigid bed flume of 10cm in width and 16° in slope by introducing the mixture of sand (D=2~4-mm, D_{50}=3.25mm, σ=2.65 g cm^{-3}) and the slurry made of kaolin powder and water (ρ=1.386 g cm^{-3}, μ_f=1.5 poise) whose sand particle concentration c_s was 0.287 (unit volume weight γ=1.74 g cm^{-3}). The depth of flow in this case was h=2.8 cm. To determine μ_T in (15), Φ_k should be known beforehand. The average value of it was obtained by experiments under various combinations of μ_f, c, θ and h. Although there are some problems to be further discussed especially for very viscous slurry case, Φ_k seems to be nearly constant as long as μ_f is within a same order of magnitude. But if μ_f changes by an order or more, it seems drastically change.

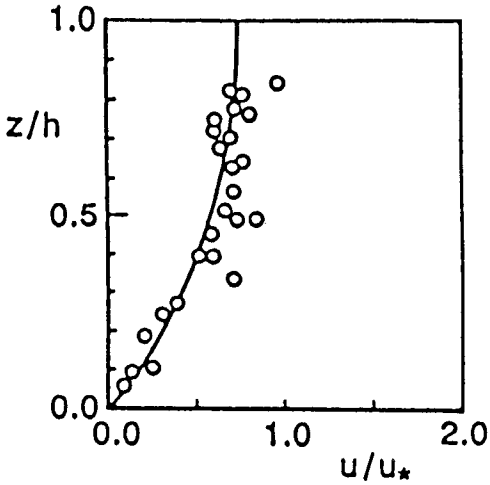

Fig.2 Velocity distribution in the viscous debris flow.

Fig.3 shows the specific viscosities versus particle concentration obtained by the experiments. This figure suggests that, in determining the apparent viscosity of the debris flow, when μ_f is comparably small, the effect of expelling flow working to disperse particles is more important than the effect of reduction of the shearing space due to occupation by particles. When μ_f is very large, the latter effect seems to become more important. The curve ``B'' in Fig.3 is Bagnold's equation (9), and in this equation, the ratio of the two effects is always constant.

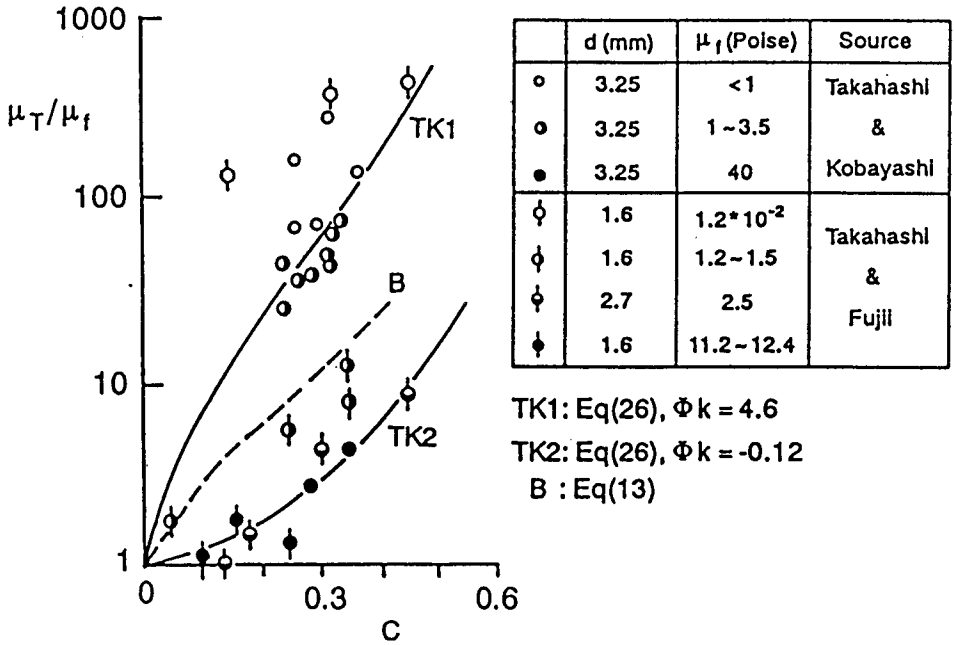

Fig.3 Specific viscosities of the viscous debris flows versus coarse particle concentration.

The magnitude of ψ obtained in the experiments (around 0.5 in the author's experiments and 0.77 in Bagnold's experiments) is worth noting. Substitution of those values in (14) gives c_∞, which is the maximum possible particle concentration in the uniform equilibrium flow and if the channel slope is flat it becomes only a small value. Nevertheless, at the Jiangjia gully in China the debris flows are observed freighting particles by concentrations far larger than thus calculated equilibrium values. What mechanism is then working for such a high fluidity in the Jiangjia gully case? The key factor might be that the material is a well graded mixture. Provided particles in a certain grade of diameters are suspended in the expelling flow which is generated by shearing, the weight of those particles is transmitted to the fluid phase and it results in an increment of the aparent density of fluid. This works to increase buoyancy acting to larger particles and diminishes the necessary intensity of expelling flow to suspend the larger grade particles. Such a hierarchic particle supporting idea, although the fundamental mechanism considered is completely different, was first suggested by Rodine and Johnson (1976). Therefore, the high fluidity may be the unique characteristics of the poorly sorted viscous debris flow and to prove this further experimental investigations are needed.

Conclusion

The constitutive equations for the viscous debris flow is given under the hypothesis that the squeezed flow arising from the shearing between the two adjacent layers of particles in the viscous fluid produces the particle sustaining dispersive pressure as well as the shear stress. Those equations are applied to the flume experiments in the laboratory and the characteristics of flow such as the equilibrium solids

concentrations, the specific viscosity and velocity distributions are deduced. The particle concentration in an equilibrium viscous flow composed of nearly uniform materials, in which the particles are transported without deposition, is not much different from that of the inertial flow on the same bed slope. This fact brings a kind of paradox that if the material is the well graded mixture, as observed in the actual viscous debris flow, the flow can transport much more dense solids concentration. A hierarchic buoyancy increment effect was suggested for a possible cause of high competence to transport particles. The viscosity of the highly freighted viscous debris flow becomes very large in comparison to that of the interstitial slurry. The specific viscosity defined as the ratio of that of the entire debris flow material to that of the slurry increases with increase in the concentration of the coarse particles,but the tendency of the change versus concentration seems different depending on the viscosity of the slurry. Detailed investigation on the mechanics of viscous flow of well graded mixture would be the key to disclose the whole aspects of the debris flows.

References

Bagnold, R. A. (1954) Experiments on a gravity-free dispersion of large solid spheres in a Newtonian fluid under shear, Proc. Roy. Soc. London, A, 225, pp.49-63

Davis, R. H., Serayssol, J. M. and Hinch, E. J. (1986) The elastohydrodynamic collision of two spheres, J. Fluid Mech., 163, pp.479-497

Rodine, J. D. and Johnson, A. M. (1976) The ability of debris, heavily freighted with coarse clastic materials, to flow on gentle slopes, Sedimentology, 23, pp.213-234

Takahashi, T. (1991) Debris flow, Monograph Series of IAHR, Balkema, pp.1-165.

Takahashi, T. and Kobayashi, K. (1993) Mechanics of the viscous type debris flow, Annuals, D.P.R.I., Kyoto Univ., 36B-2, (in printing in Japanese)

Wu, J., Kang, Z. (1990) Observation research on debris flow in Jiangjia ravin, Yunnan, Beijing Science Press, pp.1-251 (in Chinese).

Volcano-glacier interactions : field survey, remote sensing and modelling. Case study : Nevado del Ruiz, Colombia

Interactions volcan-glacier : étude de terrain, télédétection et modélisation. Cas du Nevado del Ruiz en Colombie

J.-C. THOURET*, J. VANDEMEULEBROUCK†, J.-C. KOMOROWSKI‡

*URA 10,C.R.V., Université Blaise Pascal Clermont II
5 rue Kessler, 63000 Clermont-Ferrand - France
Tel. (33) 73 34 65 90 - Fax (33) 73 34 65 44

†Laboratoire d'Instrumentation Géophysique, C.R.V., Université de Savoie, 73376 Le Bourget du Lac - France

‡Instituto de Geofisica, Universidad Nacional Autonoma de Mexico
Mexico DF, CP 04510 - Mexico and I.P.G., Université Paris VI - France

Abstract

Interactions of hot eruptive products with snow and ice have been inferred from geomorphological and glaciological perturbations on ice-clad active volcanoes. These perturbations record a variety of processes, including rapid melting, snow and ice avalanching, surficial abrasion, and mechanical scouring or gullying. The loss of large volumes of snow and ice during eruptions results mainly from: (i) the passage of pyroclastic flows and surges or hot blasts on the glacier that caps the mountain, (ii) the contact of subaerial lava flows or tephra with ice or snow, and (iii) the eruptive or geothermal activity which melts the bases of ice caps. Pyroclastic and lahar deposits, vegetation, and ice and snow were separated on a 1986 SPOT satellite image using remote sensing techniques and extensive field survey at Nevado del Ruiz, Colombia. Geomorphological and hydraulic parameters of transient, mixed avalanches (tephra, snow, and ice) which transformed to lahars point to non-channelized, unstratified, high-density, gravity-driven flows. Using 3D-ortho-images and field survey measurements to compute surface areas where snow and ice were lost from the ice cap reveal that as much as 38.5-44 x 10^6 m^3 of meltwater were released in 20-90 minutes during the November 13, 1985, eruption. Such volumes of meltwater imply a high melting rate and a vigorous heat transfer from hot eruptive products to snow and ice. Preliminary melting scenarios based on vigorous deposition of hot debris on snow point to melting rate as high as 10^{-2} m/min. Mechanical entrainment and comminution of snow and ice are important processes in triggering lahars.

Résumé

Les interactions de produits éruptifs chauds avec la neige et la glace ont été déterminés à partir des perturbations gémorphologiques et glaciologiques sur des volcans actifs recouverts de glace. Ces perturbations gardent la trace de différents processus tels que la fonte rapide, les avalanches de neige et de glace, l'abrasion de surface, le creusement par érosion de gorges. La perte d'importants volumes de neige et de glace au cours des éruptions s'explique principalement par (i) le passage d'écoulements pyroclastiques ou de bouffées chaudes sur les glaciers qui recouvrent le sommet de la montagne, (ii) le contact entre des écoulements de laves ou d'autres produits volcaniques et la glace ou la neige, (iii) l'activité éruptive ou géothermique qui fait fondre la base des couvertures de glace. Les dépôts pyroclastiques et les dépôts de lahars, la végétation, la glace et la neige ont été identifiés sur une image de satellite SPOT de 1986 en utilisant des techniques de télédétection et des relevés réalisés sur le Nevado del Ruiz en Colombie. Les paramètres géomorphologiques et hydrauliques d'avalanches transitoires, mixtes (neige et glace) qui se transforment en lahars mettent en évidence des écoulements gravitaires forte densité non canalisés et non stratifiés. L'utilisation d'orthoimages 3D et des mesures topographiques destinées à calculer les surfaces où la neige et la glace avaient disparu, a montré que jusqu'à 38,5 - 44,10 6 m3 d'eau de fonte avaient été libéré en 20-90 mm durant l'éruption du 13 novembre 1985. De tels volumes d'eau de fonte implique un taux de fonte élevé et un transfert de chaleur important des produits éruptifs chauds vers la neige et la glace.

Des scénarios de fonte basés sur une dépôt important de produits chauds sur la neige conduisent à un taux de fonte de 10 mm/mn. L'entraînement mécanique et la comminution de la neige et de la glace sont des processus importants dans le déclenchement des lahars.

Introduction

Eruptions on ice-clad volcanoes include a complex variety of mechanisms that can rapidly release enough meltwater to trigger large-scale sediment/water flows. About 110 reported historic eruptions have perturbed ice caps or snowpack and triggered lahars on at least 40 active volcanoes (e.g. Major and Newhall, 1989). For the purpose of this article, we will consider the 1985 eruption at the ice-clad and currently active Nevado del Ruiz stratovolcano (Colombia). For comparitive purposes, we will use published data from the 1980 and 1982 Mount St. Helens (Washington) eruptions, as well as unpublished data for the 1990 Mount Redoubt (Alaska) eruption (R.J. Janda, unpublished data).

Interaction of hot eruptive products with snow and ice has been inferred from geomorphological and glaciological perturbations on snowpacks and ice caps. These perturbations probably record a variety of processes such as rapid melting, snow-and-ice avalanching, surficial erosion or abrasion, and mechanical scouring or gullying. Interactions are chiefly induced by: (i) the passage of pyroclastic flows, pyroclastic surges, or hot blasts (laterally-directed eruptions) on ice or snow, (ii) the contact of subaerial lava flows or tephra with ice or snow, and (iii) basal melting of ice caps.

These disruptive interactions on ice caps, which can be generated even by relatively small eruptions, can induce mixed avalanches (tephra, ice, and snow) that transform downstream to large-volume lahars (volcanic debris flows). Lahars increase their volumes significantly by entrainment of water and eroded sediment. Valley-confined lahars can maintain relatively high velocities and have catastrophic impact as far as 100 km downstream (e.g. Nevado del Ruiz, 1985: Pierson et al., 1990).
Records of historic floods or debris flows generated by eruptions at ice-clad or snow-capped volcanoes show that volumes of meltwater can reach as much as 10^8 m^3 and peak discharges as high as 48,000 m^3/s (Table I, after Pierson, 1989). Glacier-outburst floods (jökulhlaups) can involve volumes of meltwater even larger (10^9 m^3), when dammed intra- or sub-glacial lakes are suddenly released (Bjornsson, 1983; Bjornsson and Kristmannsdottir, 1984).
This study aims to perform three primary objectives :

(1) to distinguish volcaniclastic deposits triggered by specific volcano-glacier interaction processes;
(2) to estimate the water volume generated by ice- and snow-melting and by the mechanical erosion induced by pyroclastic flowage;
(3) to consider a model of the heat transfer processes from hot eruptive products to ice and snow.

Recorded perturbations and preserved deposits

Review of types of effects

A review of eruptive processes that produced lahars or floods by the melting of snow and ice during historical volcanic eruptions indicates at least 5 causes (Major and Newhall, 1989; Thouret, 1990a,b).

1) Dense pyroclastic flows, dilute pyroclastic surges, hot blasts, and hot rock-avalanches melt, scour, and incorporate ice and snow, and quickly trigger lahars or floods (Mount St Helens, 1980, 1982: Janda et al., 1981, Pierson, 1985, 1989, Waitt et al., 1983; Nevado del Ruiz, 1985: Janda et al., 1986, Pierson et al., 1990, Thouret, 1990a).
2) Geothermal activity or subglacial eruption can melt glacier ice or an ice cap in a caldera setting, induce catastrophic breaching of a ponded intra- or sub-glacial lake, and trigger jökhulhlaups (e.g. Grimsvötn, Katla, Iceland: Bjornsson, 1983, 1984; Mt. Wrangell, Alaska: Benson and Motyka, 1978, Clarke et al., 1990).
3) Surficial lava flows can melt small to moderate volumes of snow and ice, and generate floods if a large volume of water dammed behind lava flow were to be catastrophically released (e.g. Villarica, Chile: Moreno et al., 1984; Calbuco, Chile: Klohn, 1963).
4) Catastrophic ejection of crater lakes by explosions can trigger mudflows and debris flows by mixing hot debris, snow, firn, and water while avalanches sweep down the volcano flanks (e.g. Ruapehu, New Zealand, 1969: Neall, 1976a,b).
5) Tephra fallout can slowly melt a small volume of snow and ice (Driegder, 1981). Tephra fallout usually does not trigger floods or debris flows directly.

We have observed several pertubations during the Nevado del Ruiz 1985 eruption (fig. 1, Thouret, 1990a, Thouret et al., 1987, 1992). Glacier tongues were fractured and removed by avalanching, when seismic quakes and eruptive activity set in (Fig. 2 a,b). A pattern of parallel furrows, scars and grooves scouring the snow pack and ice cap (Fig. 2 c), similar to those on Mount St. Helens (Brugman and Post, 1981), were carved by pyroclastic surges. Hollows in the ice surface were scoured by pyroclastic surges and flows, and pulverized, cross-stratified crystal-ice was redeposited infilling these hollows (Fig. 2 d). Smoothed-out seracs and abraded surfaces of glacier provide evidence for melting and surficial mechanical abrasion (Fig. 2 e). Tunnels plastered by pyroclastic debris in glacier ice at the margin of the ice cap indicate that intraglacial flowage of pyroclastic debris also took place during and after the eruption (Fig. 2 f).

Specific characteristics of tephra-laden snow-and-ice avalanche deposits

The Nevado del Ruiz 1985 eruption yielded a broad spectrum of deposits (Pierson et al., 1990; Thouret, 1990a) including tephra-fallout, dense pyroclastic flows, dilute pyroclastic surges, avalanches of tephra mixed with snow and ice, and primary lahars (debris flows and hyperconcentrated streamflows). Eruption-triggered mixed avalanches travelled a maximum of 6 km beyond the ice margin on the north flank of the Nevado del Ruiz stratovolcano prior to coalescence into major lahars (La Plazuela and Hedionda tributaries to upper Azufrado River: fig. 1). Deposits are a few hundred meters to 1 km wide, and a few decimeters to 1 m thick. The individual volume of all avalanches was in the range 6-7 x 10^6 m^3. The maximum height difference between the ice margin and the frontal lobe of the avalanche was about 1 200 m. The energy line (arctan x H/L; Hsü, 1975) was about 12°, suggesting an average apparent coefficient of friction of about 0.2. The velocity calculated from runup and superelevation of deposits was probably in excess of 15 m/s on the steep crater septum but slowed down to 10 m/s and even to 4-6 m/s on the gentle slope of the lava-flow surface above the confluence of La Plazuela with Rio Azufrado.
The avalanches spilled off the ice onto vegetated slopes and quickly transformed to viscous, relatively slow-moving soil- and vegetation-rich debris flow. They were triggered at the onset of the eruption, when pyroclastic surges swept down the snow-covered flanks and clearly before channelized lahars formed (that is within 20 minutes following the onset of the eruption: Pierson et al., 1990). Evidence for this are at least twofold: (1) avalanche-scour grooves on the bedrock cross ridges between channels that were re-excavated by later major lahars; (2) avalanche deposits on channel margins stratigraphically underlie levees of coarse debris-flow deposits which are exposed in the middle of the Rio Lagunillas channel (Fig. 3a).

Facies, sedimentary textures, and hydraulic characteristics of deposits of tephra-laden ice-and-snow avalanches are similar to those of mixed avalanches formed during the March 1982 eruption of the Mount St. Helens dome which removed a large part of the snow from the crater (Waitt et al., 1983; Pierson and Scott, 1985).

Although these mixed avalanche deposits are only transient and not well preserved in the stratigraphic record, once snow and ice have melted, the facies typically consists of a poorly sorted, nonstratified mixture of pumiceous or scoriaceous lapilli, lithic coarse ash, and chunks of dirty snow or ice (up to 1.2 m in diameter; Fig. 3b). At the margin of the deposit, steep-fronted lobes were 0.3 to 0.8 m high. Grain-size analysis indicate that the 80-cm-thick avalanche deposits (mean Phi -0.7 to -0.9, sorting index $\sigma G \sim 3.5$ and $\sigma I \sim 3.2$-3.4; skewness G ~ -0.2) are coarser than pyroclastic-surge deposits, mudflow- and hyperconcentrated-streamflow deposits but finer and better sorted than pyroclastic-flow and debris-flow deposits. In addition, they show characteristics somewhat similar to the early pyroclastic-surge and flow deposits they are related to. Several parameters: hydraulic depth, hydraulic radius, Froude number (> 1), and Mannings "n" (0.05-0.07) point to non-channelized, ill-sorted, high-density, gravity-driven flow similar to supercritical, high-concentration flows.

Lapilli-sized fragments from the mixed (tephra/snow/ice) avalanches, lahars, and pyroclastic deposits of the 1985 Nevado del Ruiz eruption were studied using backscattered-electrons imagery from the scanning electron microscope (SEM; Komorowski, 1991, Komorowski et al., 1991). Preliminary SEM images have shown that all fragments from mixed avalanche deposits, and pyroclastic-flow deposits with no contact with snow or ice, contain non-altered, porphyritic, juvenile clasts of andesitic composition, which are clearly vesiculated due to exsolution of magmatic gases prior to fragmentation and transport. The presence of vesicles (spherical to subspherical with bubble walls 5-15 μm) of two different sizes (i.e. vesicles 10 to 50 μm in diameter cut by vesicles > 100 μm), suggests that the magma was not totally degassed when it left the vent and that a last episode of vesiculation occurred at the moment of discharge at atmospheric pressure.

Satellite-based study of mixed avalanche, lahar and tephra deposits

A satellite SPOT multispectral scene (KJ 644-340 of August 9, 1986, fig. 4) was used to identify deposits generated by the 1985 eruption and post-eruptive activity. The part of the scene used covers the summit volcano and its radial headvalleys (Fig. 1). The SPOT image was studied in order to: (1) recognize different types of cover such as lahar deposits, ice, and snow; (2) establish their extent and distribution (Fig. 5), and (3) compare the satellite data with those collected during fieldwork (Figs. 1 and 6). The analysis of the SPOT image yields three results, as follows.

Three groups of objects were identified using spectral reflectances

According to characteristic spectral reflectances based on SPOT XS1 (green) and XS3 (infrared) bands, three groups of objects can be identified (Fig. 6):

(i) Bare soils with a reflectance in the visible (XS1 and 2) bands that is higher than in the infrared band. This group comprises, in order of increasing reflectance: streams, mixed avalanches, and tephra. The lowest reflectance of tephra mixed with snow or tephra mantling the ice cap is due to their high moisture content.

(ii) Vegetation with typical low reflectance in visible bands and high reflectance in the infrared band. For vegetation covered by tephra-fall

deposits, the reflectance increases in the visible bands and tends towards the tephra values. The reflectance curve decreases in the infrared band, but typically maintains a reflectance curve characteristic of vegetation.

(iii) Ice and snow. Several pixels of fresh snow and cloud show saturated DN (Digital Number) values (255) in visible bands, but the XS3 band can differentiate such pixels owing to the lower reflectance of snow in the infrared band. Ice surfaces are well separated from snow by a lower reflectance in each of three bands.

Ten objects were automatically classified using training areas

First, representative surface types were selected using our field data in order to create training areas of ten classes (Fig. 6): 1) mixed avalanches, 2) berms and channel margins of lahar deposits, 3) channelized lahars, 4) tephra-fall deposits mixed with snow, 5) recent tephra-fall beyond the ice cap, 6) vegetation covered by discontinuous tephra-fall deposits, 7) uncovered vegetation and tilled land, 8) 1985-1986 tephra-fall mantling ice near the vent, 9) fresh snowpack, and 10) uncovered ice cap. An automatic classification was then performed using a mean reflectance of each class computed from training areas. Every pixel is successively classified according to its DN values by estimating the maximum likelihood of membership. The resulting classification (Fig. 6) highlights the boundaries between geological units and helps to distinguish bare soils. Thick tephra hide the glacier ice around the crater. Thin tephra-fall deposits, with a higher spectral reflectance, have been scattered over the west and NW flanks of the volcano by the wind. Streamflow channels are distinguished from the channel margins and avalanche deposits. The tephra-laden ice-and-snow avalanches appear around the ice cap and on the channel margins. Two types of vegetation, covered or uncovered, are clearly differentiated. Vegetation has been more covered by tephra towards the NNE, reflecting the prevailing dispersal of eruptive products. The snowpack is located in the central part of the ice cap, while bare and eroded glacier ice coincides with steep slopes, cirques, collapse areas, and fractures.

Deposit differentiation using cross sections and indices

A complete classification of bare soils over the massif is difficult owing to spatial variations of reflectance within a class. First, bare soil surfaces represent heterogeneous patches, the sizes of which are smaller than that of the pixel (20 m x 20 m). Second, variations in surface orientation around the massif flanks induce differences of pixel illumination and radiance measured by the satellite. Moreover, the reflectance of the surface depends on the soil moisture content, which is related to location.

Several cross-sections of DN values are illustrated across two main channels, Rio Azufrado on the north flank of the volcano (Fig. 7a) and Rio Lagunillas on the east flank (Fig. 7b), where streamflow channels, channel margins, and avalanche deposits are exposed. Comparison between these cross-sections show that the differences of DN values between objects are similar on both profiles, although absolute levels differ, probably because of different composition, texture or moisture contents of the deposits. The similarity observed between cross-sections enables us to

extrapolate a standard reflectance profile across a drainage system, while the relative differences reflect the nature of the deposits.
To enhance further discrimination between surface types, we have investigated differences in surface heterogeneity on the SPOT image. For each bare soil class, we have computed an image homogeneity index on representative areas to determine the uniformity of a given soil at the scale of several pixels (Table in Fig. 7: Haralick, 1979; Gonzales and Wintz, 1987). This index traduces the coarseness of the image texture: a high homogeneity index implies a fine texture of image, thus a uniform surface of soil; a small index implies a coarse texture revealing a patchy structure of soil. Variations of this index show that for classes with close DN means on test areas, such as avalanches and streamflow channels, differentiation can be improved. For example, avalanche deposits are spatially homogeneous compared to streamflow channels.

Estimates of volume of meltwater released by volcano-glacier interactions

The Nevado del Ruiz ice cap is the field-test area for evaluating and modelling processes that quickly released large volumes of meltwater during the 13 November 1985 eruption (38.5-44 x 10^6 m^3 during a 20 to 90 minute duration; Thouret, 1990a).

Estimates based on air-photograph, SPOT image, and 3D-orthoimages

The amount of released water was estimated in two different ways (Fig. 8, left side):

i) The volume of water contained in the channelized lahars was computed and extrapolated back to the edge of the ice cap (11-22 x 10^6 m^3, fig. 8-left side: Pierson et al., 1990; Thouret, 1990a).

ii) The surface areas and volumes of snow and ice lost from the summit ice cap were determined using pre- and post-eruption ground photographs (38.5-44 x 10^6 m^3, fig. 8; Thouret, 1990a).

Because these estimates differed, we utilized two additional numerical and field-based approaches.

i) We compared one 1979 air photograph of the ice cap taken before the eruption (Fig. 9) with the aforementioned SPOT XS image acquired after the eruption in 1986 (Fig. 4). A digital topography model was developed by digitizing a 1/10,000-scale topographic map. A series of 3D-orthophotos of all ice-clad flanks of the volcano were constructed to show ice cap extent before and after the eruption. Two sets of 3D orthophotos point to obvious changes at the ice margin, first on the east flank (Fig. 10a,b), second on the north flank (Fig. 11a,b). The digital model and orthophotos have enabled us to calculate changes in areas of snow cover, as well as areas of ice mass removed by glacier failure (Figs. 8 and 12).

ii) Hand-drilled snow and ice cores (5035 m in elevation and at 2 km distance SW of the active Arenas crater) permitted better calculation of the water equivalent of snow, firn and ice; they also provided preliminary glacier ice mass balance and glacio-chemical data (Laj and Boutron, 1990; L. Raynaud, F. Valla, and J.-C. Thouret, unpublished data). The mean snow-accumulation

rate is about 1.5-2 m water equivalent per year. Albeit variable through the year, the snow cover was 3 to 6 m thick, and the calculated density was in range 300-550 kg/m^3. The firn-ice transition was found to be at a depth of about 10 m.

We suggest that approximately half of the released meltwater did not contribute to lahar generation, because it was lost in at least 6 ways: (1) in slush avalanches, tephra-laden ice and snow avalanches, and non-channelized small slurries; (2) within or beneath glaciers; (3) in steam resulting from passage of pyroclastic flows; (4) in firn produced by thin tephra fallout; (5) in phreatic eruptive products; (6) in wet pyroclastic-surge deposits (see Thouret, 1990a, table x for data set).

Discussion : genesis of avalanches and lahars in the light of interaction processes

According to the literature, lahars or floods can result from:

1) snow avalanche, snowmelt, and slushflows triggered by dry high-energy pyroclastic surge (e.g., Mount St Helens: Waitt et al., 1983; Waitt, 1989);
2) wet pyroclastic surges which transform to lahars (Mount St Helens: Janda et al., 1981; Pierson, 1985; Scott, 1988);
3) melting and incorporation of meter-thick snowslab avalanches (Mount St. Helens: Fairchild, 1987);
4) scouring and gullying by pyroclastic flows, transforming to ice-rich mixed diamicts into steep glaciers (Mount Redoubt: R.J. Janda, unpublished data);
5) turbulent pyroclastic flows and dilute surges which cause powerful mechanical and thermal effects such as dynamic mixing and fluid drag within a thick cover of loose snow and low-density firn (Nevado del Ruiz: Pierson et al., 1990; Janda et al., 1986; Thouret, 1990a);
6) mass failure of glacier ice caused by eruptive activity and seismic shaking.

We need to understand how considerable volumes of meltwater can be released quickly. The Nevado del Ruiz case study suggests that the ice surface was lowered an average of 3-6 m over 15 km^2 in 20-90 minutes. The most significant losses to the glaciers appear to have occurred where energetic pyroclastic flows and surges eroded or destabilized steep slopes underlain by snow and highly fractured ice. Losses were relatively minor in areas of gentle slopes were tephra-fallout was passively deposited, even though the emplacement temperatures of some deposits were probably in excess of 500°C (Pierson et al., 1990; Thouret, 1990a).

Two preliminary "melting models"

We consider three preliminary "melting models" (fig. 8b).

The first "passive" melting model is based on the non-turbulent and slow deposition of a blanket of hot debris on snow and ice. The amount of heat transferred from hot debris to snow is approximated as the heat conduction, Q, between two plates (M. Meier, in Pierson et al., 1990 ; see also Walder, 1990, 1992):

$$Q = kTo\ (t)^{0.5} / (\pi\ \alpha)^{0.5},$$

where

Q= heat flow from the hot pyroclastic layer to the snow (cal cm^{-2}),

k= thermal conductivity of pumice and lithic debris (0.6-20 x 10^{-3} cal cm^{-1} s^{-1} C^{o-1}),

To= initial temperature of pyroclastic flow (700°C),

t= time (s^{-1}),

and α= k/cγd equals thermal diffusivity (pumice and lithics 3-40 x 10^{-3} cm^2 s^{-1} ; c = specific heat, γd density of debris).

Assuming that the snowpack is free-draining and that the hot debris remains in contact with snow and ice crystals, the volume of water melted can then be computed:

$$V = [Q A / Hf \gamma i] \times 10^4$$

where

V= volume of meltwater (m^3),

Q= heat transferred (cal cm^{-2}),

A= area of contact (km^2)

Hf= heat of fusion for water (79.7 cal g^{-1}),

and γi= density of snow and ice (0.35-0.9 g cm^{-3}).

This simple mechanism of heat conduction yields a low melting rate, in the range 1-2 x 10^{-4} m/min (Fig. 8; e.g. Huppert et al., 1984). This least energetic melting model would produce about 7.4 x 10^5 m^3 of meltwater over an surface area of 15 km^2 of ice after 10 minutes or about 1.3 x 10^6 m^3 after 30 minutes. This volume is far less than that estimated from the missing snow and ice (fig. 8a). Thus, "passive" emplacement of hot rock debris on snow is insufficient to generate large heat transfer and large volume of meltwater that transform eventually to lahars.

The second "erosive" melting model is based on turbulent pyroclastic flow on snow and ice, and requires that the two materials be mechanically mixed for sufficiently rapid heat transfer. Such model has not been developped yet. However, we estimate how high is a steady melting rate necessary to obtain the volume of meltwater computed (Fig. 8a). Assuming a steady heat transfer through time and neglecting the thermal effect of hot water resulting from melt, the estimated volume of meltwater in the range 38.5-44 x 10^6 m^3 implies a more rapid melting rate, in the range 1-2 x 10^{-2} m/min over a 10-30 minute period (Fig. 8b), which is compatible with a loss of 3-6 m of snow and firn on the Nevado del Ruiz ice cap during 30 minutes on November 13, 1985. This would account for approximately 22-67 x 10^6 m^3 of liquid water, which is comparable to that given by computing the lost ice and snow from the ice cap (Fig. 8a). A less energetic melting model would also account for a comparable volume of meltwater, but only if the melting rate were steady at 3-5 x 10^{-3} m/min over a 50-90 minute period, i.e. the whole duration of the eruption (Fig.8b).

Mixing is presumably enhanced by the turbulent regime of pyroclastic surges and by other mechanical processes (dynamic mixing, fluid drag, and mass failure). Percolating meltwater, seismic shaking, and shear stress imparted by pyroclastic flows and surges may trigger large-scale mass failure and lead to mixed avalanches

that transform to lahars, like those at Mount St. Helens (1980) and Nevado del Ruiz (1985; Pierson et al., 1990). Shear stress imparted by fluid drag and particle collisions, within the high-concentration base of pyroclastic density currents, may help to trigger mixed avalanches (Waitt, 1989; Pierson et al., 1990; Fairchild, 1987; Thouret, 1990a,b).

Conclusion

The interaction of hot eruptive products with snow and ice includes a variety of processes such as rapid melting, snow and ice avalanching, surficial abrasion, mechanical scouring and gullying. Dense pyroclastic flows, dilute pyroclastic surges, and hot blasts are the most effective processes. As they melt, scour, incorporate ice and snow, they can rapidly release enough meltwater to trigger large-scale lahars or floods (10^5 to 10^9 m^3).

Field surveys and SPOT remote sensing enabled us to identify to a series of pyroclastic deposits and especially mixed avalanche deposits (tephra, snow, and ice) which contributed to lahar generation. Geomorphic and hydraulic parameters point to non-channelized, high-density or high-concentration, gravity-driven flows. Moderate-scale eruptions can trigger catastrophic lahars or floods because large volumes of meltwater are supplied by powerful mechanical and thermal processes such as dynamic mixing and fluid drag induced by turbulent flow of pyroclastic debris on and within a thick cover of loose snow and low-density firn. Approximately 38.5-44 x 10^6 m^3 of water were released from the Nevado del Ruiz ice cap during a 20-90 minute period on November 13, 1985. This estimate is based on analysis of 3D-orthoimages and on field photographs and measurements.

Two "melting models" are presented. Deposition of a blanket of hot tephra would not produce a significant volume of meltwater (e.g. Pierson et al., 1990). In contrast, the flow of hot debris across snow is presumed to produce melting at rates of 1-2 x 10^{-2} m/min. The two materials, however, must be mechanically mixed to allow rapid heat transfer. Mechanical entrainment and comminution of ice are very important in triggering lahars.

Acknowledgements

The senior author wishes to dedicate this paper to the memory of R.J. Janda and thanks T. Pierson for stimulating discussions while on sabbatical leave at the U.S. Geological Survey, Cascades Volcano Observatory. Informal review by T. Druitt and B. Hallet and two official reviews greatly improved the content and shape of this paper. We also thank our Colombian colleagues of the Observatorio Vulcanologico de Colombia (Manizales, Colombia) for technical and field assistance, Michel Sachettini from CIC Grenoble, and the French INSU-CNRS for funding fieldwork costs. This paper is a contributionto ATP DBT 3.28 from the Institut des Sciences de l'Univers, CNRS, Paris.

References

Benson C.S. and Motyka R.J., 1978. Glacier-volcano interactions on Mt. Wrangell, Alaska. Geophys. Inst., Univ. of Alaska, Fairbanks, *Annual Report* 1977-78, 25 p.

Bjornsson H., 1983. A natural calirometer at Grimsvötn ; an indicator of geothermal and volcanic activity. *Jökull* 33, AR, 13-18.

Bjornsson H.and Kristmannsdottir H., 1984. The Grimsvötn geothermal area, Vatnajökull, Iceland. *Jökull* 34, AR, 25-48.

Brugman M.M. and Post A., 1981. Effects of volcanism on the glaciers of Mount St. Helens. *Geol. Surv. Circ.* 850-D, 11 p.

Clarke G.K.C., Cross G.M., and Benson C.S., 1990. Radar imaging of glaciovolcanic stratigraphy, Mount Wrangell caldera, Alaska : interpretation model and results. *J. Geophys. Res* 94, B6, 7237-7249.

Cummans J., 1981. Chronology of mudflows in the South Fork Toutle river following the May 18 eruption. *U.S. Geol. Survey Circ.*850 B, 16 p.

Driedger C.L., 1981. Effect of ash thickness on snow ablation. *In* Lipman P.W. and Mullineaux D.R. (eds.), The 1980 eruptions of Mount St. Helens, Washington. *U.S. Geol. Survey Prof. Paper* 1250, 757-760.

Fairchild L.H., 1987. The importance of lahar initiation processes. *In* J.E. Costa and G.F. Wieczorek (eds.), Debris Flows/Avalanches: process, recognition, and mitigation. *Geol. Soc. Amer., Rev. Eng. Geol* 7, 51-61.

Gonzalez R.C. and Wintz P., 1987. *Digital Image Processing.* Addison-Wesley, Reading, Mass., 503 p.

Haralick R.M., 1979. Statistical and structural approaches to texture. *In* Proc. 4th Int. Joint Conf. Pattern Recogn., pp. 45-60

Huppert H. E., Sparks R.S.J., Turner J.S.and Arndt N.T., 1984. Emplacement and cooling of komatiite lavas. *Nature* 309, 19-22.

Hsü K.J., 1975. On sturzstroms - catastrophic debris streams generated by rockfalls. *Geol. Soc. Amer. Bull.* 86, 129-140.

Janda R.J., Scott K.M., Nolan K.M., and Martinson H.A., 1981. Lahars movement, effects and deposits. *In* Lipman and Mullineaux (eds.), The 1980 eruptions of Mount St. Helens. *U.S. Geol. Survey Prof. Paper* 1250, pp. 461-478.

Janda R.J., Banks N.G., Pierson T.C., Thouret J.C., and Calvache M.L., 1986. Interaction between ice and pyroclastic sediments erupted during the 13 November 1985 eruption of Nevado del Ruiz, Colombia. *EOS, Trans. Amer. geophys. Union* 67, 16, p.406.

Klohn E., 1963. The February 1961 eruption of Calbuco volcano. *Seism. Soc. Am. Bull* 53, 1435-1436.

Komorowski J.-C., 1991. *Scanning electron microscopy of pyroclastic matter : eruptions of Mount Vesuvius in AD 79 and Mount St. Helens in AD 1980.* Ph.D. Dissertation, Arizona State University, University Microfilms, 1-317, Ann Harbor, Michigan.

Komorowski J.-C., Glicken H.X., and Sheridan M.F., 1991. Secondary electron imagery of microcracks and hackly fracture surfaces in sand-size clasts from the 1980 Mount St. Helens debris-avalanche deposit : implications for particle-particle interactions. *Geology* 19-3, 261-264.

Laj P.G. and Boutron C.F., 1990. Trace elements in snow deposited at Nevado del Ruiz volcano, Colombia. Nevado del Ruiz Volcano, Colombia, II. *J. Volcanol. Geoth. Res.*, 42, 89-100.

Major J.J. and Newhall C.G., 1989. Snow and ice perturbation during historical volcanic eruptions and the formation of lahars and floods - a global review. *Bull. Volcanol.* 52, 1-27.

Moreno H.R. et al., 1984. Villarica volcano, S. Chile, October 1984 eruption. *SEAN Bull* 9, 11.

Neall V.E., 1976a. Lahars. Global occurrence and annoted bibliography. Victoria Univ., Wellington, *Geol. Dept. Publ.* 5, 1-18.

Neall V.E., 1976b. Lahars as major geological hazards. *Bull. Intern. Assoc. Engin. Geol.* 14, 233-240.

Pierson T.C., 1985. Initiation and flow behavior of the 1980 Pine Creek and Muddy River lahars, Mount St. Helens, Washington. *Geol. Soc. Amer. Bull.* 96, 1056-1069.

Pierson T.C., 1989. Hazardous hydrologic consequences of volcanic eruptions and goals for mitigative action : an overview. *Proc. Techn. Conf. on the Hydrology of Disasters*, November 1988, World Meteorological Organization, Geneva.

Pierson T.C. and Scott K.M., 1985. Downstream dilution of a lahar : transition from debris flow to hyperconcentrated streamflow. *Water Res. Res.* 21 (10), 1511-1524.

Pierson T.C., Janda R.J., Thouret J.C., and Calvache M.L., 1986. Initiation, bulking, and channel dynamics of catastrophic debris flows on 13 november 1985 at Nevado del Ruiz, Colombia. *EOS, Trans. Amer. geophys. Union* 67, p.406 (Abstract).

Pierson T.C., Janda R.J., Thouret J.C., and Borrero C., 1990. Perturbation and melting of snow and ice by the 13 November 1985 eruption of Nevado del Ruiz, Colombia, and consequent mobilization, flow and deposition of lahars. *J. Volcanol. Geoth. Res.* 41, 17-66.

Scott K.M., 1988. Origins, behavior, and sedimentology of lahars and lahar-runout flows in the Toutle-Cowlitz river system. *U.S. Geol. Survey Prof. Paper* 1447-A, 1-74.

Thouret J.-C., 1990a. Effects of the 13 November 1985 eruption on the ice cap and snow pack of Nevado del Ruiz (Colombia). *J. Volcanol. Geoth. Res* 41, 177-201.

Thouret J.-C., 1990b. Contribution à la définition des formations issues des interactions volcaniques et glaciaires. *In* "La Terre et les Hommes", Fac. Lettres, Université Blaise Pascal, 32, pp. 221-236.

Thouret J.-C., Janda R.J., Pierson T.C., Calvache M.L., and Cendrero A., 1987. L'éruption du 13 novembre 1985 au Nevado del Ruiz (Cordillère Centrale, Colombie): interactions entre le dynamisme éruptif, la fusion glaciaire et la genèse d'écoulements volcano-glaciaires. *Comptes-Rendus Acad. Sci.*, Paris, t. 305, Sér. II, 505-509.

Thouret J.-C., Vandemeulebrouck J., Komorowski J.-C., Valla F., and Naaim M., 1992. Interactions glace-magma et déclenchement de lahars. *Dynamique et Bilans de la Terre, Colloque National "DBT " INSU-CNRS*, Décembre 1992, Toulon, 4 p.

Waitt R.B., 1989. Swift snowmelt and floods (lahars) caused by great pyroclastic surge at Mount St Helens volcano, Washington, 18 May 1980. *Bull. Volcanol.* 52, 138-157.

Waitt R.B., Pierson T.C., MacLeod N.S., Janda R.J., Voight B., and Holcomb R.T., 1983. Eruption-triggered avalanche, flood, and lahar at Mount St. Helens - effects of winter snowpack. *Science* 221, 4618, 1394-1396.

Walder J., 1990. Melt-induced modification of contacts between pyroclastic deposits and snow or ice. *EOS, Trans. Amer. geophys. Union*, Fall meeting (Abstract V21B-2).

Walder J., 1992. Movement of pyroclastic flows over "snow" : an experimental and theoretical study. *EOS, Trans. Amer. geophys. Union*, Fall meeting (Abstract V12A-4).

Table 1

EXAMPLES OF ORIGINS AND CHARACTERISTICS OF DIFFERENT TYPES OF LARGE SEDIMENT-WATER FLOWS ORIGINATING FROM VOLCANOES (modified from PIERSON, 1989)

FLOW TYPE	LOCATION DATE	ORIGIN	VOLUME (m^3)	VELOCITY (m/s)	PEAK DISCHARGE (m^3/s)	DISTANCE TRAVELED (km)	REFERENCE
Debris flow	Mount St. Helens, 1980, North Fork Toutle River	Remobilization of debris-avalanche deposit	1.4×10^8	1.7-5.3 (front) 7-10 (peak)	7 200 6 000 6 600	at 4.5 at 26 at 40	Janda et al., 1981 Fairchild, 1987
Debris flow	Mount St. Helens, 1980, South Fork Toutle River	Rapid snow-melt by pyro-clastic surge	1.3×10^7	33 (peak) 4-8 (peak) 2.4 (front)	6 800 3 800	at 4 at 44 (59 total)	Cummans, 1981 Fairchild, 1987
Debris flow	Nevado del Ruiz 1985 (Rio Azufrado; Rio Chinchina)	Rapid snow-melt by pyro-clastic flow and surge, snow avalanches	1.2×10^7 5.5×10^7	14.6 (peak) 12 (peak) 6 (front)	48,000 27,100	at 10 at 69 (90 total)	Pierson et al., 1986, 1990
Flood	Grimsvötn, 1954	Glacier outburst flood (jökulhlaup)	$3\text{-}3.5 \times 10^9$	-	10,000	-	Björnsson, 1983

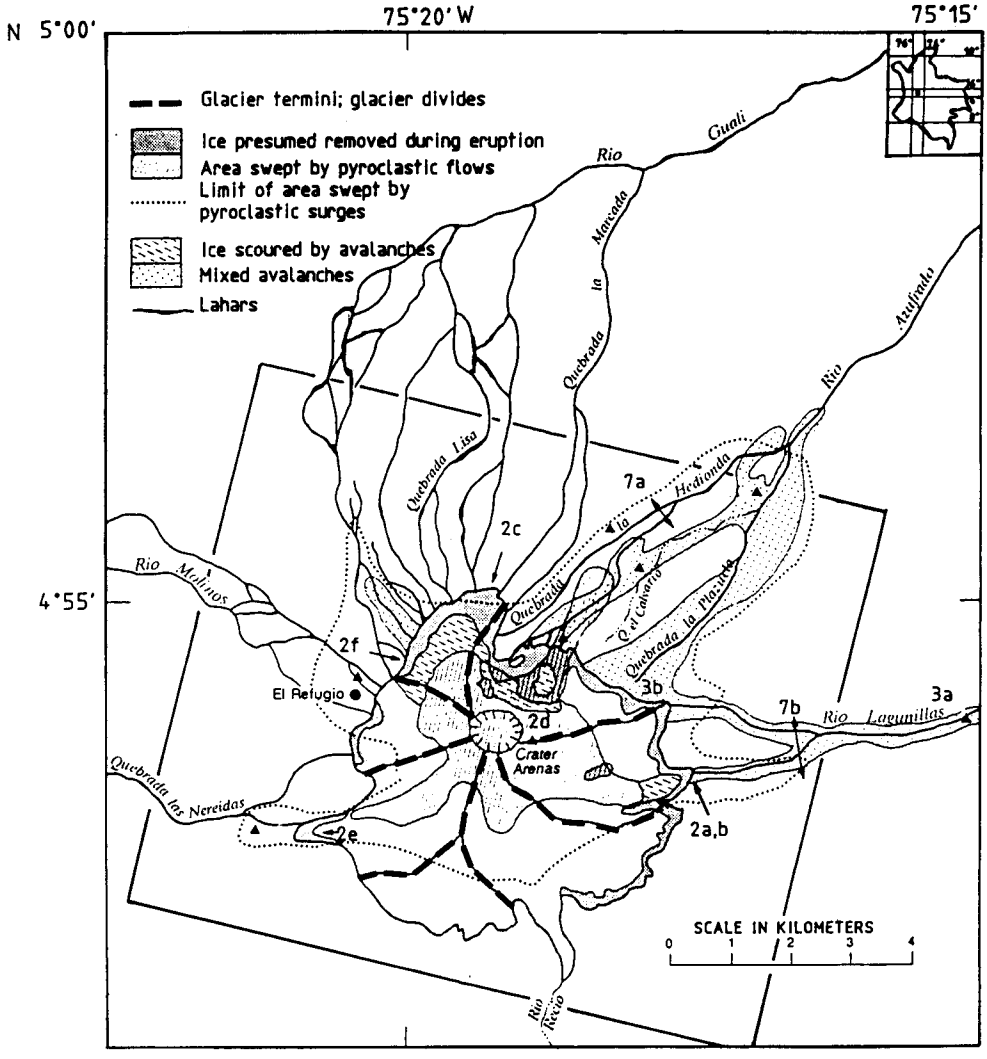

Figure 1. Approximate boundaries of the Nevado del Ruiz ice cap before and after the 13 November 1985 eruption and distributary channels that conveyed lahars. Approximate extent of pyroclastic flows, pyroclastic surges, and mixed avalanches is also shown (data compiled from aerial photographs and field surveys by J.-C. Thouret, *in*: Pierson et al., 1990; Thouret, 1990a,b). Rectangle corresponds approximately to area covered by the 1986 SPOT image (Fig. 5). Lines with arrows are cross-sections shown in Fig. 7a,b. Figures 2a,b,c,d,e,f, and 3a,b indicate the location of the corresponding photographs (see Fig. 2).

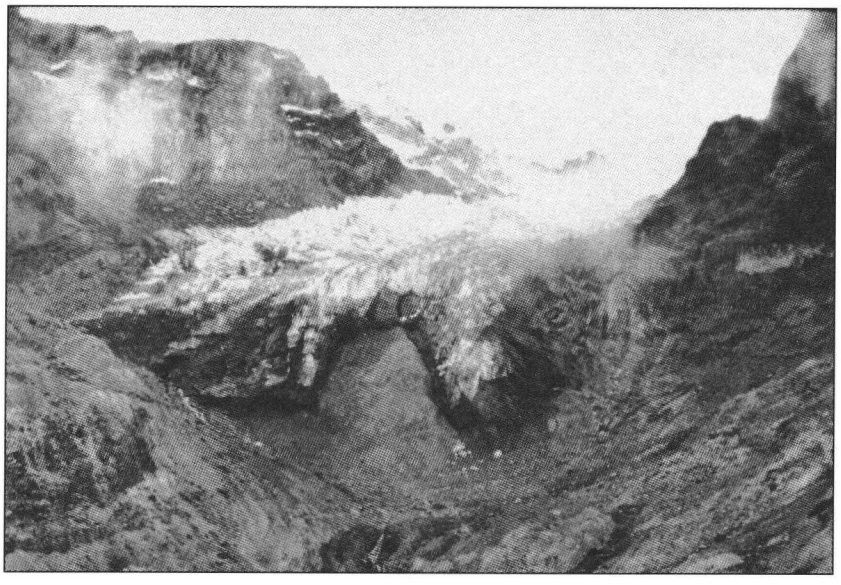

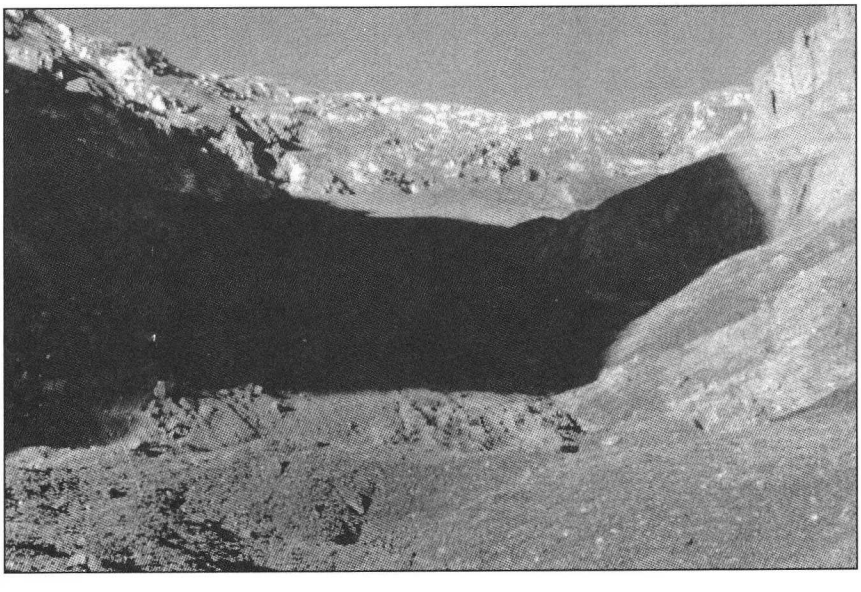

Photos 2a,b: tongue of the Lagunillas glacier (east flank of Nevado del Ruiz) before (1981) and after the 13 November 1985 eruption (December 1985).

Photo 2c: furrows, scars, and grooves on the north flank of the Nevado del Ruiz ice cap and its margin.

Photo 2d: erosive contact on pulverized, cross-stratified crystal-ice, below a thin layer of pyroclastic surge deposit and coarse pyroclastic flow deposit.

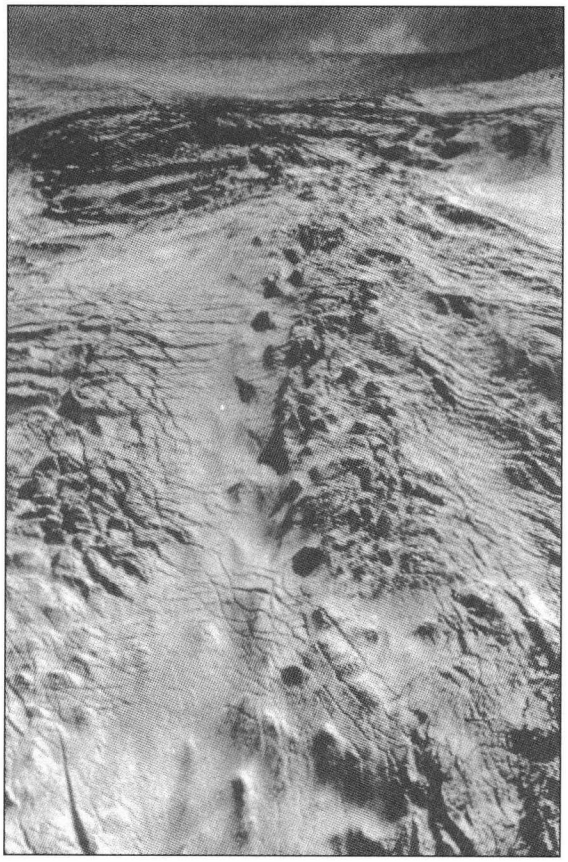

Photo 2e: smoothed out seracs and abraded surface of the Nereidas glacier on the west flank of Nevado del Ruiz.

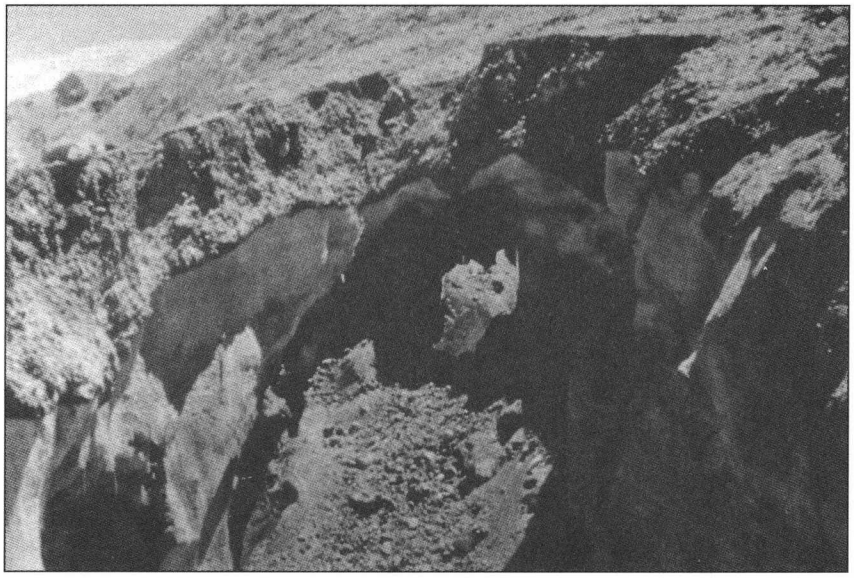

Photo 2f: tunnels plastered by pyroclastic debris in glacier ice at the northern margin of the Nevado del Ruiz ice cap. (See Fig. 1 for location of all photographs).

Figure 3a. Three types of 1985 eruption-triggered deposits exposed in the Rio Lagunillas headvalley, Nevado del Ruiz (3 500 m, 2.5 km east of the ice cap margin) : (i) early mixed avalanche deposits on the channel margins (note person for scale) ; (ii) levees of coarse and openwork debris-flow deposits ; (iii) late, thin, and massive hyperconcentrated streamflow deposits on the channel bed. (See Fig. 1 for location).

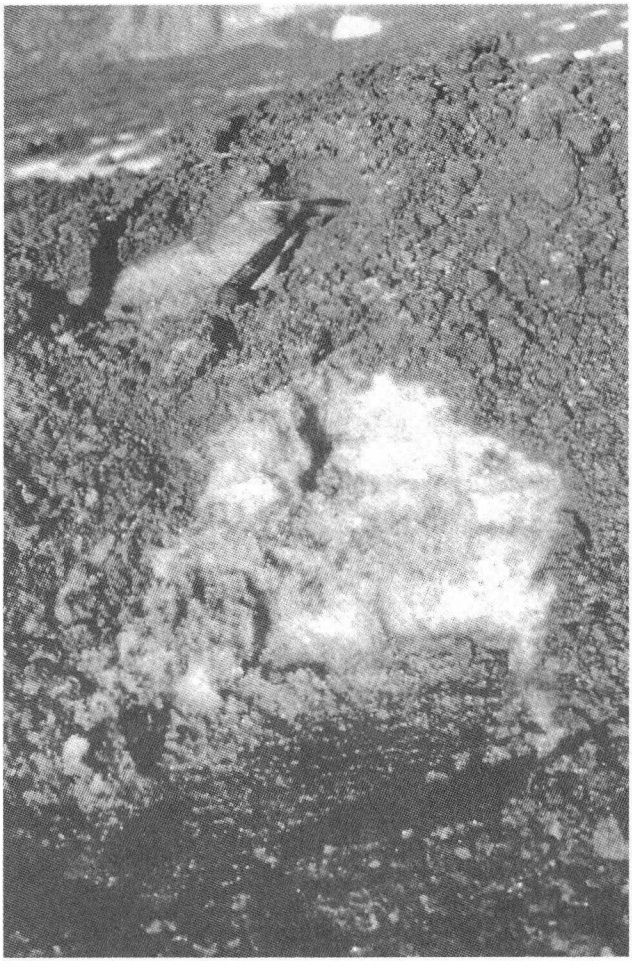

Figure 3b. Mixed avalanche deposit resting on ice, comprising a poorly sorted, nonstratified mixture of pumiceous or scoriaceous lapilli, lithic coarse ash and chunks of dirty snow and ice (note hammer for scale; section located on the NE side of the Nevado del Ruiz ice cap, December 1985). (See Fig. 1 for location).

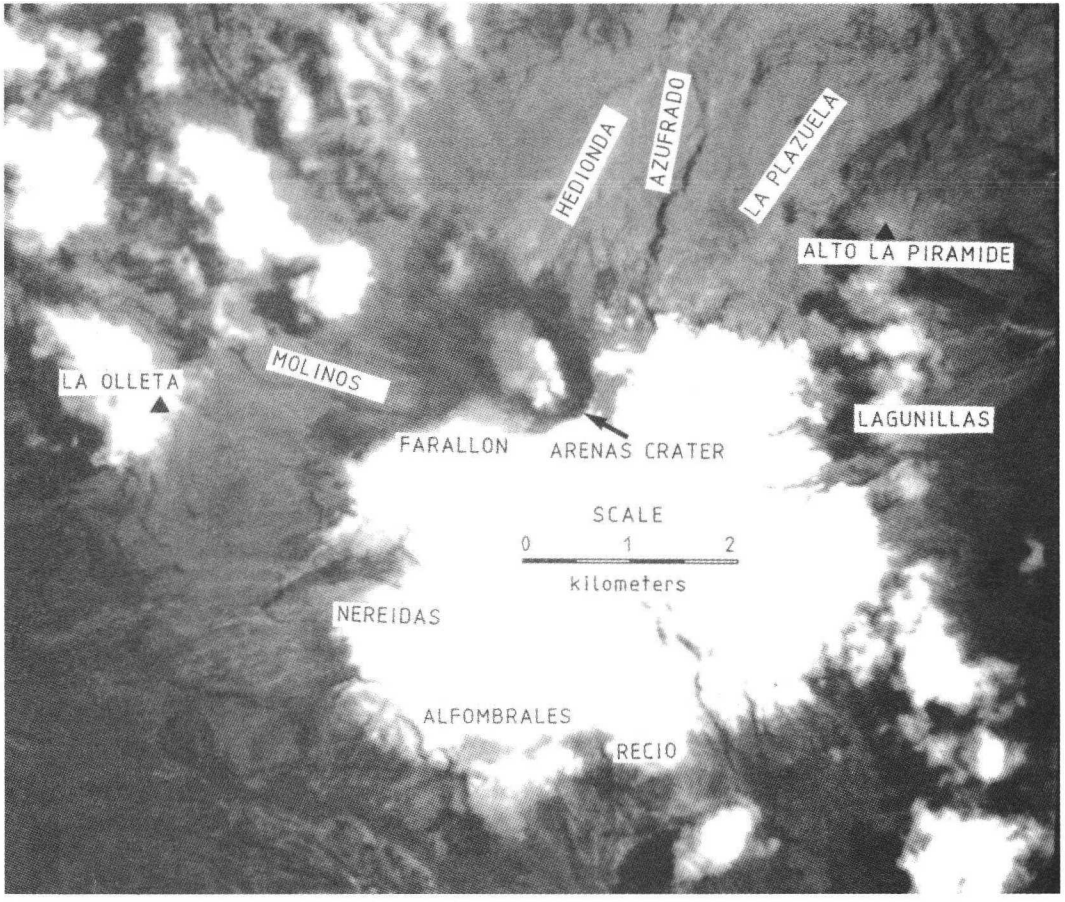

Figure 4. Photograph of the south part of the August 9, 1986, SPOT XS image (KJ 644-340, approximate scale 1/30,000). The Nevado del Ruiz summit and ice cap mantled by fresh snow, active Arenas crater with its plume on the northern edge, and the ice margins and outlets towards west (Nereidas-Molinos), north (Azufrado), and east (Lagunillas) are shown. (See Fig. 1 for location).

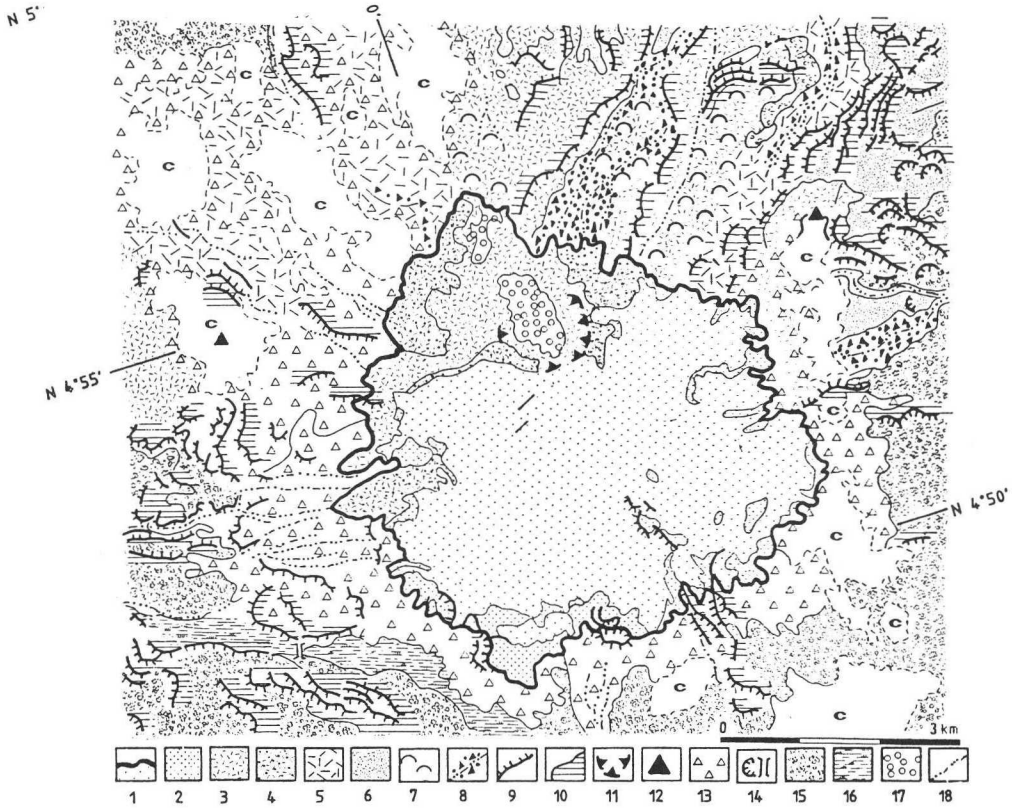

Figure 5. Interpretation of the 1986 SPOT XS image of the Nevado del Ruiz summit volcano.
I. Ice cap: 1. Post-1985 eruption boundary of ice cap and its cover of fresh snow; 2. Ice cap and bare, eroded glacier ice where snow has been removed; 3. Ice mantled by thick tephra; 4. Ice covered by thin, post-1985 tephra.
II. Eruptive products and debris-flow deposits: 5. 1985 tephra-fall deposit; 6. Thin and discontinuous tephra on paramo vegetation; 7. Mixed avalanche (tephra, snow, and ice) covered by tephra fallout; 8. Debris-flow, mudflow, and streamflow deposits.
III. Geomorphological features: 9. Scarp of lava flow; 10. Lava flow of the summit volcano of Late Pleistocene age; 11. 1985-widened Arenas crater and rims covered by thick tephra; 12. Parasitic vents of La Olleta (left) and Alto La Piramide (right).
IV. Glacial landforms and deposits: 13. Historical moraines; 14. Cirque and riegel.
V. Vegetation cover: 15. Low vegetation of paramo; 16. Peat bog.
VI. Other features: 17. Plume from the Arenas vent; 18. Rill and stream fed by meltwater from the ice cap. Letter **c** in white areas = cloud.

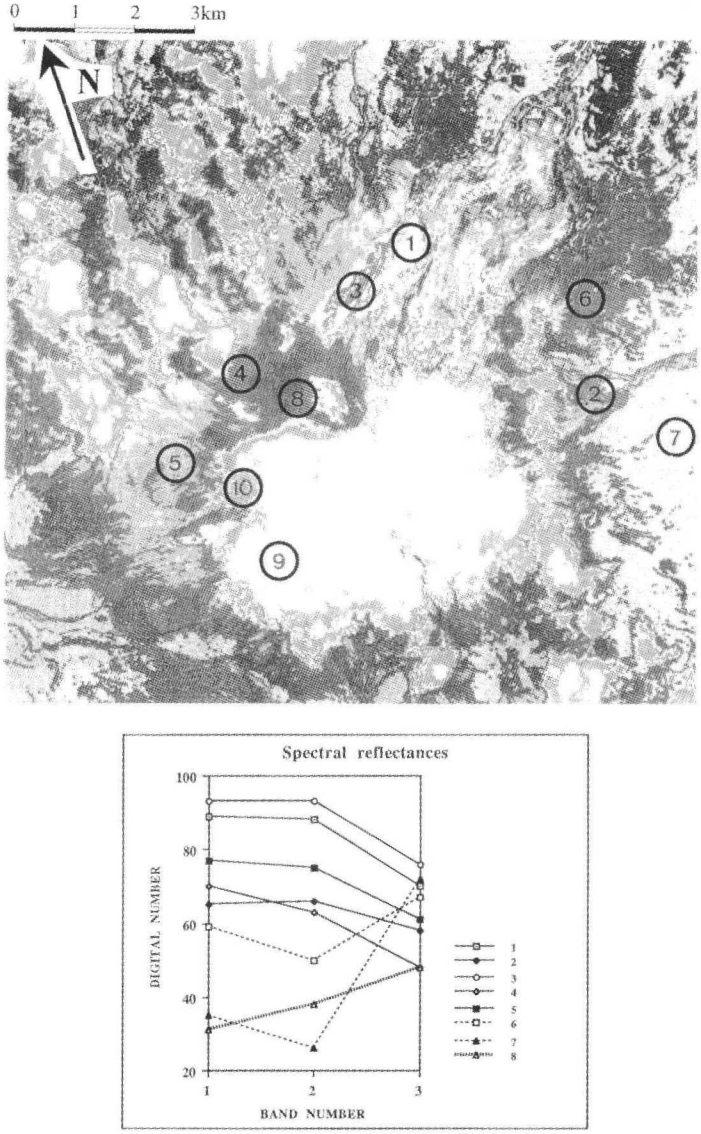

Figure 6. Geological deposits, vegetation, and ice/snow on and around the Nevado del Ruiz ice cap based on remote sensing of the August 9, 1986, SPOT XS image). Group I, bare soils: class 1: mixed avalanches; 2: berms and channel margins of lahar deposits; 3: channelized lahars; 4: tephra-fall deposits mixed with snow; 5: recent tephra fall beyond the ice cap. Group II, vegetation: class 6: vegetation covered by discontinuous tephra-fall deposits; 7: uncovered vegetation and tilled land. Group III, class 8: 1985-1986 tephra-fall mantling the ice at the vent; 9: fresh snowpack; 10: uncovered ice cap.
Table: average values of Digital Numbers (DN) in the three SPOT XS bands showing specific spectral reflectances of 8 geological units interpreted on the 1986 image. Those units are the first 8 objects listed in footnote.

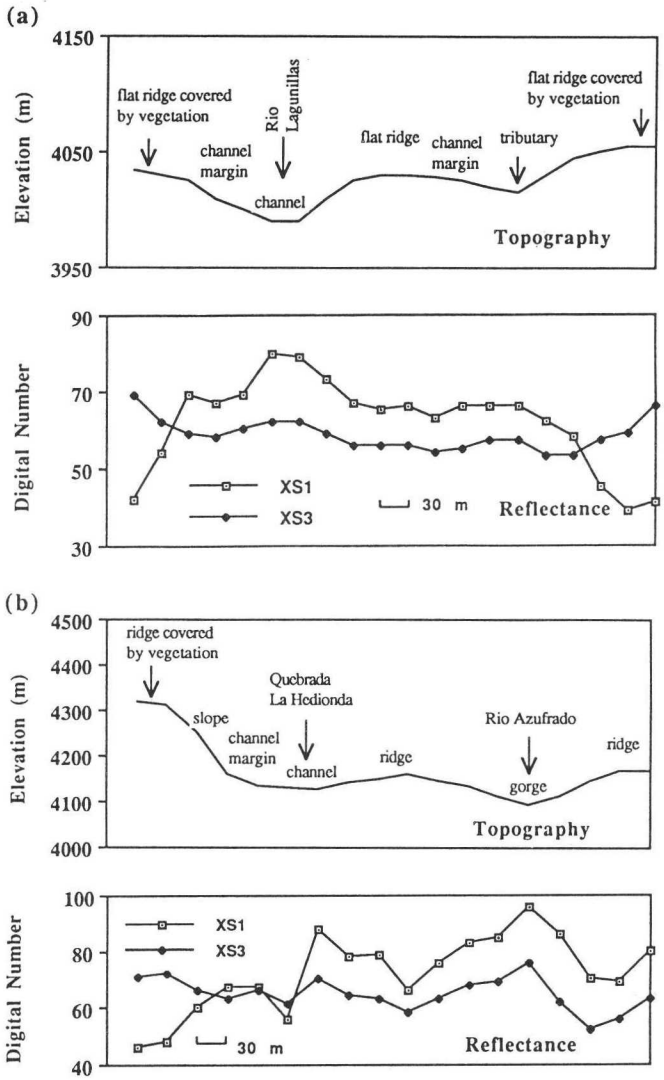

CLASSES	1	2	3	4	5	6	7	8
Homogeneity index, XS1 band	0.49	0.44	0.10	0.41	0.50	0.30	0.44	0.30
Homogeneity index , XS3 band	0.61	0.58	0.17	0.57	0.65	0.40	0.19	0.44

Figure 7. Topographic and radiometric cross-sections of XS1 and XS2 bands, perpendicular to the Rio Azufrado-Hedionda and Lagunillas headvalleys, at Nevado del Ruiz. See Fig. 1 for location. Table below: indices of texture homogeneities for listed objects in Fig.6.

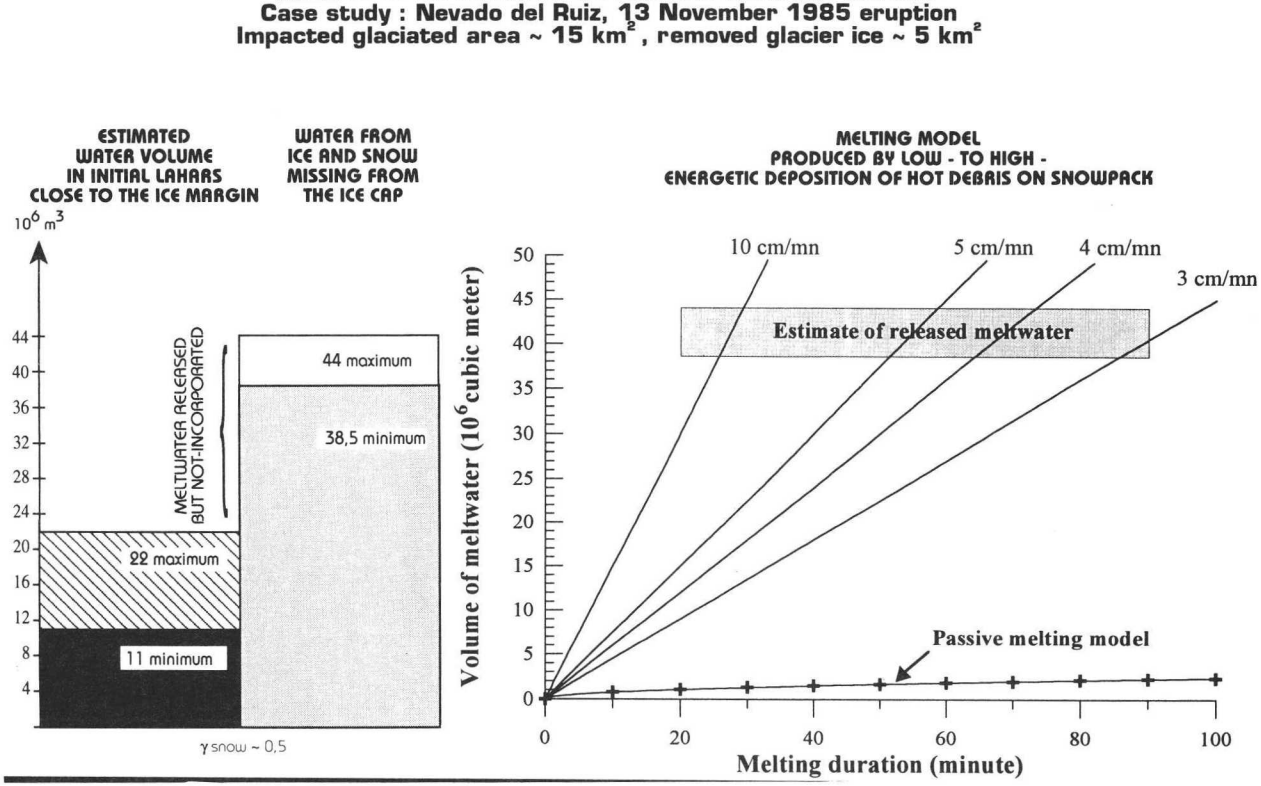

Figure 8. Comparison of estimated volumes of meltwater released from impacted snowpack and ice cap generated during the 1985 eruption of Nevado del Ruiz.
Fig. 8a: estimated water volume (i) in initial lahars close to the ice margin (Pierson et al., 1990, Thouret, 1990a); (ii) from ice and snow missing from the ice cap (Thouret, 1990a and this study).
Fig.8b: estimates of melting rates that can account for the volume of released meltwater due to volcano-glacier interactions during a 20- to 90-minute-long eruption. Line with crosses indicate a steady state melting rate for the first "passive" melting model. Lines indicate steady melting rates for different melting durations (see text for discussion).

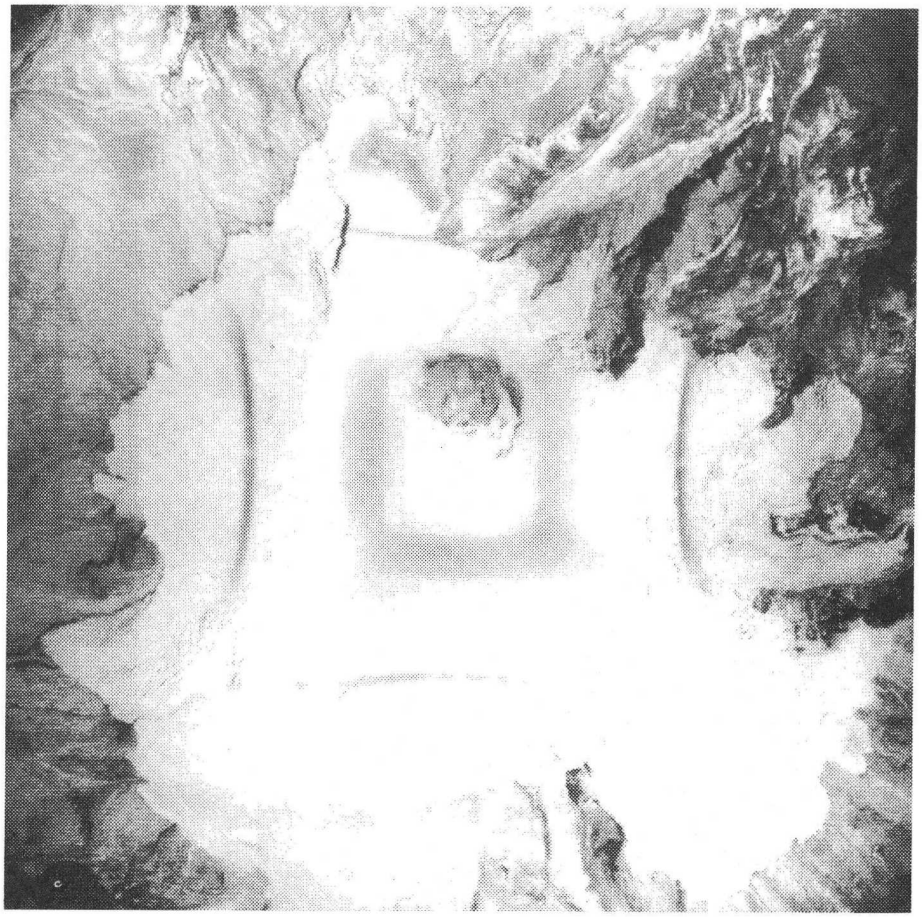

Figure 9. Aerial photograph (1979, 1/25,000 scale) of the Nevado del Ruiz ice cap providing pre-eruption data for the 3D-orthophoto.

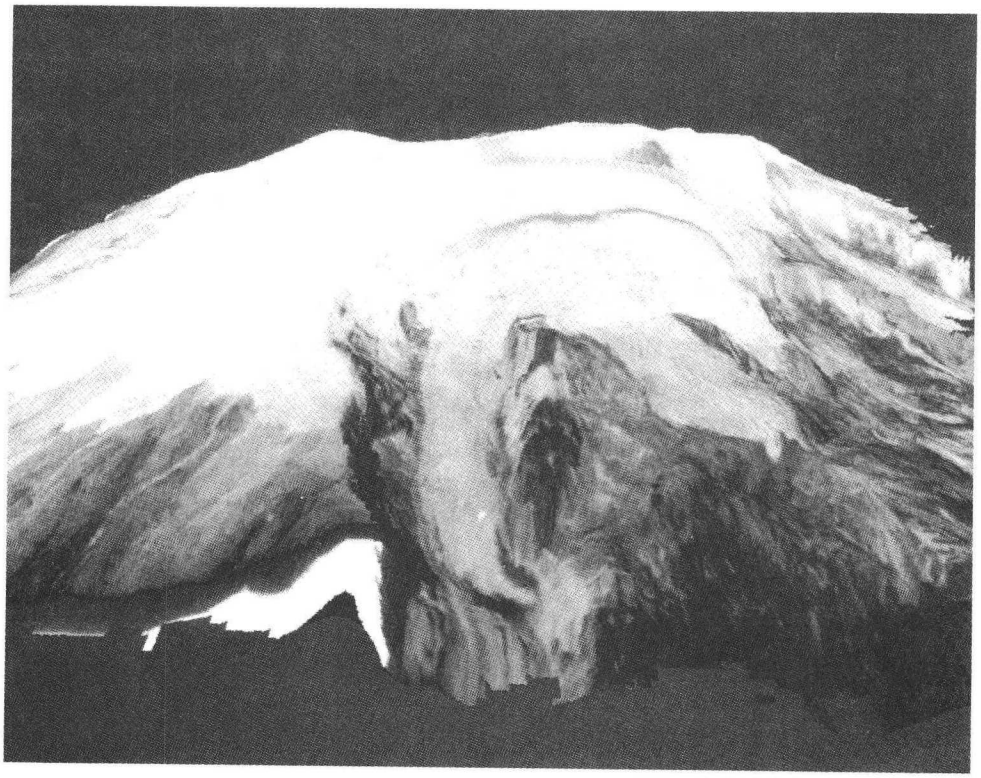

Figure 10a. Three-dimensional orthophotos of the east and NE flanks of Nevado del Ruiz before the eruption ; (b) after the eruption. Note that the tongue of the Lagunillas glacier (lower center) has been removed.

Figure 10b. Three-dimensional orthophotos of the east and NE flanks of Nevado del Ruiz after the eruption. Note that the tongue of the Lagunillas glacier (lower center) has been removed.

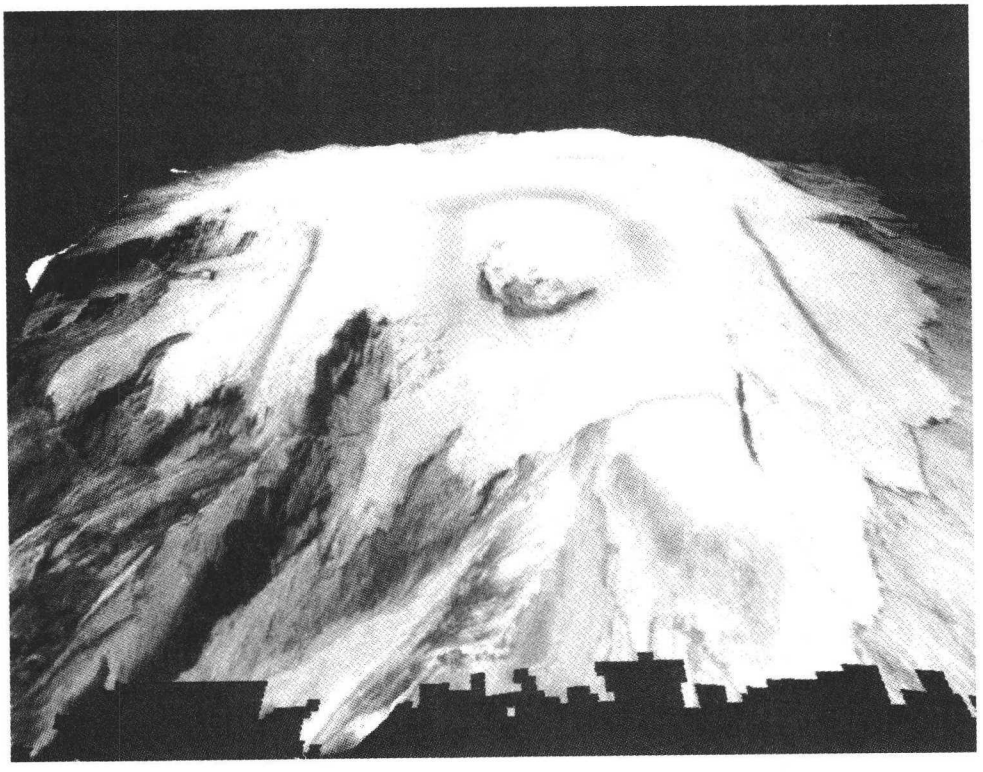

Figure 11.a Three-dimensional orthophoto of the north and NW flanks of Nevado del Ruiz before the eruption.

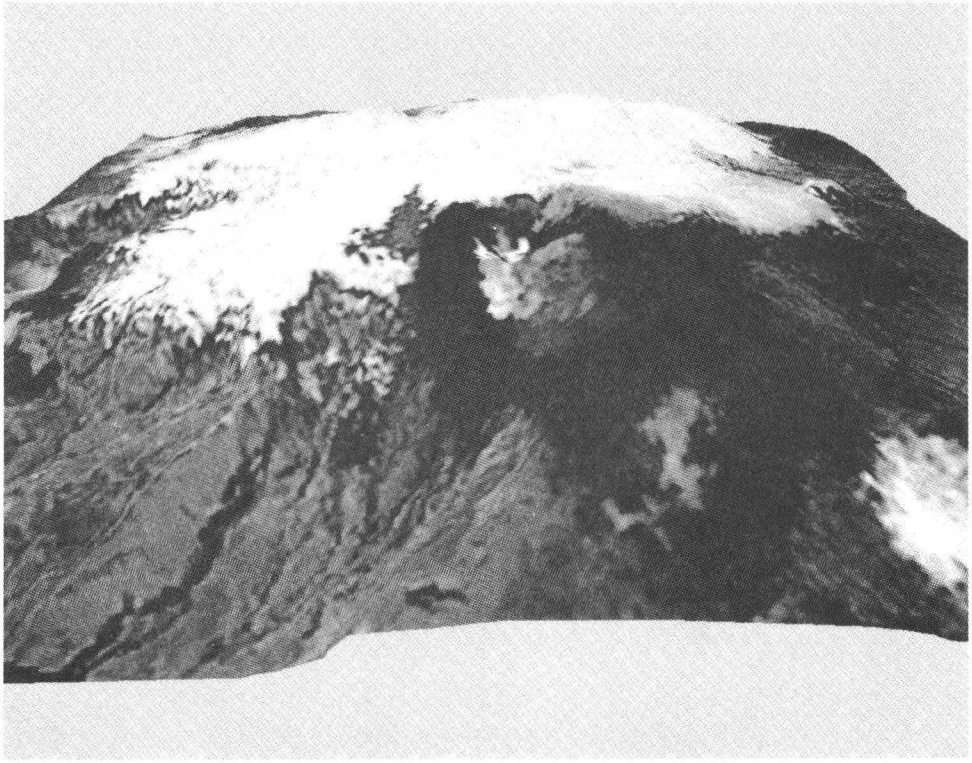

Figure 11b. Three-dimensional orthophoto of the north and NW flanks of Nevado del Ruiz after the eruption. Note active Arenas crater, eroded ice on Azufrado headwall and septum, and ice mantled by fresh tephra on Farallon (NW).

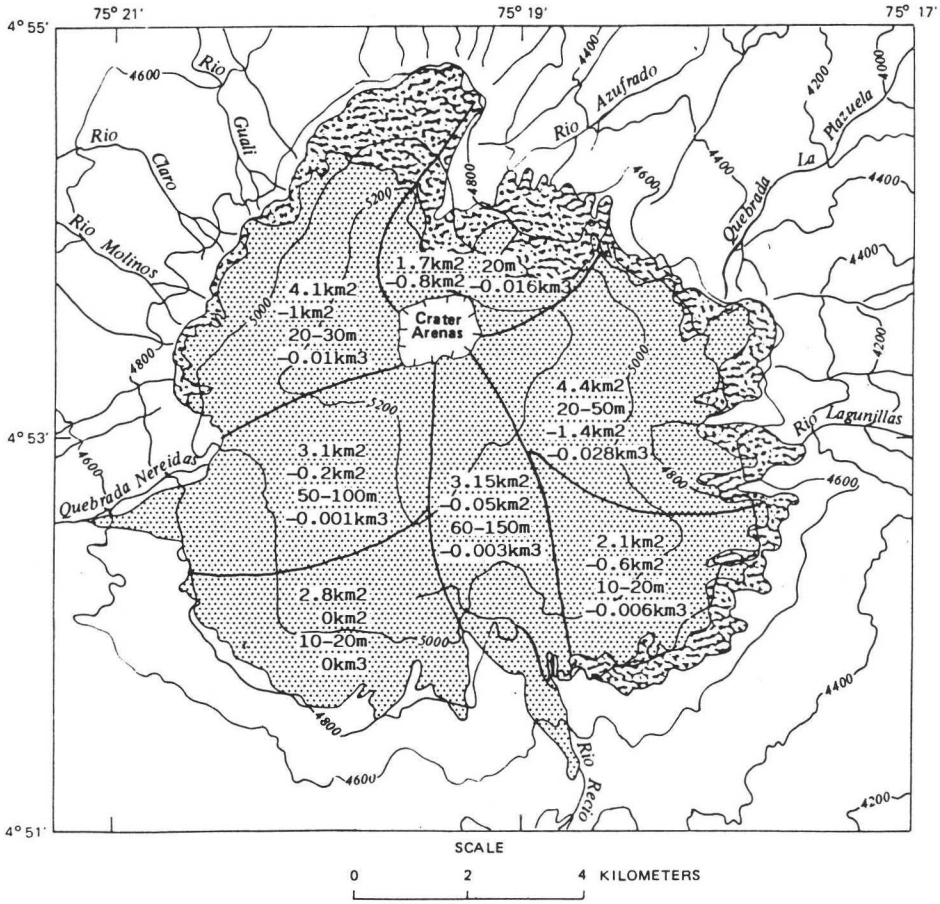

Post-eruption ice cap

Missing ice, snow and firn, and pre-eruption extent

Approximate boundary of the glacial basins

Meaning of the four figures indicated in each glacial basin :
(1) post-eruption surface area; (2) missing surface area;
(3) estimated thickness; (4) estimated missing volume

Figure 12. Map of Nevado del Ruiz ice cap after the 1985 eruption. Estimates of surface area and volume of removed ice, and the thickness of the remaining ice cap within each glacial basin are shown.

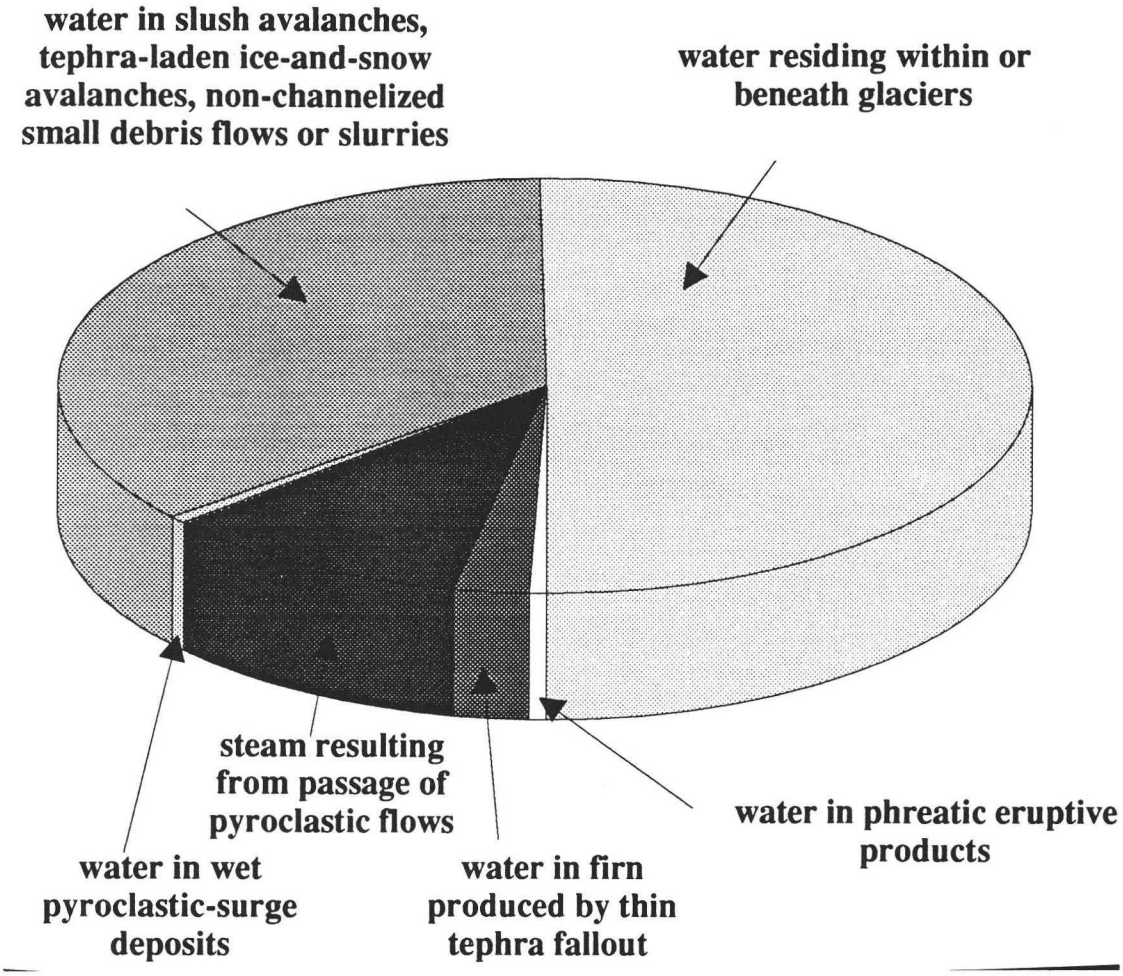

Figure 13. Estimated budget of released meltwater not contributing to lahar generation (see Thouret, 1990a for details on data set).

L O U I S - J E A N
avenue d'Embrun, 05003 GAP cedex
Tél. : 92.53.17.00
Dépôt légal : 379 — Mai 1995
Imprimé en France

The "Pierre Beghin" international workshop on *Rapid gravitational mass movements* has been supported by

L'atelier international "Pierre Beghin" sur les *Mouvements gravitaires rapides* a été organisé avec l'aide de

Institut de recherche pour l'ingénierie de l'agriculture et de l'environnement (Cemagref)

Ministère de l'Environnement Délégation aux risques majeurs (DRM)

Pôle grenoblois d'étude et de recherche sur les risques naturels (PGRN)

Grenoble, pôle européen universitaire et scientifique (GPEUS)

Service de restauration des terrains en montagne (RTM)

Région Rhône-Alpes

Cemagref Editions 1995
ISBN 2-85362-411-0
Prix : 280 F TTC